This is to certify that the

thesis entitled

OPTIMIZING THE EFFICIENCY OF TRANSVERSE JOINTS ANDCRACKS IN ROLLER-COMPACTED CONCRETE (RCC) PAVEMENTS

presented by

Jacob E. Hiller

has been accepted towards fulfillment
of the requirements for

M.S. degree in Civil Engineering

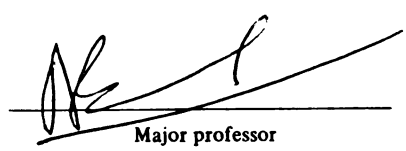

Major professor

Date 12/8/00

OPTIMIZING T
ROLI

OPTIMIZING THE EFFICIENCY OF TRANSVERSE JOINTS AND CRACKS IN ROLLER-COMPACTED CONCRETE (RCC) PAVEMENTS

By

Jacob Eskel Hiller

A THESIS

Submitted to
Michigan State University
in partial fulfillment of the requirements
for the degree of

MASTER OF SCIENCE

Department of Civil and Environmental Engineering

2000

OPTIMIZING THE

ROLLER-

Roller-compacted

e practicality of aspha

ncrete pavement RC

lume heavily loaded

ast and associated labo

nventional concrete pa

en limited due to the

ge crack widths, which

This thesis will a

of non-destructive def

ternatives (such as inc

hesives than the natura

mined in order to pro

RCC pavement rehabili

commendations will be

ABSTRACT

OPTIMIZING THE EFFICIENCY OF TRANSVERSE JOINTS AND CRACKS IN ROLLER-COMPACTED CONCRETE (RCC) PAVEMENTS

By

Jacob Eskel Hiller

Roller-compacted concrete (RCC) has been utilized since the 1930's. It combines the practicality of asphalt paving procedures with the durability of a portland cement concrete pavement. RCC pavements provide an initial cost-effective solution to low volume, heavily loaded pavements. Due to lack of forms, reinforcing steel, temperature steel, and associated labor costs, RCC pavements have resulted in savings of 10-58% over conventional concrete pavement construction. The applications of RCC pavements have been limited due to the varying surface roughness (and corresponding friction) as well as large crack widths, which develop from the long crack spacings.

This thesis will aim to evaluate existing RCC pavements in service through the use of non-destructive deflection data to estimate the stresses due to a traffic load. Alternatives (such as increased RCC design thickness, engineered joint spacing at closer distances than the natural crack spacing, or dowel bar retrofitting of natural cracks) will be examined in order to produce an efficient design based on cost. Options for in-service RCC pavement rehabilitation will be produced and future RCC pavement design recommendations will be made.

I would to thank

jects as well as with c

iversity

I would also like

its research work and p

Pasinski of PCA for pro

oncrete pavements and

I would also like

xpense regarding the I

A special thanks

ansportation and Mich

roviding FWD data of

I would like to g

ave always provided su

A final thanks go

roughout this stage of

ACKNOWLEDGEMENTS

I would to thank Dr. Neeraj Buch for his support and direction on numerous projects as well as with career objectives throughout my graduate career at Michigan State University.

I would also like to thank the Portland Cement Association (PCA) for sponsoring this research work and providing financial support. Specifically, I would like to thank Jan Prusinski of PCA for providing technical support on the subject of roller-compacted concrete pavements and Steve Kosmatka for his help on this project.

I would also like to give thanks to Tom Yu of ERES Consultants for his technical expertise regarding the ISLAB2000 rigid pavement analysis program.

A special thanks goes out to Linda Pierce of the Washington Department of Transportation and Michael Eacker of the Michigan Department of Transportation for providing FWD data of PCC retrofitted dowel sites.

I would like to give a special thanks to my parents, John and Sharon Hiller, who have always provided support and encouragement in my academic career as well as in life.

A final thanks goes to my wife, Renee, for her patience and understanding throughout this stage of our life together.

TABLE OF CONTENTS

Page

Page

TABLE

LIST OF TABLES

TABLE

C-1 RCC Design T

k=100 psi in

C-2 RCC Design T

k=250 psi in

C-3 RCC Design Th

k=400 psi in

C-4 RCC Design Th

k=100 psi in

C-5 RCC Design T

k=250 psi in

C-6 RCC Design T

k=400 psi in

C-7 RCC Design T

k=100 psi in

C-8 RCC Design T

k=250 psi in

C-9 RCC Design T

k=400 psi in

C-10 RCC Design T

k=100 psi in

C-11 RCC Design T

k=250 psi in

TABLE Page

TABLE Page

FIGURE

LIST OF FIGURES

FIGURE

FIGURE Page

FIGURE

FIGURE Page

FIGURE Page

FIGURE

A-17 Critical Tensile

Located 24" (

A-18 Critical Tensile

Located at the

A-19 Critical Tensile

Located 24" (6

A-20 Critical Tensile

Located at the P

A-21 Critical Tensile S

Located 24" (6

A-22 Critical Tensile

Located at the P

A-23 Critical Tensile

Located 24" (6

A-24 Critical Tensile

Located at the P

A-25 Critical Tensile S

Located 24" (6)

A-26 Critical Tensile S

Located at the P

A-27 Critical Tensile S

Located 24" (6)

FIGURE Page

FIGURE Page

FIGURE

FIGURE Page

FIGURE

B-18 LTE_e with R

(203 mm), k

B-19 LTE_e with R

(254 mm), k

B-20 LTE_e with Re

(254 mm), k=

B-21 LTE_e with Re

(254 mm), k=

B-22 LTE_e with Re

(254 mm), k=

B-23 LTE_e with Re

(254 mm), k=

B-24 LTE_e with Re

(254 mm), k=

B-25 LTE_e with Re

(254 mm), k=

B-26 LTE_e with Re

(254 mm), k=

B-27 LTE_e with Re

(254 mm), k=

FIGURE Page

FIGURE Page

FIGURE Page

FIGURE

B-69 Principal Ter

h=6" (152 mm

B-70 Principal Ten

h=8" (203 mm

B-71 Principal Ten

h=8" (203 mm

B-72 Principal Tens

h=8" (203 mm

B-73 Principal Ten

h=8" (203 mm

B-74 Principal Ten

h=8" (203 m

B-75 Principal Te

h=8" (203 m

B-76 Principal Te

h=8" (203

B-77 Principal T

h=8" (203

B-78 Principal T

h=8" (203

B-79 Principal

h=10" (2

FIGURE Page

FIGURE

FIGURE

B-102 Principal Te

h=14" (356

B-103 Principal Te

h=14" (356

B-104 Principal Te

h=14" (356 m

B-105 Principal Te

h=14" (356 r

E-1 Subgrade S

(152 mm) R

E-2 Subgrade S

(203 mm)

E-3 Subgrade S

(254 mm)

E-4 Subgrade S

(305 mm)

E-5 Subgrade

(356 mm)

E-6 Subgrade

(152 mm

E-7 Subgrade

(203 mm

FIGURE

FIGURE Page

FIGURE

FIGURE Page

PROBLEM STA

During the

joints were not cu

Volumetric instabi

feet (9 to 24 m)

extremely thick sect

These large

sides of the crack

stresses will be incu

designed for due to

must be developed

importance is the ne

capacities.

OBJECTIVES O

This projec

non-destructive de

RCC design thickn

spacing or dowel

- CHAPTER I -

Introduction

PROBLEM STATEMENT

During the early years of roller-compacted concrete (RCC) pavements, engineered joints were not cut in order to save on initial construction and sealant maintenance costs. Volumetric instability along with curling resulted in crack spacing ranging from 30 to 80 feet (9 to 24 m) for conventional RCC thicknesses and up to 450 feet (137 m) in extremely thick sections. These large crack spacings resulted in wide crack openings.

These large crack widths are not conducive to high load transfer between the two sides of the crack. Since the two sides of the crack may act as different slabs, higher stresses will be incurred. This will bring the pavement to failure at an earlier time than designed for due to fatigue of the concrete. To combat this problem, design strategies must be developed to ensure a long-term, cost-effective pavement. An additional issue of importance is the need to assess when and how to repair pavements with low load transfer capacities.

OBJECTIVES OF RESEARCH

This project will aim to study load stresses for in-service RCC pavements through non-destructive deflection data and finite element analysis. Alternatives (such as increased RCC design thickness, engineered joint spacing at closer distances than the natural crack spacing, or dowel bar retrofitting of natural cracks) will be examined in order to produce

an efficient desig

be discussed and

If the reco

should prove RC

that carry heavy l

consideration of R

local collector, an

SCOPE OF RESE

The recomm

following research p

provide a better und

Task 1 – Re

design proce

with RCC p

Task 2 – Ga

synthesize t

elastic mod

deflection lo

range of va

Task 3 – Fr

provide trer

comparison

an efficient design based on cost. Options for in-service RCC pavement rehabilitation will be discussed and future RCC pavement design recommendations will be made.

If the recommendations from this project are utilized, the findings from this study should prove RCC pavements are a reasonable long-term alternative for low volume areas that carry heavy loads. A secondary consideration of this project is to also promote the consideration of RCC pavement construction for other functions, such as subdivision, local, collector, and arterial roads.

SCOPE OF RESEARCH

The recommendations from this project will be made from the findings of the following research plan. The research plan has been divided into six "tasks" in order to provide a better understanding of the different phases of this project

Task 1 – Review and synthesize national and international literature as well as design procedures for RCC in order to characterize known and potential problems with RCC pavements.

Task 2 – Gather FWD and HWD data from existing RCC pavement sites and synthesize this data to backcalculate pavement structural parameters (such as elastic modulus, modulus of subgrade reaction, radius of relative stiffness, deflection load transfer efficiency, etc.). This will be done in order to describe the range of values that are typical for RCC pavements.

Task 3 – From the existing sites found in Task 2, an attempt will be made to provide trends with statistical certainties of the following parameters in comparison to deflection load transfer efficiency for each test section:

-
-
-
-
-

Task 4 – D

fatigue rela

alternatives

dowel bar re

benefit of loa

induced stres

Task 5 – De

existing RC

CONTENTS OF T

This thesis c

pavements, a discus

this study, and a sur

research. A more d

Chapter II includes

summary of the ma

design methods of

pavements, and, a

utilized. Chapter I

study. It also disc

variables from thes

- Crack width or opening
- Crack or Joint spacing
- Elastic modulus of the RCC
- Modulus of subgrade reaction
- Radius of relative stiffness

Task 4 – Develop a design scheme for new RCC pavement construction based on fatigue relationships found in Task 1 and inventory data from Task 2 including alternatives such as increased thickness design, joint cutting and maintenance, and dowel bar retrofitting of naturally cracked pavements. It will incorporate the benefit of load transfer at joints or cracks as well as the effect of temperature-induced stresses, which is not included in most design methods.

Task 5 – Develop rehabilitation strategies towards extending the service life of existing RCC pavements found in Task 2.

CONTENTS OF THESIS

This thesis contains background on information roller-compacted concrete pavements, a discussion of the analyses performed and the results obtained from data in this study, and a summary of the conclusions and recommendations derived from this research. A more detailed breakdown of the contents of individual chapters follows. Chapter II includes: background on the construction practices of RCC pavements; a summary of the material properties of RCC; a review of the most common structural design methods of RCC pavements; a review of the field performance of in-service RCC pavements; and, a description of the future application where RCC pavements are to be utilized. Chapter III provides a description of the test sites and data collected for this study. It also discusses the trends found between load transfer efficiency and many variables from these test sites. A review of a new RCC pavement structural design

method is given in

method to existing

alternatives of RC

chapter also gives a

rehabilitation altern

from the analyses p

related to the load

which concludes th

method is given in Chapter IV. Also included in Chapter IV is a comparison of this new method to existing design methods. Chapter V discusses design and rehabilitation alternatives of RCC pavements to insure the design life of an RCC pavement. This chapter also gives a detailed methodology as to the timing of dowel bar retrofitting as a rehabilitation alternative. A summary of the conclusions and recommendations arising from the analyses performed in this study as well as a listing of future research needs related to the load transfer efficiency in RCC pavements are contained in Chapter VI, which concludes this thesis.

CONSTRUCT

History

Althoug

years the idea

relatively new.

procedures wit

roller-compact

surface layer is

pavements are

The ea

pavement in 1

Another early

Japan in 1956

Roller

Oregon in the

resulting in a s

materials and

construction te

RCC p

for mass concr

- CHAPTER II -

Literature Review

CONSTRUCTION PRACTICES

History

Although the concept of soil-cement and lean concrete has been in use for over 50 years, the idea of using higher-quality aggregates to form a high-strength concrete is relatively new. Roller-compacted concrete combines the practicality of asphalt paving procedures with the durability of portland cement concrete pavement. The ability of roller-compacted concrete to carry a large of stress placed on it by an external load as a surface layer is what separates it from normal soil-cement. In this respect, RCC pavements are very similar to conventional concrete pavements.

The earliest reported use of roller-compacted concrete was as an Australian pavement in 1932 as well as in a Yakima, Washington airport pavement in 1941. Another early example of RCC was the construction of two freight yards in Hokkaido, Japan in 1956 [1].

Roller-compacted concrete was used for mass concrete dams in both Pakistan and Oregon in the early 1970s. The no-slump mixture was placed in lifts and compacted, resulting in a savings of about one-third over the costs of using conventional concrete materials and techniques. These projects demonstrated the economic advantages of this construction technique which could easily be adapted to pavement construction [2].

RCC pavements in North America were constructed on a larger scale soon after the mass concrete dams in the mid-1970s. The U.S. Army Corps of Engineers

Waterways Exper

This experiment h

rollers on RCC an

RCC pavements [2

In 1976, R

sorting and storage

as a durable and ec

pavements has been

the forestry industry

Canadian waterway

climatic conditions

In July of 1

scale RCC paveme

locks and other ar

This alternative re

concrete pavemen

construction as bo

Underlying Laye

From a pr

concrete pavemen

constructed to fu

Waterways Experiment Station (WES) built two test sections in Vicksburg, Mississippi. This experiment had two purposes. The first examined the effect of different vibratory rollers on RCC and the second studied the consequences of using marginal materials in RCC pavements [2].

In 1976, RCC pavements were constructed as a low-cost alternative for use as log sorting and storage yards in British Columbia, Canada [1]. The birth of RCC pavements as a durable and economical alternative to both conventional concrete and asphalt pavements has been attributed to this project. Due to a governmental regulation forcing the forestry industry to sort logs on land thereby reducing wood debris contamination in Canadian waterways, over 28 acres of RCC sorting yards has been built in the harsh climatic conditions of British Columbia as of 1983 [2].

In July of 1984, the U.S. Army Corps of Engineers constructed the first large-scale RCC pavement in the United States. A 20,000 yd^2 (16,700 m^2) parking area for tanks and other armored vehicles was built at Fort Hood in Texas over an 11-day period. This alternative resulted in a savings of 15 percent over a conventional reinforced concrete pavement [2]. This project was the beginning of an increase in RCC pavement construction as both military and civilian projects in the United States.

Underlying Layer Construction

From a physical standpoint, a RCC pavement is very similar to a conventional concrete pavement. Knowing this, a RCC pavement subgrade and base are designed and constructed to function in the same way as a normal PCC pavement would [2].

In frost susc

functions in consider

support so that the c

tamping and rollers

The Canadia

filling of the subgra

density in accordan

should be repaired

subgrade should be

of water from the F

Test Sections

For larger

for the contractor

before the constru

least one month in

the RCC. It is sug

28 days in order t

tensile strength of

construction site a

needed to make a

for the procedure

In frost susceptible areas, the base course should be designed with drainage functions in consideration. As the base is constructed, it should also provide enough support so that the over-lying RCC layer can be fully consolidated when compacted with tamping and rollers [2, 3].

The Canadian Portland Cement Association suggests that after excavation or filling of the subgrade, it should be compacted to a minimum of 95% Modified Proctor density in accordance with ASTM D1557. After this is done, the disturbed subgrade should be repaired and debris removed from the surface. Finally, the surface of the subgrade should be moistened without ponding or creating mud to minimize absorption of water from the RCC mixture [4].

Test Sections

For larger RCC pavement constructions sites, test sections can be utilized in order for the contractor to address mixing, transporting, placing, compaction, and curing issues before the construction of the actual pavement. These test sites should be constructed at least one month in advance in order to strength test samples can be taken directly from the RCC. It is suggested that both cores and beams be sawed from the existing RCC after 28 days in order to determine the correlation between the flexural strength and splitting tensile strength of that particular RCC mixture [2]. Samples from the actual construction site are often tedious to collect and do not provide the immediate feedback needed to make adjustments on-site [5]. Rolling patterns should be tested in order to test for the procedure which will result in optimum density with the least amount of passes.

After the site is

to achieve succ

The mo

cold joints shou

order to attain

[2]. From this

A recommende

Figure 1. Re

Production a

Since

twin-shaft pu

and can be vi

be utilized to

due to its lar

advantage of

After the site is assessed from these perspectives, techniques and designs can be modified to achieve successful construction.

The most critical component of a RCC pavement is the joint system. Fresh and cold joints should be constructed in both the transverse and longitudinal directions in order to attain smooth surface transition between the slabs as well as consistent densities [2]. From this test section, typical transverse cracking patterns can be observed as well. A recommended layout of a RCC test section can be viewed in Figure 1.

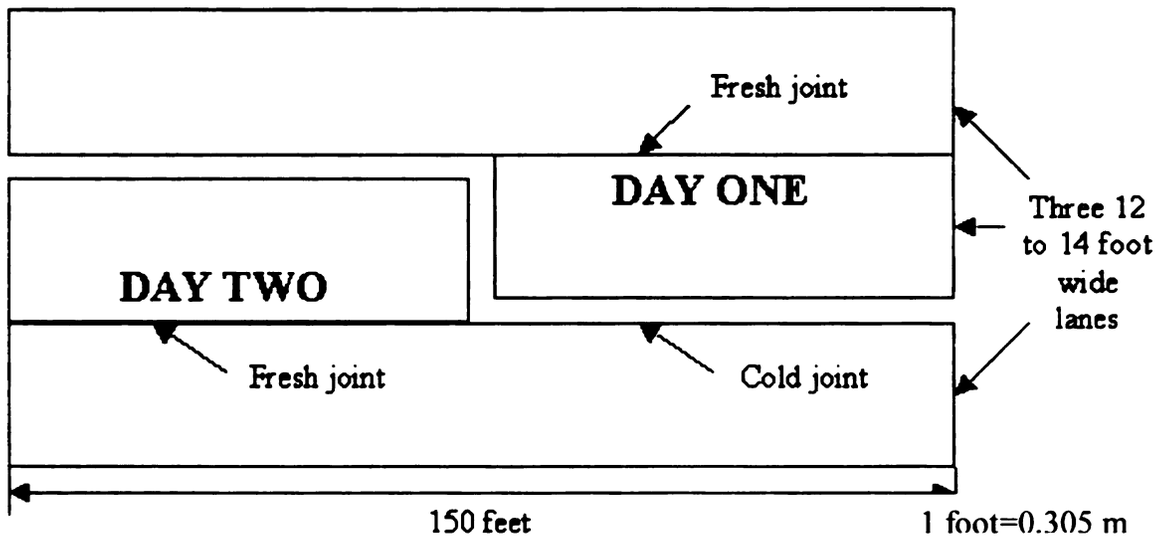

Figure 1. Recommended Test Section Setup (After Pittman [2]).

Production and Transportation

Since RCC has relatively little water in the mixture, it is typically mixed with a twin-shaft pugmill mixer. This apparatus is commonly used in asphalt concrete mixing and can be viewed in Figure 2. Both continuous mixing and weigh-batching plants can be utilized to mix RCC batches. For larger jobs, the continuous mixing plant is preferred due to its larger capacity, simpler transportation of the plant, and set-up time. The advantage of the weigh-batching plant is the superior control over the proportions of each

individual batch i

would need to de

Figure 2. Twi

The mi

minimize the ha

used to haul the

are prevalent, t

effects of precip

concrete is dur

If RCC

good condition

Using these tru

drums however

individual batch in comparison to a continuous mixing operation [2]. The contractor would need to decide which plant better suits the needs of a particular project.

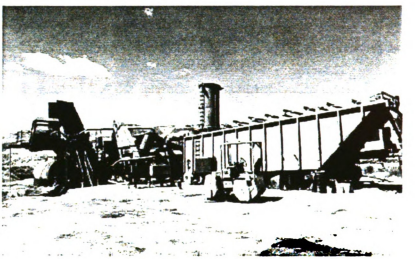

Figure 2. Twin-Shaft Pugmill Mixing Plant.

The mixing plant should be located as close to the construction site as possible to minimize the hauling time and reduce uncontrollable delays. Dump trucks are typically used to haul the RCC mix from the plant to the paving site. If environmental concerns are prevalent, the dump trucks should be equipped with protective covers to reduce effects of precipitation or extreme cold or heat. When the trucks arrive on site, the concrete is dumped directly into the paver's hopper as seen in Figure 3 [2].

If RCC material is transported using ready-mix trucks, the drum should be in good condition and as clean as possible in order to aid in the flow of the stiff mixture. Using these trucks will slow the construction process regardless of the condition of the drums however and are not recommended in most cases [6].

Figure 3. Hopper

Paving Operation

RCC pave

echnology that al

using traveling sl

pavements. Most

ber as seen in Figu

Modified Proctor

Some adju

gates between the

volume of RCC t

e front of the scr

RCC shou

form a fresh joint

Figure 3. Hopper of RCC/Asphalt Paver.

Paving Operations

RCC pavements are placed with asphalt pavers in most instances. The same technology that allows asphalt pavers to control grade and depth of asphalt pavements (using traveling skis or electronic string lines) monitors the same properties of RCC pavements. Most RCC is placed using a paver employing a vibrating screed and tamping bar as seen in Figure 4 [2]. This allows the paver to achieve compaction levels up to 90% Modified Proctor after it is initially placed and before it is rolled as tested in Figure 5.

Some adjustments are usually needed to handle RCC on asphalt pavers. Feeding gates between the hopper and screed need to be enlarged in order to accommodate the volume of RCC that is placed at a given time. Spreading screws also need to be adjusted in front of the screed to promote uniformity throughout the entire width of paving [2].

RCC should be placed as soon as possible after the initial addition of water. To form a fresh joint and assure good bond between two slabs of concrete, two adjacent

lanes need to l

together can g

Figure 4. P

Figure 5. R

lanes need to be placed within 60 minutes of each other. The use of two pavers working together can greatly minimize the chances of cold joints forming in RCC pavements [2].

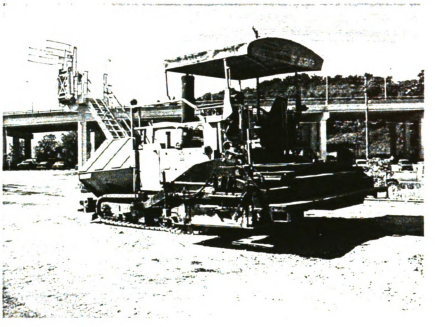

Figure 4. Paver with Double Tamping Bar Screed.

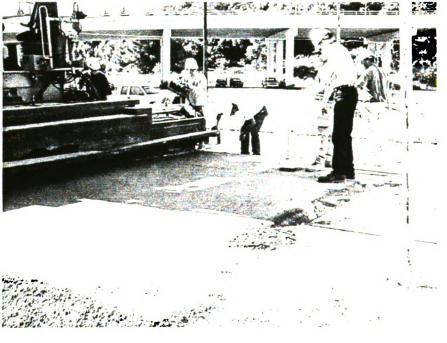

Figure 5. RCC Being Placed and Tested for Density Before Rolling.

Compaction

After pl

rollers as seen i

(89 kN) dual-d

passes of a 20-

closure of surfa

roller marks wh

plant in Spring

longitudinal co

is used, the roll

order to minimi

Figure 6. Dual

It is reco

RCC before the

Compaction

After placement using an asphalt paver, RCC pavements are compacted using rollers as seen in Figure 6. This is best achieved by making several passes of a 10-ton (89 kN) dual-drum vibratory roller in most cases. Often, this is followed by two or more passes of a 20-ton (178 kN) rubber tired roller for increased smoothness. This will aid in closure of surface voids and cracks. A dual-drum static roller can be used to remove any roller marks which may be left by the first two rollers if necessary [2]. At a Saturn auto plant in Spring Hill, Tennessee, a two roller method was implemented to minimize longitudinal cold joints between lanes with much success [7]. If a single roller technique is used, the rollers should be used in the direction parallel to the shortest dimension in order to minimize the length of possible cold joints [8].

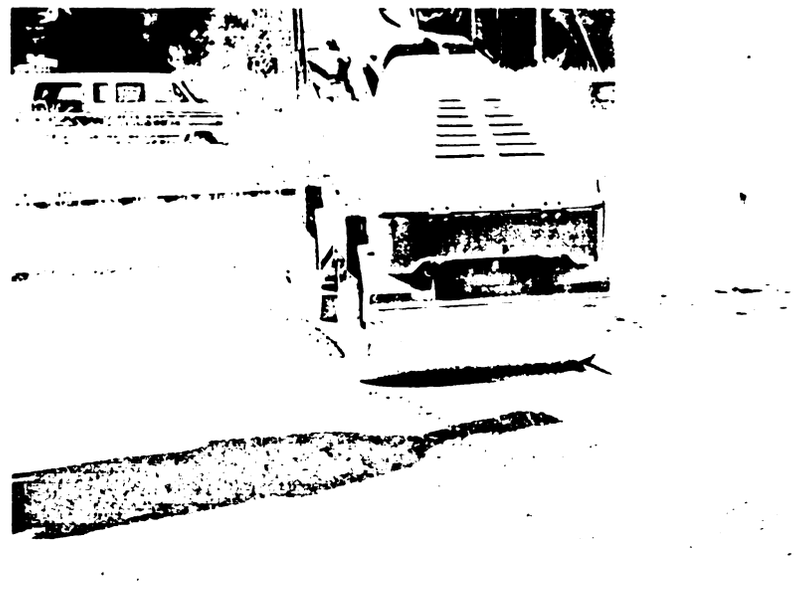

Figure 6. Dual-Drum Roller Compacting Freshly Laid RCC.

It is recommended that no more than 10 minutes elapse after the placement of the RCC before the rolling commences. The rolling should be finished within 45 minutes of

addition of v

order to atta

Curing

RCC

scaling of th

sometimes

hours using

Aft

any of the f

forming cu

must be ma

the excepti

for best re

Contracti

Si

pavements

Most proj

been note

than that

[8]. Durin

"Washington

the saw bl

addition of water at the RCC plant if possible [2]. Enough passes should be made in order to attain the necessary density required (typically 98% Modified Proctor).

Curing

RCC mixtures typically have a very low water content. To prevent drying and scaling of the freshly laid surface, a combination of moist curing and membrane curing is sometimes utilized. Freshly compacted RCC should be kept moist for a minimum of 24 hours using any of a variety of methods [2].

After the initial 24 hour curing period, RCC pavements should be covering using any of the following methods: water curing spray, wet sand, wet burlap, or a membrane-forming curing compound [2,6]. If a water spray method is employed, careful attention must be made in order to prevent the washing on fines on the surface. All traffic (with the exception of curing trucks) should be kept off the new RCC pavement until 14 days for best results [2].

Contraction Joints and Load Transfer Devices

Since RCC pavements are an economical alternative to both deep-strength asphalt pavements and conventional concrete pavements, contraction joints are often not sawed. Most projects have allowed cracks to naturally form and in many cases, no distress has been noted at these cracks. These shrinkage cracks typically form at spacings greater than that of conventional concrete pavements (between 40 to 60 feet, or 12.1 to 18.3 m) [8]. During RCC pavement construction at Fort Hood (Texas) and Fort Lewis (Washington), an attempt to saw joints in RCC pavements produced a ragged edge due to the saw blade knocking off pieces of cement paste and aggregate [2].

When cracks ar

from entering the base

However when cracks

option in many cases d

Special attention

contraction joints is atte

as high temperatures, lo

placed RCC. This sens

contraction joints [6].

In the initial co

bars or keyed joints ha

operations of RCC pa

comparison to conven

either driven into the

around with fresh RC

retrofitting is a viable

sought after threshol

RCC MATERIAL

Overview

While the cor

conventional concret

When cracks are allowed to form naturally, sealant can be used to prevent water from entering the base when freeze-thaw is a concern or when drainage is a problem [9]. However when cracks are allowed to form naturally, sealant has been discarded as an option in many cases due to aesthetic and economic reasons.

Special attention needs to be paid with respect to timing if the sawing of contraction joints is attempted. With such a low water content to start with, factors such as high temperatures, low humidity, and wind can greatly affect the hydration of freshly placed RCC. This sensitivity can seriously affect the correct timing of sawing of the contraction joints [6].

In the initial construction of RCC pavements, load transfer devices such as dowel bars or keyed joints have been very limited in use. The stiff consistency and placing operations of RCC pavements make dowel placement difficult and arduous in comparison to conventional concrete dowel placement. At this time, dowels have been either driven into the RCC pavement before final set or carefully placed and worked around with fresh RCC covering the dowels bars before rolling [2]. Dowel bar retrofitting is a viable option for placement after load transfer has diminished past a sought after threshold as is done in conventional concrete pavements.

RCC MATERIAL PROPERTIES

Overview

While the constituents of roller-compacted concrete are the same as those used in conventional concrete, the difference between the two is the proportions of these

ingredients. Norm

resembles that of

ASTM D

Cement Mixtures

Using Modified

most cases, the

However, both

between moistu

standard or mo

easily shaped by

strength while

significant amo

Figure 7. Cl

ingredients. Normal RCC is very dry and stiff mix with no slump properties. Its surface resembles that of a gray asphalt pavement as seen in Figures 7 and 8.

ASTM D558 (Standard Test Methods for Moisture-Density Relations of Soil-Cement Mixtures) and ASTM D1557 (Laboratory Compaction Characteristics of Soil Using Modified Effort) treat RCC like a soil-cement instead of conventional concrete. In most cases, the modified Proctor method is used in assessing compaction efforts on RCC. However, both of these methods treat RCC like a soil with an established relationship between moisture and density for a given compactive effort and measurable using standard or modified Proctor compaction testing [10]. When freshly mixed, RCC can be easily shaped by hand. Conventional concrete relies solely on chemical reactions to gain strength while RCC requires both from hydration as well as mechanical force to achieve a significant amount of strength.

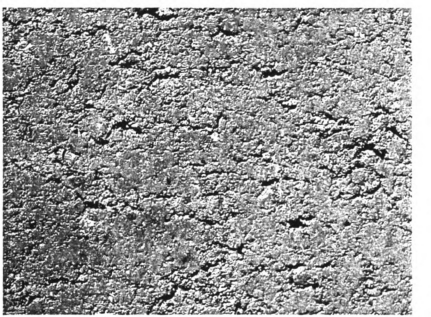

Figure 7. Close-Up View of RCC Surface (After One Day).

Figure 8. Far

RCC is

ine aggregate

9. RCC must

assure distribu

Materials

Basic

and fibers can

Aggregates

Aggre

Because of th

aggregation p

Figure 8. Far View of RCC Surface (After One Day).

RCC is generally not air-entrained, has lower water and paste contents, and higher fine aggregate volumes in comparison to conventional concretes as can be seen in Figure 9. RCC must be dry enough to hold the weight of a heavy roller, yet wet enough to assure distribution of the water available throughout the mixing and placing process [11].

Materials

Basic RCC is comprised of water, cement, and aggregates. Admixtures, fly ash, and fibers can also be found in some RCC mixes.

Aggregates

Aggregates normally comprise 75 to 85 percent of the volume of RCC mixtures. Because of this, the volume highly influences fresh RCC properties such as workability, segregation potential, and ability to consolidate properly. The volume and quality of the

aggregates have

and fatigue trend

Both fine

uncrushed grave

combination wit

seem to hold mo

flexural strength

rollers in most c

Figure 9. Clo

While g

aggregate due

recommended

aggregates have an effect on the strength, deformation characteristics, thermal properties, and fatigue trend [11].

Both fine and coarse aggregates are used in RCC mixtures. Both crushed and uncrushed gravel as well as crushed stone have been used in RCC projects in combination with both natural and manufactured sand [11]. Crushed stone and gravel seem to hold mortar better than natural aggregates in RCC and usually provides a higher flexural strength. However, crushed aggregate requires more compactive effort with rollers in most cases in comparison with natural stones [11].

Figure 9. Close-Up View of Fresh RCC.

While greater economy is usually associated with a larger nominal maximum size aggregate due to the lesser cement paste content, segregation can become a problem. It is recommended that the nominal maximum size aggregate not exceed ¾ inch (19 mm)

[11]. Since the s

larger aggregates

Fine aggr

the total aggrega

Cementitious M

Many di

These include p

as pozzolans su

Type I or II por

RCC [12]) with

volume. The fi

aggregate grad

cementitious co

[20].

As in c

the amount of

susceptible to

should be follo

Water Conten

In RC

density after c

[19] and in so

[11]. Since the surface of RCC pavement can wear down as much as ¼ inch (6 mm). larger aggregates become exposed and provide a less pleasing look aesthetically.

Fine aggregate aids in the compaction process of RCC. As much as 14 percent of the total aggregate material can pass through the #200 sieve [12].

Cementitious Materials

Many different types of cementitious materials have been used in RCC mixtures. These include portland and blended hydraulic cements, ground blast furnace slag, as well as pozzolans such as fly ash. The most typical cementitious materials used have been Type I or II portland cement (ranging from 3.5 to 6 bags/yd^3, or 4.6 to 7.8 bags/m^3, of RCC [12]) with 15 to 20 percent mixtures of Class C (binder) or F(filler) fly ash by volume. The fly ash provides additional fine material not found in many standard fine aggregate gradations to aid in compaction [11]. It is recommended that the entire cementitious content be between 12 to 14 percent of the aggregate content by weight [10].

As in conventional concrete, the design strength is the driving factor to determine the amount of cementitious materials in an RCC mixture. Since aggregates are still susceptible to chemical reactions like alkali reactivity, conventional concrete practice should be followed when setting limits on the content of cementitious materials [11].

Water Content

In RCC, the amount of water is proportioned to achieve no slump and maximum density after compaction. In most cases, the water-cement ratio is between 0.3 and 0.5 [10] and in some cases as high as 0.6 [14].

Admixtures

It is difficult t
Engineers Waterways
with air by using norm
suggested for conventi

Most RCC pav
minimized damage by
permeability of the RC
fully, it is difficult for
compactive effort als
its freeze-thaw durab

Water-reduc
only in test sections
reducing agents to l
aggregate passing t

Set retardin
for greater time for
otherwise form a c

Fibers

Research h
in RCC pavements
form at larger spac

Admixtures

It is difficult to entrain air in a RCC mixture. Research at the U.S. Army Corps of Engineers Waterways Experiment Station has showed that RCC mixes can be entrained with air by using normal air-entraining admixtures at dosages 5-10 times greater than suggested for conventional concrete [11].

Most RCC pavements that are located in freeze-thaw susceptible zones have minimized damage by using low water-cementitious ratios, thereby reducing the permeability of the RCC pavement. It has been shown that once RCC has hydrating fully, it is difficult for outside moisture to enter the RCC layer of the pavement. The compactive effort also aids in reducing the permeability of the pavement, which increases its freeze-thaw durability without air-entrainment [11].

Water-reducing admixtures have had limited use in RCC pavements and usually only in test sections and research studies. It appears that the ability for the water-reducing agents to lower water contents is dependent on the type and volume of aggregate passing the #200 sieve [11].

Set retarding admixtures have been used and are sometimes crucial in allowing for greater time for compaction as well as improving the bond between lanes that would otherwise form a cold joint [11].

Fibers

Research has been done by Nanni [13] showing the benefits of using steel fibers in RCC pavements. Most RCC pavements are allowed to crack naturally. These cracks form at larger spacings than in conventional concrete. However, the larger cracks

spacing usually

aggregate inter

can act as a "m

This increase i

increasing fati

around 25% ca

materials and l

Typically, RCC

in lifts as much

possible reduc

RCC into one

Mechanical P

Test da

similar to that

of conventiona

stress in the R

bearing layers

inches (305 to

center of the p

these areas [1

spacing usually lead to large crack openings, thereby reducing load transfer from aggregate interlock. When large diameter steel fibers are included in the RCC mix, they can act as a "micro-dowel", increasing the load transfer by keeping the cracks tighter. This increase in load transfer will benefit the RCC pavement by lowering stresses and increasing fatigue life. His research has shown that pavement thickness reductions around 25% can be utilized with proper addition of steel fibers. This will save money in materials and labor. Savings can be realized from the reduction in RCC that is produced. Typically, RCC is laid in lifts no more than 10 inches (254 mm) although it has been laid in lifts as much as 12 inches (305 mm) in some projects. Savings are made from the possible reduction in labor, which could reduce a project that once required two lifts of RCC into one lift.

Mechanical Properties

Test data from RCC pavement projects shows that the behavior of RCC is very similar to that of conventional concrete. Although its construction may differ from that of conventional concrete, it performs as a rigid plate by absorbing the vast majority of stress in the RCC layer. This allows for the subgrade and base to perform as non-load bearing layers for the most part. It is important to note that the properties within 12 to 18 inches (305 to 457 mm) of the edge of the pavements vary slightly from those near the center of the pavement as seen in Figure 10. This is due to inadequate compaction in these areas [11].

Figure 1

Compres

T

3500 psi

even wid

value is n

Flexural

T

to 4.8 M

equation

Figure 10. Edge View of RCC Pavement (After One Day).

Compressive Strength

The range of typical 28 day compressive strengths has been found to range from 3500 psi to over 5000 psi (24.1 to 34.5 MPa). Other data from cored project indicates an even wider range of compressive strengths after several years [14]. This range of tested value is not different than conventional concrete.

Flexural Strength

The range of typical flexural strengths of RCC is from 500 psi to over 700 psi (3.5 to 4.8 MPa). The Portland Cement Association recommends the following relationship in equation (1) to approximate the flexural strength of RCC:

$f_r = C (f'_c)^{1/2}$

where:

f_r
C
f'_c

Limited data has

The value of 9 w

designed using 9

flexural strength

Splitting Tensile

Tests hav

400 to over 600

tests need to be

tensile strength

specimens [11].

Modulus of Ela

Althoug

elasticity has sh

[11]. The Portl

$E = C (f'_c)^{1/2}$

$$f_r = C\,(f'_c)^{1/2} \qquad (1)$$

where:

f_r	=	flexural strength of RCC, psi.
C	=	constant (equal to 9).
f'_c	=	compressive strength at 28 days, psi.

Limited data has shown that C varied from 9.4 to 10.8 depending on the RCC mixture. The value of 9 was chosen as a conservative value. Airport pavements are typically designed using 90 day flexural strengths. This is usually about 10% greater than the flexural strength at 28 days [14].

Splitting Tensile Strength

Tests have shown that the splitting tensile strength of RCC cores has varied form 400 to over 600 psi (2.8 to over 4.1 Mpa) after 28 days of curing. The flexural strength tests need to be performed on sawed beams which can be cumbersome. The splitting tensile strength test provide more reliable results and are more easily obtained from core specimens [11].

Modulus of Elasticity

Although little data has been accumulated from RCC cores, the modulus of elasticity has shown similar to slightly higher values than those of conventional concrete [11]. The Portland Cement Association recommends the relationship in equation (2):

$$E = C\,(f'_c)^{1/2} \qquad (2)$$

where:

E
C
f_c

Limited data has s

mixture [14].

Fatigue Testing

Just like c

relationship betw

be similar based

Bond Strength

Since RC

The bond betwe

or as a partially

Bond str

strength is much

"Good"

tensile strength

constructed RC

has shown that

strength as inter

where:

E	=	elastic modulus of RCC, psi.
C	=	constant (equal to 57,000).
f'_c	=	compressive strength at 28 days, psi.

Limited data has shown that C varied from 59,000 to 67,000 depending on the RCC mixture [14].

Fatigue Testing

Just like conventional concrete, RCC is subject to fatigue behavior. The relationship between RCC fatigue and conventional concrete fatigue has been shown to be similar based on limited testing [11].

Bond Strength

Since RCC is often put down in multiple lifts, bond strength is a key property. The bond between different lifts will determine if the slab will act as one monolithic layer or as a partially bonded layer, which would signify a lower load carrying capacity [11].

Bond strength is also important for the minimization of cold joints. The bond strength is much lower for cold joints (Figure 11) than those of fresh joints.

"Good" bond strength would be regarded as at least 50 percent of the direct tensile strength of the RCC material. Based on limited data, it appears that properly constructed RCC pavements exhibit the necessary bond strength. However, some data has shown that longitudinal construction joints may not have nearly as much bond strength as interior locations exhibit [11].

Freeze-Thaw Du

Many RC
performed well.
durability using
this test for RC
the field tests th

Figure 11.

The
respect to fi
pavements i
have been u

Stu
though son

Freeze-Thaw Durability

Many RCC pavements have been built in freeze-thaw susceptible areas and have performed well. However, when RCC samples have been tested for freeze-thaw durability using ASTM C 666, the samples have performed poorly. The applicability of this test for RCC is unclear at this time. A better indication of the durability of RCC is the field tests themselves [11].

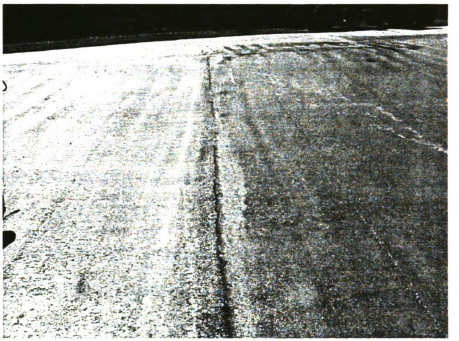

Figure 11. Longitudinal Cold Joint (After One Day).

The performance of many of the RCC pavement projects has been good with respect to freeze-that durability. Very little evidence has been found to indicate that RC pavements in cold weather regions are not durable in this aspect. Even where deicers have been used, there has been no evidence of scaling problems [15].

Studies by Ragan [16] as well as Pigeon and Malhotra [17] have shown that even though some RCC samples exhibited high bubble spacing factors that are normally

associated with

mixes contains

RCC mix whic

aggregates and

most RCC pav

Studies

thaw durability

entrained RCC

could result in

slight reductio

STRUCTUR

Overview

Since

mechanically,

limiting flexur

With this in m

depending on

create higher

discontinuities

Two p

method was d

method was d

associated with low freeze-thaw durability, the low water-cement ratios of some RCC mixes contains very little freezable water in the paste. This creates a low permeability RCC mix which is difficult to critically saturate. This along with non-frost-susceptible aggregates and proper curing conditions helps overcome the deficient air void system of most RCC pavements.

Studies by Dolen [18] have shown that air-entrained RCC samples show freeze-thaw durability factors on the order of 60 to 400 percent greater than those of non air-entrained RCC samples. These samples also showed an increase in workability which could result in a reduction in the water-cement ratio. Just as in conventional concrete, a slight reduction in compressive strength was associated with air-entraining however.

STRUCTURAL DESIGN OF RCC PAVEMENTS

Overview

Since RCC pavements respond similarly to conventional concrete pavements mechanically, the design procedures for both are alike. The procedure is based on limiting flexural stresses and the corresponding fatigue damage caused by wheel loads. With this in mind, all concrete pavements have different stress and deflection responses depending on wheel load placement. Generally, wheel loads near the edge of a pavement create higher stresses than those placed at the interior of a pavement away from discontinuities [11].

Two predominant design procedures exist for RCC pavements. One design method was developed by the Portland Cement Association (PCA) while the other method was developed by the U.S. Army Corps of Engineers (U.S. Army COE).

PCA Method

The PC

industrial RC

operations [1

the wheel loa

transfer at eit

industrial faci

the edge of t

recommends

The PCA pro

only notes th

For t

ratio. The st

strength of t

stress ratio t

equation (3)

$SR = 118.31$

or

$SR = 40$

wher

SR

NA

PCA Method

The PCA's RCC pavement design method is intended for use in the design of industrial RCC pavements [14]. However, it can also be used for similar paving operations [11]. This procedure uses the Westergaard interior stress calculation due to the wheel loads as the critical stress, thereby ignoring any variability or degree of load transfer at either natural cracks or engineered joints [1]. This assumes that wheel loads at industrial facilities do not operate like highway pavements where the wheel load is near the edge of the pavement. To account for edge loading conditions, the PCA method recommends that a 20 percent increase in the thickness of the edge be constructed [14]. The PCA procedure does not give any recommendations on contraction joint spacing, but only notes that natural cracks will form [1].

For the analysis of fatigue life, the PCA method utilizes the concept of the stress ratio. The stress ratio is defined as the stress of the design load divided by the flexural strength of the RCC used in the pavement. The PCA procedure then relates the design stress ratio to the expected load repetitions until failure of the RCC pavement using either equation (3) or (4):

$$\mathbf{SR = 118.31 - 10.73(\log_{10}(NA))} \quad \textbf{for NA} \leq \textbf{600,000 load repetitions} \quad \textbf{(3)}$$

or

$$\mathbf{SR = 40} \quad \textbf{for NA} \leq \textbf{600,000 load repetitions} \quad \textbf{(4)}$$

where:

SR = stress ratio (ratio of interior stress due to the design wheel load to the 28 day flexural strength of the RCC).

NA = number of load applications until failure.

This equation wa

samples using the

was incorporated

environmental va

U.S Army COE

The U.S.

a conservative ve

conventional cor

in a 25% maximu

transfer capabilit

are placed near c

stress equations.

30 to 60 feet (9 1

parking areas, ar

patterns [1].

In the Co

using behavioral

were simulated.

pavement tests s

This equation was derived from a series of laboratory fatigue tests on RCC beams samples using the rupture of the beams as the failure criteria. Then a conservative factor was incorporated into the equation to account for uncontrollable construction and environmental variables [2].

U.S Army COE Method

The U.S. Army Corps of Engineers method for the design of RCC pavements uses a conservative version of its conventional concrete pavement design procedure. The conventional concrete pavement design assumes load transfer at joints and cracks results in a 25% maximum bending stress reduction. The RCC design however assumes no load transfer capability and therefore, no maximum stress reduction occurs when wheel loads are placed near cracks and joints. Stresses are calculated using the Westergaard free edge stress equations. Transverse contraction joint spacings are recommended to be between 30 to 60 feet (9 to 18 m) for airfields and 50 to 75 feet (15 to 23 m) for roads, streets, parking areas, and open storage areas if utilized to control unpredictable natural crack patterns [1].

In the Corps' RCC design procedure, fatigue life of RCC pavements are modeled using behavioral data from pavement test sections on which accelerated aircraft loads were simulated. The criteria for failure was defined as one-half of the slabs in the pavement tests section exhibiting one or more structural cracks [2].

Comparison an

Both the

incorporate the

Neither of these

owner of the pa

would result in

The Co

pavement test

of conventiona

life is similar a

but uses the b

fatigue crackin

performance l

FIELD PER

In a p

pavements fr

these sites. I

than normal

asphalt pave

of new conv

more RCC p

drive.

Comparison and Contrast

Both the PCA and Corps' method for the design of RCC pavements do not incorporate the benefits of load transfer at discontinuities in the RCC pavement slab. Neither of these methods includes reasoning on transverse contraction joint spacing if the owner of the pavement would like to incorporate this feature. Both of these methods would result in thicker pavement sections than needed from a stress viewpoint [2].

The Corps of Engineers' method does incorporate physical conventional concrete pavement test section data into their fatigue performance model. Although the mechanics of conventional concrete and RCC pavements are similar, this assumes that their fatigue life is similar as well. The PCA RCC design method instead incorporates RCC test data, but uses the beam rupture point as failure. Although this model may help in predicting fatigue cracking in RCC pavements, the criteria generally does not signal the end of the performance life of a pavement.

FIELD PERFORMANCE OF RCC PAVEMENTS

In a PCA study, Piggott [15] reviewed the performance of 34 in-service RCC pavements from across North America and reported on the general condition of 18 of these sites. He found that, in general, RCC pavements tend to have a rougher surface than normal PCC or asphalt pavements. However, due to the introduction of high-density asphalt pavers, newer RCC pavements have been found to have ride qualities near those of new conventional PCC or asphalt pavements. This important quality should lead to more RCC pavements being used as roads which require a certain level of smoothness to drive.

Structur

[15] attributes th

factor which co

be that they are

military facilitie

pavements coul

RCC pa

many years of s

qualities in mar

widths which w

problem. Agai

thickness in ma

Overal

durable pavem

the same surfa

than adequate

cost alternativ

FUTURE OF

Piggot

traffic on all b

pavements bui

density asphal

Structural failures were found to be very uncommon in RCC pavements. Piggott [15] attributes this in part to the high strength that RCC achieves over time. An other factor which could have influenced the general good condition of RCC pavements could be that they are over-designed. Since most RCC pavements are currently in use in military facilities, storage areas, and intermodal terminals, the design traffic for these pavements could have been overestimated, resulting in an increased life of the pavement.

RCC pavements that have shown extensive cracking have only done so after many years of service. These cracks have not been a factor in deterring its service qualities in many cases though. Although many pavements have shown large crack widths which would lead to higher stresses, faulting does not appear to be a major problem. Again, Piggott [15] attributes this to possible over-design of the RCC pavement thickness in many cases.

Overall, Piggott notes that most of the RCC projects surveyed have provided a durable pavement to their respective users. While the RCC pavements did not provide the same surface quality of conventional PCC pavements, they were found to be more than adequate for service in low volume, high load areas and provided the users a low-cost alternative in these cases.

FUTURE OF RCC PAVEMENTS

Piggott notes in [26] that "RCC pavements can be successfully built to carry traffic on all but the highest class of multi-lane highway." Many of the newer RCC pavements built in North America have enjoyed excellent surface smoothness due to high density asphalt pavers and the quality of the rolling after the initial placement.

Studies

as a pavement s

multiple layers

with the adequa

though. RCC p

surface texture

Along

recently been

Portland, OR

residential stre

construction.

traffic that ha

pavements.

Studies in Australia [19, 20] have been developed in order to test the use of RCC as a pavement surface material for residential and high-speed arterial roads. The use of multiple layers of RCC has been found to aid in the construction of smoother pavements with the adequate roughness and skid resistance for high-speed travel. In many cases though, RCC pavements were designed to be overlaid with a small amount of asphalt for surface texture consistency.

Along with the Australian RCC pavement experiments, RCC pavements have recently been used as secondary highways (Williams Lake, BC), collector streets (Portland, OR and Edmonton, AB), internal roads and parking, (Spring Hill, TN), and residential streets (Alliance, KS and Fort St. John, BC) with great success. With quality construction, more RCC pavements will eventually be built to support larger volumes of traffic that have historically needed smooth riding asphalt and conventional concrete pavements.

DESCRIPTIO

Non-des

(FWD), heavy-w

lip vibrator (WI

North America.

Engineers Water

AB was conduct

Edmonton. The

summarize the ir

Austin, TX

The RCC

load pavements.

trailers to move

as an access roa

other nearby loca

Both the

6" (152 mm) lim

50/50 mix of Ty

surface layer wit

- CHAPTER III -

RCC Pavement Sites

DESCRIPTION OF TEST SITES

Non-destructive testing (NDT) deflection data from falling-weight deflectometer (FWD), heavy-weight deflectometer (HWD), and the Waterways Experiment Station 16-kip vibrator (WES) was utilized from six different RCC pavement sites located across North America. Testing for the first five sites was conducted by the U.S. Army Corps of Engineers Waterways Experiment Station, while the testing for the last site in Edmonton, AB was conducted by Construction Technology Laboratories, Inc. (CTL) and the City of Edmonton. The six sites are described in the following sections. Tables 1 and 2 summarize the inventory data for these sites.

Austin, TX

The RCC pavement sites in Austin, TX were generally used as low volume, high load pavements. The Central Freight site is a terminal site which was utilized by tractor trailers to move freight around the terminal. The Tuscany Way site in Austin, TX served as an access road to the trucks which serviced the Central Freight Line Terminal and other nearby locations [1].

Both the Austin, TX sites were comprised of a 7" (178 mm) RCC surface over a 6" (152 mm) lime-stabilized base and were constructed in April 1987. The RCC was a 50/50 mix of Type I Portland Cement and Class C fly ash producing a relatively weak surface layer with a flexural strength of 550 psi (3792 kPa). The test data used from both

of these sites

Tuscany Way

Table 1. RC

1 in= 25.4 mm

Location
Austin, TX
Ft. Campbell, KY
Ft. Drum, N
Ft. Hood, T
Spring Hill, TN

*WES = WE
FWD = Fal
HWD = He

of these sites was originally collected in September 1991 using a HWD device. The Tuscany Way access road was tested again in January 1992 using a HWD device [1].

Table 1. RCC Pavement Site Information (After Pittman [1]).

1 in= 25.4 mm

Location	Area	Size (sq yd)	Date Const.	Date(s) Tested	Test Device [a]	RCC Layer (in.)	Base Layer (in.)	Base Type [b]
Austin, TX	Central Freight	90,000	Apr-87	Sep-91	HWD	7	6	LSB
	Tuscany Way	14,670	Apr-87	Sep-91 Jan-92	HWD HWD	7	6	LSB
Ft. Campbell, KY	63rd Chemical Company	66,500	Jul-87	Jan-91 Aug-91	FWD HWD	7.5	4	CLS
Ft. Drum, NY	PN69A	20,200	Oct-89	Aug-91	HWD	10	10	CGB
	PN69B	23,500	Jul-89	Apr-90 Aug-91	FWD HWD	10	10	CGB
	PN187	18,000	Aug-89	Apr-90 Aug-91	FWD HWD	10	10	CGB
	PN203	3,700	Aug-89	Aug-91	HWD	10	10	CGB
Ft. Hood, TX	Bldg. 26027	20,000	Jul-84	Mar-85 Feb-90 Sep-91	WES FWD HWD	10	12	LSB
	Bldg. 38033	18,600	Aug-88	Feb-90 Sep-91	FWD HWD	9	6	LSB
	Bldg. 3850	63,900	Oct-87	Feb-90 Sep-91	FWD HWD	8.35	6	LSB
	Wash Rack	20,000	Sep-89	Feb-90 Sep-91	FWD HWD	9	6	LSB
	Tank Trail	5,200	Sep-89	Feb-90 Sep-91	FWD HWD	9	6	LSB
Spring Hill, TN	Zenith Road	13,200	Nov-88	Jan-91	HWD	6	--	CGB

[a] WES = WES 16-kip Vibrator
FWD = Falling-Weight Deflectometer
HWD = Heavy-Weight Deflectometer

[b] LSB = Lime-Stabilized Base
CLS = Crushed Limestone Base
CGB = Crushed Granular Base

Table 2. RCC Pavement Mix Proportion Information (After Pittman [1]).

1 lb/yd^3=432.5 kg/m^3 1 psi=6.89 kPa

Table 2. RCC Pavement Mix Proportion Information (After Pittman [1]).

1 in=25.4 mm 1 lb/yd^3=432.5 kg/m^3 1 psi=6.89 kPa

Location	Area	Type I Cement	Fly Ash		Water	Coarse Aggregate		Fine Aggregate	Water-Cementitous	RCC Flexural
		Weight [a]	Type	Weight [a]	Weight [a]	Max. Size	Weight [b]	Weight [b]	Ratio [c]	Strength [d]
Austin, TX	Central Freight	260	C	260	182	3/4"	1610	1610	0.35	550
	Tuscany Way	260	C	260	182	3/4"	1610	1610	0.35	550
Ft. Campbell, KY	63rd Chemical Company	400	F	211	205	3/4"	1785	1465	0.34	760
Ft. Drum, NY	PN69A	450	F	150	210	3/4"	2321	988	0.35	820
	PN69B	450	F	150	210	3/4"	2321	988	0.35	820
	PN187	450	F	150	210	3/4"	2321	988	0.35	820
	PN203	450	F	150	210	3/4"	2321	988	0.35	820
Ft. Hood, TX	Bldg. 26027 -- Mix 1	312	C	155	158	1 1/2"	2275	1372	0.34	830
	Bldg. 26027 -- Mix 2	376	C	186	130	3/4"	2165	1366	0.23	830
	Bldg. 38033	293	F	146	176	7/8"	2006	1669	0.40	800
	Bldg. 3850	293	C	118	176	3/4"	1821 to 1275	1972 to 2495	0.43	835
	Wash Rack	293	F	146	176	7/8"	2006	1669	0.40	800
	Tank Trail	293	F	146	176	7/8"	2006	1669	0.40	800
Spring Hill, TN	Zenith Road	400	F	150	192	3/4"	1890	1550	0.35	600

[a] Weight in pounds per cubic yard

[b] Weight in pounds per cubic yard in saturated surface-dry condition

[c] Water/(Cement + Fly Ash) ratio, by weight

[d] After 28 days using third-point loading (psi)

Fort Campb

The R

military vehic

maintenance

Chemical Co

This

(102 mm) cr

Type I Portl

to give an av

constructed

HWD respec

Fort Drum.

The

New York.

of this pave

sub-divided

numbers (P

All

10" (254 m

at different

The mix de

l ratio. Th

Fort Campbell, KY

The RCC pavement site at Fort Campbell, KY was used to provide access for military vehicles including tanks, trucks, and other vehicles to motor pools and maintenance shops. These pavements were located in low-speed areas of the 63rd Chemical Company military installation [1].

This cross section was comprised of a 7.5" (191 mm) RCC layer resting on a 4" (102 mm) crushed limestone base for drainage. The RCC in this pavement utilized a Type I Portland Cement along with a Class F fly ash as filler in a 1.9 to1 ratio by weight to give an average flexural strength of 760 psi (5240 kPa). This pavement was constructed in July 1987 and tested in January 1991 and August 1991 using an FWD and HWD respectively [1].

Fort Drum, NY

The third RCC pavement site considered in this study is at Fort Drum in upstate New York. As with the RCC pavement site at Fort Campbell, KY, the primary purpose of this pavement was to provide low-speed access for large military vehicles. This site is sub-divided into four sections, PN69A, PN69B, PN187, and PN203, based on project numbers (PN) denoted during construction [1].

All of the projects at Fort Drum consist of a 10" (254 mm) RCC layer resting on a 10" (254 mm) crushed granular base. Although all of the different PN's were constructed at different times during the summer of 1989, they all utilize the same RCC mix design. The mix design consists of Type I Portland Cement mixed a Class F fly ash filler in a 3 to 1 ratio. This resulted in a high average flexural strength of 820 psi (5654 kPa) for this

RCC mix. Sections

sections were then t

Fort Hood, TX

The fourth R

site is sub-divided in

38033, and Building

the Building numbe

used for washing ta

Tank Trail. Projec

RCC pavements [

The Buildi

12" (305 mm) lift

further subdivided

coarse aggregate

section with the

a Class C fly ash

normal sized co

but in greater qu

these sections a

curing. This pa

WES in March

RCC mix. Sections PN69B and PN187 were tested using an FWD in April 1990 and all sections were then tested in August 1991 using an HWD [1].

Fort Hood, TX

The fourth RCC pavement site considered in this study is at Fort Hood, TX. This site is sub-divided into five sections. The first three sections, Building 26027, Building 38033, and Building 3850, were access roads for military vehicles and were denoted by the Building number. The final two sections were located at a Wash Rack which was used for washing tanks and the access road to get to the Wash Rack which is noted as the Tank Trail. Projects at Fort Hood varied in mix design as well as thickness design of the RCC pavements [1].

The Building 26027 section consisted of a 10" (254 mm) RCC layer resting on a 12" (305 mm) lime-stabilized base and was constructed in July 1984. This section was further subdivided into two different mix designs, one used a 1.5" (38 mm) top size coarse aggregate and another used a 0.75" (19 mm) top size coarse aggregate. The section with the lager coarse aggregate used Type I Portland Cement in conjunction with a Class C fly ash in a 2 to 1 ratio by weight with a water-cementitious ratio of 0.34. The normal sized coarse aggregate section used the same constituents and ratios of binders, but in greater quantities and with a very small water-cementitious ratio of 0.23. Both of these sections attained an average flexural strength of 830 psi (5723 kPa) after 28 days of curing. This particular section was tested using all three deflection testing devices, the WES in March 1985, the FWD in February 1990, and the HWD in September 1991 [1].

The Buil

mm) lime stabili

The mix design

aggregate with

Cement with a

strength of 8(

and the HWD i

The RC

8.35" (212 mm

October 1987.

filler in a 2.5 t

This strength

0.43 for RCC.

February 199(

The ta

September 19

stabilized base

top size coars

Cement with

average flexur

tested using t

The Building 38033 section was built as a 9" (229 mm) RCC layer over a 6" (152 mm) lime stabilized base. This particular section was constructed in August of 1988. The mix design for this RCC pavement consisted of a 0.875" (22 mm) top size coarse aggregate with a 0.40 water-cementitious ratio. The binder consisted of a Type I Portland Cement with a Type F fly ash filler in a 2 to 1 ratio resulting in an average flexural strength of 800 psi (5516 kPa). This section was tested using the FWD in February 1990 and the HWD in September 1991 [1].

The RCC pavement section located near Building 3850 was specified to be a 8.35" (212 mm) RCC layer on a 6" (152 mm) lime stabilized base when constructed in October 1987. The binder consisted of a Type I Portland Cement with a Type C fly ash filler in a 2.5 to 1 ratio resulting in an average flexural strength of 835 psi (5757 kPa). This strength was high when compared to the relatively high water-cementitious ratio of 0.43 for RCC. As with Building 38033, this section was also tested using the FWD in February 1990 and the HWD in September 1991 [1].

The tank washing area and access road to the wash rack were both constructed in September 1989 and are comprised of a 9" (229 mm) RCC layer over a 6" (152 mm) lime stabilized base. The mix design for this RCC pavement consisted of a 0.875" (22 mm) top size coarse aggregate with a 0.40 water-cementitious ratio. A Type I Portland Cement with a Type F fly ash filler in a 2 to 1 ratio was used for both sections. The average flexural strength for these sections was 800 psi (5516 kPa). This section was tested using the FWD in February 1990 and the HWD in September 1991 [1].

Spring Hill.

The S

Road. This r

main assembl

The S

pavement lay

mix design fo

Type I Portla

resulting aver

site was teste

Edmonton.

The E

171th Avenu

originally de

years) and ev

[21].

This

cement stabi

consisted of

strength of t

to test the ef

September

Spring Hill, TN

The Spring Hill, TN RCC pavement site is part of the Saturn Plant on Zenith Road. This road provides access to tractor-trailers as well as normal sized vehicles to the main assembly building [1].

The Spring Hill, TN RCC pavement site consists solely of a 6" (152 mm) RCC pavement layer on a stiff roadbed soil. This site was constructed in November 1988. The mix design for this site used a 0.35 water-cementitious ratio with a binder combination of Type I Portland Cement and a Class F fly ash as filler material in a 2.67 to 1 ratio. The resulting average flexural strength of this mix was 600 psi (4137 kPa) after 28 days. This site was tested only once with an HWD in January 1991 [1].

Edmonton, AB, Canada

The Edmonton, AB RCC pavement site is part of 112th Street between 167th and 171th Avenues in Edmonton, AB. This road is a two-lane city arterial road and was originally designed to be an RCC surface road for a short evaluation period (up to 5 years) and eventually was converted to an RCC base for an asphalt-surfaced pavement [21].

This site consists of a 8" (203 mm) RCC pavement layer resting on a 6" (152 mm) cement stabilized subgrade constructed in August 1992. The binder for this project consisted of Canadian Type 10 Portland Cement only. The resulting average flexural strength of this mix was 404 psi (2782 kPa). This site had joints cut at different intervals to test the effect on load transfer efficiency. This site was tested twice with an FWD in September 1992 and September 1993 [22]. Since this site was set up with cut joints and

did not in

Waterway

DATA C

D

Waterway

the follow

1.
2.
3.
4
5.
6.
7.

This stud

Corps of

and joint

D

allows fo

accuracy

were mea

no spallin

sealant o

[1].

T

Experime

did not include the same information which the U.S. Army Corps of Engineers Waterways Experiment Station studies did, it was analyzed separately.

DATA COLLECTION

Data collected for every crack or joint during the U.S. Army Corps of Engineers Waterways Experiment Station study [1] and subsequently utilized in this study includes the following:

1. Project location
2. Date of tests
3. Pavement surface temperature
4. Crack or joint width
5. Crack or joint spacing
6. Deflections from FWD/HWD testing at cracks/joints
7. Midslab deflections from FWD/HWD testing

This study focused only on data from transverse cracks and joints while the U.S. Army Corps of Engineers Waterways Experiment Station study included many types of cracks and joints including both fresh and cold joints, longitudinal cracks, and others.

Data for crack widths was determined using an optical scale lupe. This apparatus allows for magnification of the crack up to 7 times the normal size resulting in an accuracy of the crack width to the nearest 0.001 inches (0.0254 mm). The crack widths were measured at locations closest to the LTE testing location for the FWD/HWD where no spalling, wearing, or excessive damage was done to the crack. In cases where joint sealant or excessive fines closed the surface of the crack, no measurements were taken [1].

To measure crack spacings during the U.S. Army Corps of Engineers Waterways Experiment Station study, a rolling measuring wheel was used resulting in an accuracy of

0.1 feet (30.5 mm)

distances to the ne

Data from

1. Da
2. Joi
3. De
4. M

The Edmonton. A

sections which w

provided.

In additi

material propert

DATA ANAL

Two di

consistency of

deflections we

represent a va

the different b

concrete. radi

applied to the

Table 3.

0.1 feet (30.5 mm). The resulting crack spacing was found by averaging the two distances to the nearest cracks for every crack tested using the FWD/HWD.

Data from each joint in the Edmonton, AB [22] study included the following:

1. Date of test
2. Joint spacing
3. Deflections from FWD/HWD testing at joints/cracks
4. Midslab deflections from FWD testing

The Edmonton, AB study focused on engineered joints at various spacings. With the few sections which were allowed to naturally crack in this study, crack spacings were not provided.

In addition to the data on each joint or crack from both studies, cross-section and material properties were also found as provided earlier in this chapter.

DATA ANALYSIS

Two different backcalculation methods were analyzed in order to verify the consistency of these individual procedures. Thicknesses, loads, and the corresponding deflections were randomly selected for 10 different RCC pavement sites. These sites represent a variety of soil support conditions, mix designs, and locations. After analyzing the different backcalculation procedures, a typical range of elastic modulus of the concrete, radius of relative stiffness, modulus of subgrade reaction can be determined and applied to the RCC pavement site analyses. The deflection information is summarized in Table 3.

Table 3. De

1 in=25.4 mm

Case No.	Loc
1	Carr K
2	Ft. I T
3	Sp Hil
4	Ft. I N
5	Ft. I N
6	Ft. I N
7	Ft. I N
8	Edm A
9	Edm A
10	Edm A

ERES Meth

In the

basin area (A

deflection bas

deflection sen

the sensor dir

Table 3. Deflection Data from Different RCC Test Sites.

1 in=25.4 mm 1 lb = 4.45 N

Case No.	Location	RCC Thickness (in.)	Load (lb)	Deflections (mils)						
				Distance from Load (in.)						
				0	12	24	36	48	60	72
1	Ft. Campbell, KY	7.5	26648	14.3	13.1	10.4	7.8	5.9	4.2	3.2
2	Ft. Hood, TX	10	25908	11.4	10.1	8.9	7.6	6.3	5.3	4.2
3	Spring Hill, TN	6	26224	7.9	5.9	3.7	2.2	1.2	0.6	0.4
4	Ft. Drum, NY	10	9546	2.34	2.00	1.61	1.23	0.88	0.67	0.53
5	Ft. Drum, NY	10	13992	3.48	3.03	2.34	1.75	1.30	1.00	0.73
6	Ft. Drum, NY	10	19284	4.67	3.95	3.22	2.45	1.83	1.29	0.89
7	Ft. Drum, NY	10	23844	6.59	5.62	4.45	3.34	2.38	1.65	1.15
8	Edmonton, AB	8	6439	4.67	3.76	2.85	2.19	1.75	1.46	1.12
9	Edmonton, AB	8	9374	7.03	5.73	4.35	3.35	2.68	2.17	1.73
10	Edmonton, AB	8	12316	9.47	7.72	5.89	4.51	3.58	2.87	2.30

ERES Method

In the ERES method of backcalculation, the first parameter to be calculated is the basin area (AREA). This parameter can be defined as the cross-sectional area of the deflection basin between the center of the FWD or HWD load plate and the outermost deflection sensor, normalized with respect to the maximum deflection (i.e., deflection at the sensor directly below the center of the load plate, δ_0) [23]. Due to this normalization

to the max

computed

Υ (0. 8.

center of t

deflection

$ARE.1 =$

w

Al
$\hat{\alpha}$

Tl

parameter

with ARE

found in

mm):

$t = \left[\ln\right.$

w

A

to the maximum deflection, AREA has units of length rather than area. It can be computed by using deflection data measured at sensors located at various radial distances "r" (0, 8, 12, 18, 24, 36, and 60 in, or 0, 203, 305, 457, 610, 914, 1524 mm) from the center of the FWD or HWD load plate. This should be done once for each set of deflection data. Equation (5), from [23], can be used to calculate this parameter:

$$AREA = \left[\begin{array}{l} 4 + 6\left(\frac{\delta_8}{\delta_0}\right) + 5\left(\frac{\delta_{12}}{\delta_0}\right) + 6\left(\frac{\delta_{18}}{\delta_0}\right) + \\ 9\left(\frac{\delta_{24}}{\delta_0}\right) + 18\left(\frac{\delta_{36}}{\delta_0}\right) + 12\left(\frac{\delta_{60}}{\delta_0}\right) \end{array} \right] \quad (5)$$

where:

AREA = deflection basin area, in.
δ_r = deflection of the r^{th} sensor, mils.

The next parameter that is calculated is the radius of relative stiffness. This parameter characterizes the combined stiffness of the slab-foundation system [23]. As with AREA, this should be calculated once for every set of deflection data. Equation (6), found in [24], is used to compute ℓ and is only valid for a load plate radius of 6 in (150 mm):

$$\ell = \left[\ln\left\{\frac{(60 - AREA)}{289.708}\right\} / (-0.698) \right]^{2.566} \quad (6)$$

where:

ℓ = radius of relative stiffness, in.
AREA = deflection basin area, in.

A

dimension

regression

sensor loc

deflection

$\delta_r^* =$

w

a

Table 4.

Radia Distance (in)
0
8
12
18
24
36
60

A

modulus c

each senso

thesis are

After computing the radius of relative stiffness for a given set of deflections, a non-dimensional regression coefficient must be calculated for each sensor. Equation (7) is a regression equation for which the regression coefficients (a, b, and c) differ for each of the sensor location, as seen in Table 4. δ_r^* takes into account the decreasing pavement deflections as a function of distance from the load plate.

$$\delta_r^* = ae^{[-be^{(-cl)}]} \tag{7}$$

where:

a,b,c = regression coefficients from [23] (see Table 4)
ℓ = radius of relative stiffness, mm.

Table 4. Regression Coefficients for δ_r^* (After [23]).

Radial Distance, r (in)	a	b	c
0	0.12450	0.14707	0.07565
8	0.12323	0.46911	0.07209
12	0.12188	0.79432	0.07074
18	0.11933	1.38363	0.06909
24	0.11634	2.06115	0.06775
36	0.10960	3.62187	0.06568
60	0.09521	7.41241	0.06255

After computing δ_r^*, the next step in the ERES method is to calculate the elastic modulus of the concrete (E). A value for the elastic modulus of concrete is computed for each sensor's deflection, noted here as E_r. The reported elastic modulus values in this thesis are the average elastic modulus values calculated from each sensor for a given set

of deflect

from [23]

$$E_r = \frac{12(}{}$$

w

E

v

P

ô

h

ô

T

subgrade

foundatio

$$k = \frac{}{12(1}$$

w

k

E

h

v

of deflections. The elastic modulus for each sensor can be computed using equation (8) from [23]:

$$E_r = \frac{12(1-\nu^2)P\ell^2\delta_r^*}{\delta_r h^3} \quad \textbf{(8)}$$

where:

E_c	=	concrete modulus of elasticity based on δ_r, psi
ν	=	Poisson's ratio for concrete (assumed to be 0.15)
P	=	applied load, lb
ℓ	=	radius of relative stiffness, in
δ_r	=	deflection of the r^{th} sensor, mils
h	=	concrete slab thickness, in
δ_r^*	=	nondimensional deflection coefficient at radial distance "r"

The final step in the ERES backcalculation procedure is to compute the modulus of subgrade reaction (k). The modulus of subgrade reaction estimates the stiffness of the foundation under the RCC layer. It can be calculated using equation (9) from [25]:

$$k = \frac{Eh^3}{12(1-\nu^2)\ell^4} \quad \textbf{(9)}$$

where:

k	=	modulus of subgrade reaction, psi/in
E	=	concrete modulus of elasticity, psi
h	=	concrete slab thickness, in
ν	=	Poisson's ratio for concrete (assumed to be 0.15)
ℓ	=	radius of relative stiffness, in

ECOPP

T

Pavemer

theoretic

range of

T

using eq

$SF = \frac{(a$

ECOPP

[26]:

$t = \frac{}{[0.0}$

ECOPP Method

The second method for backcalculation is the ECOPP (Estimation of Concrete Pavement Parameters). This method was developed through regression analysis on theoretical, load-induced deflections of 288 pavement sections which represented a large range of dimensions and material properties.

The first step in this analysis is to calculate the deflection basin slope factor (SF) using equation (10) from [26]:

$$SF = \frac{(\delta_0 - \delta_{24})}{\delta_0} \qquad \textbf{(10)}$$

where:

SF	=	deflection basin slope factor
δ_0	=	deflection of sensor at load plate, mils
δ_{24}	=	deflection of sensor located 24 inches (610 mm) from load plate, mils.

After the deflection basin slope factor has been calculated, the next step in the ECOPP process is to calculate the radius of relative stiffness (ℓ) using equation (11) from [26]:

$$\ell = \frac{1}{[0.00401148 + 0.102021(SF) - 0.00443311 * \log(SF)]} \qquad \textbf{(11)}$$

where:

ℓ	=	radius of relative stiffness, in
SF	=	deflection basin slope factor.

A

calculate

backcalcu

equation

$ND_* = ($

v

N
d
F

U

compute

for slabs

(13) and

$\log(k) =$

$\log(k) =$

v

k
N
(
r
L
a

After the radius of relative stiffness has been computed, the next step is to calculate the modulus of subgrade reaction (k) of the foundation layers. For this backcalculation procedure, the normalized δ_{36} deflection must be calculated first using equation (12) from [26]:

$$ND_{36} = \delta_{36} * \left(\frac{9000}{P}\right) * 1000 \qquad \textbf{(12)}$$

where:

ND_{36}	=	normalized δ_{36} deflection, in
δ_{36}	=	sensor deflection located 36 inches from the load plate, mils
P	=	applied FWD or HWD load from load plate, lb.

Using this normalized deflection, the modulus of subgrade reaction can then be computed using equation (13) for slabs thicker than 6 inches (152 mm) or equation (14) for slabs thicker than 8 (203 mm) inches from [26]. Regression coefficients for equations (13) and (14) are listed in Table 5.

$$\log(k) = a_0 + a_1 * [\log(ND_{36})] + a_2 * (\ell) + a_3 * \left(\frac{r}{\ell}\right) \qquad \textbf{(13)}$$

$$\log(k) = a_0 + a_1 * [\log(ND_{36})] + a_2 * (\ell) + a_3 * \left(\frac{\ell}{L}\right) \qquad \textbf{(14)}$$

where:

k	=	modulus of subgrade reaction, psi/in
ND_{36}	=	normalized δ_{36} deflection, in
ℓ	=	radius of relative stiffness, in
r	=	radius of load plate, in
L	=	RCC slab length, in
a_0, a_1, a_2, a_3	=	regression coefficients from [26] (See Table 5).

Table 5.

RCC
Thickn

modulu

only or

$E = \frac{12}{}$

Table 5. Regression Coefficients for a_1, a_2, a_3, and a_4 (After [26]).

RCC Slab Thickness (in)	a_1	a_2	a_3	a_4
5	4.67014	-1.00366	-0.04159	-2.93908
6	4.08076	-0.99399	-0.02821	-1.88585
8	3.19287	-0.99076	-0.01298	0.40057
10	3.21337	-1.00799	-0.01342	0.42543
12	3.20290	-0.99595	-0.01353	0.48629
15	3.14526	-0.98294	-0.01243	0.56773
18	3.07694	-0.97320	-0.01160	0.65605
20	3.03577	-0.96488	-0.01079	0.71466

The final step in the ECOPP backcalculation procedure is to compute the elastic modulus of the concrete (E). Unlike the ERES procedure, the elastic modulus is calculated only once using equation (15) from [26]:

$$E = \frac{12(1-\nu^2)k\ell^4}{h^3} \qquad \textbf{(15)}$$

where:

E	=	concrete modulus of elasticity, psi
ν	=	Poisson's ratio for concrete (assumed to be 0.15)
k	=	modulus of subgrade reaction, psi/in
ℓ	=	radius of relative stiffness, in
h	=	concrete slab thickness, in

Backc

ECOF

analy

Tabl

Cas
No.

1

2

3

4

5

6

Backcalculation Procedure Comparison

A backcalculation analysis was done using both the ERES method and the ECOPP method for the 10 deflection cases found in Table 3. The results from this analysis are listed in Table 6.

Table 6. Comparison of Backcalculated Parameters from Different RCC Test Sites.

1 in=25.4 mm 1 psi/in=.271 kPa/mm 1 psi=6.89 kPa

Case No.	Location	Radius of Relative Stiffness (in.)			Modulus of Subgrade Reaction (psi/in.)			RCC Elastic Modulus (10^6 psi)		
		ECOPP	ERES	% Diff.	ECOPP	ERES	% Diff.	ECOPP	ERES	% Diff.
1	Ft. Campbell, KY	29.12	30.00	2.93	258	248	-4.32	5.16	5.58	7.38
2	Ft. Hood, TX	34.12	37.65	9.36	223	197	-12.85	3.54	4.65	23.82
3	Spring Hill, TN	16.82	18.10	7.08	1,163	1,295	10.25	5.05	7.54	33.08
4	Ft. Drum, NY	26.26	27.83	5.63	672	629	-6.91	3.75	4.42	15.25
5	Ft. Drum, NY	25.26	27.35	7.61	712	638	-11.64	3.40	4.18	18.68
6	Ft. Drum, NY	26.36	27.55	4.31	679	650	-4.46	3.85	4.39	12.38
7	Ft. Drum, NY	25.44	26.69	4.69	632	605	-4.40	3.10	3.60	13.87
8	Edmonton, AB	21.94	25.26	13.17	276	257	-7.55	1.47	2.40	38.87
9	Edmonton, AB	22.34	25.60	12.72	260	242	-7.56	1.49	2.38	37.59
10	Edmonton, AB	22.50	25.56	11.99	253	237	-6.92	1.48	2.31	35.86

Elastic Mod

The

backcalcula

all cases, th

as seen in F

In (

than those

over predic

elastic mod

10,000 and

not have b

Figure 12.

Elastic Modulus of Concrete Comparison

The elastic modulus of the concrete differed greatly depending on the backcalculation procedure and in some cases resulted in a discrepancy of up to 40%. In all cases, the ERES method estimated a greater elastic modulus than the ECOPP method as seen in Figure 12.

In Cases 8-10 in Edmonton, AB, deflections at the outmost sensors were greater than those of other RCC pavement sections and may have caused the ERES model to over predict the elastic modulus of the concrete. These sections also had a very low elastic modulus predicted from both methods (about $1.5*10^6$ psi and $2.4*10^6$ psi, or 10,000 and 16,500 MPa) for the ECOPP and ERES methods, respectively) which may not have been addressed when the regression models for backcalculation were developed.

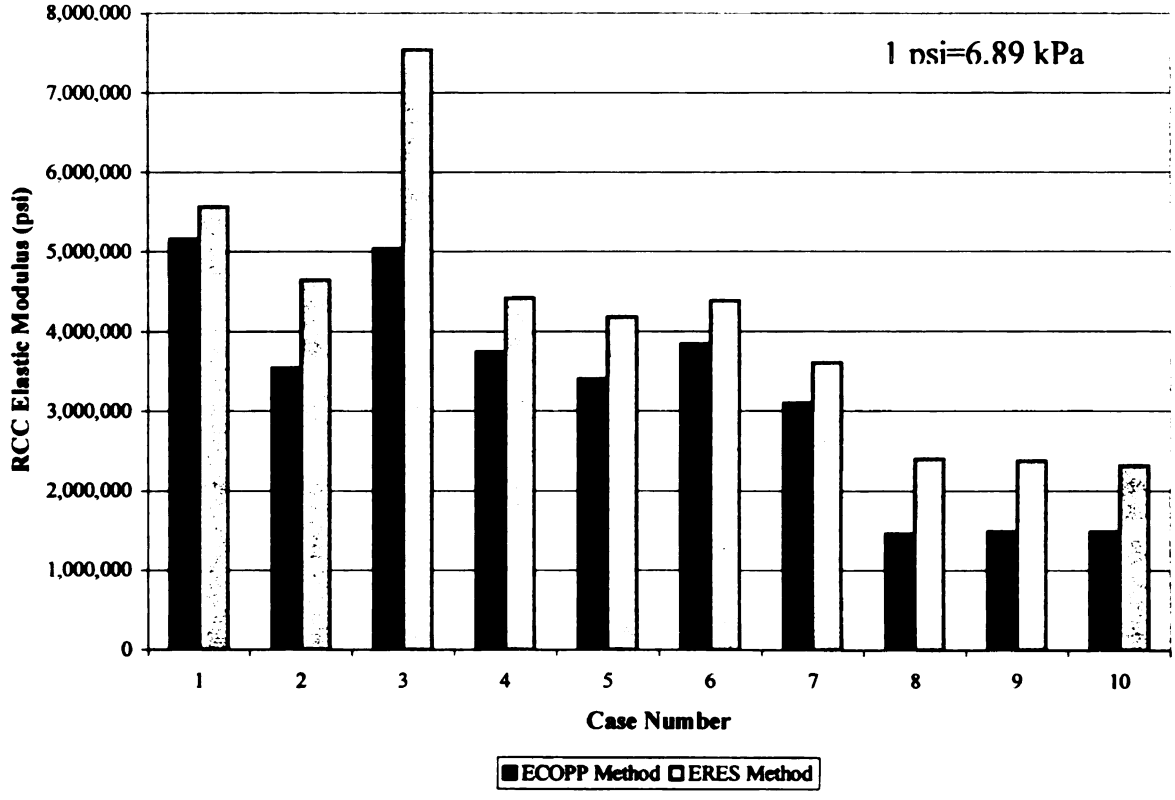

Figure 12. Results of Backcalculated Elastic Modulus of the Concrete Comparison.

In Case 3 in Spring Hill, TN, the deflection for all sensors were extremely low in comparison to other RCC pavement sites. This pavement was also the thinnest slab tested at 6 inches (152 mm). Since the ERES method predicts an elastic modulus of the concrete for every sensor and the average is reported, an abnormal deflection could influence the results slightly. However, every sensor deflection in this case predicted a reasonably consistent, yet high, elastic modulus value.

Although the results from this portion of the backcalculation analysis vary greatly, it is safe to suggest that the elastic modulus of the concrete for RCC pavement sections is similar to PCC pavement sections with an average elastic modulus of the concrete value of approximately 4,000,000 psi (27,500 MPa).

Modulus of Subgrade Reaction Comparison

The modulus of subgrade reaction results were in better agreement (Figure 13). In every case but one (Case 3-Spring Hill, TN), the ECOPP method predicted higher levels of foundation support than the ERES method.

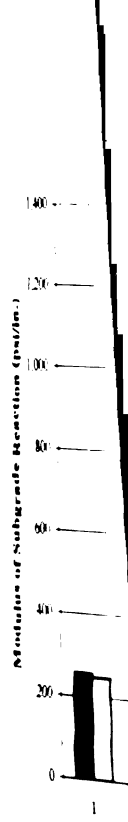

Figure 13. Resu

Since Cas

from three differ

limestone, lime-s

expected to diffe

produced an exc

1295 psi in. or 3

due to the low d

have been out o

of subgrade reac

preceding sectio

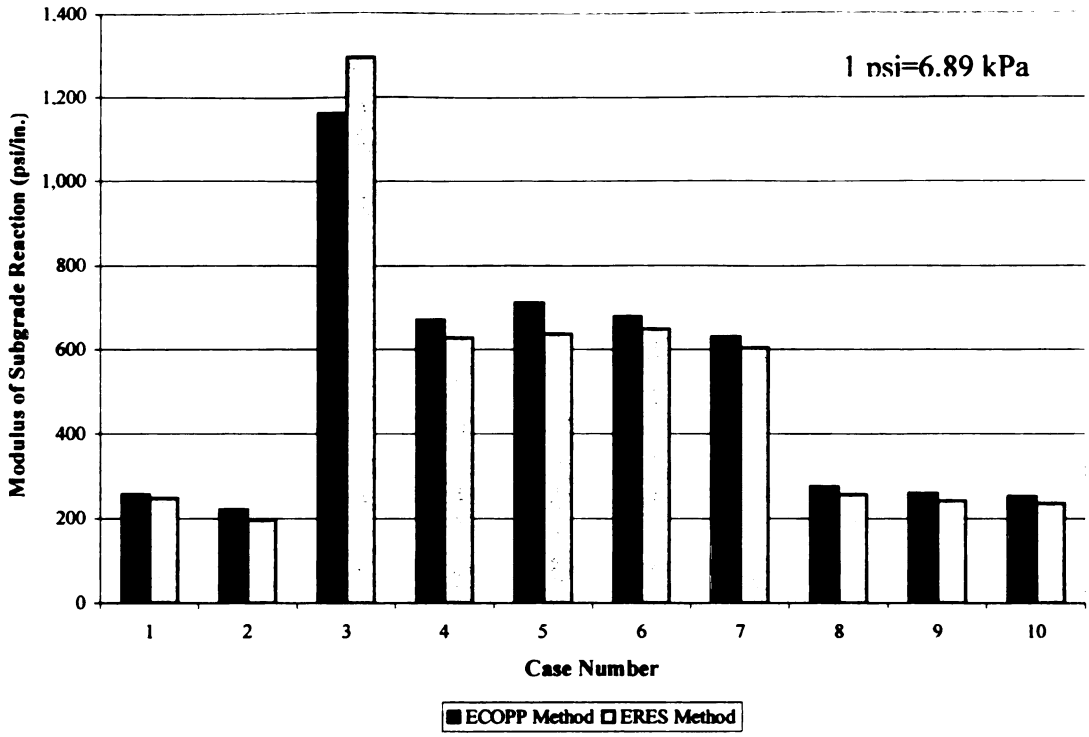

Figure 13. Results of Backcalculated Modulus of Subgrade Reaction Comparison.

Since Cases 1-3, from Ft. Campbell, KY, Ft. Hood, TX, and Spring Hill, TN, are from three different locations and represent three separate base conditions (crushed limestone, lime-stabilized, and crushed granular base, respectively), the results should be expected to differ in comparison to each other. However, Case 3 in Spring Hill, TN produced an exceptionally high modulus of subgrade reaction values (1163 psi/in and 1295 psi/in, or 316 and 352 kPa/mm) for the ECOPP and ERES methods, respectively) due to the low deflections and thin slab (6 inches, 152 mm) at this site. These values may have been out of the intended range for both methods which over estimated the modulus of subgrade reaction (in addition to the elastic modulus of the concrete from the preceding section).

C

AB (cem

different

the modu

methods

differenc

U

subgrade

Values o

backcalc

reaction.

Radius o

A

found to

in Figure

values (k

incorrect

Cases 4-7 at Ft. Drum, NY (crushed granular base) and Cases 8-10 in Edmonton, AB (cement-stabilized subgrade) showed consistency within the methods with respect to different loads. In all of these cases however, the ECOPP method slightly over predicted the modulus of subgrade reaction in comparison to the ERES method. The results of both methods in these cases are relatively equal with almost every result within a 10% difference between the two methods.

Using these two backcalculation analyses, it is suggested that most modulus of subgrade reaction values would range from 150 to 450 psi/in (40.7 to 108.6 kPa/mm). Values over 450 psi/in (108.6 kPa/mm) could have been over estimated by the backcalculation procedures and can be modeled using a lower modulus of subgrade reaction.

Radius of Relative Stiffness Comparison

Although similar in magnitude, the backcalculated radius of relative stiffness was found to be greater in every case using the ERES method for the set of deflections as seen in Figure 14. Since the radius of relative stiffness is a calculated value, it relies on other values (k, E, h, and ν) to be determined. If any of these other values were estimated incorrectly, it could affect the calculation of the radius of relative stiffness adversely.

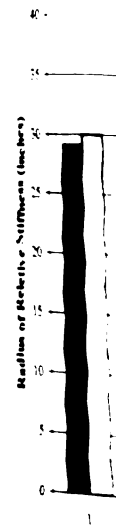

Figure 14. F

In all

RCC paveme

mm) in comp

deflections a

concrete. H

only a 7% di

LOAD TR

Loa

by a term ca

indication o

transfer effi

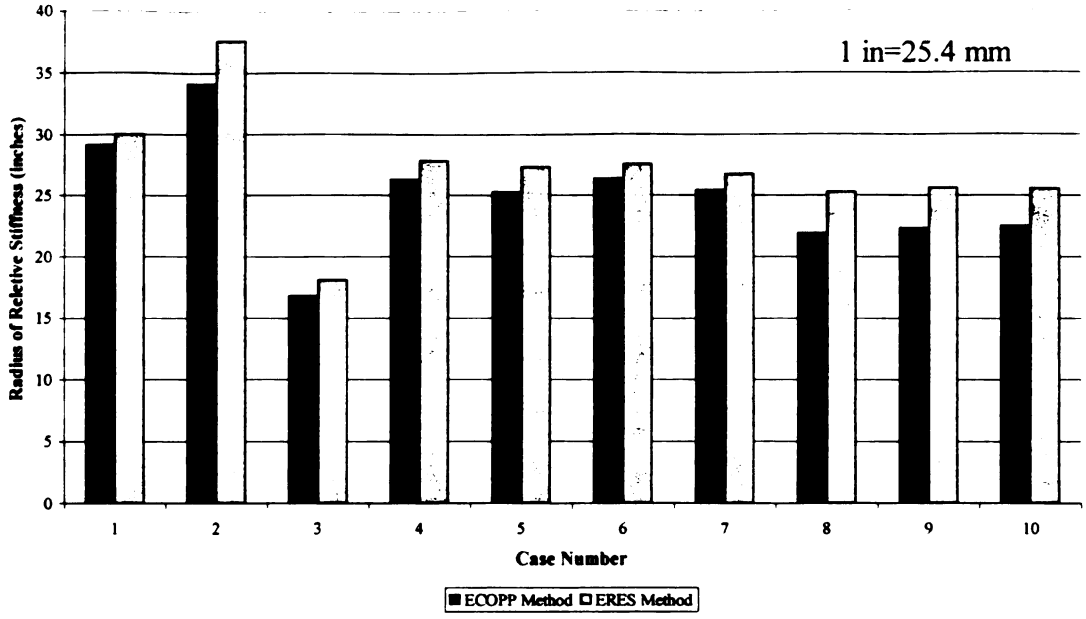

Figure 14. Results of Backcalculated Radius of Relative Stiffness Comparison.

In all cases except Case 3 in Spring Hill, TN, the radius of relative stiffness for these RCC pavement sites was found to be within a reasonable range (22-35 inches, or 559-889 mm) in comparison to PCC pavement sites. Case 3 was affected by the extremely low deflections and resulting high modulus of subgrade reaction and elastic modulus of the concrete. However, both methods predicted a similar radius of relative stiffness resulting in only a 7% difference, which may add to validity of the results found in this case.

LOAD TRANSFER EFFICIENCY BACKGROUND

Load transfer across cracks or joints in RCC pavements is commonly quantified by a term called load transfer efficiency (LTE). Expressed as a percentage, LTE gives an indication of the effectiveness of a crack in transferring load. Computation of load transfer efficiency based on deflections near a crack under an applied load is a very

useful metho

approach is t

Use

proportiona

LTE_δ was us

load. Detle

(16) from [

$$LTE_\delta = \frac{\delta}{\delta}$$

wh

LT

δ_t

δ_t

LTE_δ can

or heavy-v

load, using

the resulti

computing

HWD test

higher imp

Fi

cases - (p

load P is

useful method of determining the LTE. The load transfer efficiency computed using this approach is termed as the deflection load transfer efficiency (LTE_δ) [26].

Use of LTE_δ assumes that the amount of load transfer across a crack is directly proportional to the relative deflections of the unloaded to loaded sides of the crack [28]. LTE_δ was used in this study to characterize the ability of cracks and joints to transfer load. Deflection load transfer efficiency was computed in this study by using equation (16) from [27]:

$$\mathbf{LTE_\delta = \frac{\delta_U}{\delta_L} \times 100\%} \qquad \mathbf{(16)}$$

where:

LTE_δ	=	deflection load transfer efficiency, %
δ_U	=	deflection on the unloaded side of a crack or joint, mils
δ_L	=	deflection on the loaded side of a crack or joint, mils.

LTE_δ can be easily computed using field data from a falling weight deflectometer (FWD) or heavy-weight deflectometer (HWD). An FWD is a device that applies an impulse load, using a 12 inch (300 mm) diameter circular load plate, to a pavement and measures the resulting pavement deflections through a series of sensors. Deflection data for computing LTE_δ is thus readily available when this device is used. The principal behind HWD testing is identical to that of FWD testing except that an HWD is best suited for higher impulse loads and thicker pavements.

Figures 15 and 16 illustrate the meaning of LTE_δ by considering the two extreme cases - 0% and 100% deflection load transfer efficiency, respectively. In these figures, a load P is shown to be applied to one side of a crack or joint. In the case of field testing,

this load P wou

resulting deflect

Figure 15 that w

has no deflection

case scenario, as

This can eventua

RCC pavement ir

Figure 16, where

of the crack or jo

shared by both s

on the pavement

of the discontinu

undergo.

this load P would be provided by an impulse by means of the FWD or HWD. The resulting deflections from this load P are depicted in the figures as well. It is seen in Figure 15 that when there is no load transferred (0% LTE_{δ}), the unloaded side of the slab has no deflection and thus does not share in the carrying of the load. This is the worst-case scenario, as all the load must be carried by one side and increased deflections result. This can eventually lead to other distresses as well as increase fatigue damage of the RCC pavement in the vicinity of the crack or joint. The best-case scenario is depicted in Figure 16, where the LTE_{δ} is 100%. Here, it can be seen that the deflections on each side of the crack or joint due to the applied load P are equal. Thus, the load is being equally shared by both sides of the discontinuity, and the minimum amount of damage is inflicted on the pavement. In this case, the stress caused by this load is also shared by both sides of the discontinuity, thereby reducing the maximum stress a pavement system would undergo.

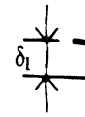

Figure 15

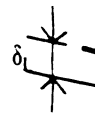

Figure 16

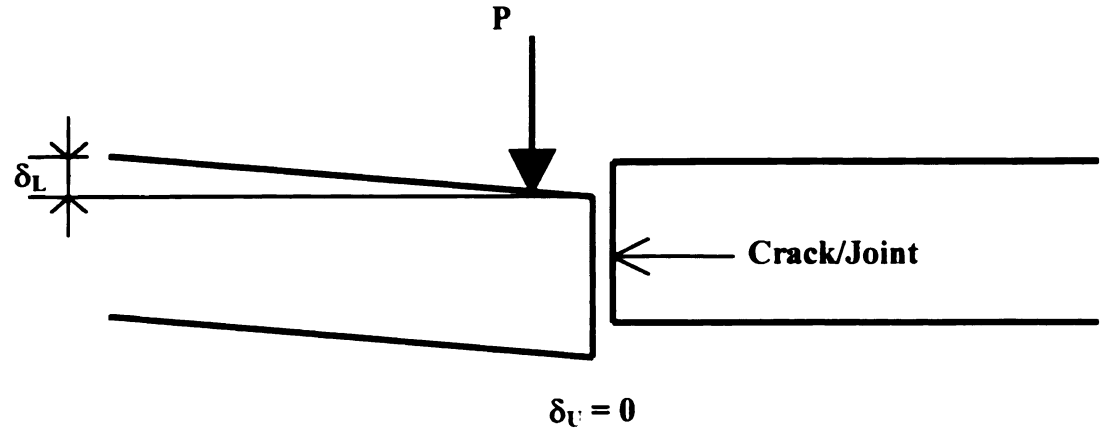

Figure 15. Depiction of 0% Deflection Load Transfer Efficiency (After Buch [29]).

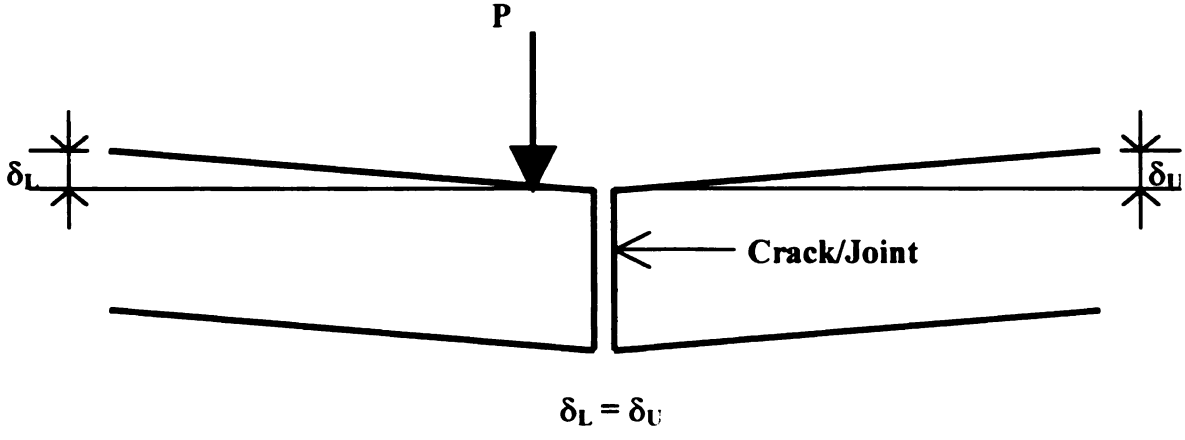

Figure 16. Depiction of 100% Deflection Load Transfer Efficiency (After Buch[29]).

LOAD TRAN

Load tr

Experiment Sta

the effects of pa

reaction, radius

relationships bet

This section has

Waterways Expe

Waterways Exp

Data fro

Experiment Stat

different paveme

reaction, and rad

Most of the pave

to save on costs

transverse cracki

pavements from

thickness, age, a

Transverse Crac

With RC

between these cr

LOAD TRANSFER EFFICIENCY TRENDS

Load transfer efficiency data from the U.S. Army Corps of Engineers Waterways Experiment Station [1] and the Edmonton, AB [22] study was analyzed in order to study the effects of pavement variables, such as such as elastic modulus, modulus of subgrade reaction, radius of relative stiffness, etc., on load transfer efficiency. In particular, relationships between crack or joint spacing and load transfer efficiency were studied. This section has been divided into two parts: one for the U.S. Army Corps of Engineers Waterways Experiment Station and one for the Edmonton, AB study.

Waterways Experiment Station Study Trends

Data from all five sites of the U.S. Army Corps of Engineers Waterways Experiment Station Study were grouped together in order to study the general trends of different pavement parameters such as crack spacing, crack width, modulus of subgrade reaction, and radius of relative stiffness on load transfer efficiency in RCC pavements. Most of the pavements from these sites have been allowed to naturally crack transversely to save on costs related to joint cutting. The first part of this section will focus on natural transverse cracking RCC pavements while the second section will analyze jointed RCC pavements from the study in [1]. It should be noted that many variables such as thickness, age, and traffic were not analyzed in this study.

Transverse Cracked RCC Pavements

With RCC pavements that are allowed to naturally crack, many times the spacing between these cracks tend to be quite large in comparison to conventional concrete

pavem

be distr

increas

with re

the spa

the cas

Experi

data fr

relatio

betwee

Crack Width (in.)

Figure

I

pavemen

pavements. With these large crack spacings, volumetric changes in the concrete can not be distributed to many crack openings, but instead to very few openings. This tends to increase the crack widths in RCC pavements. Figure 17 shows a trend of crack width with respect to crack spacing. Again, the crack spacings in this study are the average of the spacing before and after a particular crack to the most nearby transverse cracks. In the case of this figure and others from the U.S. Army Corps of Engineers Waterways Experiment Station study, each observation on the figure represents an average of a set of data from different sites and subsections of the study. Although scatter is noticed in this relationship, a clear trend of increasing crack widths are noticed with increasing spacings between these cracks.

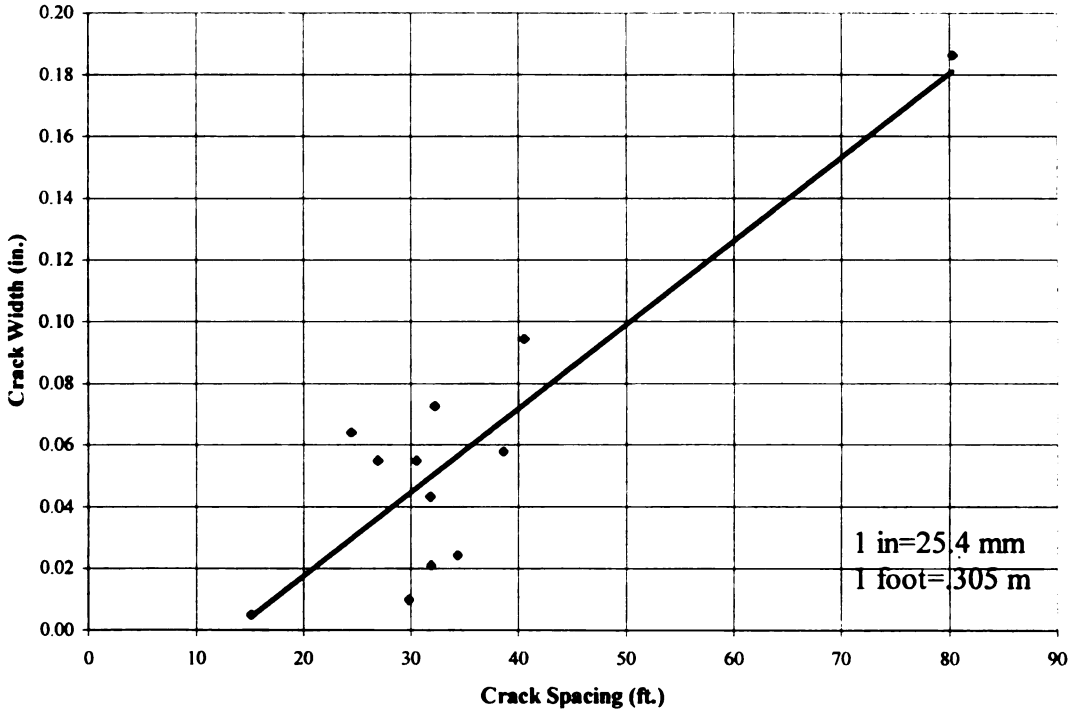

Figure 17. Relationship Between Crack Width and Crack Spacing.

In general, large crack widths are not conducive to high load transfer in rigid pavements structures. The trend from Figure 17 would suggest that smaller crack

spacings would

slabs. This hig

stresses on both

transfer also de

surface for user

large problem in

can be limited by

Figures 1

spacings and defl

is exhibited which

larger crack width

cracks resulted in

crack widths less

0.08 inches (2 mm

past 0.08 inches (

inches (2 mm) wa

low level of LTE,

an external load r

high crack spacin

spacings over 40

shorter crack spa

spacings are more

spacings would increase the chance for high load transfer between discontinuities in slabs. This high LTE would decrease stresses incurred by external loads and share the stresses on both sides of the discontinuity. It is commonly believed that high load transfer also deters faulting of cracks and joints thereby providing a smooth driving surface for users. Although Piggott [15] suggests that faulting does not seem to be a large problem in his RCC pavement visual field study, it is still a potential problem which can be limited by increased load transfer between slabs.

Figures 18 and 19 show the relationships between crack widths and crack spacings and deflection load transfer efficiency, respectively. In both cases, a clear trend is exhibited which follows the theory explained in the above paragraph. In Figure 18, larger crack widths led to low levels of deflection load transfer efficiency while tighter cracks resulted in improved load transfer. A fairly clear delineation was seen in LTE_δ for crack widths less than 0.04 inches (1 mm) and those between 0.04 inches (1 mm) and 0.08 inches (2 mm). Again, a clear delineation was seen in LTE_δ as crack widths opened past 0.08 inches (2 mm). However, the average LTE_δ for crack widths greater than 0.08 inches (2 mm) was found to be around 51%. These cracks would fall into a dangerously low level of LTE_δ which would increase the stresses experienced by the pavement under an external load near the crack. In Figure 19, lower levels of LTE_δ were associated with high crack spacings and vice versa. A similar difference in LTE_δ was seen for crack spacings over 40 feet (12.2 m) in distance as with the crack widths when compared to shorter crack spacings. This data would tend to support the theory that larger crack spacings are more detrimental to load transfer between cracks.

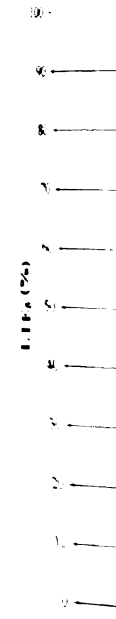

Figure 18.

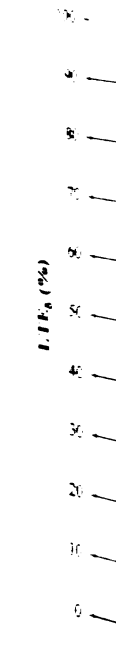

Figure 19.

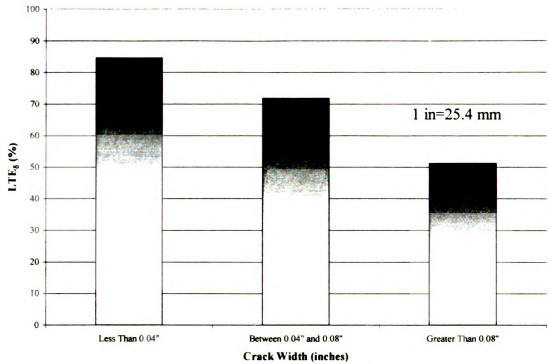

Figure 18. Relationship Between Crack Width and LTE_δ.

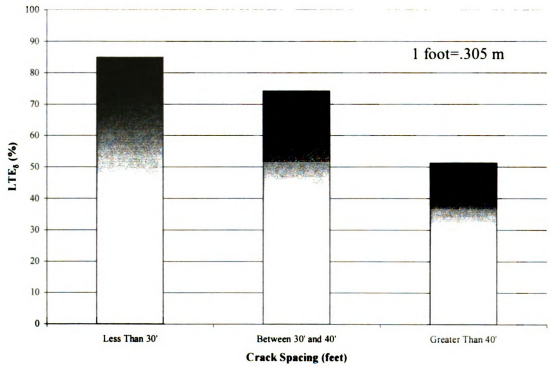

Figure 19. Relationship Between Crack Spacing and LTE_δ.

As

Experimen

20. Points

the figure)

suggested

American

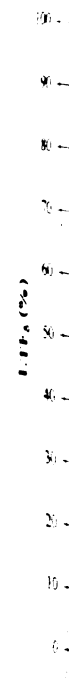

Figure 2

P

curling a

cracks) a

artificial

opposing

which lea

As the modulus of subgrade reaction (k) increased, data from the Waterways Experiment Station study showed that LTE_δ also increased. This can be seen in Figure 20. Points that tend to disagree from the general trend (three points on the upper left of the figure) were tested at temperatures in excess of 90°F (32°C) which is over the suggested range of 50 to 85°F (10 to 29°C) for FWD testing as suggested by the American Association of State Highway and Transportation Officials (AASHTO).

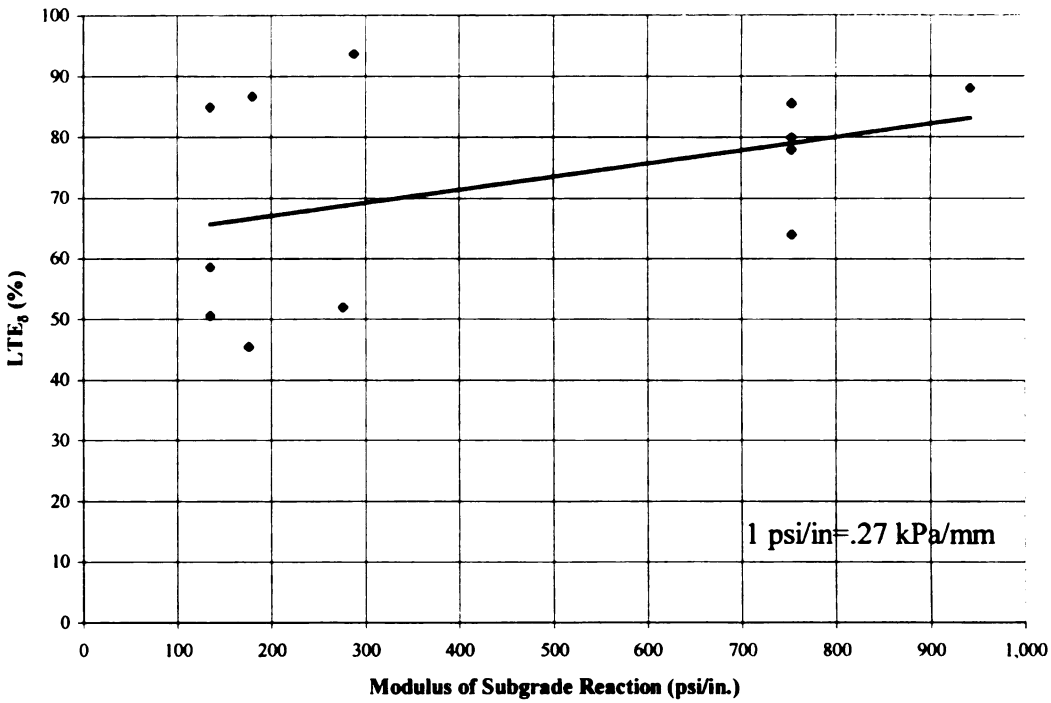

Figure 20. Relationship Between Modulus of Subgrade Reaction and LTE_δ.

Pavement temperature can affect the performance of transverse cracks through curling and thermal expansion/contraction mechanisms. Downward curling (at the cracks) and thermal expansion of slabs can occur at high temperatures, resulting in artificially smaller crack widths. This results in a greater potential for contact between opposing crack faces (and thus greater potential for aggregate interlock between slabs), which leads to higher load transfer efficiencies for such cracks.

A re

order to pr

high load tr

of scatter t

appear that

and a highe

modulus ar

contradicts

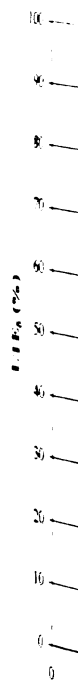

Figure 21

A relationship between the radius of relative stiffness (ℓ) and LTE_δ was sought in order to provide a guide to designing RCC pavements for shorter crack spacings with high load transfer. The results of this focus can be seen in Figure 21. This trend has a lot of scatter to it and does not appear to be a true trend. From this graph however, it would appear that greater stiffness characteristics (Eh^3) of the RCC would lead to lower LTE_δ and a higher resulting stress near the crack. If this were true, both a higher elastic modulus and thicker RCC slab would contribute to a loss in load transfer, which contradicts the common belief.

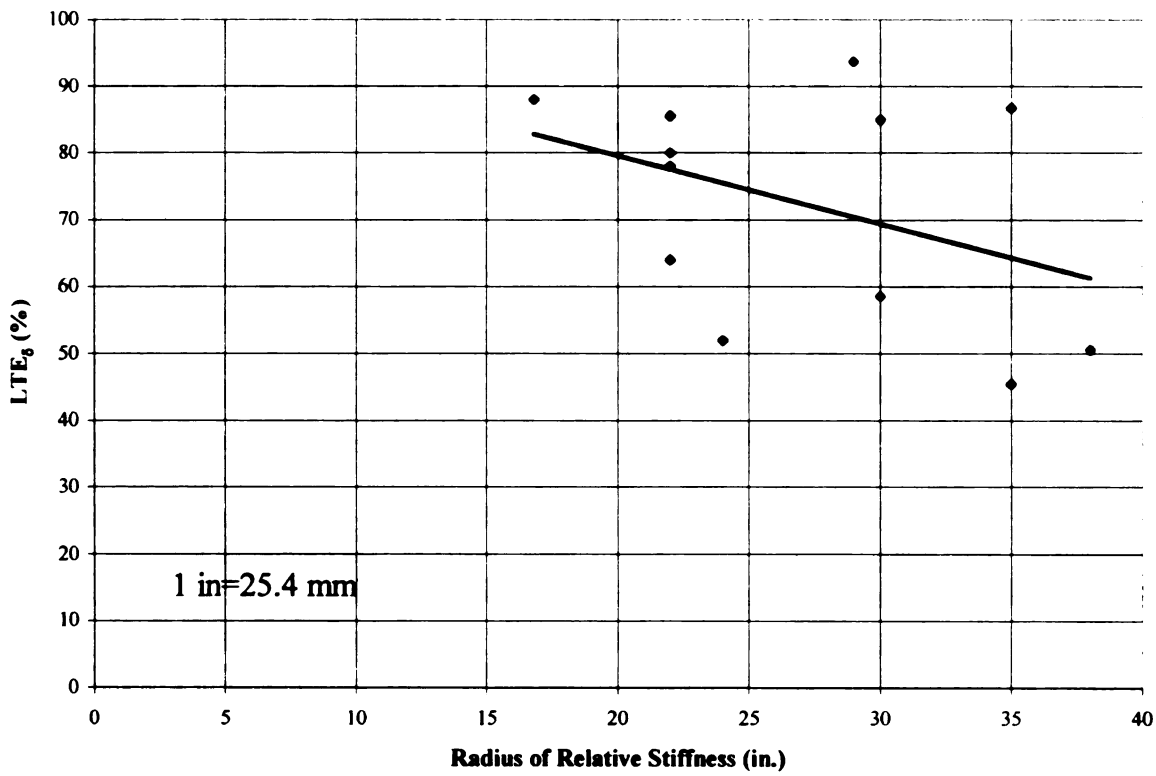

Figure 21. Relationship Between Radius of Relative Stiffness and LTE_δ.

Transverse Jo

Joints

Hood, TX to

the purely fu

[30]. Nanni

of 40 to 60°

90°. How

feet (3.0 to

also noted

unaffected

Fr

investigat

with this

amount o

RCC pav

or HWD

possible

Ft. Drum

than the

section de

pavement

Transverse Jointed RCC Pavements

Joints were sawed at some of the RCC pavements at Fort Drum, NY and Ft. Hood, TX to provide a better riding surface as well as a more aesthetic appearance than the purely functional naturally cracked RCC pavements of other sites. In a field study [30], Nanni found that saw cut joints in RCC pavements tended to range from an LTE_δ of 40 to 60% while naturally cracked RCC pavements had increased LTE_δ's of 60 to 90%. However, he noted that when the average slab length is in the range of 10 to 30 feet (3.0 to 9.1 m), the LTE_δ remains unaffected by classification as a joint or crack. He also noted that the width and aggregate interlock of the crack or joint seemed to remain unaffected by the choice to saw cut at these spacings.

From the Waterways Experiment Station study, joint spacing was analyzed to investigate its effect on LTE_δ as seen in Figure 22. A large amount of scatter was found with this trend (R^2=0.03) as well as a large range of LTE_δ. This may be due to the small amount of data available from the Waterways Experiment Station study in [1] on jointed RCC pavements. Each point found in Figure 22 represents one joint tested with the FWD or HWD instead of a set of data as with the naturally cracked RCC pavements. Another possible reason for the scatter is the lack of joint spacing data found on joints tested from Ft. Drum, NY with high LTE_δ's. These data points could have helped form a better trend than the one presented in Figure 22. The Edmonton, AB study discussed in the next section deals primarily with saw cut joints and their effect on load transfer in RCC pavements.

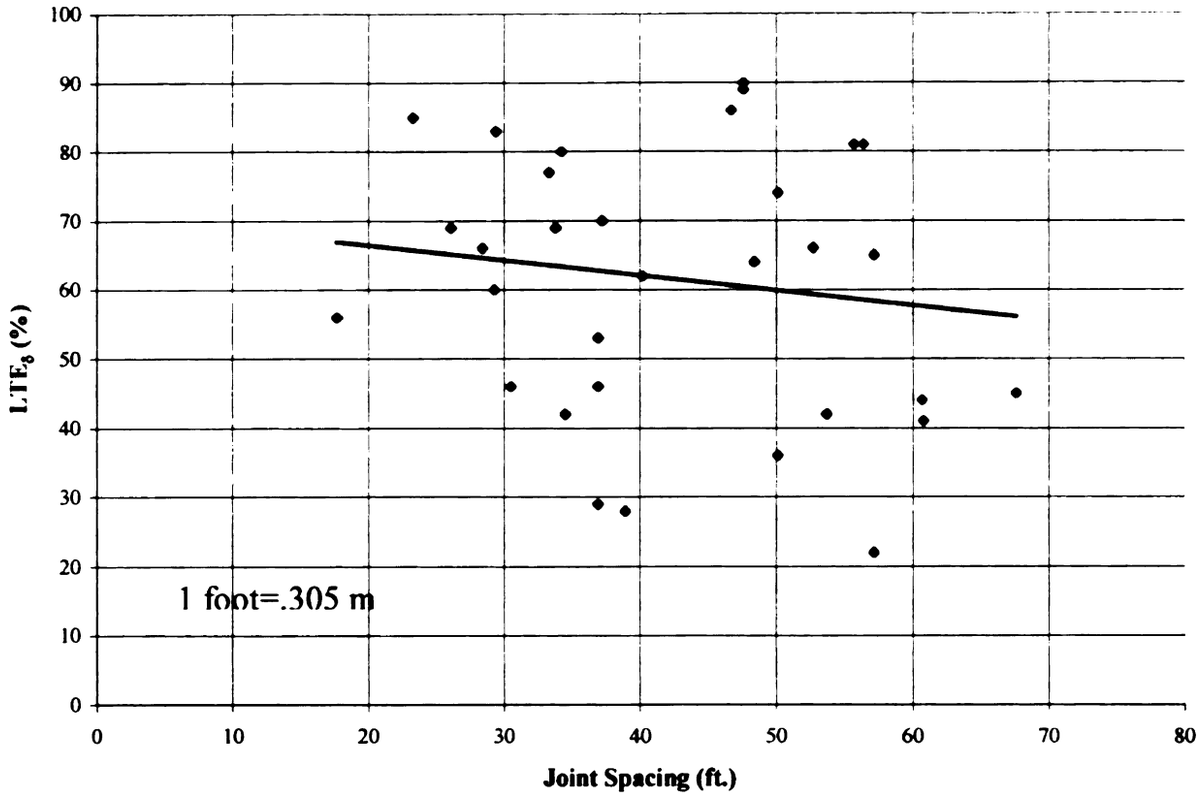

Figure 22. Relationship Between Average Joint Spacing and LTE_δ.

Edmonton, AB Study Trends

The study from the Edmonton, AB RCC pavement is a more controlled analysis on load transfer than that of the Waterways Experiment Station. It focuses on the effect of joint spacing on load transfer without great changes in RCC thickness, support conditions, and traffic that are associated with the Waterways Experiment Station study. While most of the data deals with jointed RCC pavements at different joint spacing, some of this study dealt with naturally cracked RCC pavements in order to test the effect of saw cutting on LTE_δ on a gross basis.

Transverse J

The

and 49.2 fee

spacings ten

23 shows th

with increas

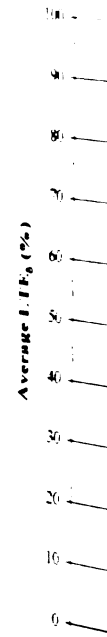

Figure 23.

Radiu

joints at the

showed a dec

natural cracks

less scattering

Transverse Jointed RCC Pavements

The Edmonton, AB study focused on four distinct joint spacings, 14.8, 21.3, 32.8, and 49.2 feet (4.5, 6.5, 10.0, and 15 m) to test its effect on load transfer. These joint spacings tend to agree to the range that most rigid pavements have designed for. Figure 23 shows the effect of joint spacing on LTE_δ. A clear trend of decreasing LTE_δ is noticed with increased joint spacing although the levels of LTE_δ is fairly low overall.

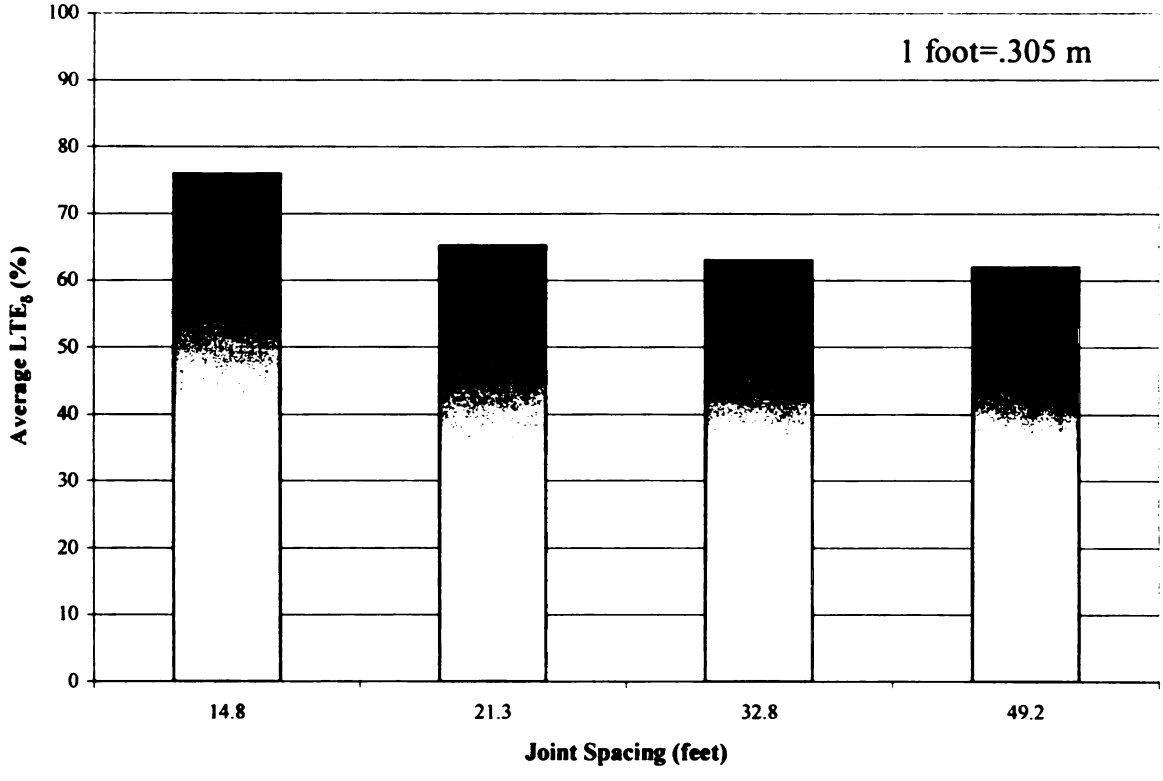

Figure 23. Relationship Between Joint Spacing and LTE_δat Edmonton, AB Site.

Radius of relative stiffness was found to have an effect on load transfer at the joints at the Edmonton, AB site. In Figure 24, an increasing radius of relative stiffness showed a decreasing load transfer efficiency. This tends to agree with the findings on natural cracks from the Waterways Experiment Station in the preceding section, but with less scattering of the data.

Figure 24. Rel

From th

reaction was fo

pavements. Ho

clear trend was

established as s

In the p

stiffness (Eh^3)

stiffness on the

two variables a

is on the order

modulus is the

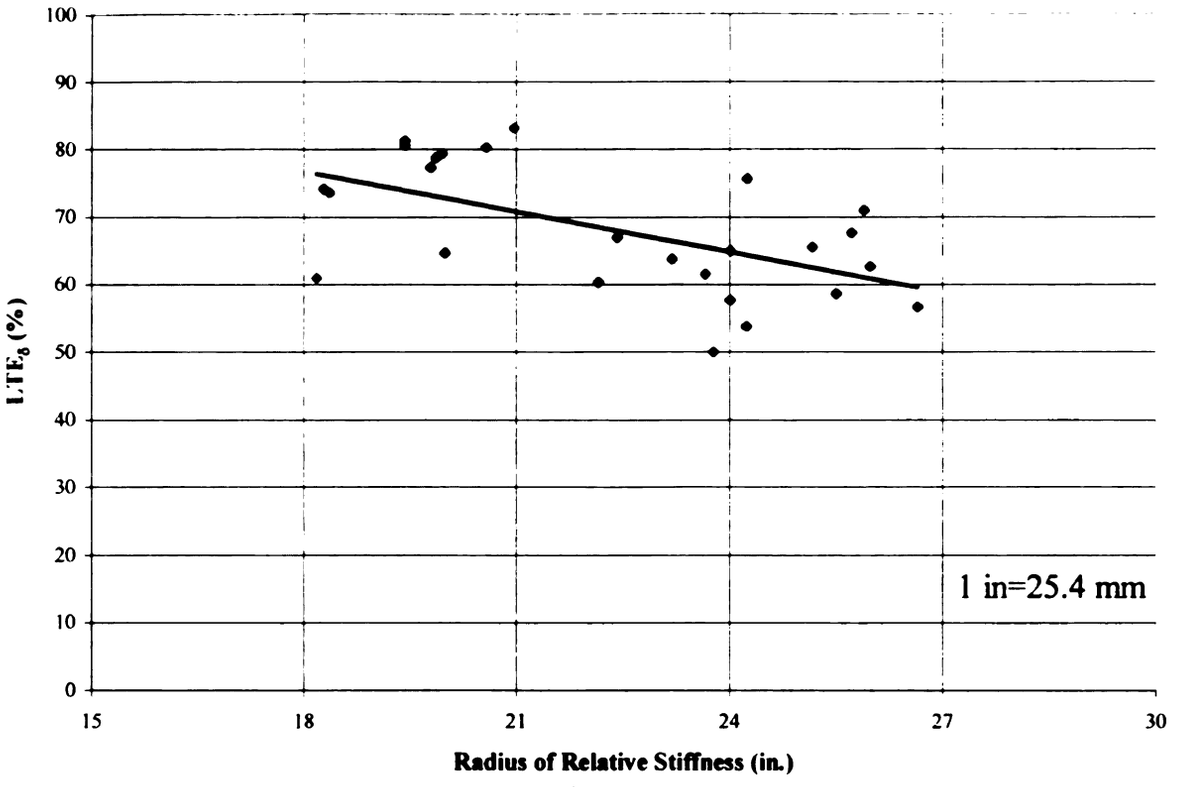

Figure 24. Relationship Between ℓ and LTE$_\delta$at Edmonton, AB Site.

From the Waterways Experiment Station study, an increased modulus of subgrade reaction was found to have positive effect on load transfer in naturally cracked RCC pavements. However, with the high amount of variation in the results from that study, no clear trend was established. From the Edmonton, AB study, no clear trend was again established as seen in Figure 25.

In the previous section on naturally cracked RCC pavements, increasing slab stiffness (Eh^3) was found to have a negative effect on LTE$_\delta$. A brief analysis of slab stiffness on the RCC pavements from this site shows a good correlation between these two variables as seen in Figure 26. Since the elastic modulus value used in this analysis is on the order of 10^6 while the RCC thickness value is much smaller value, the elastic modulus is the controlling variable in the computation of the slab stiffness.

Figure 2

Figure 26.

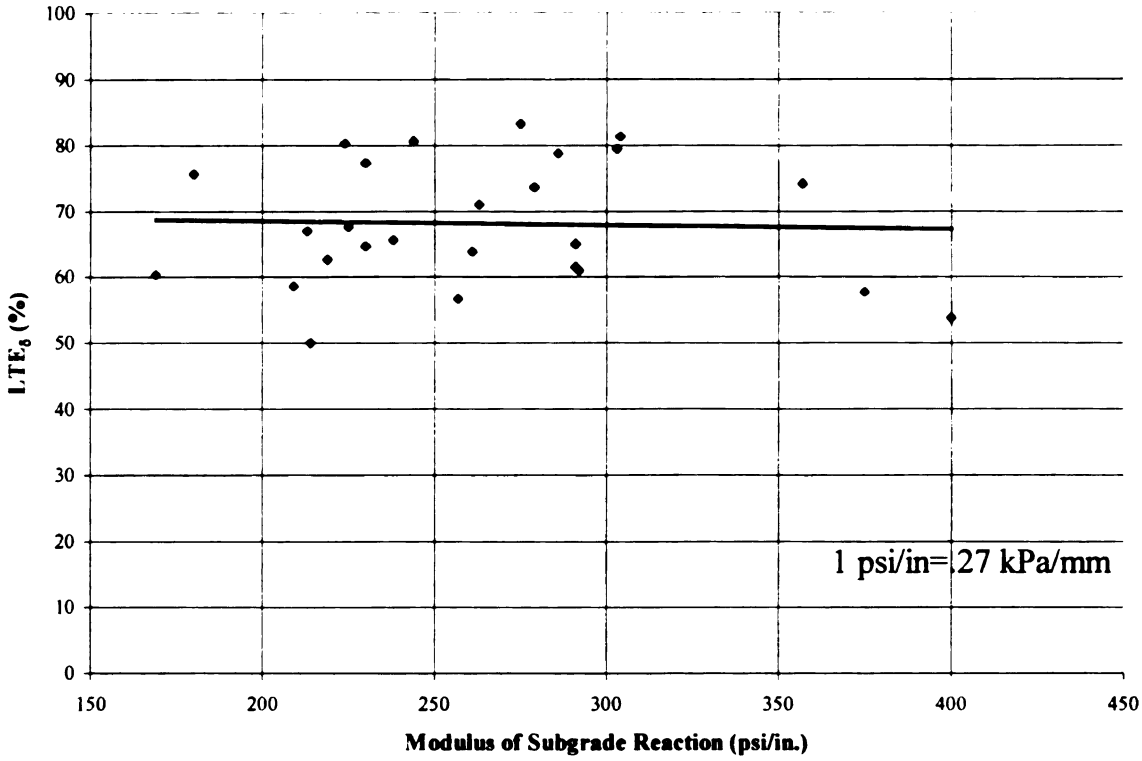

Figure 25. Relationship Between k and LTE_δ at Edmonton, AB Site.

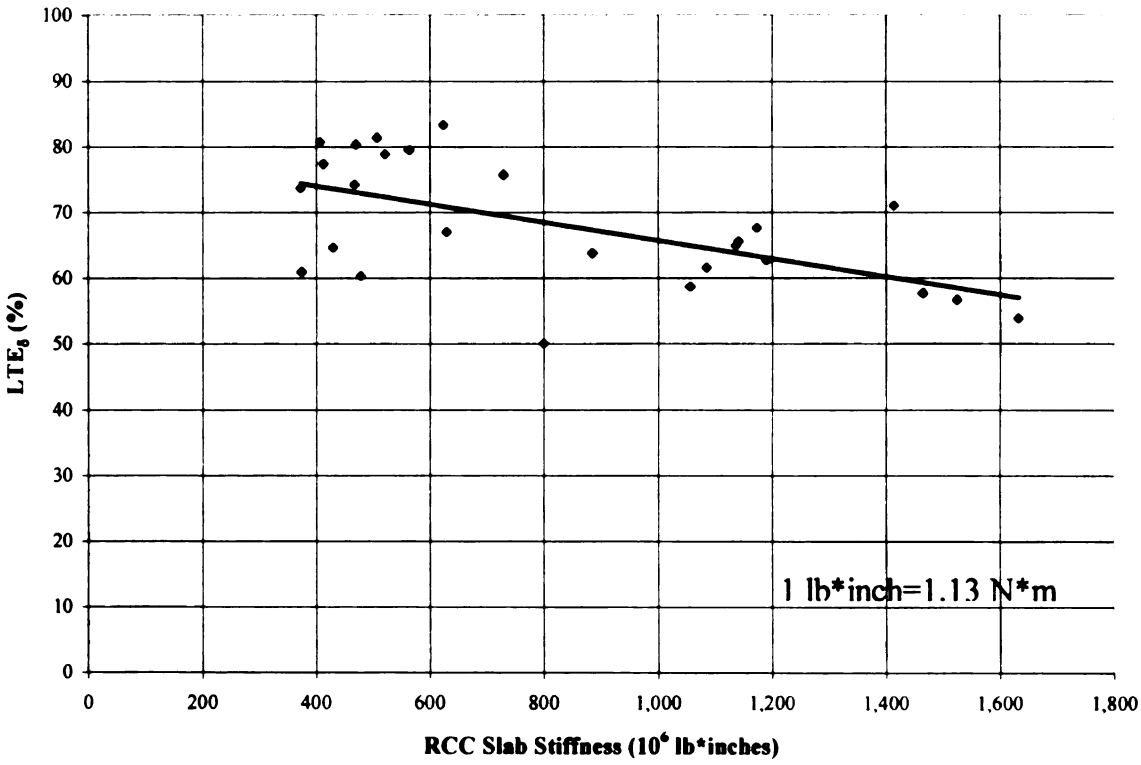

Figure 26. Relationship Between Eh^3 and LTE_δ at Edmonton, AB Site.

It i

transfer at

small incre

Ioannides

studies in

similar no

absolute d

therefore

Transvers

A

naturally a

While no

of 68% w

This woul

versus joi

It is generally thought that increasing thickness results in an increased load transfer at a crack or joint. A brief finite element analysis using ISLAB2000 shows a small increase in the calculated LTE_δ when the RCC slab thickness is increased. Ioannides [27] reports that an increase in slab stiffness generates a lower LTE_δ. Other studies in [31, 32, 33] presented both numerical and experimental data that conclude similar notions on slab stiffness. It is noted however that as the LTE_δ's are decreased, the absolute deflections will be reduced thereby increasing pavement life. The lower LTE_δ's therefore can be sustained over a longer period of time.

Transverse Cracked RCC Pavements

A few sections of the Edmonton, AB RCC pavement site were allowed to crack naturally as a comparison to the jointed RCC pavements with respect to load transfer. While no crack spacing data was available, the jointed RCC pavements averaged an LTE_δ of 68% while the naturally cracked RCC pavements at this site averaged an LTE_δ of 59%. This would tend to contradict the findings of Nanni [30] on load transfer in cracked versus jointed RCC pavements which were discussed earlier in this chapter.

OVERVIEW

This ma
influence the fa
temperature gra
respect to the e
the joints or cra
the magnitude a

Effect of Load

Load tr
stress when in
approximately
load placemen
joints or crack
where a negat
higher than th
crack. Howe
design of RC
at the top of t
tensile stress a

- CHAPTER IV -

RCC Pavement Design

OVERVIEW OF DESIGN METHODOLOGY

This method of RCC pavement design incorporates many different factors which influence the fatigue life of a pavement. These factors include load on the design axle, temperature gradient within the RCC slab, foundation support, and load placement with respect to the edge of the pavement. Other parameters, such as load transfer efficiency at the joints or cracks, slab length, and slab width, were also investigated for their impact on the magnitude and location of the critical stress in a RCC pavement.

Effect of Load Positioning on Tensile Stress

Load transfer efficiency was found to only affect the magnitude of the tensile stress when in the vicinity of the joint or crack. This range in most cases was approximately 5-7 feet (1.5-2.1 m) from the discontinuity in the pavement. The critical load placement was found in virtually all cases to be midway between the transverse joints or cracks along the edge of the pavement as seen in Figure 27. In some cases where a negative temperature gradient (temperature at the bottom of the RCC slab is higher than the top of the slab) existed, the critical stress was due to a load at the joint or crack. However, this occurred so infrequently that it should not be considered in the design of RCC pavement thickness. In these few cases, the critical tensile stress occurred at the top of the RCC slab whereas the vast majority of scenarios resulted in a critical tensile stress at the bottom of the RCC slab.

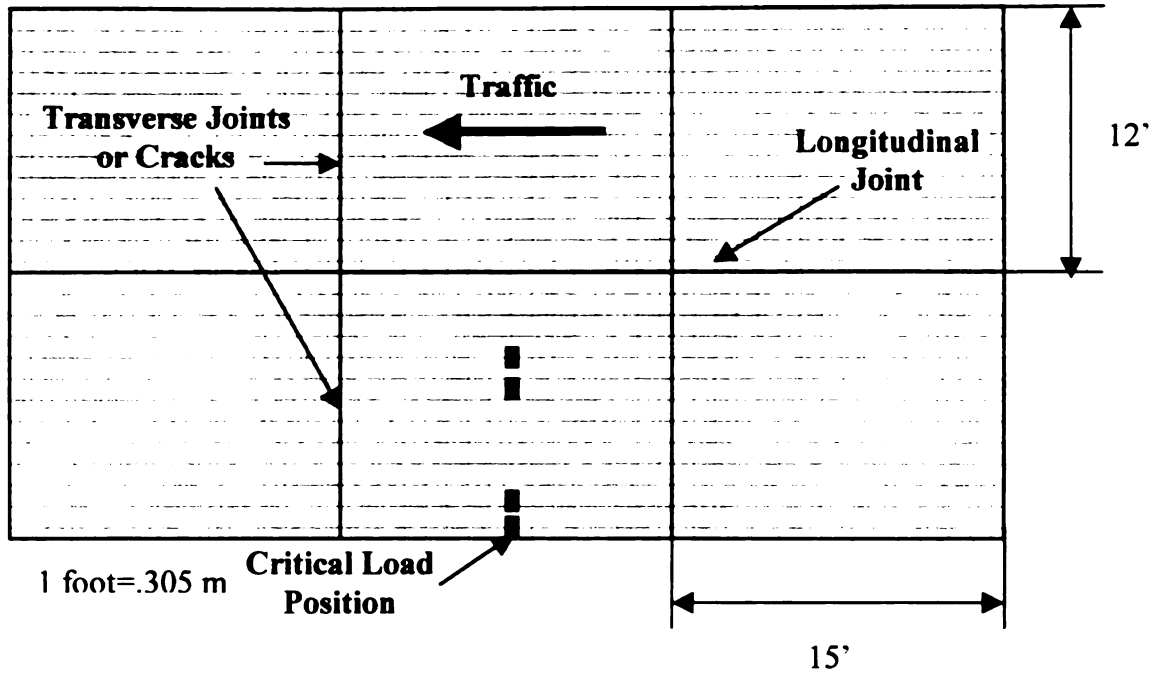

Figure 27. Slab Dimensions and FEA Mesh for Critical Load Position at Edge.

Effect of Slab Dimensions on Tensile Stress

Slab length had an effect on the magnitude of the critical stress when the slab length was at an extremely short distance. When slab lengths were less than 15 feet (4.6 m), the critical stresses tended to decrease slightly. For slab lengths greater than 15 feet (4.6 m), critical stresses tended to remain constant. This supports the findings of Ioannides and Korovesis [27] who claimed that with a slab length (L) divided by radius of relative stiffness (ℓ) value greater than 5 under full slab contact support conditions, the responses of the pavement approach infinite slab-like conditions. For a common radius of relative stiffness of 36 inches (914 mm), the slab length would be required to be equal to or greater than 15 feet (4.6 m) to meet this criterion. This study showed that even with a low radius of relative stiffness of 25 inches (635 mm), shorter slab lengths had little effect on the critical stress level. With the vast majority of natural crack spacings in RCC

pavements gre

than 25 inches

fatigue life des

Slab wi

location as slab

restrictions on t

much smaller ra

structure. In all

effect on critical

that a slab width

affect pavement

radius of relative

decreased below

the study in [27]

of relative stiffne

level to adversely

GUIDE TO RC

A "new" r

method incorpora

gradients in the RC

of the design metho

pavements greater than 15 feet (4.6 m) with a radius of relative stiffness (ℓ) values greater than 25 inches (635 mm), slab length does not appear to be a major consideration in fatigue life design.

Slab width appears to have a similar effect on the critical stress magnitude and location as slab length. However since practical restrictions from truck widths place restrictions on the slab width to minimum limits of 10-12 feet (3.0-3.7 m) in most cases, a much smaller range of values were examined for the effect in critical stress in a pavement structure. In all cases examined, increases in slab length over 12 feet (3.7 m) had no effect on critical slab stress magnitude or location. Ioannides and Korovesis [27] found that a slab width (W) divided by radius of relative stiffness (ℓ) value less than 4 tended to affect pavement performance parameters such as load transfer. Again using the common radius of relative stiffness of 36 inches (914 mm), the slab width would have to be decreased below 12 feet (3.7 m) to adversely affect the pavement structure according to the study in [27]. This corresponds well with findings from this study. With low radius of relative stiffness (ℓ) values, slab widths would need to be reduced to an impractical level to adversely affect the critical stress magnitude.

GUIDE TO RCC PAVEMENT STRUCTURAL DESIGN

A "new" method for RCC thickness design is described in this section. This method incorporates axle load and configuration, foundation support, temperature gradients in the RCC layer, and the effect of load placement in the design. A flowchart of the design methodology can be seen in Figure 28.


Traffic

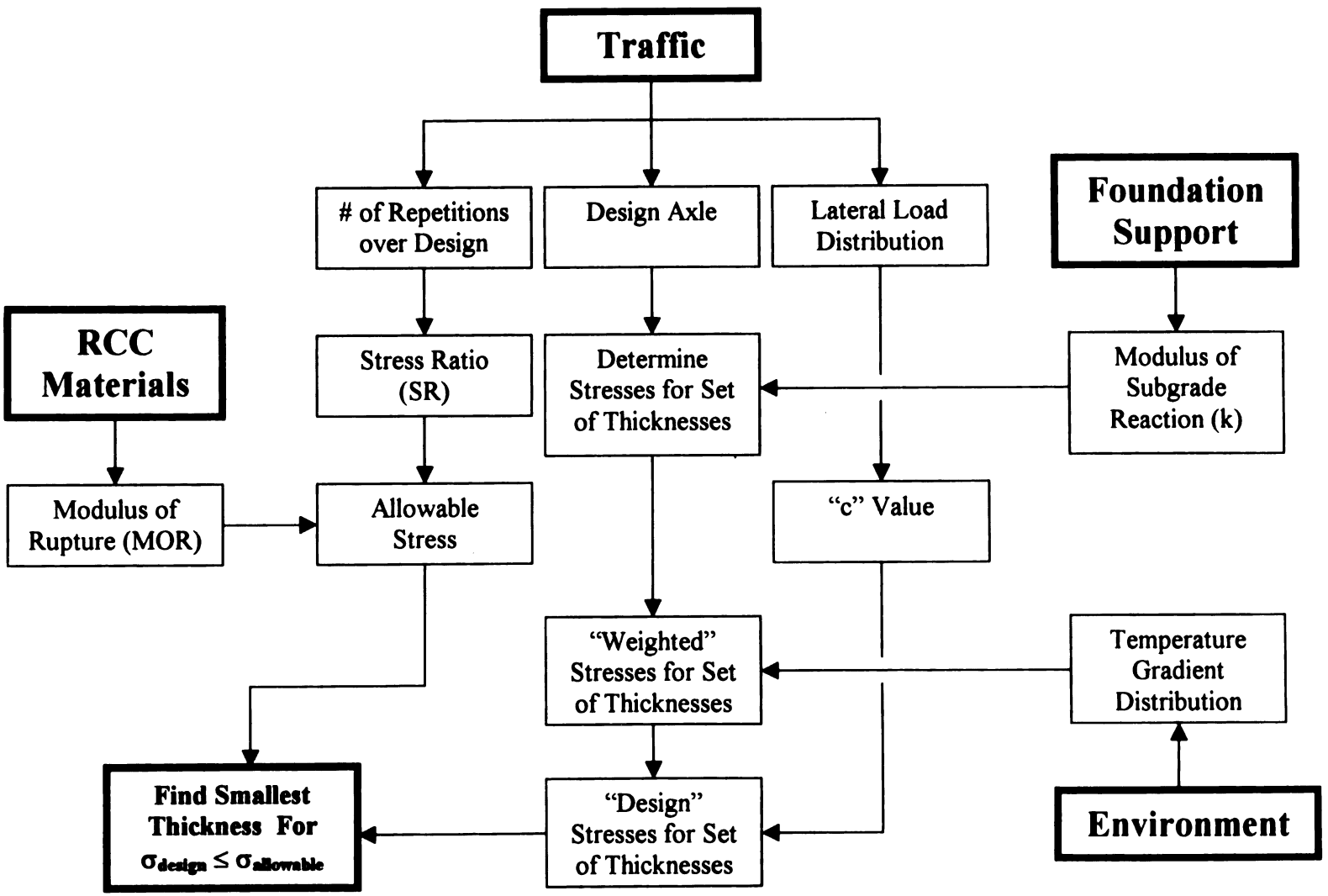

Figure 28. Flow Chart for Methodology of "New" RCC Pavement Design Process.

This section describes the methodology and an example design of an RCC pavement thickness for the following conditions:

- RCC pavement to be used as an access road for a factory, servicing mainly trailers
- 100,000 allowable repetitions of 18 kip (160.1 kN), dual-tired axle for design life
- Average modulus of subgrade reaction of 250 psi/in (67.9 kPa/mm)
- Tires are assumed to be at a pressure of 100 psi (689 kPa)
- RCC flexural strength of 700 psi (4826 kPa)
- Assumed to be a positive temperature gradient 30% of the time, a negative gradient 15% of the time, and no gradient for the remainder of the time.

Stress Ratio and Allowable Stress

The first step in the design of the RCC slab thickness is to determine the stress ratio as a function of load repetitions from Table 7. In this case for 100,000 repetitions, the corresponding stress ratio is 0.47. Table 7 is formulated based on the relationship between stress ratio and allowable repetitions in RCC pavements used by PCA [14] as outlined in Chapter 2.

Alternatively, Tayabji and Halpenny [34] developed a similar relationship for RCC pavement fatigue relationships. Their fatigue relationship encompasses a larger range of stress ratios as seen in Table 8.

A comparison of both relationships (Figure 29) shows that the PCA model for fatigue of RCC pavements is much more conservative than that of the Tayabji and Halpenny model. The Tayabji and Halpenny model will result in thinner RCC pavements. However, Table 8 is added for purposes of comparison to the PCA model and can be used in the same capacity. In the case of this example, the stress ratio would be approximately 0.65.

Table 7. Fati

Stress Ra
0.41
0.42
0.43
0.44
0.45
0.46
0.47
0.48
0.49
0.50
0.51
0.52
0.53
0.54
0.55

[a] Load stress

Table 7. Fatigue Relationship (After PCA [14]).

Stress Ratio [a]	Allowable Repetitions	Stress Ratio [a]	Allowable Repetitions
0.41	465000	0.56	9700
0.42	360000	0.57	7500
0.43	280000	0.58	5800
0.44	210000	0.59	4500
0.45	165000	0.60	3500
0.46	130000	0.61	2700
0.47	100000	0.62	2100
0.48	76000	0.63	1600
0.49	59000	0.64	1200
0.50	46000	0.65	950
0.51	35000	0.66	740
0.52	27000	0.67	570
0.53	21000	0.68	440
0.54	16000	0.69	340
0.55	12000	0.70	260

[a] Load stress divided by modulus of rupture

Tabl

S

[a] Loa

Table 8. Fatigue Relationship (After Tayabji and Halpenny [34]).

Stress Ratio [a]	Allowable Repetitions	Stress Ratio [a]	Allowable Repetitions
0.45	6800000	0.71	25600
0.46	5500000	0.72	20700
0.47	4400000	0.73	16700
0.48	3600000	0.74	13500
0.49	2900000	0.75	10900
0.50	2300000	0.76	8800
0.51	1900000	0.77	7100
0.52	1500000	0.78	5700
0.53	1200000	0.79	4600
0.54	980000	0.80	3700
0.55	800000	0.81	3000
0.56	640000	0.82	2400
0.57	520000	0.83	1950
0.58	420000	0.84	1575
0.59	340000	0.85	1275
0.60	270000	0.86	1025
0.61	220000	0.87	830
0.62	175000	0.88	670
0.63	140000	0.89	540
0.64	115000	0.90	435
0.65	93000	0.91	350
0.66	75000	0.92	280
0.67	60000	0.93	230
0.68	49000	0.94	185
0.69	39000	0.95	150
0.70	32000		

[a] Load stress divided by modulus of rupture

Figure 29. Co

Using ec

and the design r

$\sigma_{allowable} = SR * M$

where:

$\sigma_{allowable}$
SR
MOR

Using the values

329 psi (2270 kP

design load, the s

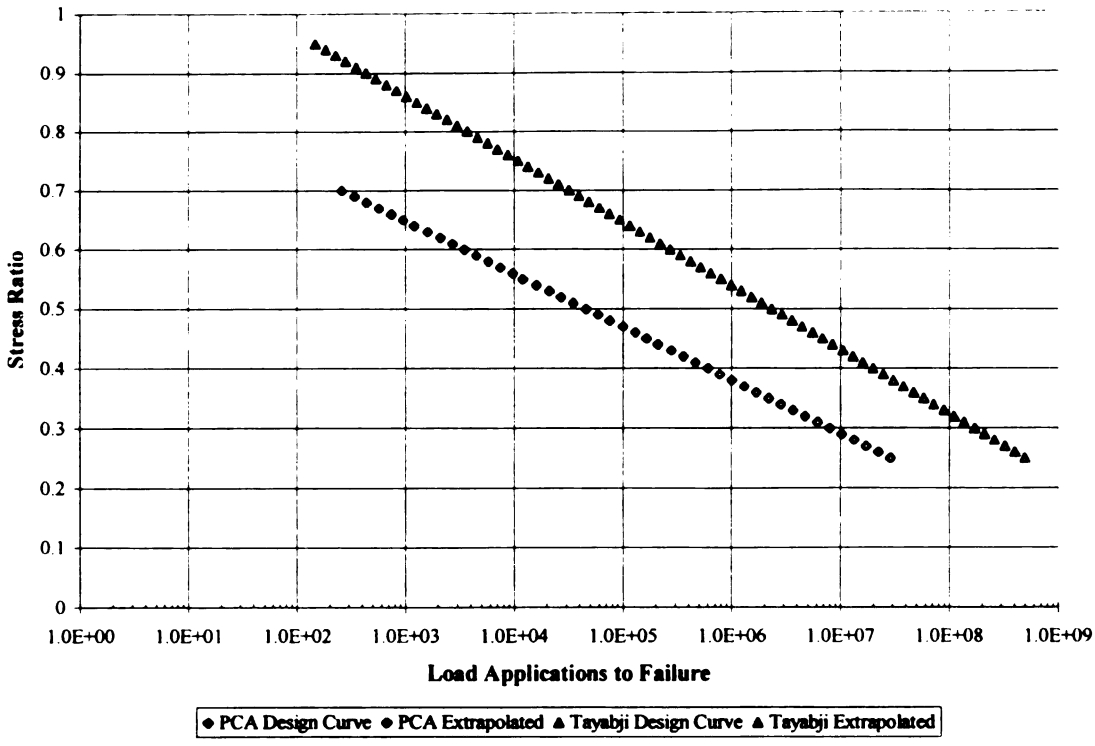

Figure 29. Comparison of PCA and Tayabji/Halpenny Fatigue Relationships.

Using equation (17), the allowable stress can be determined from the stress ratio and the design modulus of rupture of the RCC for both fatigue relationships.

$$\sigma_{allowable} = SR * MOR \qquad (17)$$

where:

$\sigma_{allowable}$	=	allowable design stress, psi
SR	=	stress ratio (found from Table 7)
MOR	=	modulus of rupture of RCC, psi

Using the values of SR = 0.47 and MOR = 700 psi, the allowable stress for this design is 329 psi (2270 kPa). This means that to achieve the desired 100,000 repetitions of the design load, the stress caused by this load cannot exceed 329 psi (2270 kPa). Based on

the Ta

an incr

Temp

slab of

thickn

analys

the ter

tempe

divide

chang

Winkl

deflec

forces

this ty

on th

(posit

down

upwa

Figure

the Tayabji and Halpenny fatigue relationship, the allowable stress is 455 psi (3140 kPa), an increase of 38% over the PCA allowable stress.

Temperature Gradients

Three temperature differentials from the top to the bottom of the RCC pavement slab of 0, -15, and +15°F (0, -8.3, +8.3°C) were selected for use in the fatigue-based RCC thickness design. For simplicity in modeling, all temperatures differentials in this analysis were assumed to change linearly with depth of the RCC pavement slab. Since the temperature differentials were held constant at the three values stated above, the temperature gradients (defined as the temperature differential across the depth of the slab divided by the depth of the slab) changed as the thicknesses of the RCC pavement slabs changed. These temperature gradients lead to a curling action of the RCC pavement slab.

The subgrade in this analysis was assumed to be a Winkler foundation. A Winkler, or liquid, foundation models the subgrade as a set of independent springs. The deflection of each "spring" is proportional to the force at that point and independent of all forces elsewhere [35]. By assuming an RCC pavement to be a rigid plate supported by this type of foundation under a temperature differential, additional stresses will transpire on the slab that would not occur with exterior loads only.

Downward curling occurs when the top of the slab is warmer than the bottom (positive gradient). In this case, the top of the slab elongates and consequently curls downward. The springs on the edges of the slab are in compression and push the slab upward, while the interior springs are in tension and pull the slab downward as seen in Figure 30. This results in compression at the top portion of the slab and tension in the

bottom portion of the slab. The maximum compression and tension occur at the extreme top and bottom of the slab, midway between the edges. The reverse situation (negative gradient) can be seen in Figure 31. The points if tension and compression are the exact opposite in this case. All of these situations assume that no curling is evident when no temperature differential is present in the RCC pavement slab [35].

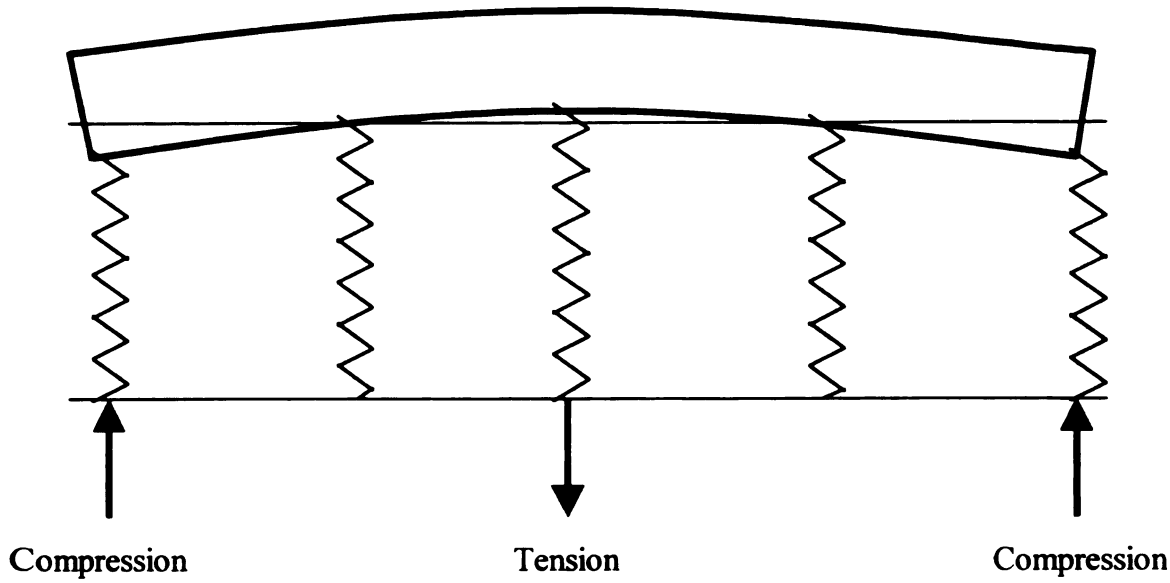

Figure 30. Downward Slab Curling due to Positive Gradient.

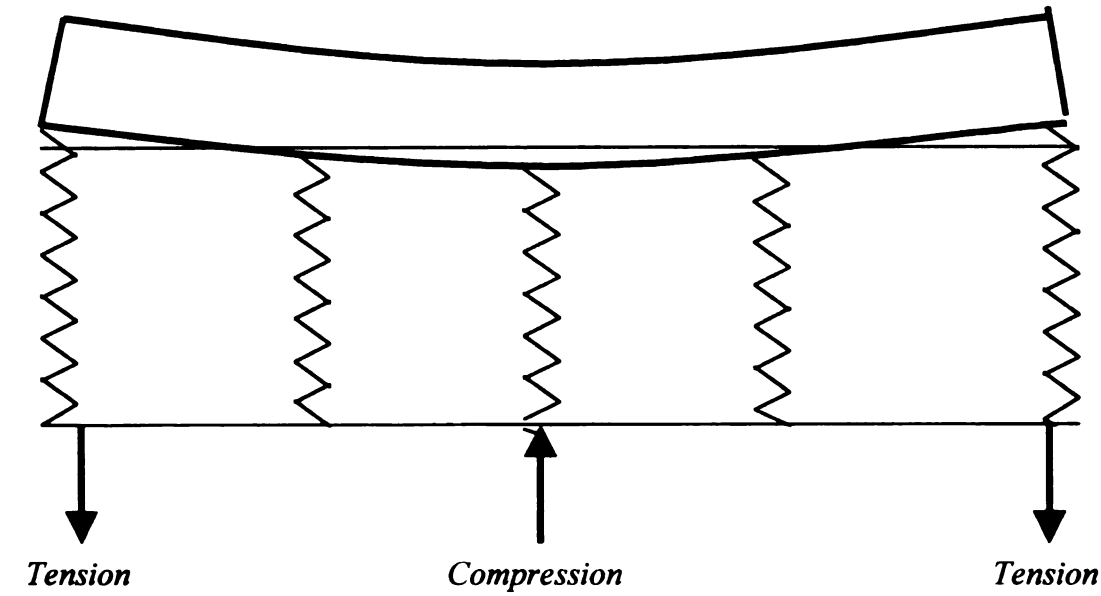

Figure 31. Upward Slab Curling due to Negative Gradient.

Lateral Load Location

Most RCC pavement design methods based on stress calculations assume that the load positioning is either at the critical location at the edge of the pavement slab or at a point near the interior of the pavement slab, which would result in a lesser stress under the same load. In reality, the location with respect to the longitudinal edge (or shoulder) varies with each pass of an axle due to drifting of the vehicle. Over time, the accumulation of these passes result in a lateral load distribution as illustrated in Figure 32. Figure 32 represents a normal distribution with an expected value (E[x]) of 24 inches (610 mm) and standard deviation (σ_{dev}) of 10 inches (254 m) from the slab edge on a 12 foot (3.6 m) lane width. The zero point on the x-axis represents the slab edge and all positive values along the x-axis represent distances from the slab edge which are located on the mainline slab. This distribution is an amalgamation of many field tests [36, 37, 38, 39, 40, 41] which attempted to characterize the lateral load distributions of many different vehicle types on both concrete and asphalt pavements. From Figure 32, it can be seen that a vast majority of vehicles remained more than 24 inches (610 mm) away from the pavement edge, thereby reducing the stress induced by the axle load on the pavement slab. However, some axles drift towards the slab edge causing an increased tensile stress. This drifting towards the slab edge would underestimate the design stress if an interior slab loading conditions were employed. Conversely, if the edge loading condition were used for design, it would overestimate the design stress and result in a conservative slab thickness.

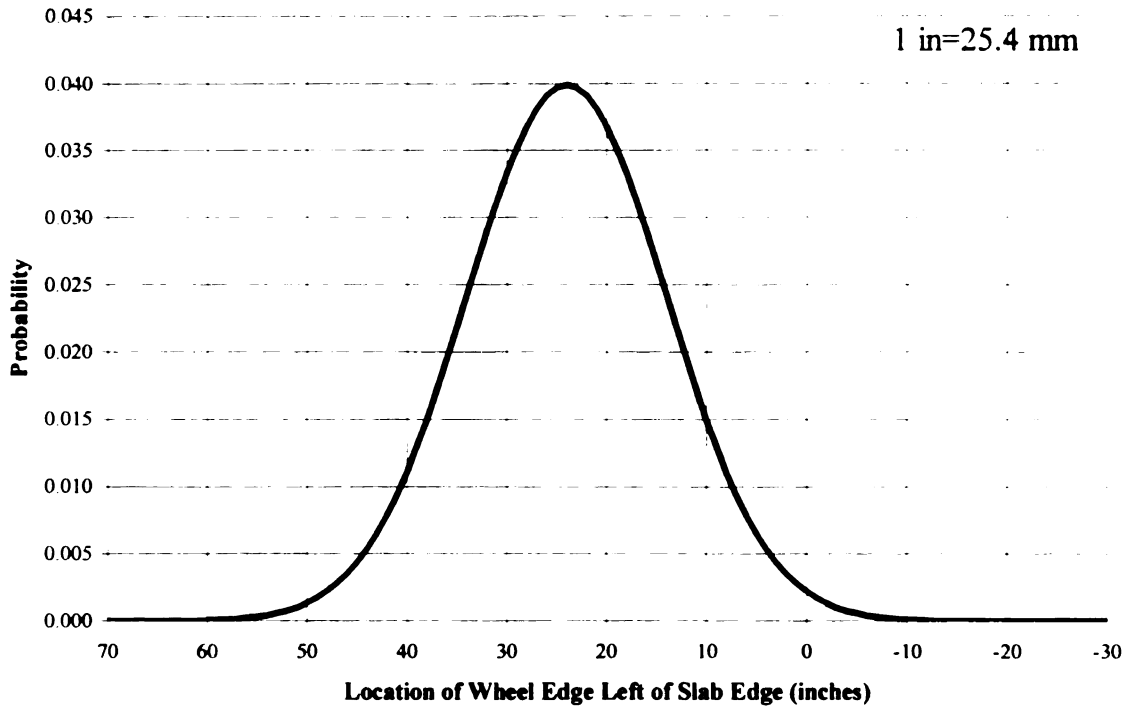

Figure 32. Typical Probabilistic Lateral Load Distribution on 12' Wide Lane.

To assess the effect of lateral load distribution on RCC slab thickness design, a level of reliability must be chosen as defined in equation (18).

$$R = (1 - P[F]) * 100\% \qquad (18)$$

where:

R	=	reliability, %
$P[F]$	=	probability of failure

The higher the level of reliability is, the lower probability that the level of design stress will be surpassed. For instance, if the chosen level of reliability is 70% (or 0.70), then the probability that a random wheel positioning would be closer to the edge than designed for would be 1 - 0.70 = 0.30 or 30%. The level of reliability chosen for any particular pavement design should be related to the use and expected life of the facility in question.

If a pavement is to be used as low volume roadway with little significance then the level of reliability should be low although in no case should a pavement be designed below the 50% reliability level. Conversely, if the pavement is to be traversed by vehicles requiring a better ride quality, then a higher level of reliability should be designed for.

Figure 33 represents the level of reliability for the lateral load distribution data shown in Figure 32. A level of reliability of almost 100% is achieved if the edge loading condition is utilized. On the other hand the reliability level is only 50% when using E[x] = 24 inches (610 mm) from the slab edge.

Figure 33. Level of Reliability for Load Positioning on 12' Wide Lane.

The next step in this design would be to choose the level of reliability with respect to the lateral load distribution using Tables A-1 though A-5 and/or the corresponding figures in Appendix A. In the example problem, the design load is an 18-kip dual-tire axle so Table A-2 or Figures A-7 through A-12 should be utilized. Table 9 gives a

summary of the levels of reliability for different distances from the pavement slab edge as well as a list of "c" values which are associated with certain levels of reliability. These "c" values can be used in conjunction with Appendix A to design RCC pavement thicknesses for certain levels of lateral load reliability. These "c" values in Table 9 were developed through a series of ISLAB2000 iterations to determine the effect of the lateral load placement on the critical tensile stress and are only approximate values. The "c" value is defined by equation (19).

$$c = \frac{(\sigma_R - \sigma_{24})}{(\sigma_{edge} - \sigma_{24})} \qquad (19)$$

where:

c	=	"c" value, from Table 9
σ_R	=	tensile stress for reliability level in question, psi
σ_{24}	=	tensile stress for load placed at slab edge, psi
σ_{edge}	=	tensile stress for load placed 24" (0.6 m) from slab edge, psi

Table 9. Reliability Levels for Different Wheel Load Locations.

1 in=25.4 mm

Distance of Wheel Edge from Slab Edge (inches)	Level of Reliability (%)	"c" Values
24	50	0.000
17.25	75	0.065
11	90	0.163
7.5	95	0.313
0.75	99	0.900
0	99.5	1.000

Determination of Pavement Thickness

The final steps can now be taken from the example problem cited earlier in this chapter. The allowable stress found earlier using the PCA fatigue relationship was 329 psi (2270 kPa). This should be entered in a worksheet like the one found in Table 10 along with the modulus of subgrade reaction. In this case, the value of k was assumed to be 250 psi/in (67.9 kPa/mm). A level of reliability must be chosen based on the importance of the facility. Since this pavement is to provide service to trailers primarily, a level of reliability for the lateral load distribution will be assumed to be 95%. This corresponds to a "c" value of 0.313 according to Table 9.

The next task is to input the critical tensile stresses for the specific design wheel load and modulus of subgrade reaction for the problem. These stresses should be entered for both the edge loading condition and the condition where the load is two feet (0.6 m) from the edge if the lateral load distribution is to be considered. In this example, these values can be found in Table A-2 of Appendix A and have been entered into the RCC pavement design worksheet in Table 10. A blank worksheet for further computations of RCC thickness design can be found in Table 11.

After this has been completed, the assumption of the percentage of time that the pavement will be under each temperature gradient must be decided. For this example, the problem statement assumes that a positive temperature gradient occurs 30% of the time, a negative gradient occurs 15% of the time, and no gradient occurs for the remainder of the time. While positive and negative gradients do exist virtually all of the time in concrete pavements, the assumption that no gradient occurs 55% of the time helps balance out

periods when the assumed temperature differential is greater than reality. These values are also entered into Table 10 near the top of the table.

The next step is to use these temperature differential assumptions to compute the weighted values of tensile stress for all thicknesses and in both loading position cases as seen in Table 10. After this, the differential between the weighted tensile stresses for each loading position can be computed by subtracting the weighted stress when the load is two feet from the edge from the weighted edge stresses. These values were found for all the RCC pavement thicknesses and entered in the column in the upper portion of Table 10.

To determine the design stresses for each RCC pavement thickness when considering the lateral load distribution, the "c" value must be used. The design stresses can be computed by multiplying the differential of the weighted stresses by this "c" value (in this case 0.313) and adding that to the weighted stress found for when the load is located two feet (0.6 m) from the edge as seen in Table 10.

The final step is to choose the thickness of the RCC pavement using the allowable stress value calculated earlier (329 psi, or 2270 kPa) and the design stresses for each RCC thickness found in Table 10. The design stress should not exceed the allowable stress, so the thickness should be greater than 6 inches (152 mm) according to Table 10. However, since the allowable stress is near the design stress for the RCC thickness of 6 inches (152 mm), a final design thickness of 6.5 inches (165 mm) was chosen.

Table 10. Worksheet for Example on Determination of RCC Thickness.

1 in=25.4 mm 1 psi=6.89 kPa 1 psi/in=0.271 kPa/mm

	ΔT_{RCC}	0°F	15°F	-15°F	Weighted Stress Value (psi)	Differential Between Weighted Stresses from Edge and 2' Away (psi)	Design Tensile Stress (psi)
	% Time Under Gradient	0.55	0.3	0.15			
RCC Thickness (in.)							
Load is 2' from edge	5	336.2	483.0	250.1	367.3	180.6	423.9
	6	258.0	404.0	203.9	293.7	135.4	336.1
	7	206.1	351.5	184.2	246.4	102.8	278.6
	8	169.8	315.8	176.4	214.6	84.4	241.0
	9	143.1	290.2	168.2	191.0	71.1	213.3
	11	107.0	255.5	152.8	158.4	53.0	175.0
	13	84.0	231.7	149.7	138.2	40.7	150.9
	15	68.3	212.8	144.9	123.1	32.8	133.4
Load is at edge	5	528.0	659.0	399.0	548.0	k (psi/in.)	250
	6	409.0	541.0	279.0	429.1	Lateral Load Reliability (%)	95
	7	328.6	462.0	199.1	349.2		
	8	271.1	407.0	185.2	299.0	"c" Value	0.313
	9	228.4	367.7	174.5	262.1	Allowable Stress (psi)	329
	11	170.2	314.0	157.3	211.4		
	13	132.8	278.0	149.7	178.9	**Design Thickness (in)**	**6.5**
	15	107.3	250.5	144.9	155.9		

Table 11. Worksheet for Determination of RCC Thickness.

1 in=25.4 mm 1 psi=6.89 kPa 1 psi/in=0.271 kPa/mm

	ΔT_{RCC}	0°F	15°F	-15°F	Weighted Stress Value (psi)	Differential Between Weighted Stresses from Edge and 2' Away (psi)	Design Tensile Stress (psi)
	% Time Under Gradient						
RCC Thickness (in.)							
Load is 2' from edge	5						
	6						
	7						
	8						
	9						
	11						
	13						
	15						
Load is at edge	5					k (psi/in.)	
	6					Lateral Load Reliability (%)	
	7						
	8					"c" Value	
	9					Allowable Stress (psi)	
	11						
	13					Design Thickness (in)	
	15						

A catalog of designs can be found in Appendix C. These tables provide the final design thickness for 2,430 cases which are based on the following design inputs:

- Five axle weights and configurations
- Modulus of subgrade reaction (k): 100, 250, 400 psi/in(27.1, 67.9, 108.6 kPa/mm)
- Allowable stress ($\sigma_{allowable}$): Ranging from 100 psi to 500 psi (689 to 3450 kPa)
- Lateral load reliability: 75, 95, 99%
- Percentage of time with positive temperature gradient: 0, 25, 50%
- Percentage of time with negative temperature gradient: 0, 25, 50%

To use this catalog of design, the allowable stress must first be calculated from the from the stress ratio (Table 7) for the allowable repetitions desired and the expected modulus of rupture of the RCC pavement slab. Then using the other input parameters, the design thickness can be chosen from the appropriate table in Appendix C. The tables are organized by axle weight and configuration as well as the modulus of subgrade reaction.

For cases where the design inputs are between the values listed in the table, a weighted thickness can be computed from the nearest thickness values to that of the desired design. If the thickness values for the nearest design inputs vary greatly, the complete design method should be employed in order to find the correct design thickness.

Limiting Subgrade Stress

From a slab tensile stress standpoint, the load transfer efficiency at cracks and joints has little effect on the maximum tensile stress. The "maximum" tensile stress is almost always experienced when the axle is midway between the transverse joints or cracks, along the edge. When the load is at or near a discontinuity, the slab tensile stress is affected by the load transfer efficiency but not to the point where the "maximum" tensile stress is exceeded.

One way that load transfer efficiency aids in the pavement performance is by controlling the stress felt in the subgrade. When the underlying layers of a concrete pavement system are stressed, the probability of pumping in the underlying materials increases. This usually results in premature cracking in the corners of the slabs by creating a cantilever beam effect on the slab corner.

The design method incorporates a design check against an excessive subgrade stress. This design check was developed using ISLAB2000 and modeling an axle load at the joint or crack. No temperature gradients were used when modeling these cases. As the load transfer efficiency was increased, the subgrade stress was found to decrease. This effect promotes the use of joints at distances less than 30 feet (9.1 m) in order to keep the cracks tight and promote higher load transfer between slabs. A decrease in subgrade stress was also exhibited when the RCC thickness is increased.

It is important to note that the use of retrofit dowels analytically reduced the subgrade stress for a given thickness and modulus of subgrade reaction. Typically, PCC pavements are designed to limit the subgrade stress to no more than 5 psi (34.5 kPa). From the ISLAB2000 analysis, the subgrade stress would always exceed this level under the 12 and 18 kip (53.4 and 80.1 kN, respectively) single axle loads unless it was retrofitted with dowels and may prove to be unpractical from a design standpoint. While no particular threshold is recommended to limit the subgrade stress to, this should provide a check for the designer in order to deem the design thickness as adequate for long-term protection of the underlying layers. It may also indicate the need for retrofit dowels for in-service pavements that indicate low load transfer at the cracks or joints. The figures used to check against an excessive subgrade stress are found in Appendix E.

Mixed Traffic Designs

When multiple axle designs are required for design of the RCC thickness, another step should be utilized in the design. To do this, the cumulative fatigue damage caused by the mixed traffic must be calculated. This step is modeled after a Miner's hypothesis model of cumulative damage from [14].

First, a trial RCC thickness must be chosen and then the tensile stress for each axle type and temperature gradient combination in the traffic mix must be found from Appendix A. Next, the stress ratio must then be determined from the stresses found and the assumed modulus of rupture of the RCC mix. From the stress ratio, the allowable repetitions for each axle type must be computed using Table 7. The number of allowable load repetitions for each axle design in the traffic mix should be calculated. After this, the fatigue consumption for each axle type should be computed using equation (20).

$$F_n = \frac{N_{expected,\,n}}{N_{allowable,\,n}} * 100\% \qquad (20)$$

where:

F_n	=	fatigue consumption for wheel load *n*, %
$N_{expected,\,n}$	=	expected number of load repetitions of wheel load *n*
$N_{allowable,\,n}$	=	allowable number of load repetitions of wheel load *n*

The fatigue consumption for all of the axle types in the traffic mix should then be added. If the total fatigue consumption is greater than 100%, then the trial pavement thickness should be increased and the process should be repeated. If the total fatigue consumption is less than 100%, the process can be repeated using a thinner trial pavement thickness to see what the thinnest slab thickness is possible which does not result in fatigue consumption over 100%.

To demonstrate this adaptation of the "new" RCC pavement design method, an example design is provided. Three axle types will be used in this example although more can be accommodated. Common design parameters for this example will include the following:

- Modulus of subgrade reaction = 250 psi/in (67.9 kPa/mm)
- RCC modulus of rupture of 600 psi (4140 kPa)
- Positive temperature gradient 25% of the time
- Negative temperature gradient 25% of the time
- No temperature gradient 50% of the time
- Lateral load reliability of 95%

The design parameters that are specific to each axle type for this example are listed in Table 12.

Table 12. Data to be Used in Mixed Traffic RCC Design Example.

	Design Axle Number		
	1	2	3
Design Axle (kips)	12	18	36
Single or Dual tired?	Dual	Dual	Dual
Single or Tandem Axle?	Single	Single	Tandem
Expected Repetitions	200,000	200,000	100,000

The first trial thickness used in this example is 8 inches (203 mm) as seen in Table 13. Using the temperature distribution and lateral load distribution for this case, the design tensile stresses are 183.0, 231.6, and 212.3 psi (1260, 1600, and 1460 kPa) for design axles 1, 2, and 3 respectively. Using the modulus of rupture for this example, the calculated stress ratio would be 0.37, 0.46, and 0.42 for design axles 1, 2, and 3 respectively. Using Table 7 from earlier in this chapter, the allowable repetitions for

these stress ratios can be seen in Table 13. Using equation (20) and summing the results. the total fatigue consumption for all three axles is 182%, larger than the 100% limit for a satisfactory thickness design.

Since the total fatigue consumption for the first trial thickness was greater than 100%, the second trial thickness should be increased. In this example, the trial thickness was increased to 9 inches (229 mm) and the process was repeated as seen in Table 13. In this case, the total fatigue consumption was 43% and the thickness was deemed as the final design thickness.

Table 13. Worksheet for Mixed Traffic RCC Design Example.

1 in=25.4 mm 1 psi=6.89 kPa

	Design Axle Number		
	1	**2**	**3**
Trial Thickness #1 (in)	8		
Design Tensile Stress (psi)	183.0	231.6	212.3
Calculated Stress Ratio	0.37	0.46	0.42
Allowable Repetitions	Unlimited	130,000	360,000
Fatigue Consumption (%)	0	154	28
Total F_N (%)	182		
Decision	**Total F_N is too high Increase trial thickness**		
Trial Thickness #2 (in)	9		
Design Tensile Stress (psi)	165.0	206.1	190.9
Calculated Stress Ratio	0.33	0.41	0.38
Allowable Repetitions	Unlimited	465,000	Unlimited
Fatigue Consumption (%)	0	43	0
Total F_N (%)	43		
Decision	**Total F_N is below 100% Final design thickness is 9"**		

Comparison of Results to Other RCC Pavement Design Methods

Five cases were analyzed using three separate RCC pavement design thickness methods ("new" method outlined in this thesis, PCA method, and the U.S. Army Corps of Engineers method) to make comparisons between the results of each method. The "new method" was analyzed both with and without temperature gradients using both the PCA and Tayabji/Halpenny fatigue relationships summarized earlier in this chapter. The five cases are outlined in Table 14.

Table 14. Data to be Used in RCC Design Comparisons.

1 kip=4.45 kN 1 psi/in=0.271 kPa/mm 1 psi=6.89 kN

	Case No.				
	1	**2**	**3**	**4**	**5**
Design Axle (kips)	12	18	24	30	36
Single or Dual tired?	Dual	Dual	Dual	Dual	Dual
Single or Tandem Axle?	Single	Single	Tandem	Tandem	Tandem
Allowable Repetitions	200,000	300,000	300,000	400,000	1,000,000
k (psi/in)	100	250	400	250	100
RCC MOR (psi)	400	500	800	700	600
Positive gradient	25%	30%	35%	40%	45%
Negative gradient	10%	15%	20%	25%	30%
No gradient	65%	55%	45%	35%	25%
Lateral Load Reliability	75%	95%	90%	99%	99.5%

Case 1 represents an RCC pavement designed under moderate loading conditions with poor subgrade support. Case 2 in Table 14 is the same problem discussed in the example design problem. Case 3 incorporates conditions with good subgrade support and the load

distributed under a tandem axles instead of a single axle. The conditions for Case 4 represent average subgrade support conditions and level of design traffic. Case 5 represents the severe case of the five and should result in the thickest RCC pavement thickness. The results of the design method analysis are listed in Table 15.

Table 15. RCC Thickness Results of RCC Design Comparison in Inches.

1 in=25.4 mm

	Case No.				
Design Method	**1**	**2**	**3**	**4**	**5**
New Method[a] (with temp)	8.5	9	5[c]	7	12
New Method[a] (no temp)	7	8	5[c]	6.5	9.5
New Method[b] (with temp)	6.5	7	5[c]	5.5	8.5
New Method[b] (no temp)	6	6.5	5[c]	5	7.5
PCA Method	8	8	5	6.5	8
U.S. Army Corps of Engineers	7.5	7.5	4.5	6	8

[a] Using PCA fatigue relationship

[b] Using Tayabji/Halpenny fatigue relationship

[c] 5 inches (127 mm) is the thinnest RCC pavement section using this method

In all cases, the "new" method using the conservative PCA fatigue relationship while incorporating temperature gradients resulted in the thickest RCC pavement sections. The same method and fatigue relationship were also utilized without a temperature differential across the depth of the pavement, resulting in 7-20% thinner pavements. Using the "new" method with the Tayabji/Halpenny fatigue relationship and temperature considerations resulted in 21-29% thinner pavements than designs using the

same method using the PCA fatigue relationship. When temperature was not considered, the Tayabji/Halpenny fatigue relationship resulted in 14-23% thinner pavements than those cases designed using the PCA fatigue relationship.

In general, the PCA and U.S. Army Corps of Engineers RCC design methods predicted similar RCC thicknesses with the PCA design method predicting a thickness of 0.5 inches (13 mm) greater than the U.S Army Corps of Engineers method in almost every case. Both the U.S. Army Corps of Engineers and PCA design methods resulted in similar thicknesses when compared to the "new" method at 75 or 90% lateral load reliability and no temperature considerations. This seems logical since the "new" method is based on the same fatigue relationships used in the PCA design method, which also does not incorporate temperature-related stresses.

A significant increase in the design thickness can be seen by increasing the reliability of the lateral load location as seen in Figure 34. It is important to note that the lateral load reliability does not represent the reliability of the entire pavements design. Variability in other design variables such as load magnitude, modulus of rupture for the RCC, modulus of subgrade reaction, etc. could lessen the cumulative reliability level of the design. In Case 1 and 2, a 43% increase in thickness was required when the lateral load reliability went from 50% to 99.5%. Other cases (except for Case 3) showed similar increases in the design thickness in order to attain higher levels of reliability. Case 3 did not require an increase in thickness because for all levels of lateral load reliability, the design required was less than the minimum thickness design attainable by this method.

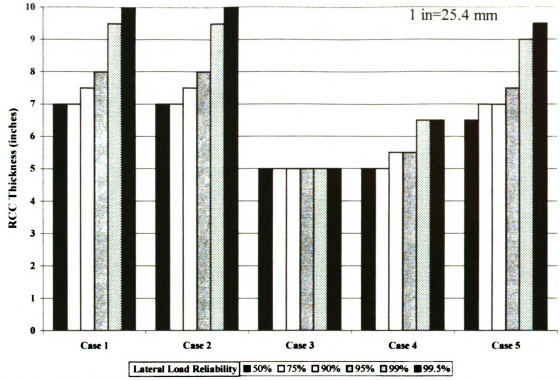

Figure 34. Effect of Reliability on "New" Method Thickness Without Temperature.

If the various temperature conditions are considered using the "new" method, an average increase in thickness of 18% resulted in comparison to when the temperature considerations were not employed. The impact of the lateral load placement reliability when temperature conditions are considered on the pavement thickness for all five cases can be seen in Figure 35. Again, no change in the design thickness for Case 3 was realized because the design required was less than the minimum thickness design possible using this method.

If both the temperature gradients and the level of lateral load placement reliability are considered as in the "new" method, thicker RCC pavements will be designed. However, thicker RCC slabs with the same level of aggregate interlock factor will analytically produce higher load transfer across transverse cracks, resulting in an increased fatigue life. This will be discussed more in Chapter 5 of this thesis.

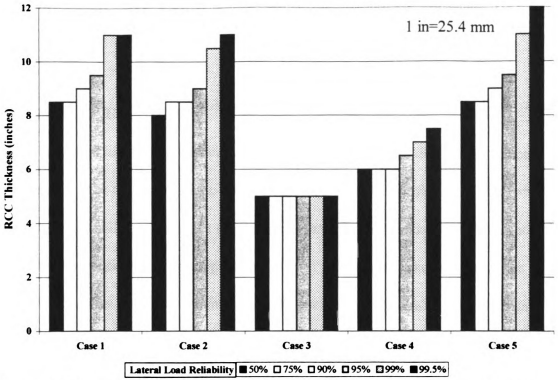

Figure 35. Effect of Reliability on "New" Method Thickness With Temperature.

- CHAPTER V -

Investigation of RCC Pavement Alternatives

DESIGN ALTERNATIVES

Although load transfer efficiency was found to have little effect on the critical tensile stress to be used in a fatigue-based design, a high load transfer aids in the reduction of faulting and spalling potential at the crack or joint. From an initial design standpoint, two alternatives exist for increasing load transfer at a transverse crack or joint. The first alternative includes saw cutting joints at closer spacings than natural cracks spacings in order to decrease crack widths while the second alternative involves increasing the design thickness so that the stress can be distributed over a larger depth.

Engineered Joint Spacing

As discussed in Chapter 3, RCC pavements that are allowed to naturally crack in the transverse direction often crack at spacings much larger than those of conventional concrete sections (typically 15 to 30 feet, or 4.6 to 9.1 m). With thermal and volumetric changes of the RCC pavement, large crack widths result which are not conducive to effective load transfer. This low load transfer, in turn, results in high deflections and tensile stresses as a load passes over the crack resulting in premature fatigue damage as well as an increased potential for faulting. Water and other incompressibles can easily enter the crack and underlying layers of the pavement resulting in pumping of the base material and locking up of the crack. When incompressibles enter the joint or crack of a rigid pavement, there is a loss of movement between the slab and stress concentrations

occur near the discontinuity. In combination with thermal expansions and/or exterior loadings, these stresses can surpass the strength of the concrete material and cause the joint or crack to spall. When pumping of the underlying materials occurs, a loss of support usually occurs on the leave side of the crack or joint. This loss of support can cause a cantilever effect of the concrete slab, thereby increasing tensile stresses and causing corner cracks. These phenomenon can be avoided if addressed in the design and maintenance of the pavement.

If joints are engineered at spacings less than 30 feet (9.1 m), data from Chapter 3 and Appendix D has shown that crack widths have been fairly tight and the resulting load transfer efficiencies have been above an acceptable level (generally over 80%).

Joints are normally sawed after the RCC has begun the hydration process and as closely timed to after the rolling process has occurred. This technology requires water to cool the saw blade since the RCC has already been rolled and achieved considerable strength. Another way joints may be cut involves the use of a vibrating plate (Figure 36) at a very early age before final rolling of the RCC pavement. This technology has produced effective joints in RCC bases in the United Kingdom as seen in Figure 37. To do this, the vibrating plate is used to cut a groove into the freshly laid RCC pavement. A bitumen fill is then poured into the groove using a watering can and the pavement and joint are then re-rolled. The cracks then open up after a few days due to temperature and volumetric changes. This process has the benefit of lower construction costs over the saw blade cutting procedure with similar success in forming joints in RCC pavements.

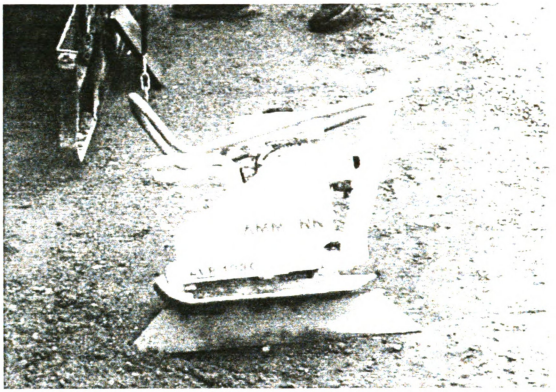

Figure 36. Vibrating Plate with Welding Fin for Use in Inducing Joints.

Figure 37. Inducing of Joints Using the Vibrating Fin in an RCC Base.

Increased RCC Slab Thickness

Analytically for a constant level of AGG, an increased thickness will not provide a substantial increase in load transfer across a crack or joint. Under a given load however, the increased thickness will reduce the tensile stresses near the crack or joint in a rigid pavement.

Figures 38, 39, and 40 represent trends developed using ISLAB2000 to determine stress levels near the joint or crack for an 18 kip (80 kN) dual-tired axle placed at that joint or crack for modulus of subgrade reaction levels of 100, 250, and 400 psi/in (27.1, 67.9, and 108.6 kPa/mm), respectively. These figures can be used to determine relative stress levels for different RCC thicknesses as related to the level of deflection load transfer efficiency. From these figures, it can be concluded that tensile stress levels decrease with very high levels of LTE_{δ}. A breaking point can be seen in all three figures. At LTE_{δ} levels below these thresholds, LTE_{δ} has little bearing on the tensile stress near the joint or crack. For thicker pavements, this threshold point is at levels of LTE_{δ} greater than 90%. For thinner pavements such as the 6 and 8 inch (152 and 203 mm) thick RCC pavements, this breaking point is at a level of LTE_{δ} closer to 70 or 80%. This would suggest that the thicker slabs would tend to have less reliance on load transfer to reduce tensile stresses. By doing this, the thicker pavements provide a more reliable method of stress reduction than thinner pavements. If the thinner pavements lose load transfer due to aggregate attrition, opening of the crack due to temperature, etc., they will undergo a much larger level of tensile stress than desirable.

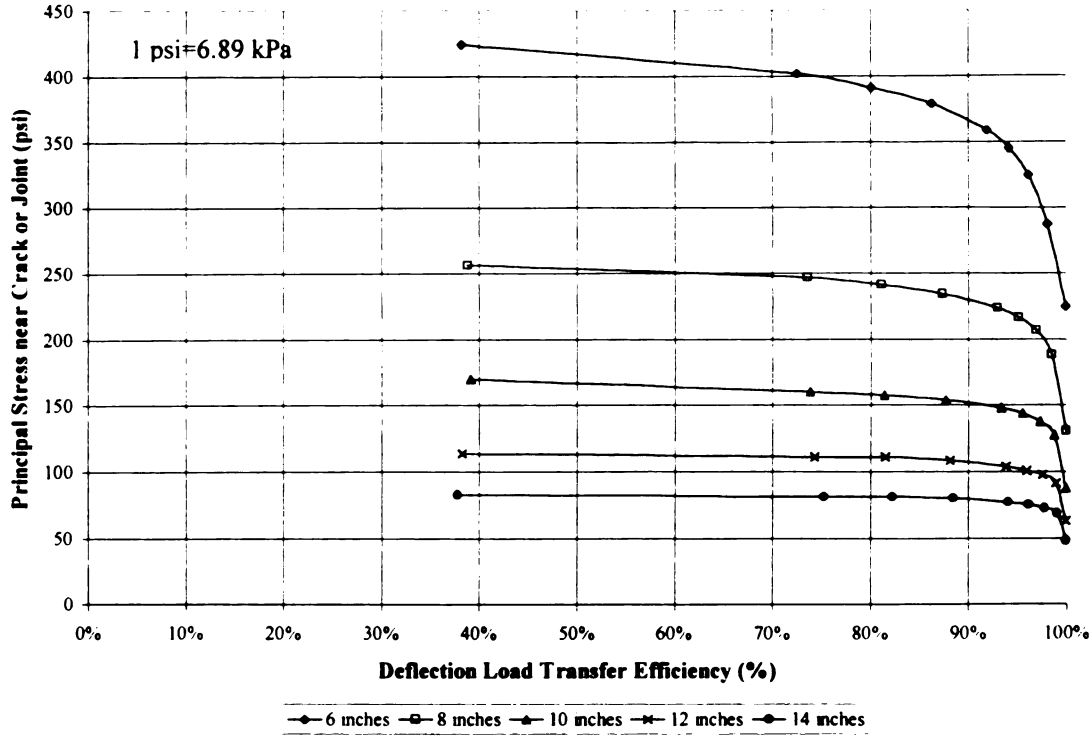

Figure 38. Effect of LTE_δ on Tensile Stress near the Crack or Joint for k=100 psi/in (27.1 kPa/mm) and No Temperature Gradient.

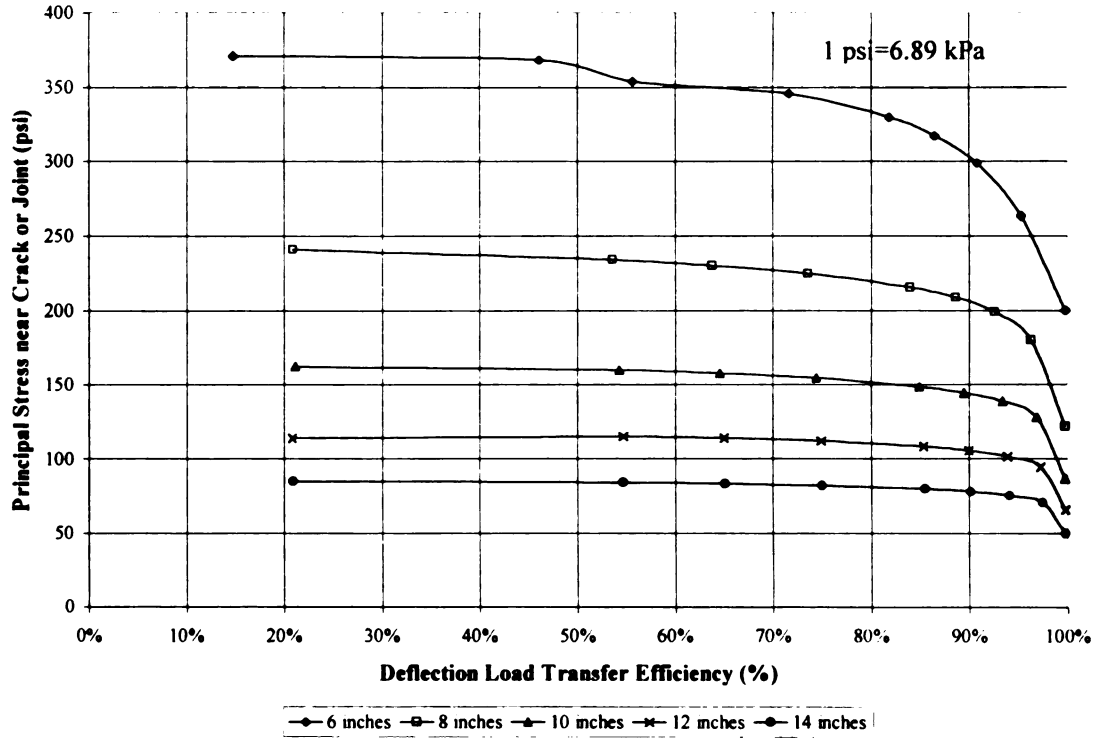

Figure 39. Effect of LTE_δ on Tensile Stress near the Crack or Joint for k=250 psi/in (67.9 kPa/mm) and No Temperature Gradient.

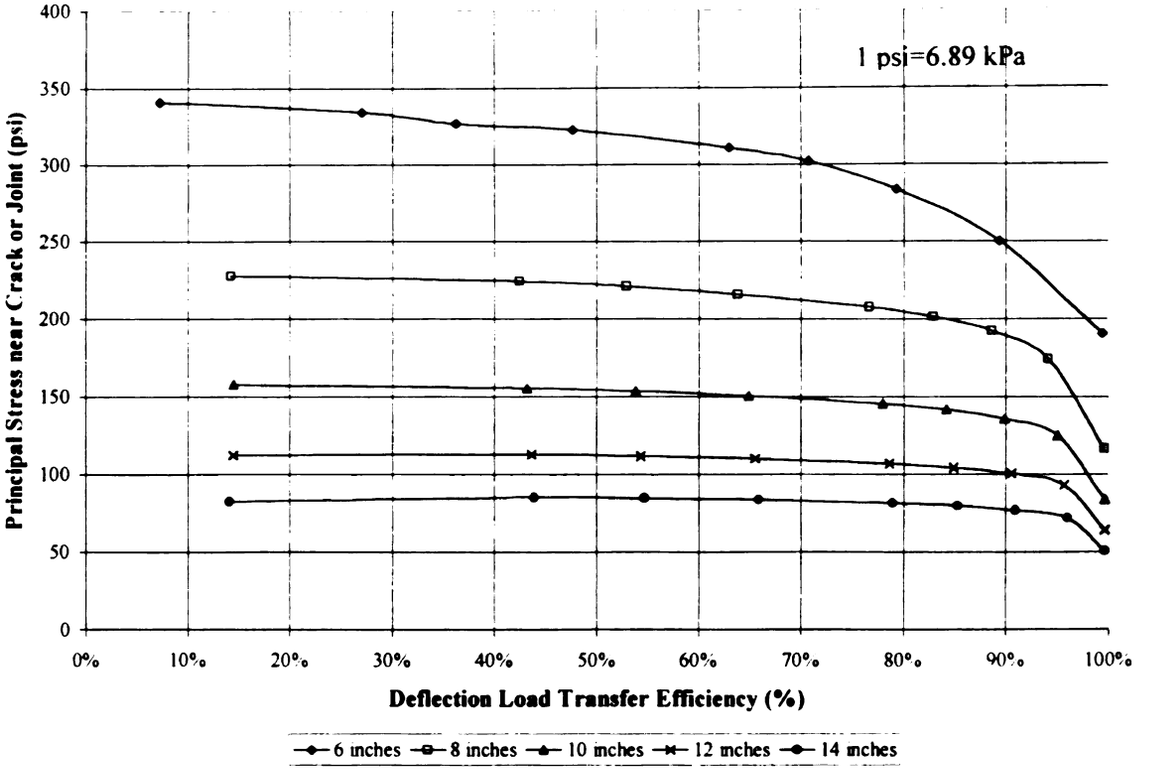

Figure 40. Effect of LTE_δ on Tensile Stress near the Crack or Joint for k=400 psi/in (108.6 kPa/mm) and No Temperature Gradient.

DOWEL BAR RETROFITTING AS A REHABILITATION ALTERNATIVE

After an RCC pavement is constructed, few options exist for increasing load transfer across a joint or crack. An economical and reliable option is dowel bar retrofitting (DBR).

This section aims to study the benefits of DBR as both preventive and corrective maintenance on transverse cracks in RCC pavements. Using the finite element computer program ISLAB2000, iterations were made to model cracks with aggregate interlock as the sole means of load transfer at various levels of AGG. The same cases were then analyzed with dowel bars inserted so that load transfer could be achieved through aggregate interlock as well as through the dowel bars. In both cases, load transfer

efficiency and the critical tensile stress were computed in order to examine the immediate theoretical benefits of retrofitted transverse cracks in RCC pavements.

To test the validity of these theoretical benefits, data from FWD tests of actual PCC pavement dowel bar retrofitted sites in both Michigan and Washington was utilized. The field tests were found to correlate well with the theoretical prediction of load transfer efficiency in most cases. Cases where the theoretical and field data did not match well were investigated for possible explanations of disparity.

In conjunction with long-term performance data on dowel bar retrofitted sites, this study should help pavement engineers develop a better understanding of the proper timing of dowel bar retrofits.

Overview

Load transfer across transverse cracks is critical to the maintenance of satisfactorily performing RCC pavements. In an ideal situation, both sides of a crack or joint an RCC pavement should share in supporting the load as it is transferred from one side of the crack or joint to the other. By doing this, deflections and their ensuing damage to the pavement can be reduced [42].

Back in 1933, Benkelman [28] noted that when the crack faces of two slabs are held firmly together, the aggregate interlock can be expected to function permanently as a load transfer mechanism. While this may be true to a certain extent, wear of the aggregates and opening of the joints due to time and traffic can cause loss of load transfer capacity. However, this type of load transfer is highly dependant on material properties of the concrete, such as coarse aggregate type and size, mix design, and gradation [43].

Low severity shrinkage cracks can also develop into structural fatigue cracks through a loss of load transfer. Raja and Snyder [44] note that abrasion of the crack faces and opening of the cracks over time can lead to intrusion of water and incompressibles into the cracks. This phenomenon can lead to a loss of load transfer, resulting in increased slab deflections, pumping, faulting, and spalling at the crack.

Loss of load transfer across transverse cracks results in increased internal tensile stresses in the pavement and can lead to more fatigue cracking and loss of structural integrity in the pavement [45].

Just like many RCC pavements, many older PCC pavements have initially relied on aggregate interlock for load transfer at engineered joints. Transverse cracks that have formed between these joints have relied on aggregate interlock to maintain the adequacy of the pavement structure. With the United States Interstate Highway system deteriorating, a method for increasing load transfer at these joints and cracks was needed. A rehabilitation method of retrofitting dowel bars at these transverse cracks and joints was then utilized.

Although dowel bar retrofitting has been in use since a 1975 German project, it was not until 1980 when the Federal Highway Administration (FHWA) awarded a research project to the Georgia Department of Transportation (DOT) to evaluate multiple devices aimed at restoration load transfer on I-75, including dowel bars. After 10 years of performance, the dowel retrofitted sites were evaluated using an FWD. Surprisingly, many of the dowel bars were still performing at optimum efficiency. While other dowel bars did not exhibit the same performance, the Georgia DOT was satisfied with the overall results of these first dowel bar retrofits [46]. In another study, Snyder et al. [45] also

concluded that retrofit dowels were most effective device to increase load transfer in both joints and cracks of PCC pavements.

Since the early 1980's, other states have utilized dowel bar retrofitting with much success as well. Over time, dowel bar retrofit construction has been refined to combat problems with overconsolidation of the concrete covering, spalling of the sawed slots, and misalignment of the dowels.

Importance of Dowel Bar Retrofitting

Dowel bar retrofitting can be utilized as either a preventive or corrective maintenance tool for rigid pavements. Mamlouk et al. [47] defines preventive maintenance as "the planned strategy of cost effective treatments to an existing roadway system and its appurtenances that preserves the system, retards future deterioration, and maintains or improves the functional conditions of the system without necessarily increasing structural capacity." Therefore, DBR as a preventive maintenance measure is applied only to rigid pavements in a satisfactory condition in an attempt to eliminate or reduce future faulting, pumping, corner breaks, and spalling.

In the case of preventative maintenance, the dowel bar retrofit does not immediately benefit the pavement from a structural standpoint after the rehabilitation in terms of stresses or load transfer efficiency. However, the deterioration of stress and load transfer efficiency over time is widely believed to occur at a lesser rate, thereby increasing the structural life of a concrete pavement. While reliable deterioration models for DBR cracks do not exist at this time, field evaluation of dowel bar retrofits on a repeated basis has been occurring (most notably in Washington state [48,49]) for many years in PCC

pavements. This data will eventually be used in part to assess the long-term benefits of dowel bars versus aggregate interlock as a means of long-term load transfer.

Laboratory testing of dowel bar retrofits in cracked PCC slabs is currently being conducted at the University of Minnesota using the Minnesota Accelerated Loading Facility (Minne-ALF). The goals of these tests are to determine the effects of selected design and construction variables, such as joint face texture, repair backfill material, and dowel material and length, on retrofit dowel load transfer system performance as well as to determine the variability in Minne-ALF test results [50]. The results of these tests will eventually be able to provide relative comparisons of the benefits of aggregate interlock and various design features in dowel bar retrofits.

Corrective maintenance is a necessary action conducted on a pavement to increase its performance to a satisfactory level. The defining distinction between preventive and corrective maintenance is the timing of the rehabilitation as seen in Figure 41. When the rehabilitation occurs below a given threshold, it is deemed as corrective maintenance. In general, there has not been clear threshold universally accepted by the pavement community for dowel bar retrofitting [51]. The corrective maintenance procedure for dowel bar retrofitting is similar to that of the preventive maintenance process except that faulted joints or cracks may need to be diamond ground.

In corrective maintenance cases, dowel bar retrofitting usually provides increased load transfer efficiency and reduced stresses at the cracks or joints, thereby increasing the life of a rigid pavement. While the performance of dowel bars which were inserted in corrective maintenance cases may differ than that of preventive maintenance cases, corrective maintenance provides an initial increase in performance and extended pavement

life as seen in Figure 42. The performance of the pavement for any period of time can be maximized by increasing the total area under a curve similar to one from Figure 42 [52]. In both preventive and corrective maintenance scenarios, dowel bar retrofitting provides a mechanism by which cracks and joints may have prolonged load transfer and its associated benefits.

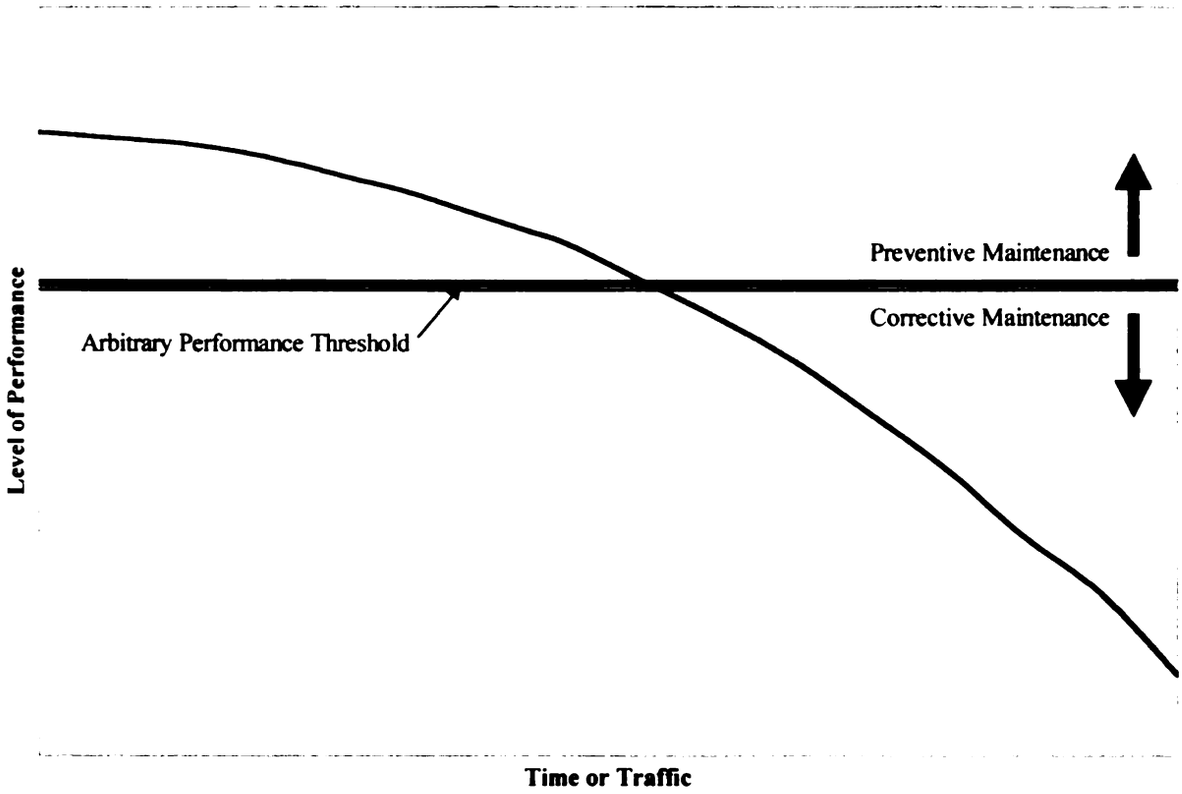

Figure 41. Distinction Between Preventive and Corrective Maintenance.

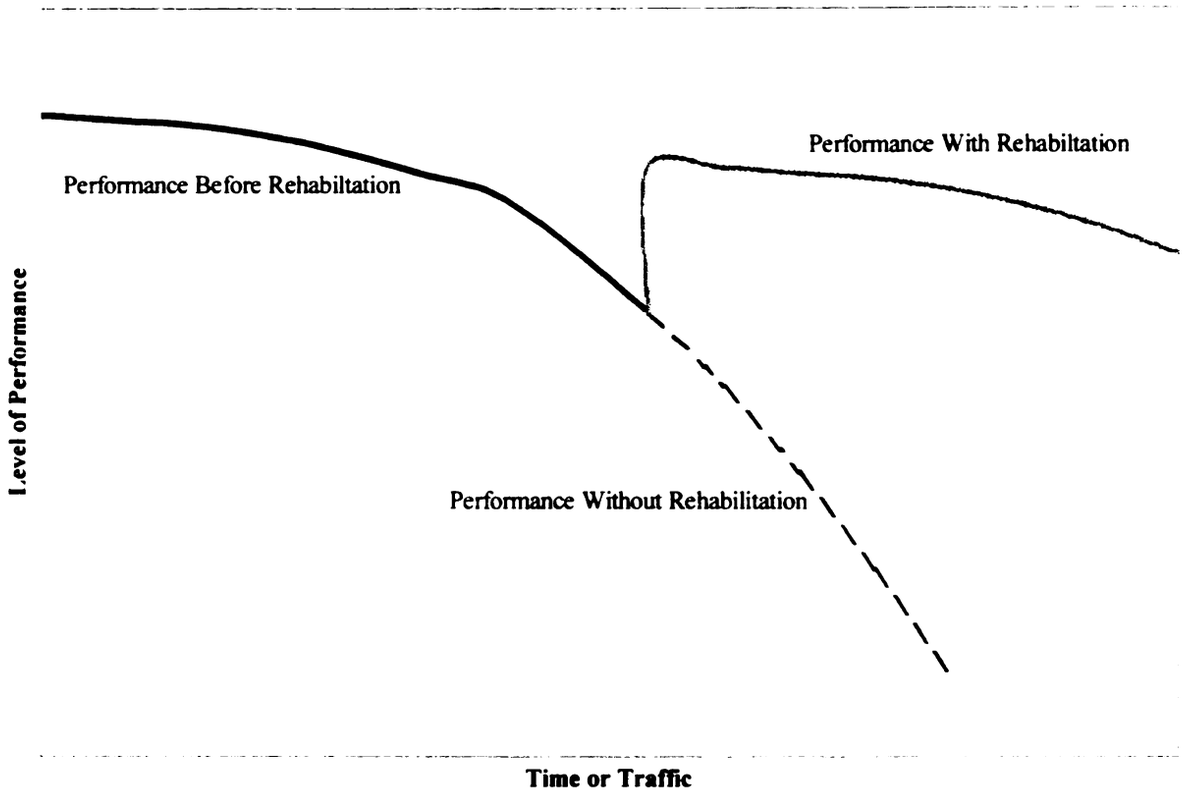

Figure 42. Comparison of Performance Benefits of Rehabilitation Over Time.

Current Methodology of Selection

For PCC pavements, most agencies select cracks and joints that are candidates for dowel bar retrofitting on a project basis. Each project would include many miles of structurally sound concrete pavement with unspalled, primarily transverse cracks that extend to the shoulder. All cracks (or joints if originally undoweled) that match these criteria would be retrofitted with dowel bars provided that the spacing allowed such rehabilitation. Severely spalled transverse cracks are normally treated with full-depth patches since the concrete near the crack is not structurally adequate to hold dowel bars over time. As of this time, dowel bar retrofitting has not been widely used as a method of

rehabilitation of load transfer in RCC pavements. However, the criteria for such rehabilitation would be concurrent with that of PCC pavements.

Cracks or joints can be selected for dowel bar retrofitting on the basis of falling-weight deflectometer (FWD) testing. An FWD is a device that applies an impulse load, using a circular load plate, to a pavement and measures the resulting pavement deflections through a series of sensors. When one side of a crack or joint is loaded by the FWD, the other side will respond as well. The amount of response on the unloaded side of the joint or crack is proportional to its load transfer capability. The response of the unloaded side to the loaded side is termed deflection load transfer efficiency (LTE_δ) as mentioned in Chapter 3 of this thesis.

Analytical Modeling

Finite element analysis using ISLAB2000 was conducted on RCC pavement sections representing ranges of variables which are typical of all rigid pavements including:

- Modulus of subgrade reaction (k): 100, 250, 400 psi/in. (27.1, 67.9,108.6 kPa/mm)
- Concrete thickness (h): 6, 8, 10, 12, 14 inches (152, 203, 254, 305, 356 mm)
- Aggregate interlock factor (AGG): 100 to 1,000,000 psi (1.0 to 6,900 MPa)
- Temperature difference: 0, -15, +15°F (0, -8.3, +8.3°C)

Other material and geometric properties were set at constant values for this analysis. These constant values included the following:

- Slab length: 30 feet (9.1 m)
- Slab width: 12 feet (3.7 m)
- Elastic Modulus: 4,000,000 psi (27,600 MPa)
- Poisson Ratio: 0.15
- Coefficient of Thermal Expansion: $4.4*10^{-6}$ in/in/°F ($7.9*10^{-6}$ mm/mm/°C)
- Unit Weight: 150 lb/ft^3 (2,400 kg/m^3)
- Dowel Bar Properties

- Diameter: 1.25 inches (32 mm)
- Elastic Modulus: 20,000,000 psi (138,000 MPa)
- Poisson's Ratio: 0.20
- Dowel Length: 18 inches (460 mm)
- Locations 12, 24, and 36 inches (0.3, 0.6, 0.9 m) from longitudinal edges as seen in Figure 43.

All of the pavements in this analysis assumed no contribution to the load transfer occurred from a shoulder. This is usually the case when either an asphalt or gravel shoulder is present which is the case in the vast majority of older PCC pavements and almost all RCC pavements.

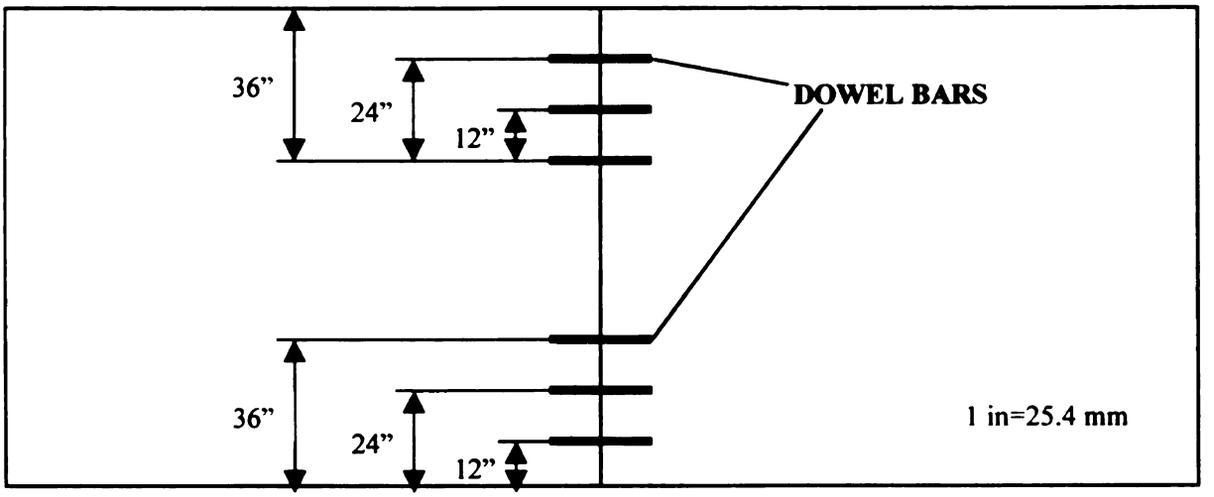

Figure 43. Dowel Bar Retrofit Locations for ISLAB2000 Modeling.

To simulate the load placed by an FWD while testing for deflection load transfer efficiency, a 18,000 lb (80 kN) axle load was placed on one side of a modeled crack as seen in Figure 44. The same matrix of parameters was analyzed with and without dowel bars in order to characterize the benefits of a simulated dowel bar retrofit. To simulate the dowel retrofit, two sets of three dowel bars were placed at mid-depth in the wheel paths at 12 inch (0.3 m) spacings. The elastic modulus of the patching mix that covers the embedded dowel bars was assumed to be the same as that of the rest of the concrete.

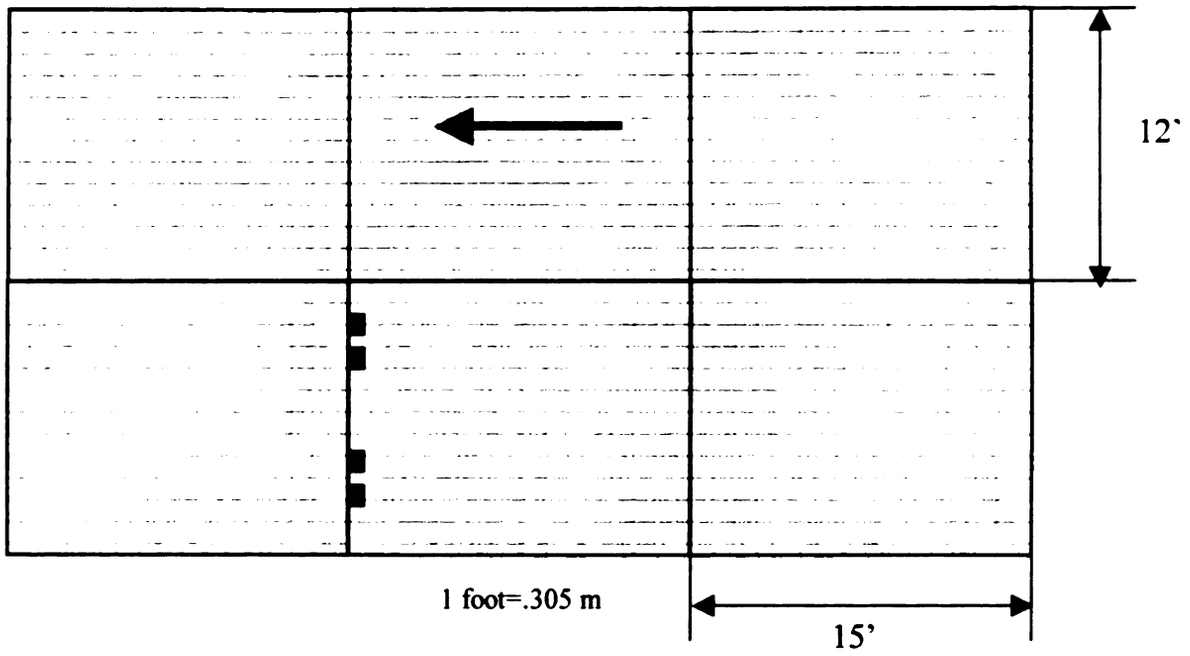

Figure 44. Slab Dimensions and FEA Mesh for Joint/Crack Load Position.

For all cases without dowel bars, the load transfer efficiency was analytically found for different levels of AGG. The same cases were then evaluated with dowel bars and the same levels of AGG. This method of analysis assumes that no loss of aggregate interlock was achieved by cutting slots for the retrofit dowels. The load transfer efficiencies in both cases were then compared to assess the increase in load transfer due to dowels. Figure 45 provides an example for LTE_δ with respect to AGG for both before and after a dowel bar retrofit for the case of h = 8 inches (203 mm), k = 250 psi/in (67.9 kPa/mm), and ΔT = 0°F (0°C). Figure 63 shows the principal tensile stresses near the crack for before and after a dowel bar retrofit for the same levels of h, k, and ΔT as in Figure 45.

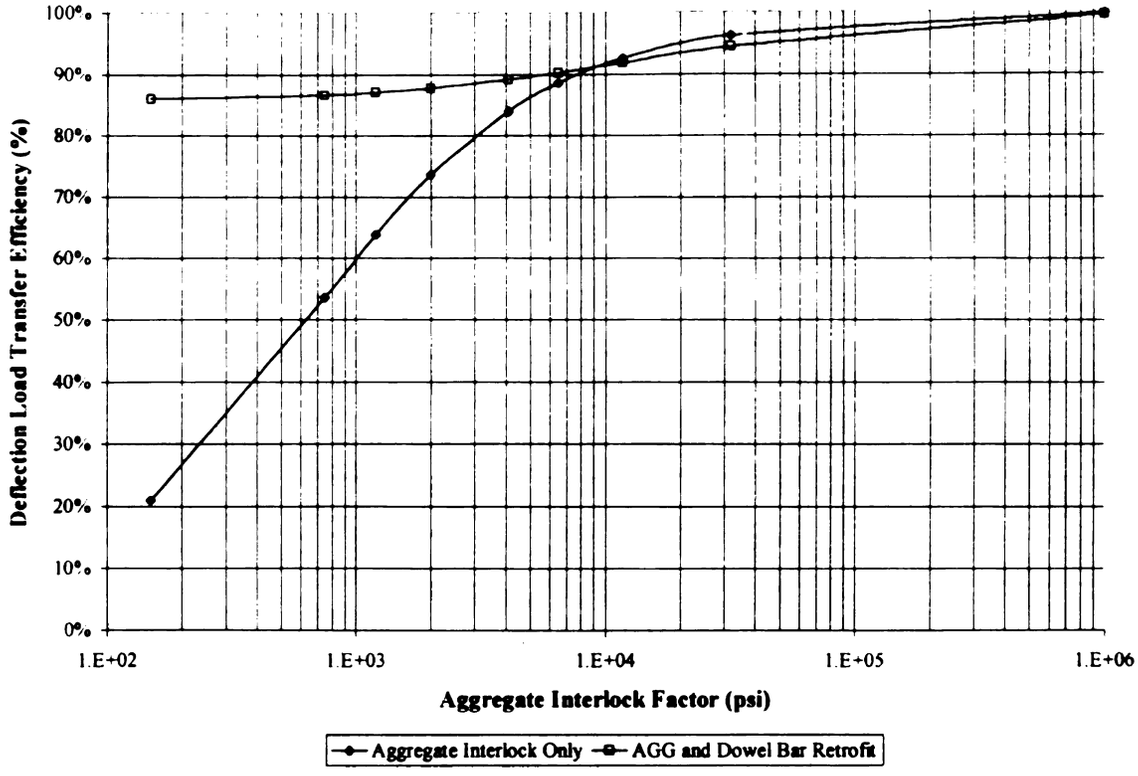

Figure 45. Example of LTE_δ Increase for Given Levels of AGG.

In Figure 46, there is a distinct separation between the curve representing aggregate interlock as the sole means of load transfer and the curve representing aggregate interlock with the benefit of retrofit dowels to aid in load transfer. This break represents the point where dowels aid in increasing LTE_δ for a given crack or joint. In this case, the break is near an LTE_δ of 91%. If a dowel bar retrofit occurs when LTE_δ is greater than this level for h = 8 inches (203 mm), k = 250 psi/in (67.9 kPa/mm), and ΔT = 0°F (0°C), these analytical trends would suggest that no immediate benefit in LTE_δ would be realized. This is important to note for any pavement owner that is considering using dowel bar retrofitting as a rehabilitation method.

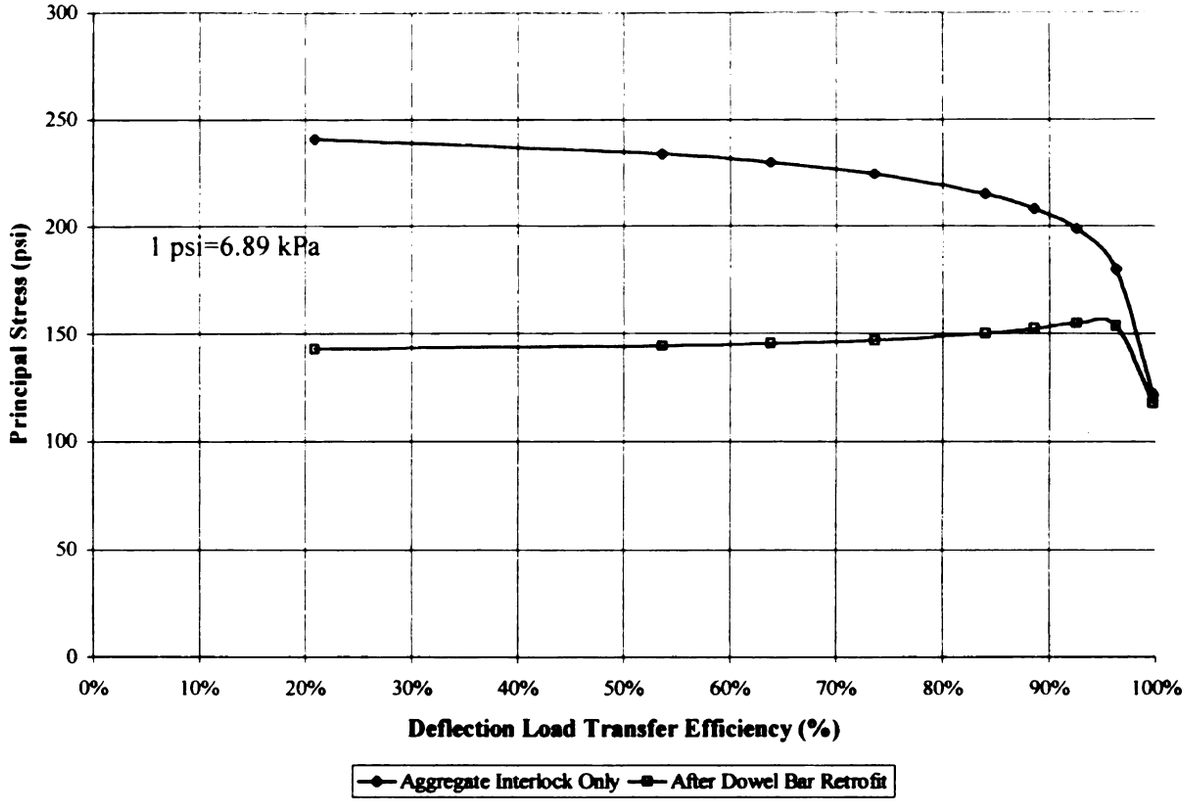

Figure 46. Example of Reduction in Maximum Tensile Stresses By Using DBR.

Figure 47 shows the same data as in Figure 45, but instead avoids the immeasurable parameter of AGG to determine LTE_δ after a dowel bar retrofit from the initial LTE_δ for the case of h = 8" (203 mm), ΔT = 0°F (0°C), and various levels of k. From Figure 47 (and for other similar curves for different levels of h, k, and ΔT), it is seen that a significant improvement in LTE_δ can be achieved through dowel bar retrofitting. Increases of up to 85% can be achieved in LTE_δ, theoretically. Figure 47 also illustrates that the increase in LTE_δ is dependant on the modulus of subgrade reaction. Lower levels of subgrade support generally provide greater increases in LTE_δ.

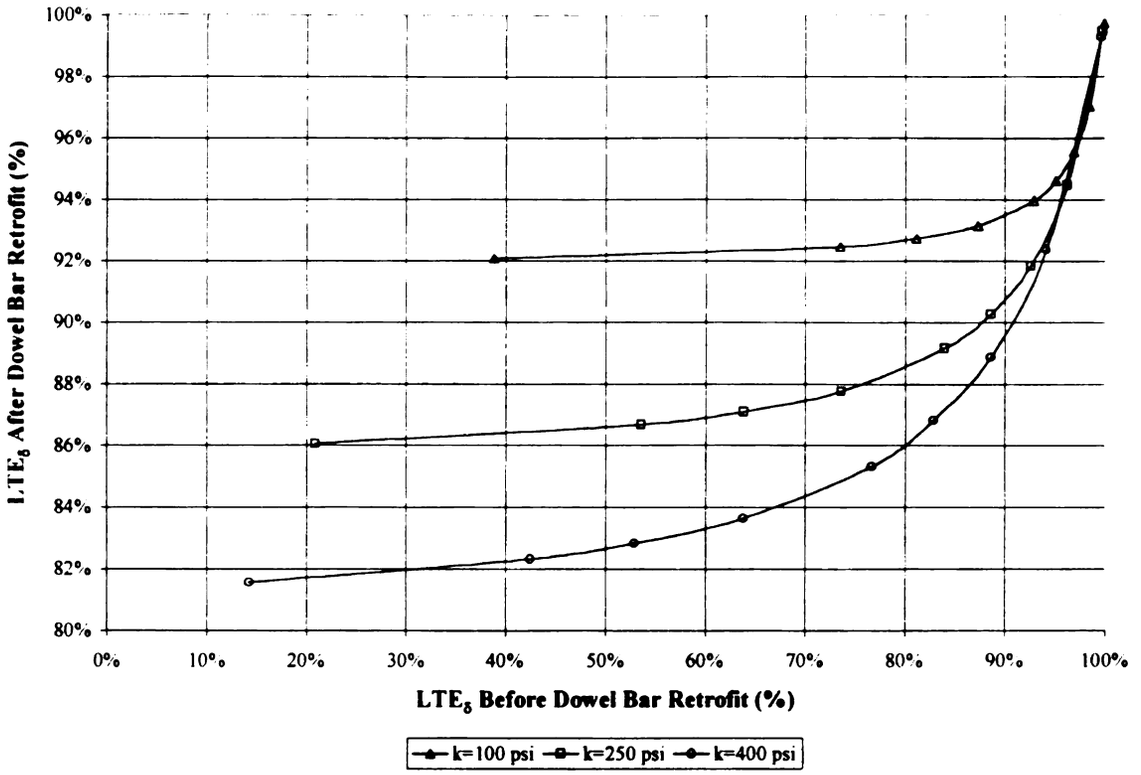

Figure 47. Example of Final LTE$_\delta$ for Given Levels of Original LTE$_\delta$.

Field Validation of Analytical Results

To justify the analytical models which were produced using ISLAB2000, FWD data from actual dowel bar retrofit sites were utilized. FWD data from both before and after the dowel bar retrofits were utilized from both Michigan and Washington state sites. This data is from conventional PCC pavement sites. However, the predicted gains in load transfer should be applicable to all types of rigid pavements, including RCC pavements, if proper construction and selection criteria are maintained.

Michigan Dowel Bar Retrofit Sites

In the state of Michigan, the dowel bar retrofit sites include the following:

- I-69, Eaton County, South of Lansing, MI
- I-75, Monroe County, North of Toledo, OH
- M-14, Washtenaw County, East of Ann Arbor, MI

With the exception of some cracks on the I-69 site, the Michigan sites have been primarily preventive maintenance projects with the intention to increase the LTE_δ of tight transverse cracks over the design period of the dowels.

The trend in Figure 48 was developed by analyzing a dowel bar retrofit with h = 9 inch (229 mm), the design thickness of the I-69 pavement. By using a backcalculation method (ERES method described in Chapter 3) to estimate the modulus of subgrade reaction to model for this site, it was determined that k = 250 psi/in (67.9 kPa/mm), modeled as a Winkler foundation, was appropriate. Each triangle in Figure 48 and the following figures represents a crack retrofitted with dowels and non-destructively evaluated using an FWD. The analytical trend corresponds well with the field-tested cracks at all levels of LTE_δ. Unlike the other Michigan sites, several cracks on the I-69 site exhibited low levels of LTE_δ before dowel bar retrofitting to help substantiate the predicted trend for the entire range of LTE_δ values.

The I-75 site was designed to be an 11 inch (279 mm) PCC pavement with an asphalt shoulder serving as the main north-south interstate route in Michigan. Backcalculation procedures resulted in a modulus of subgrade reaction value near 250 psi/in (67.9 kPa/mm) for use in modeling this site. The trend developed using these values in modeling the dowel bar retrofit is seen in Figure 49. As a preventive maintenance section, the expected values of LTE_δ after the dowel retrofit should be very near the initial high values of LTE_δ.

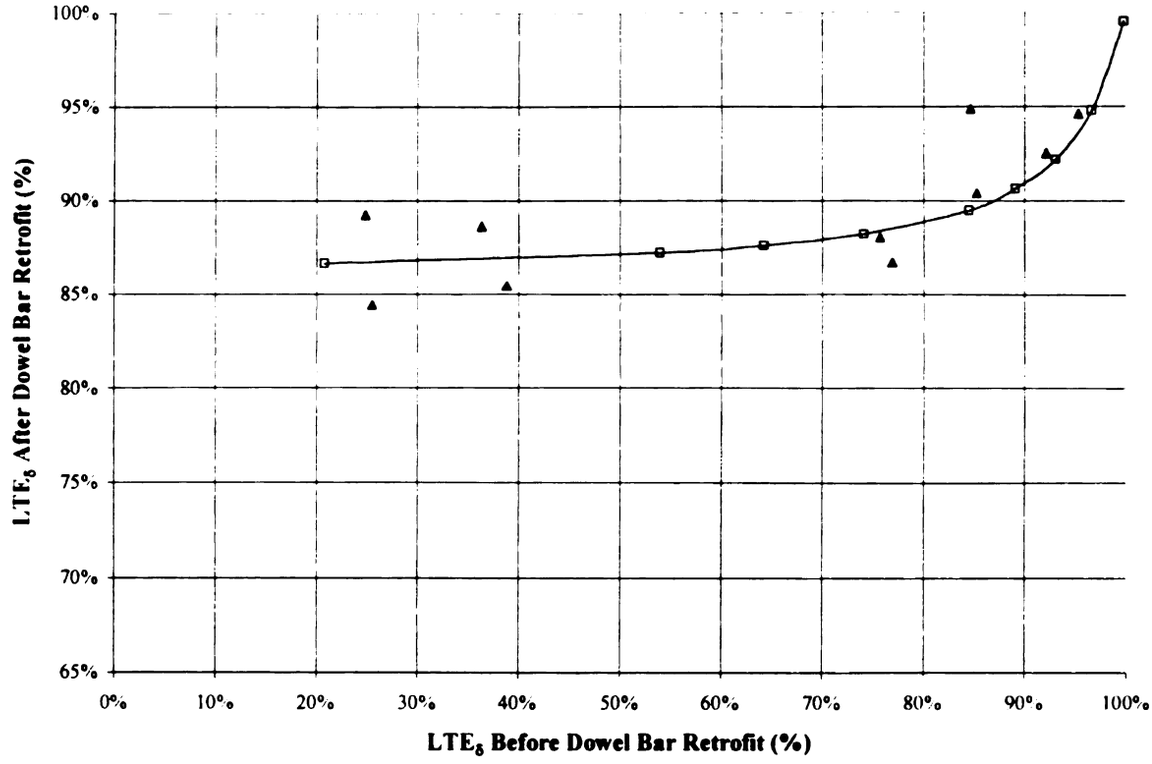

Figure 48. Field Verification of LTE$_\delta$ for DBR Site on I-69 in Michigan.

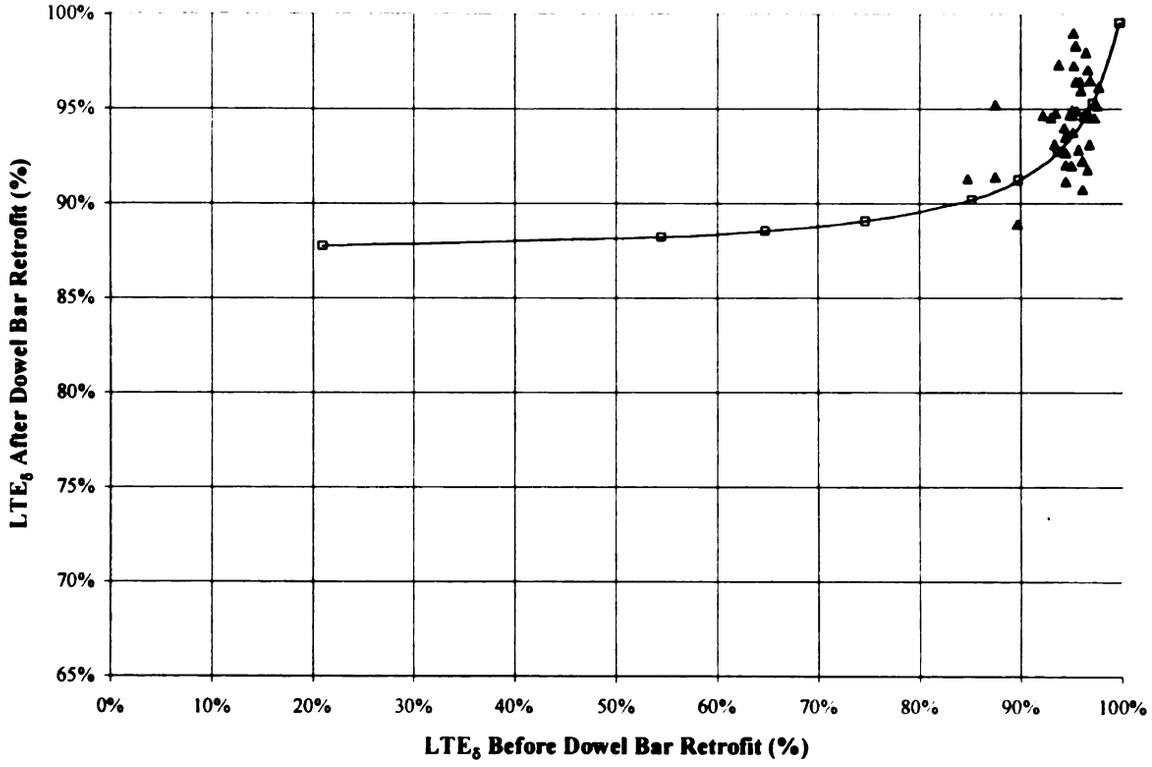

Figure 49. Field Verification of LTE$_\delta$ for DBR Site on I-75 in Michigan.

The data points and trend in Figure 49 demonstrate that little loss or gain in LTE_δ is developed initially following dowel retrofitting in these cases. The benefits of these dowel bar retrofits are based upon long-term preservation of load transfer across these cracks.

As with the I-75 site, the dowel bar retrofitting on M-14 in Michigan was a preventive maintenance measure. The PCC layer was designed to be 9 inches (229 mm) thick with an asphalt shoulder. A modulus of subgrade reaction was found to be near 250 psi/in (68.7 kPa/mm) again using backcalculation of mid-slab FWD tests. However, Figure 50 illustrates a very poor correlation between the cracks which were tested using the FWD and the predictive trend. In over 80% of the cases, the cracks exhibited lower levels of LTE_δ after the dowel bar retrofittings than before any rehabilitation occurred.

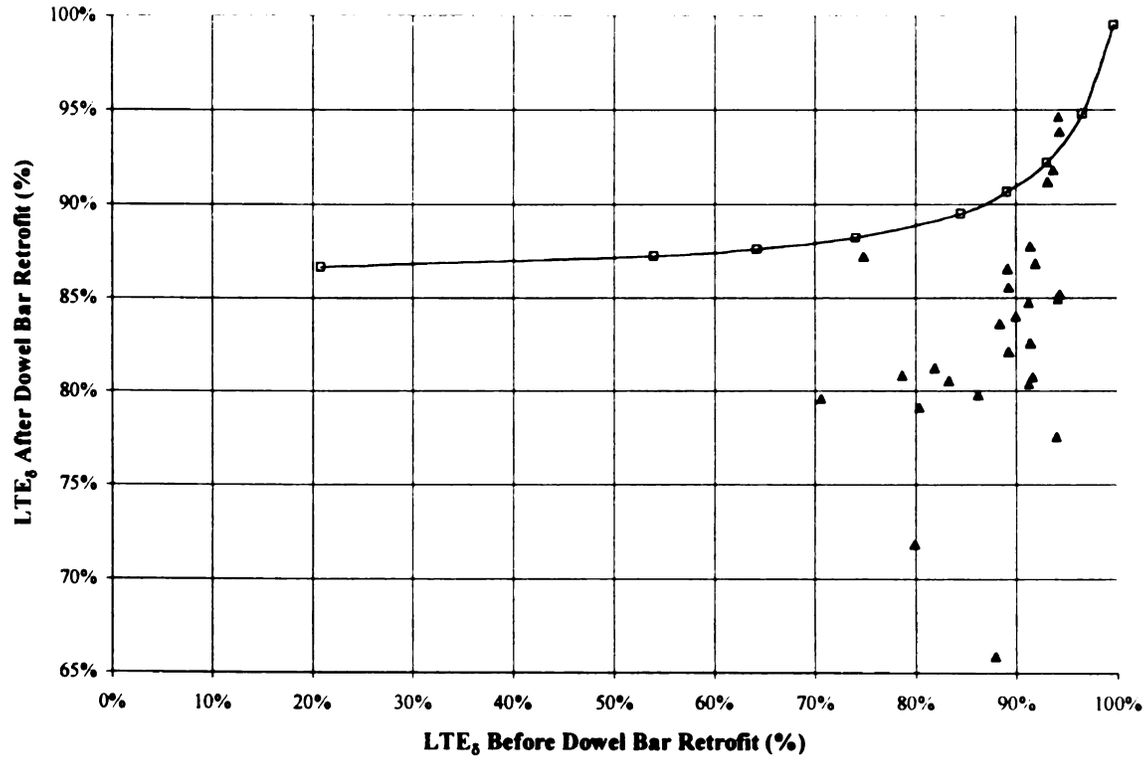

Figure 50. Field Verification of LTE_δ for DBR Site on M-14 in Michigan.

A visual observation of the M-14 site in Figure 51 reveals a problem with spalling of the grout material covering the retrofit dowels, which may have lead to this

discrepancy. Without a solid base of concrete for the dowel bars to bear against as loads cross these cracks, the retrofits could not provide added load transfer. An investigation of the rehabilitation construction found that there was a problem controlling the consistency of the grout material as it came out of the mobile mixer. The mix was originally very dry, so water content was increased on site. This resulted in a very wet consistency with many of the fines rising to the surface after vibration. This reduced the air voids near the surface, thereby increasing delamination potential and decreasing freeze-thaw resistance. A petrographic investigation of cores taken from the site by the Michigan Department of Transportation revealed that the top 1 to 1 ½ inches (25 to 38 mm) of the grouting material had very few air voids and led to the premature delamination [47].

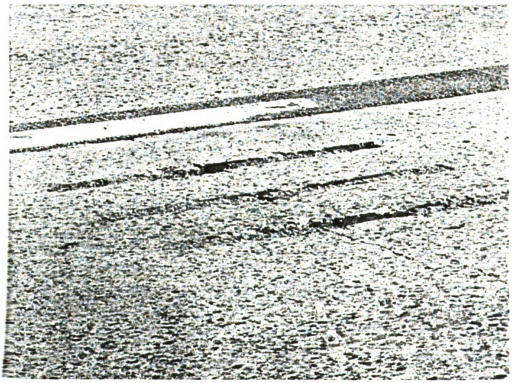

Figure 51. View of Spalling in Grout Covering of M-14 DBR Site.

Washington State Dowel Bar Retrofit Sites

In Washington State, the Washington Department of Transportation set up a PCC Pavement Rehabilitation Test Section on I-90 west of Cle Elum, WA which included some sections which were retrofitted with dowel bars as a rehabilitation technique for transverse cracks. This site was a 9 inch (229 mm) thick plain jointed concrete pavement resting on a crushed stone base with an asphalt shoulder [48]. A modulus of subgrade reaction of 400 psi/in (108.6 kPa/mm) was assumed since no information of the level of stiffness of the subgrade was found. This assumption tended to correlate well with the tested transverse cracks as seen in Figure 52 although some scatter was noticed in the data. However, in general, the predictive trend did forecast the increase in LTE_δ due to the dowel bar retrofits.

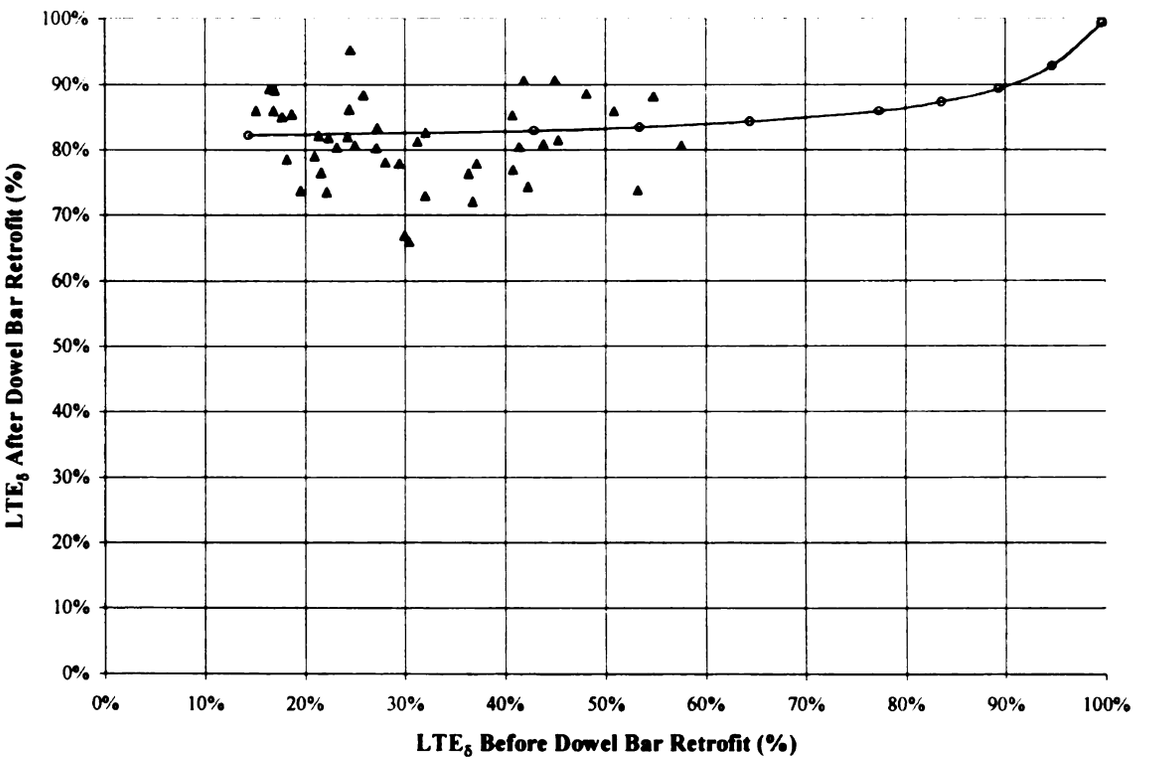

Figure 52. Field Verification of LTE_δ for DBR Site on I-90 in Washington.

Benefits of Selective Retrofitting

Analytical trends, such as the ones in Figures 45-47, can help pavement owners set thresholds for levels of LTE_δ in order to gain the maximum benefit of existing load transfer at a crack. Similar figures were developed for the entire range of modulus of subgrade reaction, pavement thickness, and temperature difference across the depth of the slab and can be found in Appendix B of this thesis.

As discussed earlier, the break between the two curves in the example in Figure 45 represents the point where dowel bar retrofits start to have immediate impact on LTE_δ analytically. Therefore, as a corrective maintenance measure, the threshold using FWD testing for LTE_δ would be set at a point less than this level (in this case LTE_δ = 91%). Also in Figure 45, a distinct drop in the difference between aggregate interlock only and the curve representing both aggregate interlock and dowels occurs around LTE_δ = 80%. Consequently, an ideal threshold value to trigger a dowel bar retrofit would be this level of load transfer.

Figure 46 can also be used as a guide to set threshold values by limiting the maximum tensile stress analytically. When the LTE_δ is below a level of 75-80% the critical values of tensile stress in the concrete tend to remain near the same levels. Therefore no significant benefit can be gained by waiting for the crack performance to deteriorate past those levels. A pavement owner could set the threshold near LTE_δ =75-80% for this level of h, k, and ΔT (when testing the pavement using the FWD) to activate a dowel bar rehabilitation action.

By using the predictive LTE_{δ} trends developed using ISLAB2000, a pavement owner could use non-destructive evaluations of potential rehabilitation candidates in order to make more efficient use of existing load transfer in transverse cracks in corrective maintenance situations. This will result in construction savings by reducing the amount of dowel bars placed if every transverse crack in a PCC pavement was retrofitted.

From 1993-1997, the Washington Department of Transportation granted contracts for dowel bar retrofits ranging from $34.40 to $42.33 per dowel placed with a total of over 300,000 dowels retrofitted over this period [49]. Assuming that one-third of the retrofits could be avoided, a potential savings of more than $3,000,000 over this period could be achieved.

- CHAPTER VI -

Conclusions, Recommendations, and Future Research Needs

CONCLUSIONS AND RECOMMENDATIONS

Backcalculation Procedures

FWD data from both Pittman [1] and Wu and Todres [22] was analyzed using two different backcalculation methods for pavement support and stiffness parameters. This was done in order to verify the consistency of the results of the two methods. If the results of the two methods were analogous, then backcalculated values from these two studies would be valid in comparison. Three parameters, k, E, and ℓ, were of particular of interest since they have an effect of the design of the pavement.

- The results of the modulus of subgrade reaction comparison tended to correlate well. The ECOPP method predicted larger values in all, but one case. The ECOPP method predicted values 4-12% greater than the ERES method. When the modulus of subgrade reaction was very high, the ERES method tended to predict greater values than the ECOPP method of backcalculation.
- A fairly large discrepancy was found between the results of the elastic modulus comparison. In some cases, the difference in the two values approached 40%. In all cases, the ERES method predicted greater values than the ECOPP method. In extreme cases (very low values of E), the discrepancy between the two methods was the greatest. For values within the normal range, $3\text{-}5*10^6$ psi ($2.1\text{-}3.4*10^4$ MPa), for rigid pavements, the values correlated fairly well.

- The backcalculation results of the radius of relative stiffness were found to correlate well using both methods. The differences between both methods ranged from 2-13% difference in results. Since the radius of relative stiffness is a derived parameter dependant on E, k, ν, and h, large differences between the two methods in E and k will result in differences in the values of ℓ. This was the case as the greatest difference in ℓ for these two methods correlated with the same cases where the values of E differed most.

In general, the results of the two backcalculation methods correlated well enough to make comparisons between backcalculated values from both studies mentioned above.

Load Transfer Efficiency Correlations

In addition to the above analyses involving FWD data, several other analyses were performed on field data from the studies in [1] and [22] to view the effects of various factors on load transfer in transverse cracks of RCC pavements. Findings related to these analyses are summarized below.

- An approximate relationship was found to exist between the crack width and the natural crack spacing of RCC pavements. As the pavements crack at larger spacings, the cracks tended to open more resulting in less aggregate interlock between both sides of the crack. The reduction in aggregate interlock resulted in lower load transfer efficiencies and increased tensile stress at the crack. Lower load transfer efficiencies tended to add to the potential for faulting of the pavement as well.

- As with crack spacing, an increased sawed joint spacing was found to have detrimental effects on load transfer at the joints. This was true from data from both studies [1,22] examined in this thesis.
- An increasing modulus of subgrade reaction tended to improve the load transfer efficiencies of RCC pavements. This was found to be true for natural cracks, but the results from the jointed RCC pavements was found to be inconclusive. This is probably due to the lack of data available on joints in RCC pavements.
- An increasing radius of relative stiffness tended to decrease the load transfer efficiency for both cracks and joints in RCC pavements.
- Increasing thickness generally results in an increased load transfer at a crack or joint. A finite element analysis showed a small increase in the derived LTE_δ when the RCC slab thickness was increased.
- Trends from naturally cracked and jointed RCC pavements showed a decrease in load transfer when the Eh^3 was increased. This correlated well with Ioannides' [27] contention as well as from results of other numerical and experimental studies [31, 32, 33]. However, Ioannides notes that as the LTE_δ's are decreased, the absolute deflections are reduced and can be sustained over a longer period of time.
- It is generally thought that higher concrete strength and the corresponding high values of elastic modulus provide higher load transfer efficiency. However, no clear trend from this field data was found between load transfer and concrete strength or elastic modulus.

RCC Pavement Design

A fatigue-based RCC pavement design method was developed and summarized in Chapter 4 of this thesis. In developing this design process, many conclusions were established and are listed below.

- With the exception of a few cases with extreme negative temperature gradients, the critical tensile stress occurred when the axle was placed midway between transverse cracks, immediately next to the pavement edge. This load position, as well as a position 24 inches (0.6 m) from the longitudinal edge, was used in the development of the fatigue-based design method for RCC pavements.
- Load transfer efficiency had no bearing on the level of the critical tensile stress of RCC pavements. The level of LTE_δ had an effect on stresses only within a short distance of 5-7 feet (1.5-2.1 m) when a load was placed at the crack or joint in question. In virtually every case, this tensile stress was less than the stress when the load was placed midway between transverse cracks and at the pavement edge.
- The slab length did not have an effect on the tensile stress calculations using ISLAB2000 when it was larger than 15 feet (4.6 m). The tensile stresses remained unaffected by a change in slab width as long as the slab width was greater than reasonable values set by lane delineation.
- The effect of the lateral load distribution was noted on pavement stresses and the resulting design. Using a typical distribution for the drift of an axle, a modification to the RCC design method was incorporated. The impact of the level of reliability was demonstrated with very high levels of reliability impacting

the design thickness by as much as 40% over cases where the average load location and the resulting stresses were employed.

- The impact of temperature differences across the depth of an RCC pavement slab was discussed and utilized in the RCC design method. By incorporating temperature gradients and their resulting tensile stress increases, RCC design thicknesses increased by as much as 30% in the design examples considered.
- The theory of using subgrade stress as a limiting factor in RCC pavement design was incorporated. Increased load transfer efficiency and thickness helped limit subgrade stresses and influence the decision to reduce joint spacing or retrofit dowels. Joint spacing was recommended to be below 30 feet (9.1 m) in order to maximize load transfer at the discontinuities and reduce the subgrade stress.

RCC Pavement Rehabilitation Alternatives

- The idea of engineered joint spacing was studied in order to provide tighter cracks and higher load transfer efficiencies in RCC pavements. Trends from field data in Edmonton, AB showed that shorter joint spacings resulted in increased load transfer at the joints. Naturally cracked pavements at closer crack spacings also had similar results. If joints are utilized in RCC pavements, a recommended distance less than 30 feet (9.1 m) should be employed. This increased load transfer reduced the tensile stress as the loads pass over the crack or joint, thereby increasing the fatigue life of the pavement. This increased load transfer also aids in the reduction of faulting potential at the crack or joint.

- Figures were introduced which analytically relate load transfer efficiency, RCC thickness, and the modulus of subgrade reaction to the tensile stress felt by the RCC pavement under an 18 kip (80 kN) design load. These figures can be used as a final check for the design of the RCC pavement thickness in order to efficiently use the predicted load transfer efficiency at cracks or joints. Raw data on load transfer efficiency for the sites in this study can be found in Appendix D.
- The use of dowel bars was analytically proven to be beneficial in restoring load transfer in all types of rigid pavements. Figures for a range of different pavement parameters such as h, k, and ΔT were introduced which can aid a pavement owner in developing performance thresholds using an FWD to optimize the timing of a dowel bar retrofit. Methods for developing these thresholds using analytical modeling were also introduced. The use of dowels to decrease the subgrade stress was also introduced.

FUTURE RESEARCH NEEDS

The work performed in this study revealed a few areas where future research is warranted. These future research needs are listed below.

- More FWD tests on RCC pavements need to be conducted in order to better clarify the trends described in this thesis. These tests need to be systematically designed to include both jointed and naturally cracked RCC pavements.
- A life-cycle cost analysis needs to be utilized in order to better characterize the benefit of RCC pavements as a low-cost alternative to asphalt pavements over a design life.

- Tests should be conducted on RCC samples in order to characterize the coefficient of thermal expansion for a scientifically designed set of mixes. It is apparent that the coefficient of thermal expansion for RCC mixes tend to have unique effects on the crack widths in RCC pavements.
- More reliable flexural strength relationships for RCC mixes should be developed by incorporating the water-cementitious ratio, aggregate properties, density, and other factors in order to better predict the fatigue of RCC.
- The effect of aggregate properties on the load transfer of cracks needs to be addressed in order to better understand its impact.
- Better temperature profiles need to be developed in order to characterize the magnitude of the temperature gradients in RCC pavements as well as the length of periods at which each gradient is impacting the pavement. This will help pavement engineers better incorporate temperature effects in the design of RCC pavements.
- Dowel bar rehabilitations of cracks and joints in RCC pavements should be constructed and monitored in order to evaluate the effectiveness of such rehabilitation. Long-term benefits should also be inspected using FWD testing in order to characterize the deterioration of load transfer over time in comparison to other sites which solely rely on aggregate interlock as a load transfer mechanism.
- Thresholds for subgrade stress should be investigated in order to better understand its impact to RCC pavement design.

APPENDICES

Metric Conversions for Appendices

1 foot=.305 m

1 in=25.4 mm

1 psi=6.89 kN

1 psi/in=.27 kPa/mm

APPENDIX A: TABULATED CRITICAL TENSILE STRESSES

Table A-1. Critical Stresses (psi) for a 12 Kip Single Axle Load.

	RCC Thickness (in.)	ΔTRCC = 0°F			ΔTRCC = 15°F			ΔTRCC = -15°F		
		k = 100 psi/in.	k = 250 psi/in.	k = 400 psi/in.	k = 100 psi/in.	k = 250 psi/in.	k = 400 psi/in.	k = 100 psi/in.	k = 250 psi/in.	k = 400 psi/in.
Load is 2' from edge	5	276.3	237.0	219.2	422.0	384.2	368.2	192.8	220.1	227.1
	6	211.7	181.1	167.4	357.8	326.6	314.3	181.1	184.3	198.4
	7	168.9	144.2	133.2	316.5	289.5	278.7	169.2	175.1	174.7
	8	138.9	118.4	109.2	287.4	264.4	254.8	158.2	168.5	170.2
	9	116.9	99.5	91.7	265.3	246.6	238.2	151.4	161.6	165.1
	11	87.2	74.1	68.2	231.8	222.6	216.4	146.0	152.5	154.8
	13	68.6	58.0	53.4	215.5	205.7	202.1	137.3	149.7	152.0
	15	56.1	47.1	43.3	202.2	191.5	191.2	126.2	144.9	149.4
Load is at edge	5	437.0	369.0	337.2	570.0	500.0	468.0	303.0	239.0	226.5
	6	335.4	284.8	261.1	472.0	416.0	392.0	198.5	189.1	196.2
	7	267.6	227.9	209.3	408.0	361.5	340.9	181.4	177.0	175.9
	8	219.6	187.5	172.5	363.3	323.9	305.8	167.4	170.3	171.6
	9	184.2	157.7	145.2	329.3	297.1	281.1	155.3	163.3	166.3
	11	136.3	117.1	108.1	279.7	261.0	249.0	146.0	152.5	156.6
	13	106.1	91.2	84.3	255.0	236.4	228.5	137.3	149.7	152.0
	15	85.8	73.5	68.0	225.9	216.7	213.2	126.3	144.9	149.4

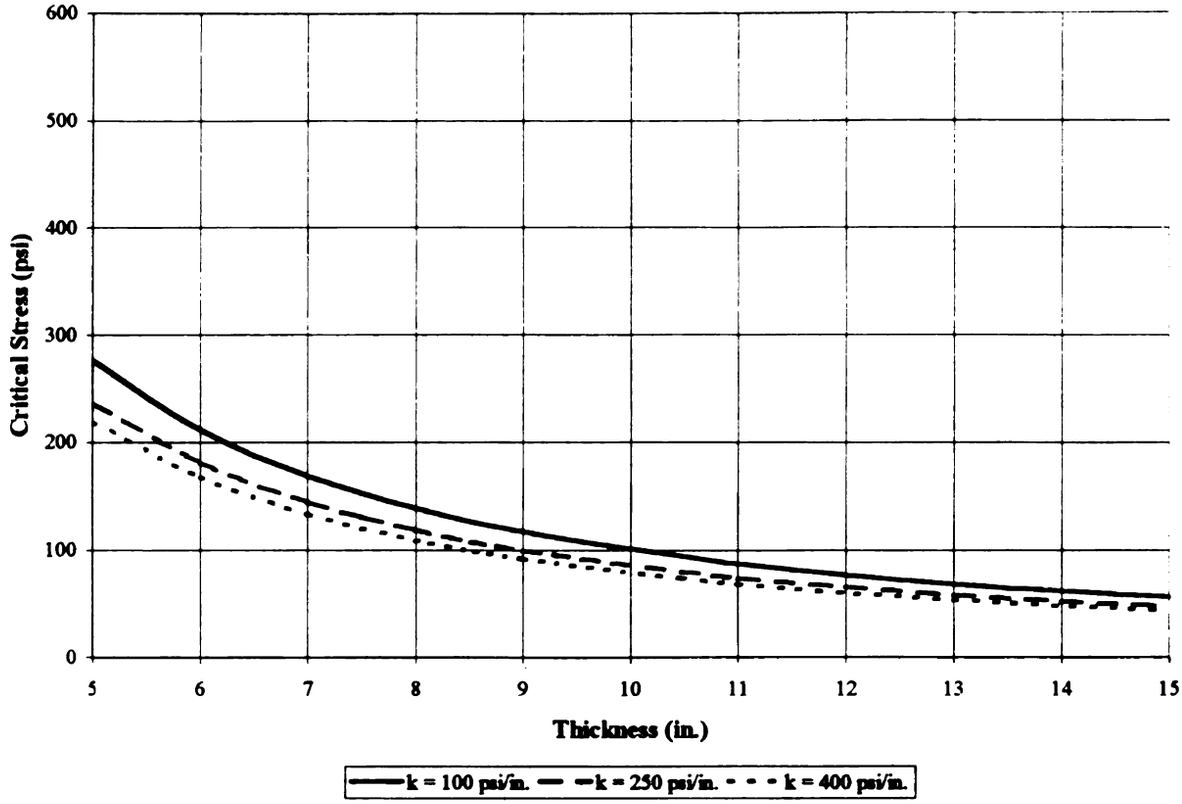

Figure A-1. Critical Tensile Stresses for a 12 kip (53.4 kN) Dual-Tired Single Axle Located 24" (61 mm) from the Pavement Edge with ΔT=0°F (0°C).

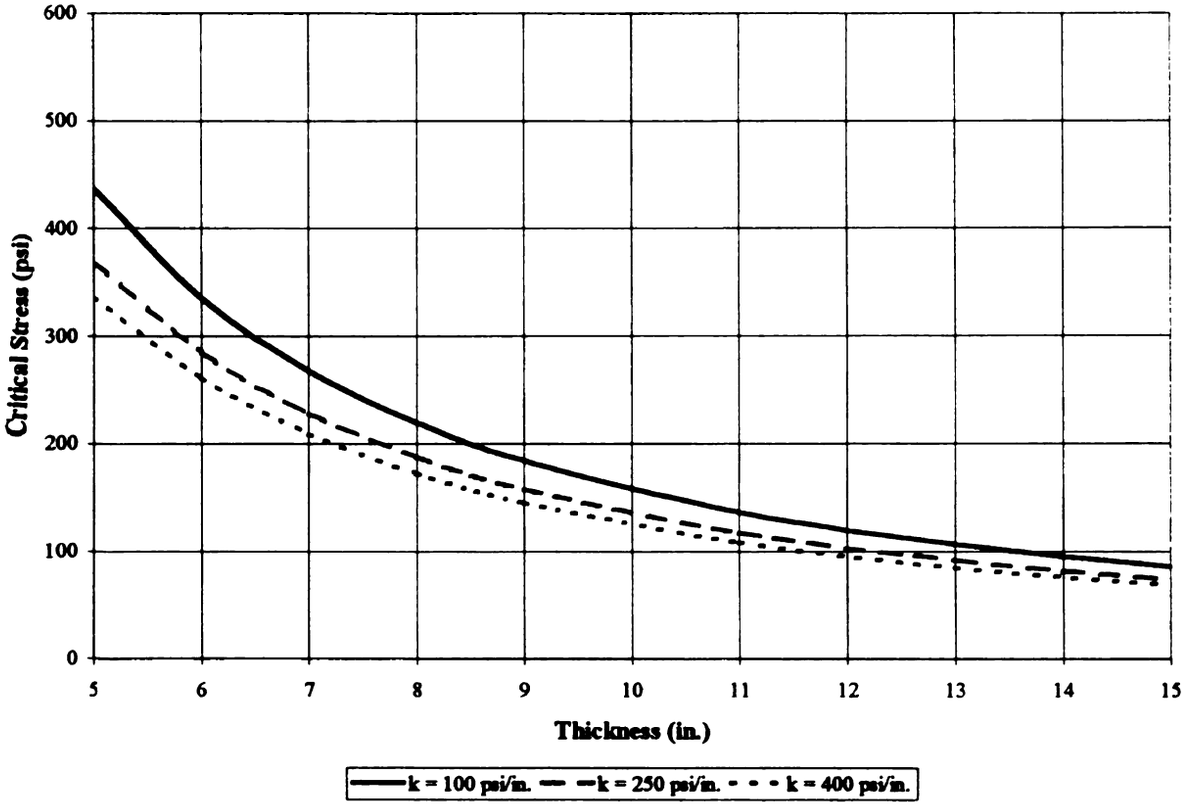

Figure A-2. Critical Tensile Stresses for a 12 kip (53.4 kN) Dual-Tired Single Axle Located at the Pavement Edge with ΔT=0°F (0°C).

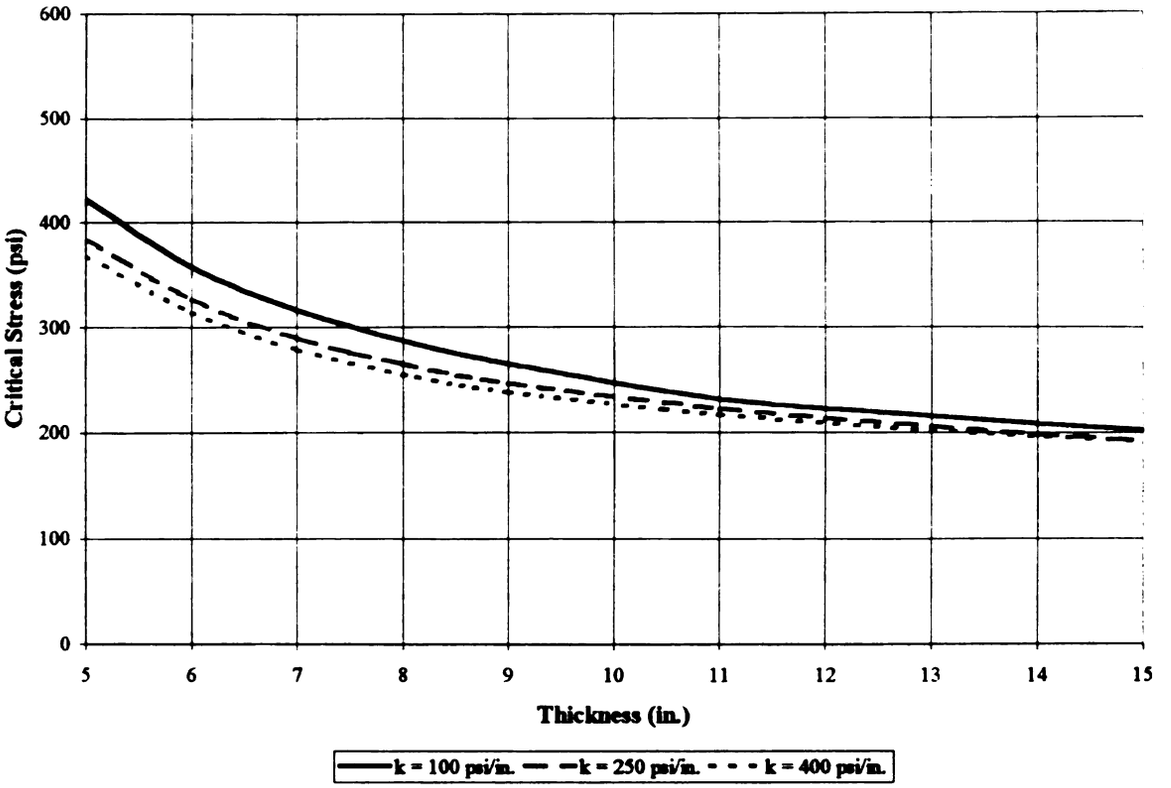

Figure A-3. Critical Tensile Stresses for a 12 kip (53.4 kN) Dual-Tired Single Axle Located 24" (61 mm) from the Pavement Edge with ΔT=15°F (8.3°C).

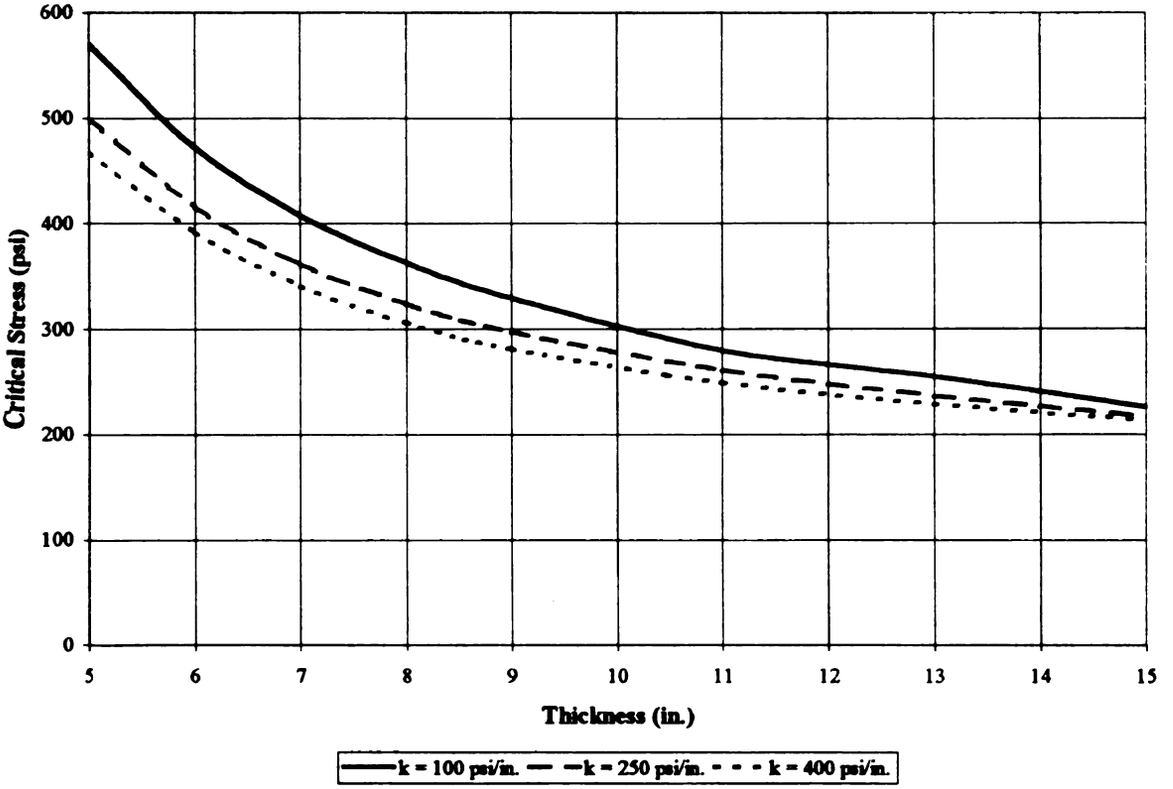

Figure A-4. Critical Tensile Stresses for a 12 kip (53.4 kN) Dual-Tired Single Axle Located at the Pavement Edge with ΔT=15°F (8.3°C).

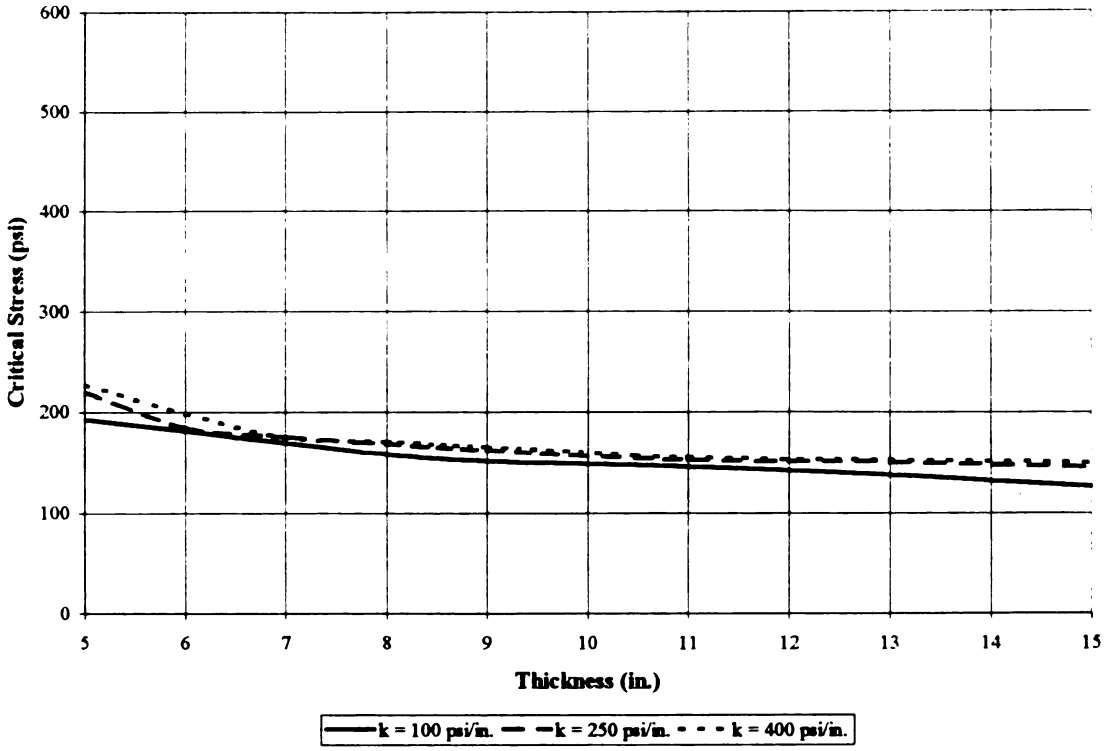

Figure A-5. Critical Tensile Stresses for a 12 kip (53.4 kN) Dual-Tired Single Axle Located 24" (61 mm) from the Pavement Edge with ΔT=-15°F (-8.3°C).

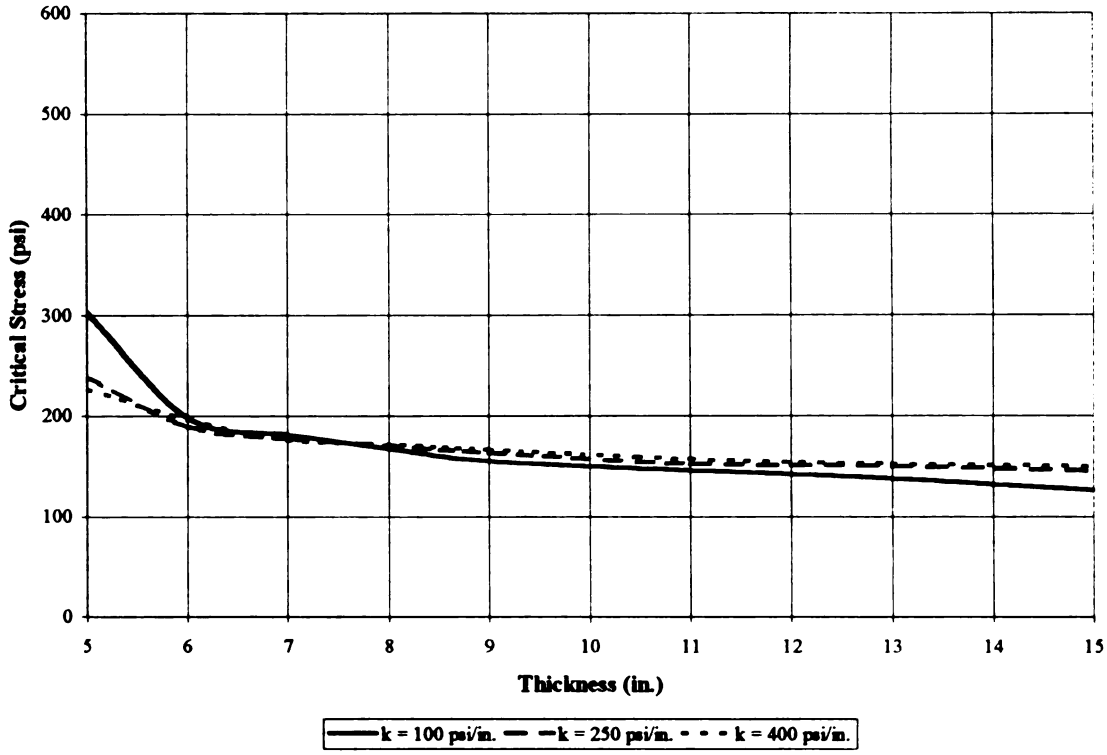

Figure A-6. Critical Tensile Stresses for a 12 kip (53.4 kN) Dual-Tired Single Axle Located at the Pavement Edge with ΔT=-15°F (-8.3°C).

Table A-2. Critical Stresses (psi) for an 18 Kip Single Axle Load.

	RCC Thickness (in.)	ΔTRCC = 0°F			ΔTRCC = 15°F			ΔTRCC = -15°F		
		k = 100 psi/in.	k = 250 psi/in.	k = 400 psi/in.	k = 100 psi/in.	k = 250 psi/in.	k = 400 psi/in.	k = 100 psi/in.	k = 250 psi/in.	k = 400 psi/in.
Load is 2' from edge	5	395.0	336.2	309.7	540.0	483.0	459.0	249.0	250.1	257.5
	6	303.7	258.0	237.7	450.0	404.0	384.5	195.3	203.9	220.0
	7	243.2	206.1	189.7	391.0	351.5	335.3	190.3	184.2	186.7
	8	200.5	169.8	156.1	349.0	315.8	301.7	166.7	176.4	177.2
	9	169.1	143.1	131.5	317.5	290.2	277.9	154.6	168.2	171.2
	11	126.7	107.0	98.2	271.3	255.5	246.2	146.0	152.8	158.7
	13	99.9	84.0	77.1	236.7	231.7	225.7	137.3	149.7	152.0
	15	81.9	68.3	62.6	224.1	212.8	210.6	126.1	144.9	149.4
Load is at edge	5	629.0	528.0	481.0	763.0	659.0	612.0	496.0	399.0	352.0
	6	485.0	409.0	374.0	622.0	541.0	505.0	348.0	279.0	246.0
	7	388.0	328.6	300.9	529.0	462.0	432.0	247.5	199.1	192.8
	8	319.1	271.1	248.6	463.0	407.0	381.9	186.2	185.2	182.1
	9	268.2	228.4	209.8	413.0	367.7	345.6	169.7	174.5	173.3
	11	199.0	170.2	156.7	342.3	314.0	297.5	146.0	157.3	160.8
	13	155.2	132.8	122.5	291.8	278.0	266.6	137.2	149.7	152.0
	15	125.7	107.3	99.1	252.1	250.5	244.3	126.3	144.9	149.4

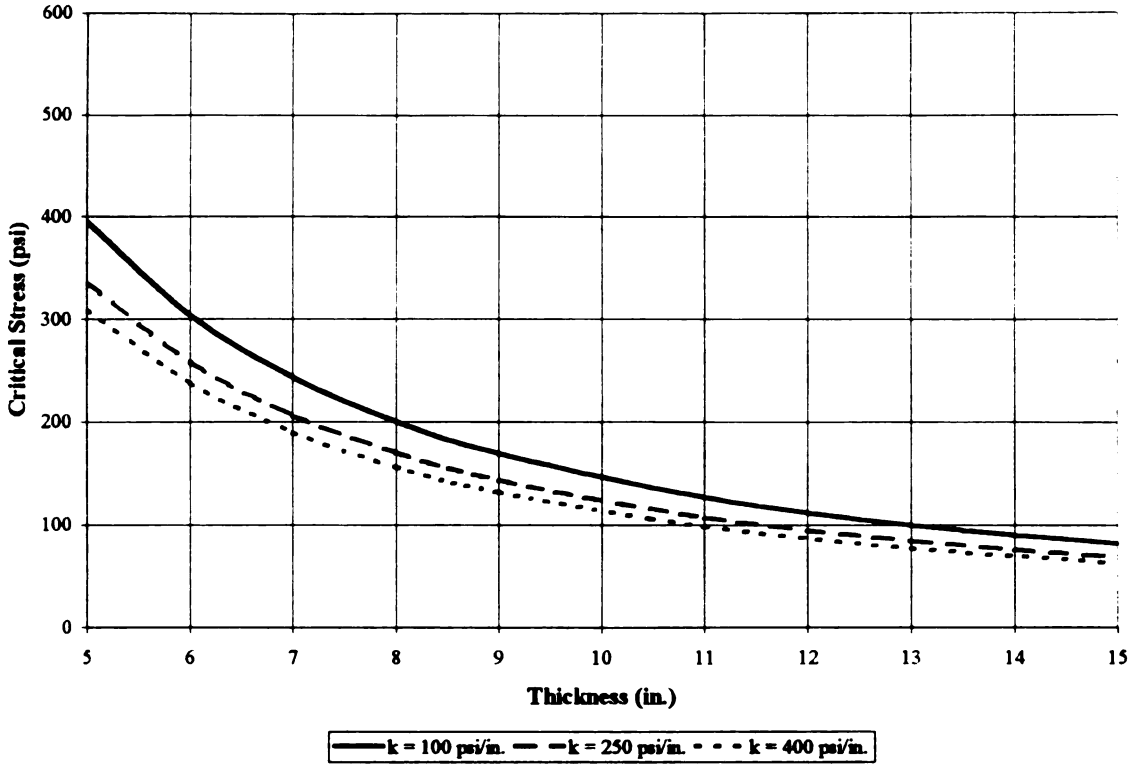

Figure A-7. Critical Tensile Stresses for an 18 kip (80.1 kN) Dual-Tired Single Axle Located 24" (61 mm) from the Pavement Edge with ΔT=0°F (0°C).

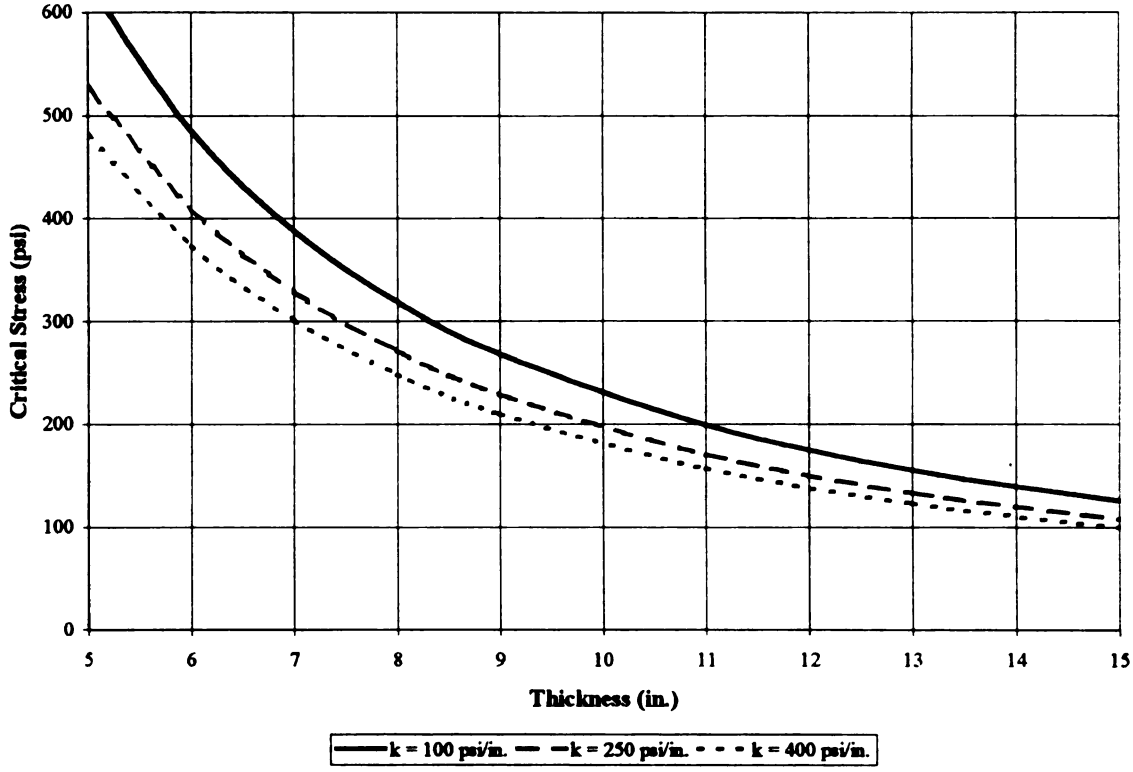

Figure A-8. Critical Tensile Stresses for an 18 kip (80.1 kN) Dual-Tired Single Axle Located at the Pavement Edge with ΔT=0°F (0°C).

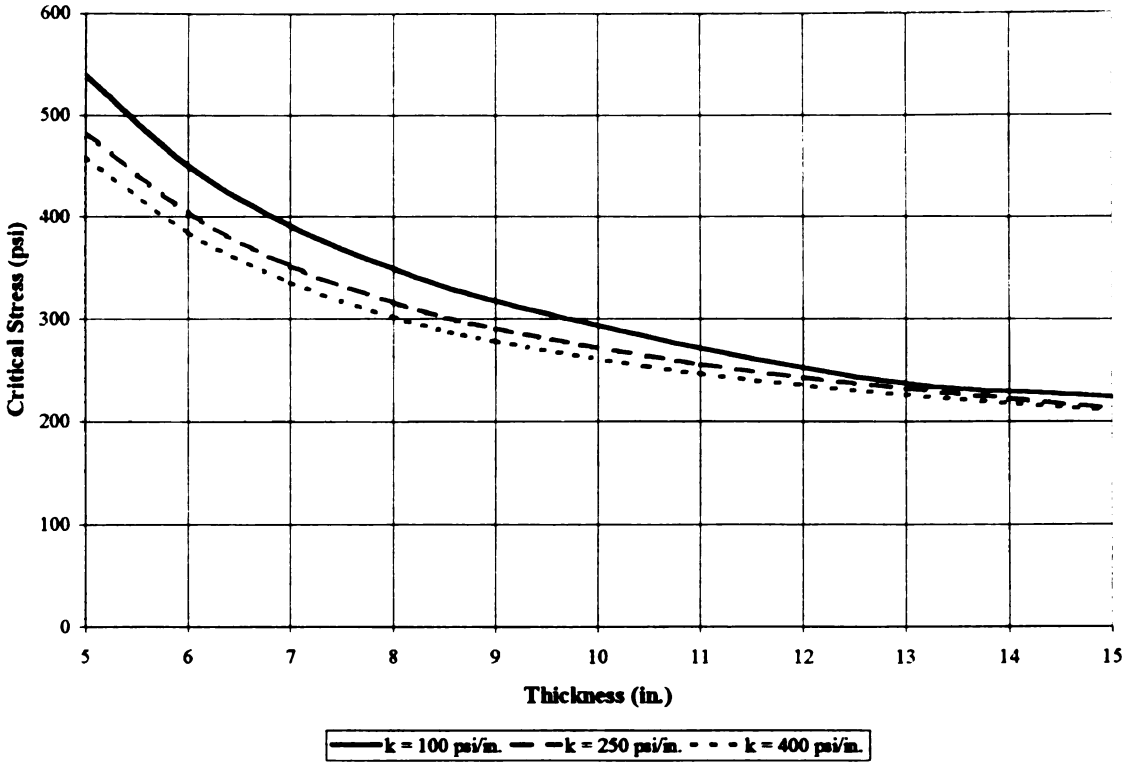

Figure A-9. Critical Tensile Stresses for an 18 kip (80.1 kN) Dual-Tired Single Axle Located 24" (61 mm) from the Pavement Edge with ΔT=15°F (8.3°C).

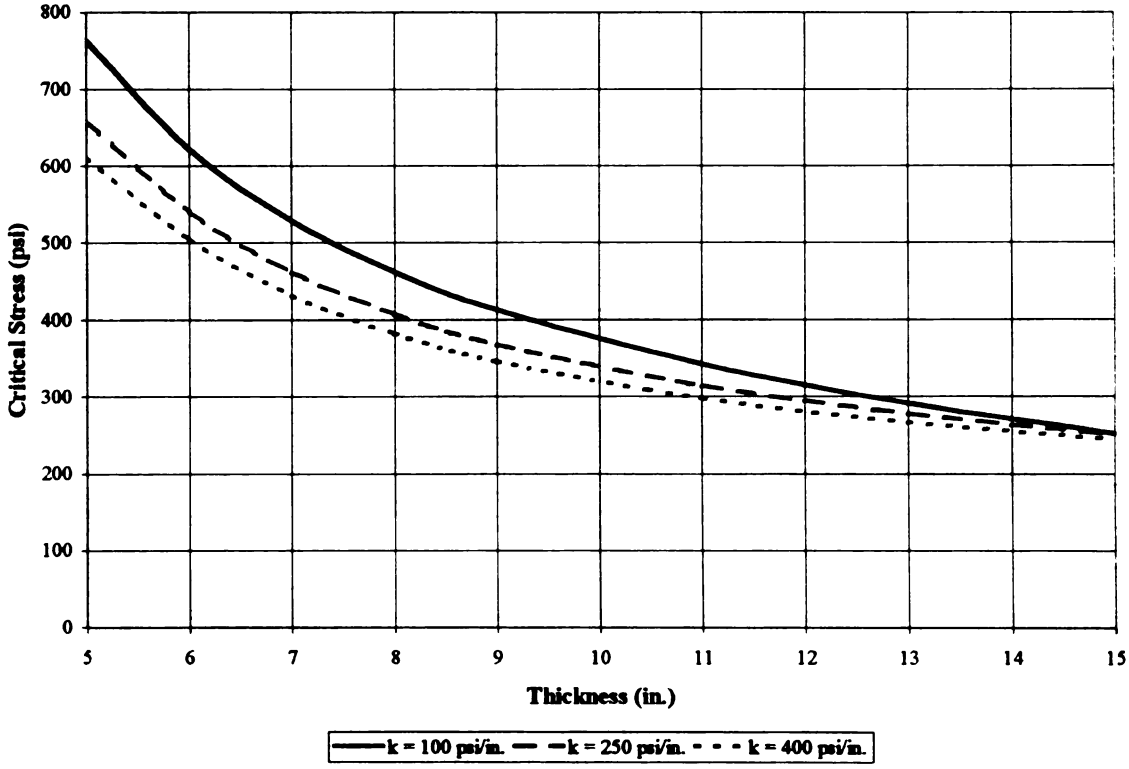

Figure A-10. Critical Tensile Stresses for an 18 kip (80.1 kN) Dual-Tired Single Axle Located at the Pavement Edge with ΔT=15°F (8.3°C).

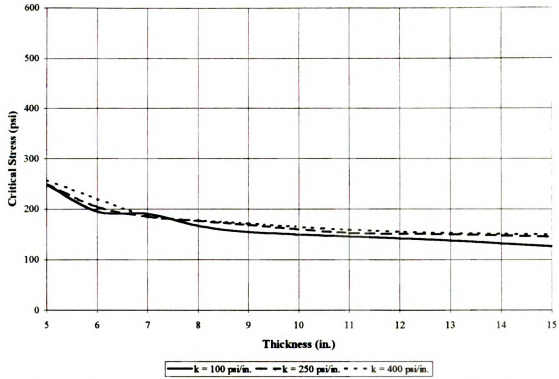

Figure A-11. Critical Tensile Stresses for an 18 kip (80.1 kN) Dual-Tired Single Axle Located 24" (61 mm) from the Pavement Edge with ΔT=-15°F (-8.3°C).

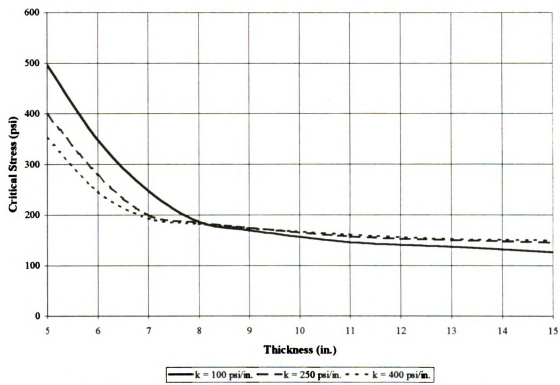

Figure A-12. Critical Tensile Stresses for an 18 kip (80.1 kN) Dual-Tired Single Axle Located at the Pavement Edge with ΔT=-15°F (-8.3°C).

Table A-3. Critical Stresses (psi) for a 24 Kip Tandem Axle Load.

	RCC Thickness (in.)	ΔTRCC = 0°F			ΔTRCC = 15°F			ΔTRCC = -15°F		
		k = 100 psi/in.	k = 250 psi/in.	k = 400 psi/in.	k = 100 psi/in.	k = 250 psi/in.	k = 400 psi/in.	k = 100 psi/in.	k = 250 psi/in.	k = 400 psi/in.
Load is 2' from edge	5	237.3	207.4	196.0	383.7	355.0	345.1	204.4	230.3	236.6
	6	183.4	155.9	146.1	330.2	302.4	293.4	190.1	191.0	206.6
	7	149.1	123.9	114.7	296.5	270.2	261.3	175.2	180.2	179.3
	8	125.5	102.4	93.8	272.9	249.1	240.5	161.2	171.6	173.6
	9	108.3	87.1	79.1	254.8	234.3	226.2	151.4	162.7	166.8
	11	85.2	67.1	60.1	226.7	214.4	207.8	146.0	152.5	153.6
	13	70.5	54.5	48.4	203.7	200.0	195.7	137.2	149.7	152.0
	15	60.4	46.0	40.5	195.5	187.4	186.2	126.1	144.8	149.3
Load is at edge	5	367.0	312.2	290.5	499.0	442.0	421.0	254.3	247.4	243.2
	6	286.3	238.7	220.4	422.0	369.7	350.5	225.4	207.7	213.1
	7	233.8	191.7	175.5	372.4	324.8	306.6	203.3	193.3	185.7
	8	197.0	159.7	145.0	337.7	295.2	277.9	183.8	180.7	176.3
	9	169.8	136.5	123.1	311.3	274.5	258.4	166.7	170.4	169.2
	11	132.4	105.3	94.2	271.3	246.7	233.6	146.0	152.5	156.7
	13	108.1	85.3	76.0	240.0	227.1	217.8	137.2	149.7	152.0
	15	91.2	71.5	63.5	213.1	210.7	205.5	126.5	144.8	149.3

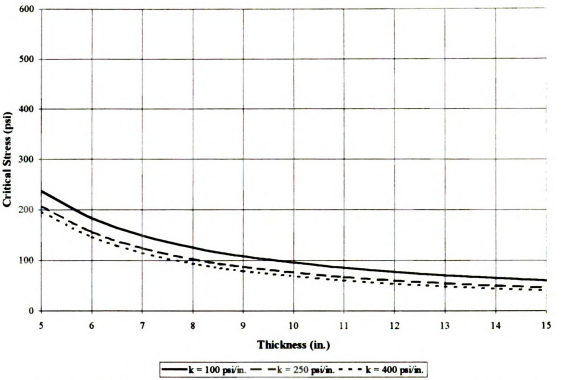

Figure A-13. Critical Tensile Stresses for a 24 kip (106.8 kN) Dual-Tired Tandem Axle Located 24" (61 mm) from the Pavement Edge with ΔT=0°F (0°C).

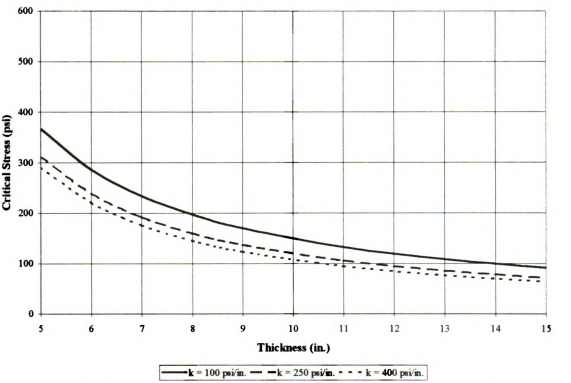

Figure A-14. Critical Tensile Stresses for a 24 kip (106.8 kN) Dual-Tired Tandem Axle Located at the Pavement Edge with ΔT=0°F (0°C).

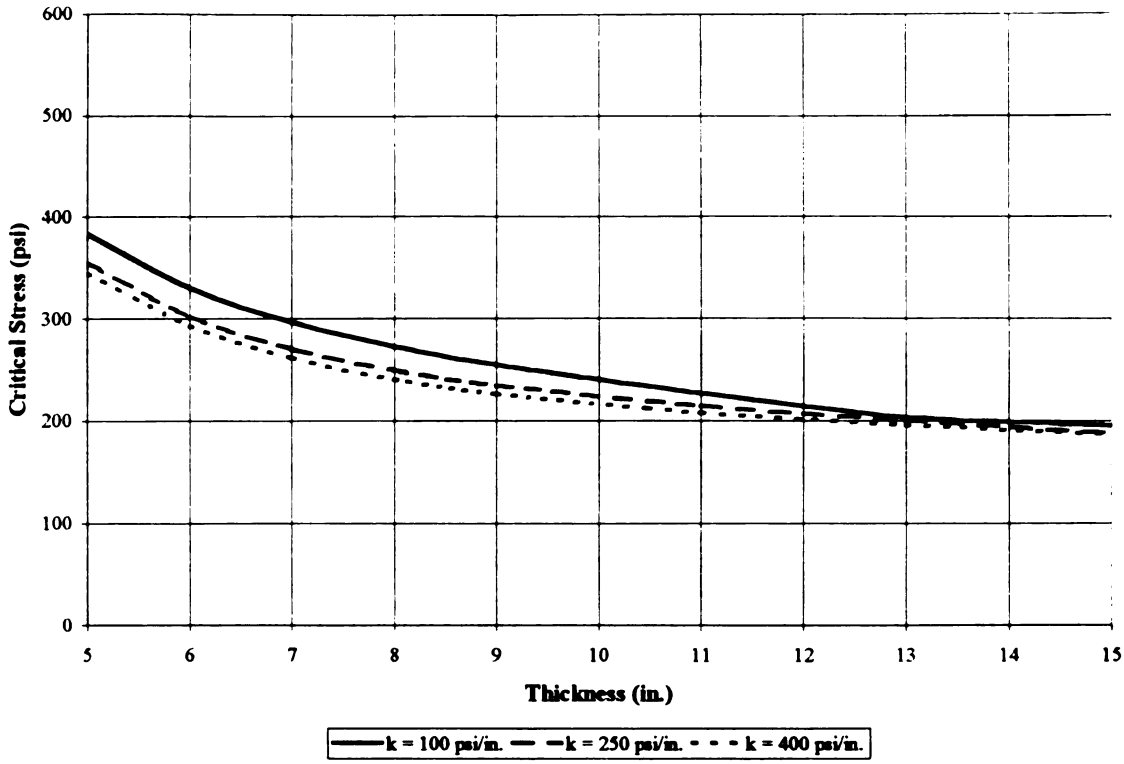

Figure A-15. Critical Tensile Stresses for a 24 kip (106.8 kN) Dual-Tired Tandem Axle Located 24" (61 mm) from the Pavement Edge with ΔT=15°F (8.3°C).

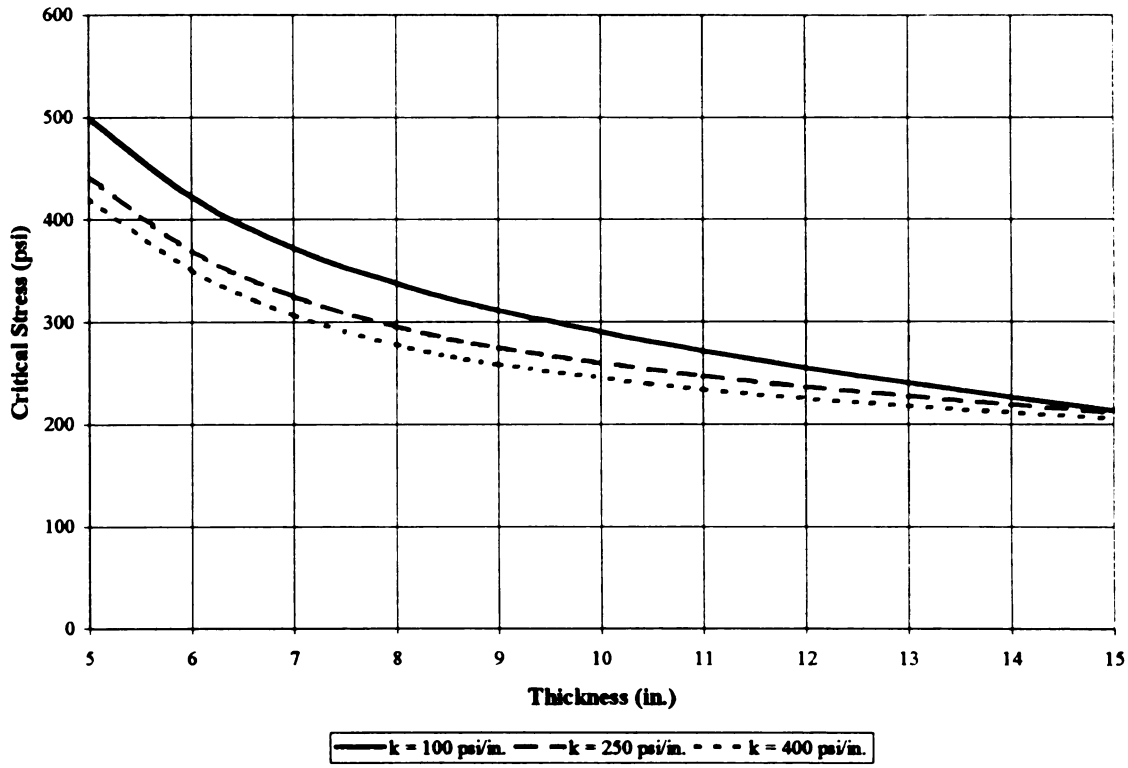

Figure A-16. Critical Tensile Stresses for a 24 kip (106.8 kN) Dual-Tired Tandem Axle Located at the Pavement Edge with ΔT=15°F (8.3°C).

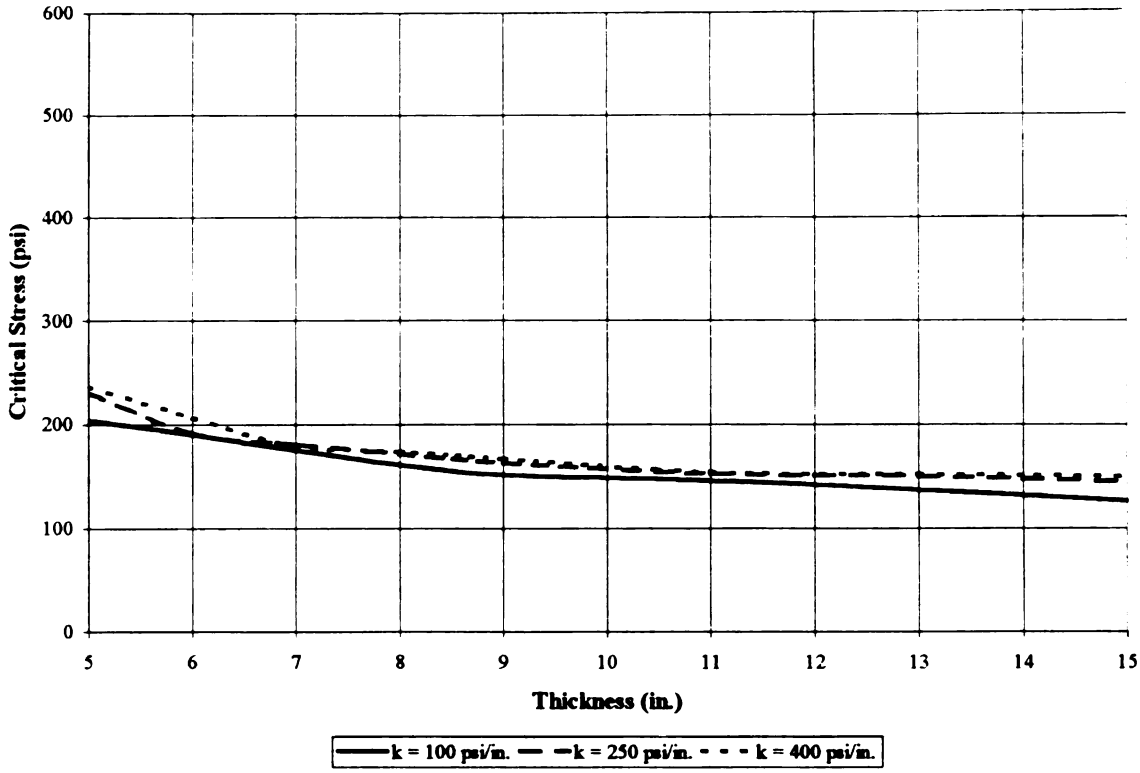

Figure A-17. Critical Tensile Stresses for a 24 kip (106.8 kN) Dual-Tired Tandem Axle Located 24" (61 mm) from the Pavement Edge with ΔT=-15°F (-8.3°C).

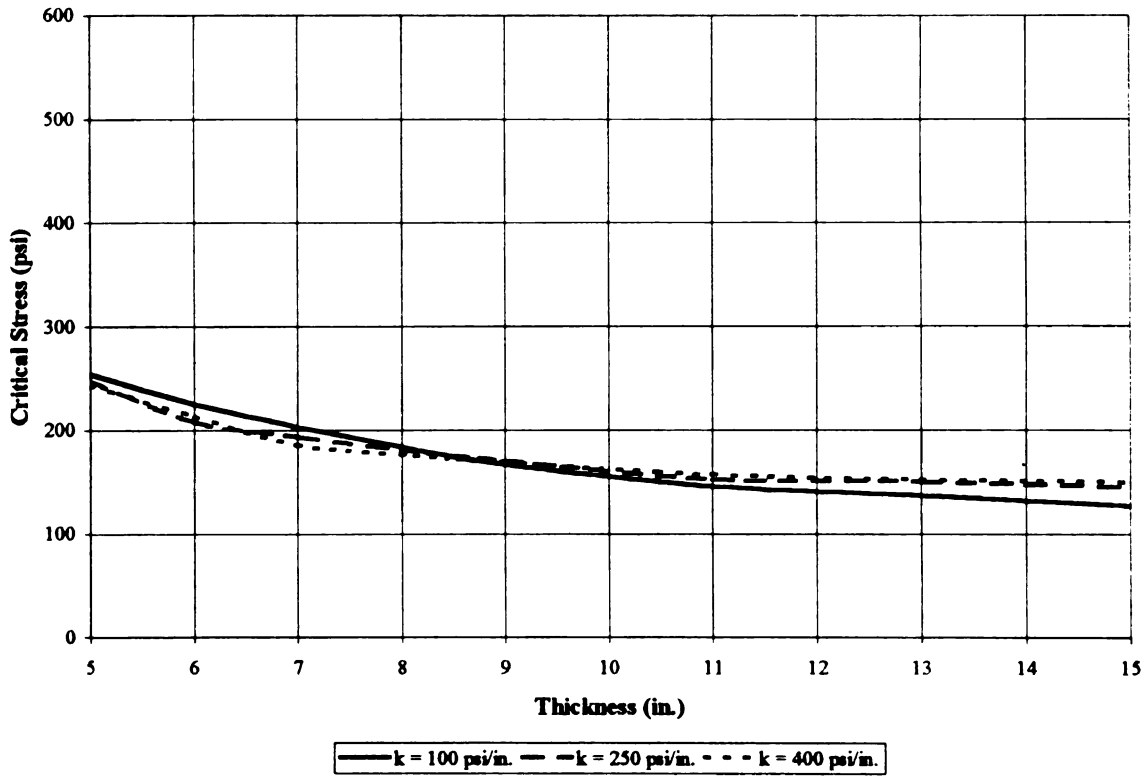

Figure A-18. Critical Tensile Stresses for a 24 kip (106.8 kN) Dual-Tired Tandem Axle Located at the Pavement Edge with ΔT=-15°F (-8.3°C).

Table A-4. Critical Stresses (psi) for a 30 Kip Tandem Axle Load.

	RCC Thickness (in.)	ΔTRCC = 0°F			ΔTRCC = 15°F			ΔTRCC = -15°F		
		k = 100 psi/in.	k = 250 psi/in.	k = 400 psi/in.	k = 100 psi/in.	k = 250 psi/in.	k = 400 psi/in.	k = 100 psi/in.	k = 250 psi/in.	k = 400 psi/in.
Load is 2' from edge	5	305.9	267.1	252.4	452.0	415.0	401.0	217.3	247.9	254.2
	6	236.5	200.9	188.2	383.3	347.4	335.5	200.0	202.7	218.8
	7	192.2	159.7	147.8	339.6	306.0	294.4	182.6	186.4	186.8
	8	161.8	132.0	120.9	309.1	278.8	267.6	166.6	176.7	178.2
	9	139.5	112.4	102.0	286.0	259.6	249.1	152.4	166.7	170.7
	11	109.5	86.5	77.5	251.1	233.8	225.1	145.9	152.5	155.1
	13	90.5	70.2	62.4	223.7	215.7	209.7	137.1	149.7	152.0
	15	77.4	59.2	52.2	210.7	200.6	197.9	125.9	144.8	149.3
Load is at edge	5	467.0	397.0	369.0	600.0	527.0	500.0	335.0	274.7	266.9
	6	365.0	303.4	280.0	501.0	435.0	411.0	249.5	228.8	232.5
	7	297.9	244.0	223.1	437.0	377.5	354.7	221.9	208.7	199.7
	8	251.1	203.3	184.4	392.0	339.3	317.8	198.0	193.8	187.2
	9	216.5	173.9	156.8	358.3	312.3	292.4	177.5	181.0	176.8
	11	168.7	134.3	120.1	307.8	275.9	259.7	145.9	158.8	159.5
	13	137.7	108.8	96.9	269.7	250.7	238.8	137.1	149.7	152.0
	15	116.0	91.1	80.9	238.0	230.4	230.4	126.5	144.8	149.3

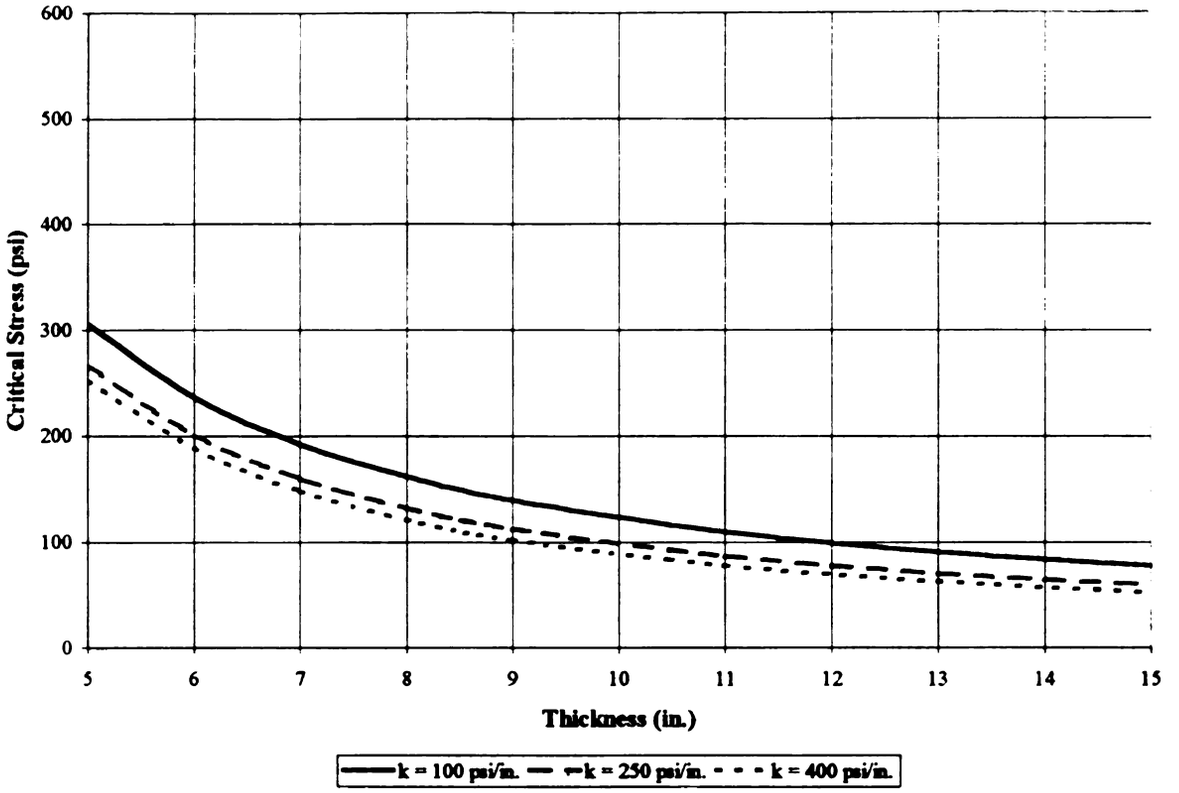

Figure A-19. Critical Tensile Stresses for a 30 kip (133.4 kN) Dual-Tired Tandem Axle Located 24" (61 mm) from the Pavement Edge with ΔT=0°F (0°C).

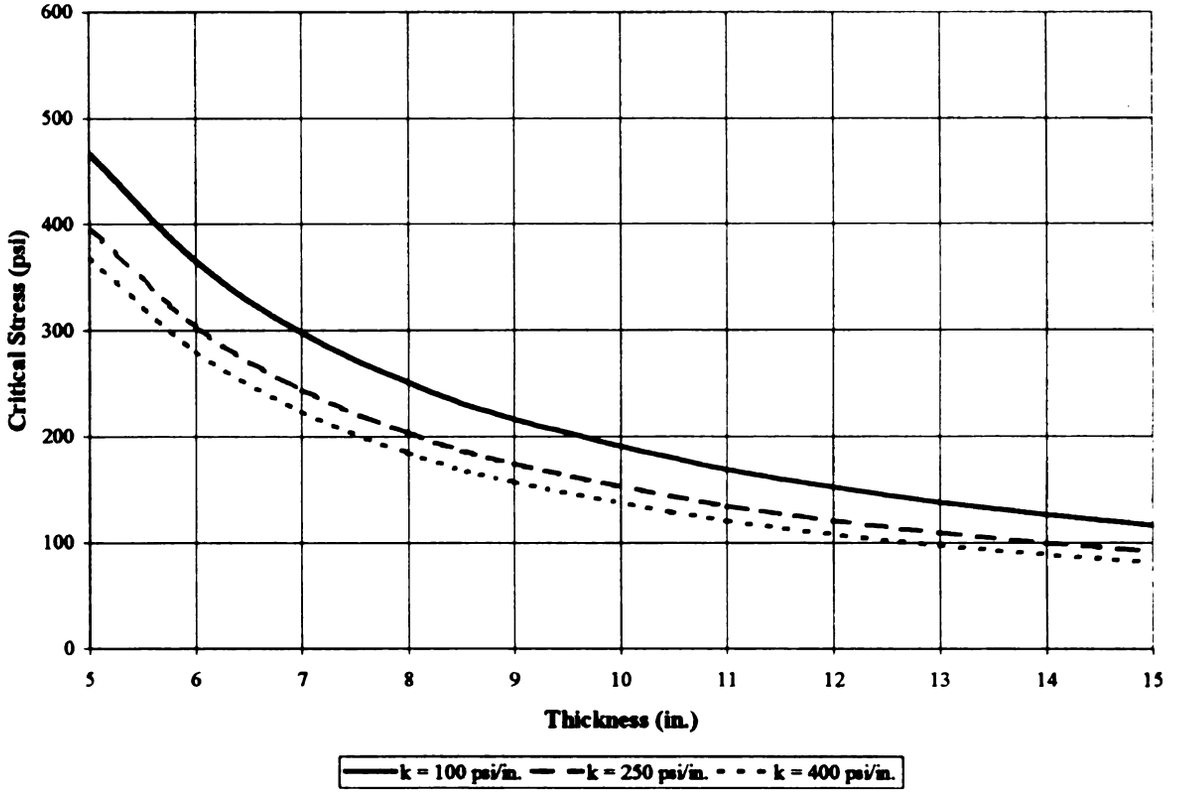

Figure A-20. Critical Tensile Stresses for a 30 kip (133.4 kN) Dual-Tired Tandem Axle Located at the Pavement Edge with ΔT=0°F (0°C).

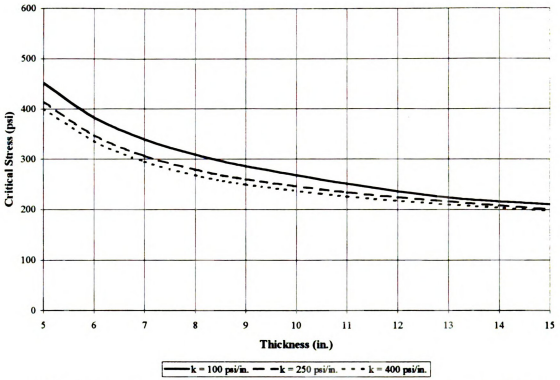

Figure A-21. Critical Tensile Stresses for a 30 kip (133.4 kN) Dual-Tired Tandem Axle Located 24" (61 mm) from the Pavement Edge with ΔT=15°F (8.3°C).

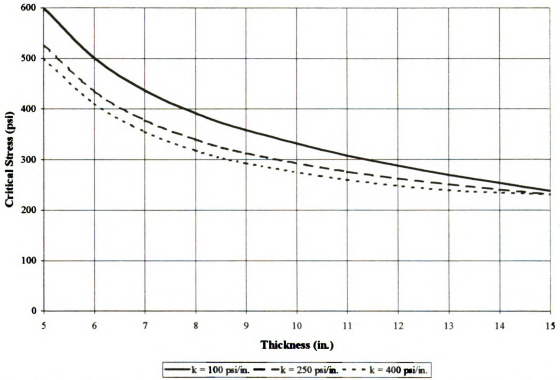

Figure A-22. Critical Tensile Stresses for a 30 kip (133.4 kN) Dual-Tired Tandem Axle Located at the Pavement Edge with ΔT=15°F (8.3°C).

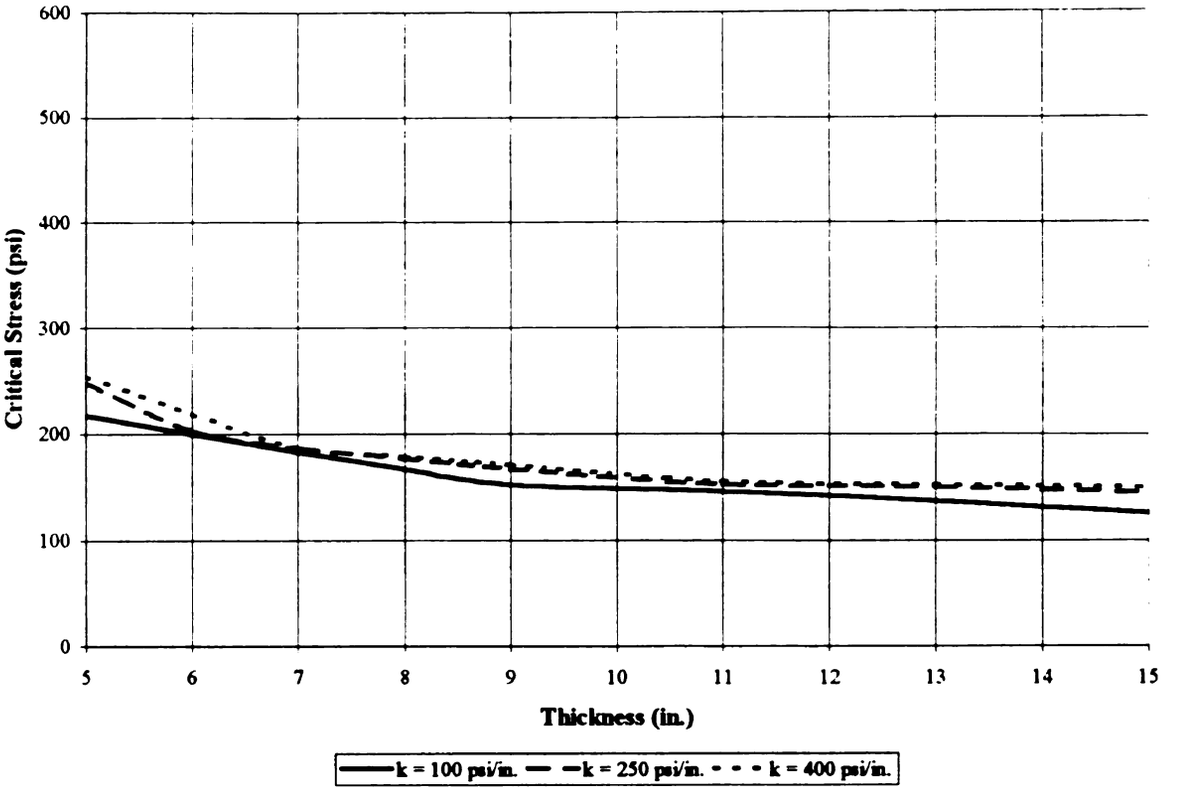

Figure A-23. Critical Tensile Stresses for a 30 kip (133.4 kN) Dual-Tired Tandem Axle Located 24" (61 mm) from the Pavement Edge with ΔT=-15°F (-8.3°C).

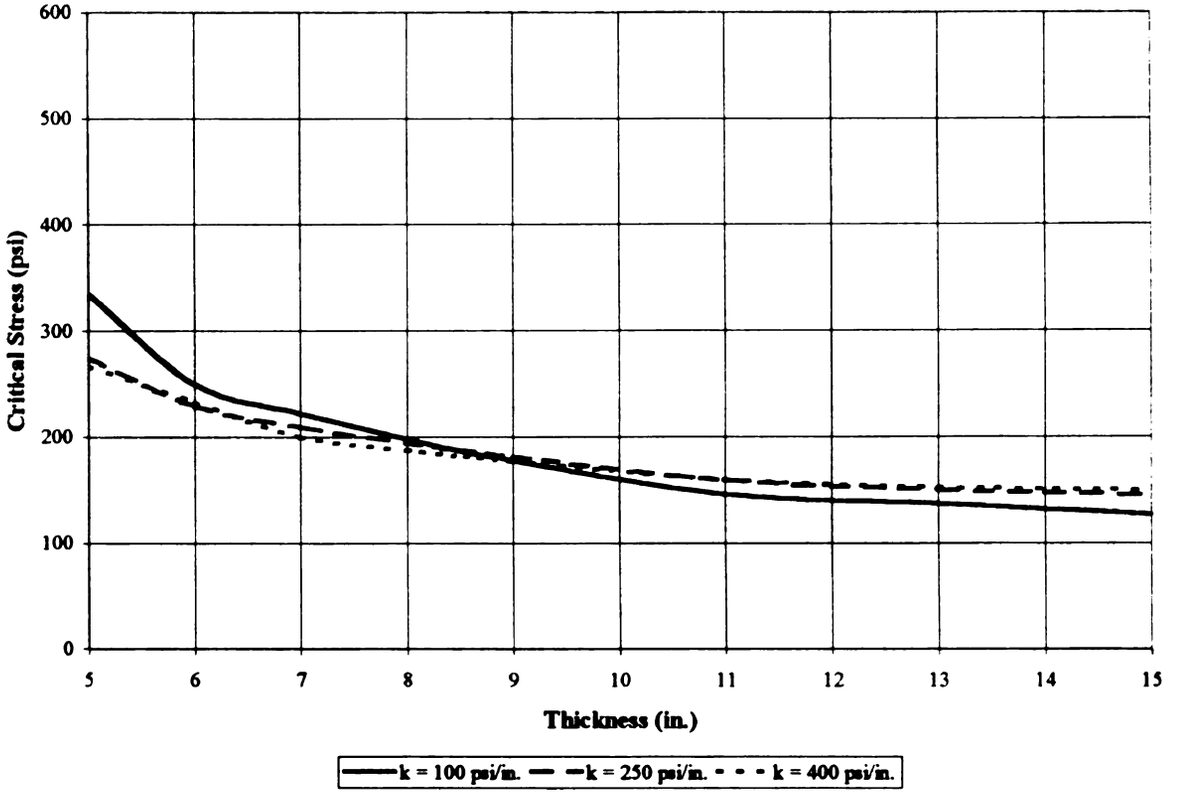

Figure A-24. Critical Tensile Stresses for a 30 kip (133.4 kN) Dual-Tired Tandem Axle Located at the Pavement Edge with ΔT=-15°F (-8.3°C).

Table A-5. Critical Stresses (psi) for an 36 Kip Tandem Axle Load.

	RCC Thickness (in.)	ΔTRCC = 0°F			ΔTRCC = 15°F			ΔTRCC = -15°F		
		k = 100 psi/in.	k = 250 psi/in.	k = 400 psi/in.	k = 100 psi/in.	k = 250 psi/in.	k = 400 psi/in.	k = 100 psi/in.	k = 250 psi/in.	k = 400 psi/in.
Load is 2' from edge	5	336.4	292.7	275.8	483.0	440.0	425.0	229.0	265.0	271.5
	6	260.8	220.6	206.3	408.0	367.0	353.5	211.3	213.6	231.2
	7	212.8	175.7	162.2	360.1	322.0	308.8	192.6	192.8	195.2
	8	179.6	145.6	133.0	327.0	292.3	279.6	175.3	182.8	182.9
	9	155.5	124.2	112.4	301.9	271.4	259.4	159.7	172.3	175.1
	11	122.9	96.1	85.8	264.4	243.4	233.4	145.9	152.8	158.9
	13	102.1	78.4	69.4	235.3	223.9	216.7	137.0	149.7	152.0
	15	87.8	66.4	58.3	210.3	207.8	204.0	125.9	144.8	149.3
Load is at edge	5	526.0	446.0	414.0	658.0	575.0	543.0	398.0	320.0	291.8
	6	412.0	341.8	314.8	547.0	472.0	444.0	281.0	251.1	252.8
	7	337.5	275.3	251.3	475.0	408.0	381.7	242.1	225.0	216.1
	8	285.0	229.8	208.1	425.0	364.6	340.3	215.4	206.6	200.0
	9	246.2	196.8	177.1	386.9	334.1	311.6	192.3	192.4	187.8
	11	192.6	152.4	136.0	330.9	293.1	274.7	155.1	167.7	167.9
	13	157.7	123.9	110.0	289.1	265.0	251.2	137.0	149.7	152.1
	15	133.3	104.0	92.1	254.8	242.7	233.6	126.6	144.8	149.3

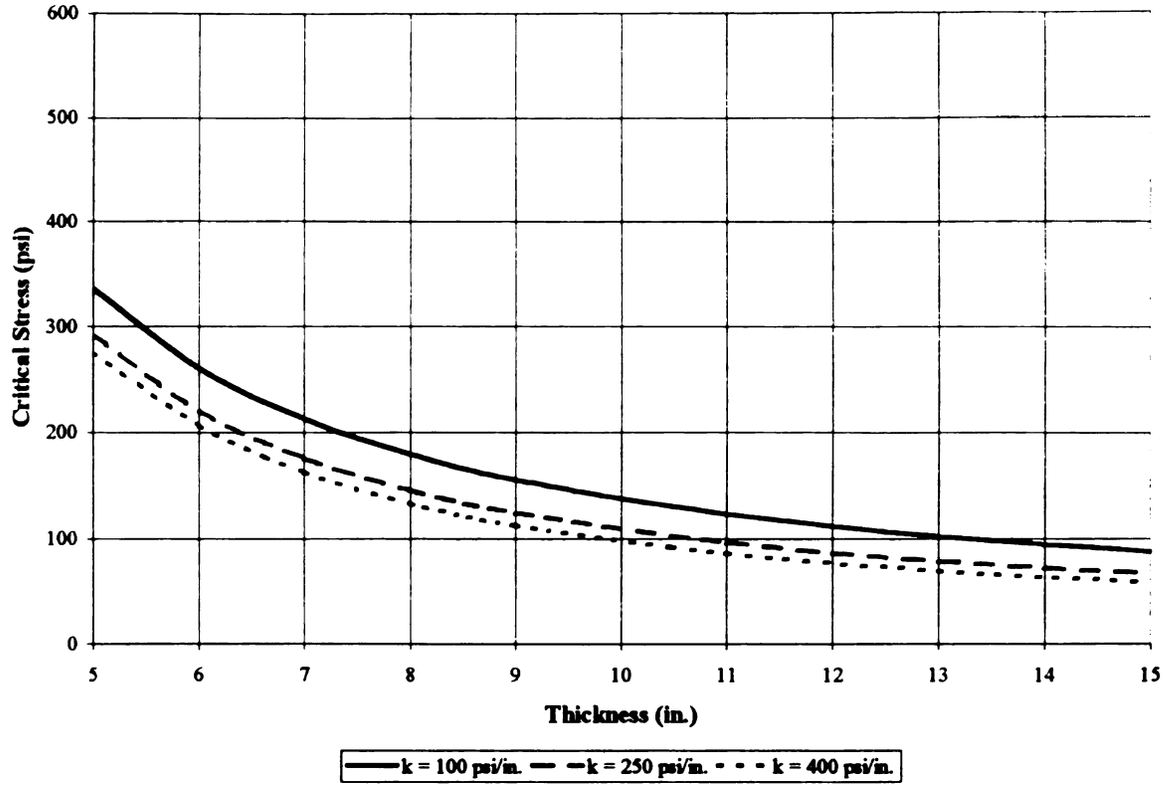

Figure A-25. Critical Tensile Stresses for a 36 kip (160.1 kN) Dual-Tired Tandem Axle Located 24" (61 mm) from the Pavement Edge with ΔT=0°F (0°C).

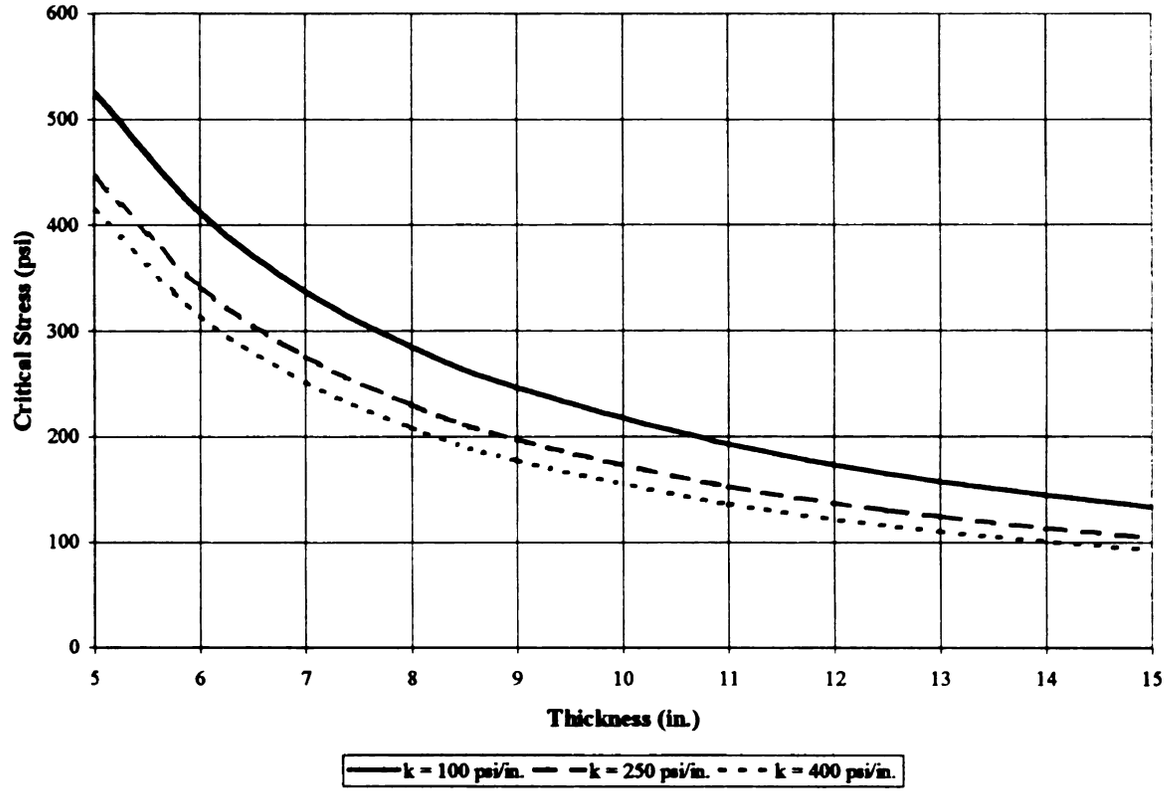

Figure A-26. Critical Tensile Stresses for a 36 kip (160.1 kN) Dual-Tired Tandem Axle Located at the Pavement Edge with ΔT=0°F (0°C).

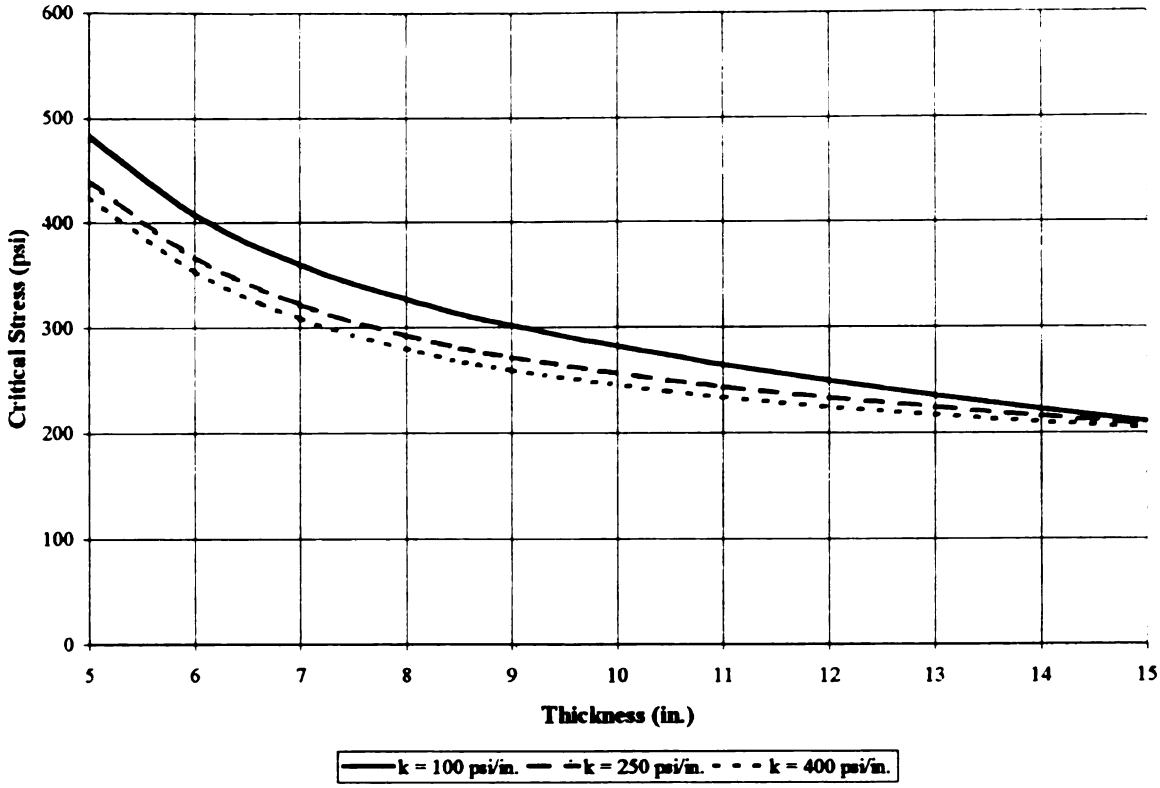

Figure A-27. Critical Tensile Stresses for a 36 kip (160.1 kN) Dual-Tired Tandem Axle Located 24" (61 mm) from the Pavement Edge with ΔT=15°F (8.3°C).

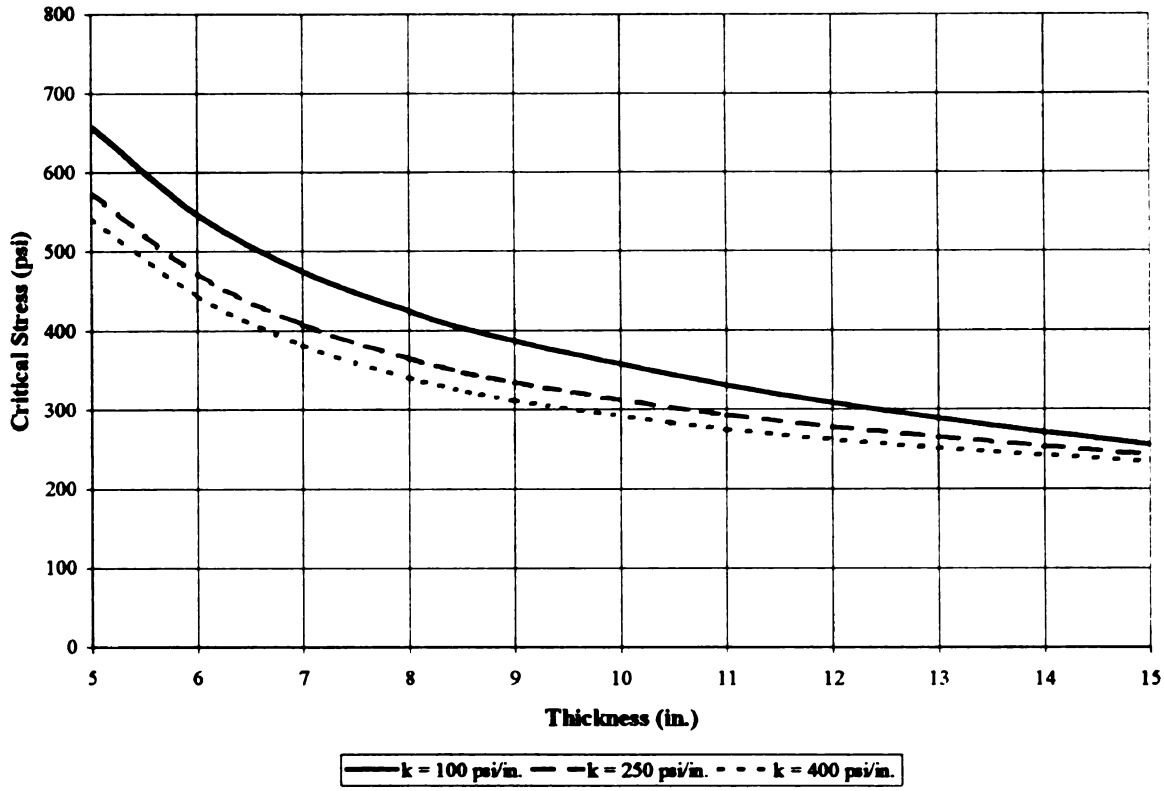

Figure A-28. Critical Tensile Stresses for a 36 kip (160.1 kN) Dual-Tired Tandem Axle Located at the Pavement Edge with ΔT=15°F (8.3°C).

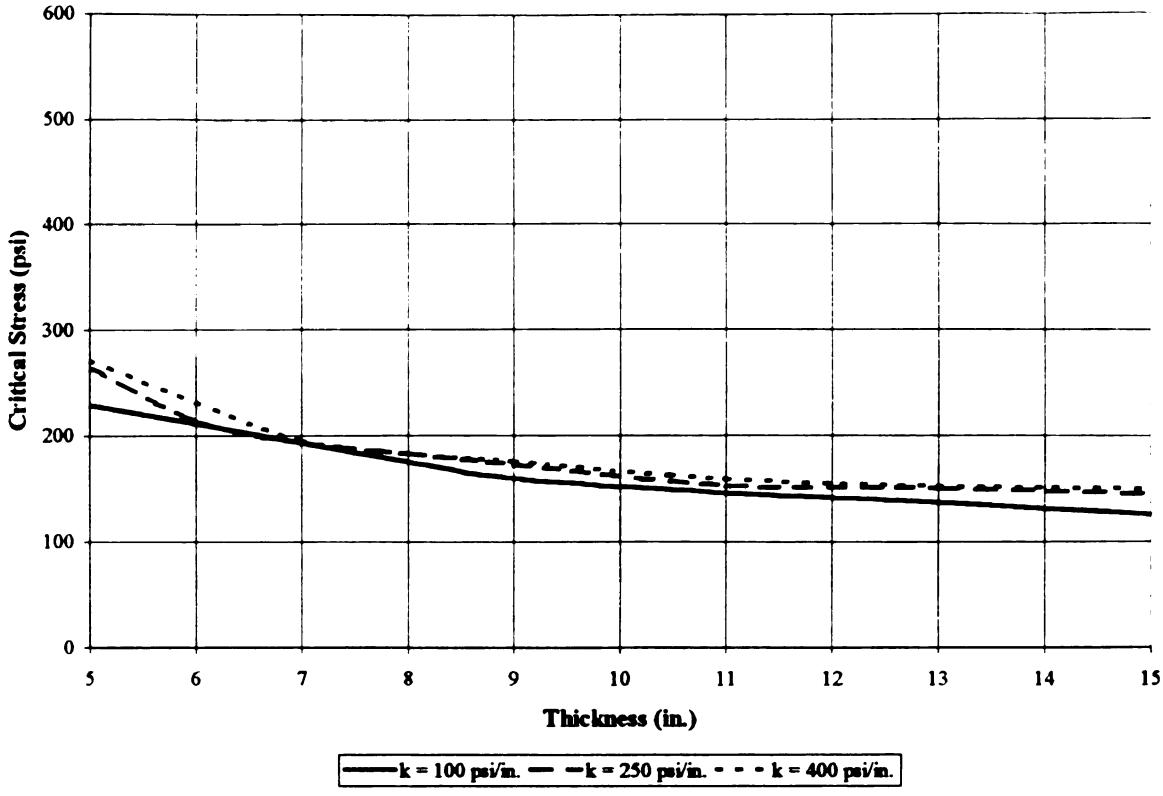

Figure A-29. Critical Tensile Stresses for a 36 kip (160.1 kN) Dual-Tired Tandem Axle Located 24" (61 mm) from the Pavement Edge with ΔT=-15°F (-8.3°C).

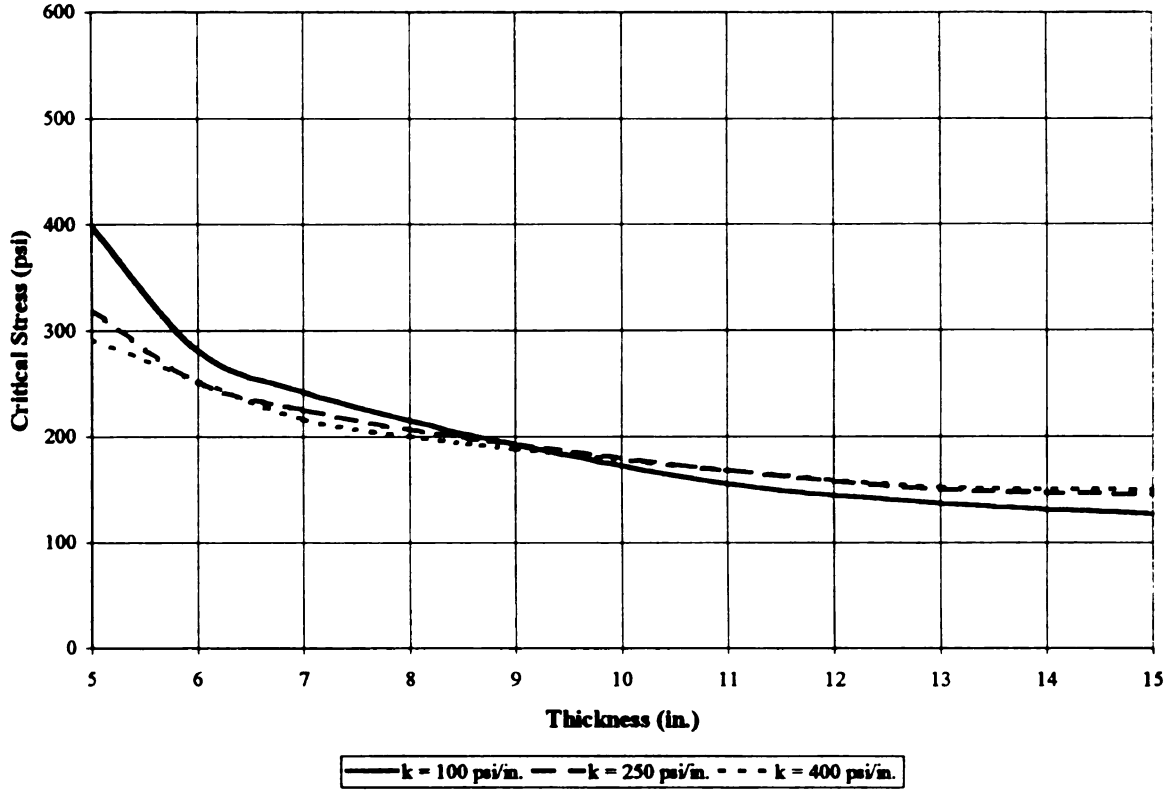

Figure A-30. Critical Tensile Stresses for a 36 kip (160.1 kN) Dual-Tired Tandem Axle Located at the Pavement Edge with ΔT=-15°F (-8.3°C).

APPENDIX B: DOWEL BAR RETROFIT GUIDE

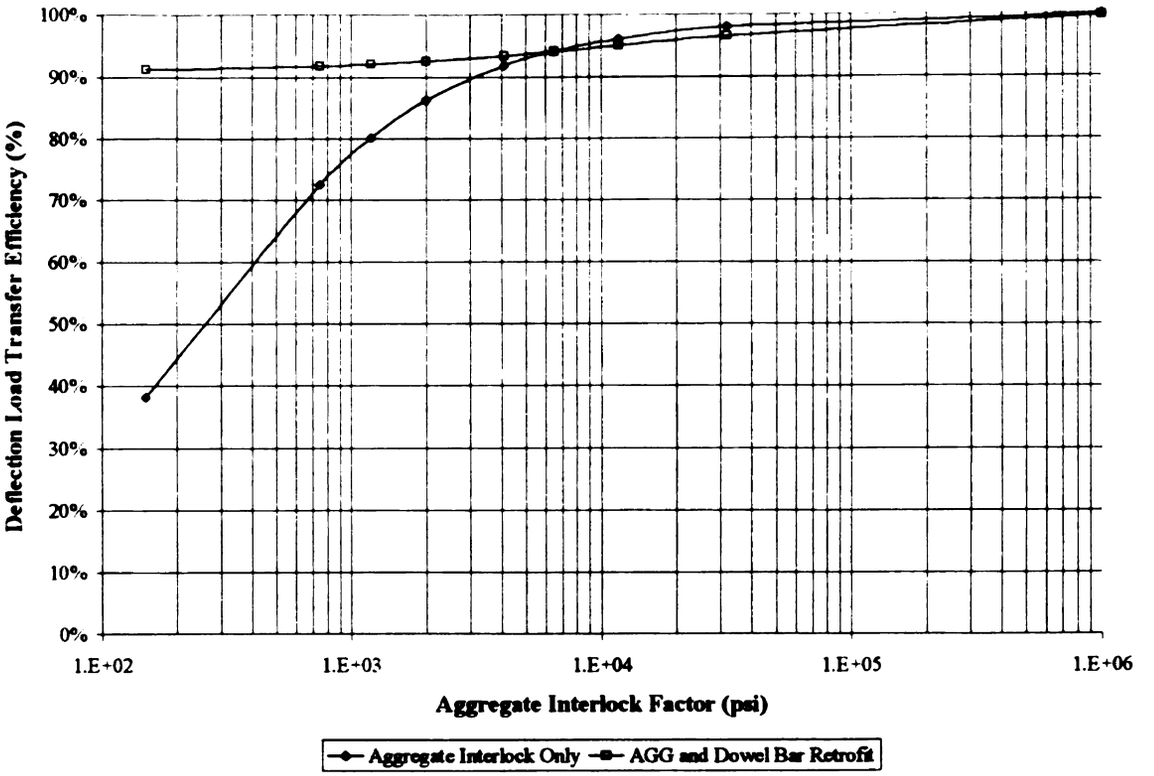

Figure B-1. LTE_δ with Respect to AGG Before and After Dowel Bar Retrofit for h=6" (152 mm), k=100 psi/in (27.1 kPa/mm), and ΔT=0°F (0°C).

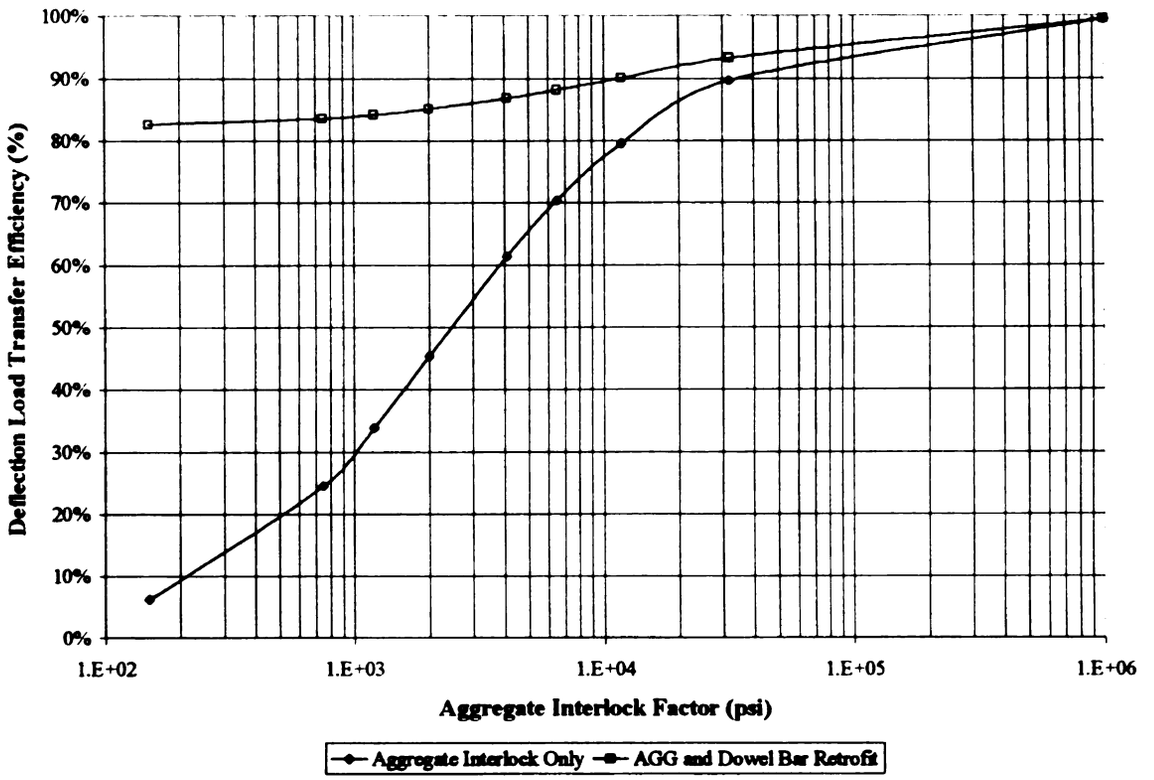

Figure B-2. LTE_δ with Respect to AGG Before and After Dowel Bar Retrofit for h=6" (152 mm), k=100 psi/in (27.1 kPa/mm), and ΔT=+15°F (+8.3°C).

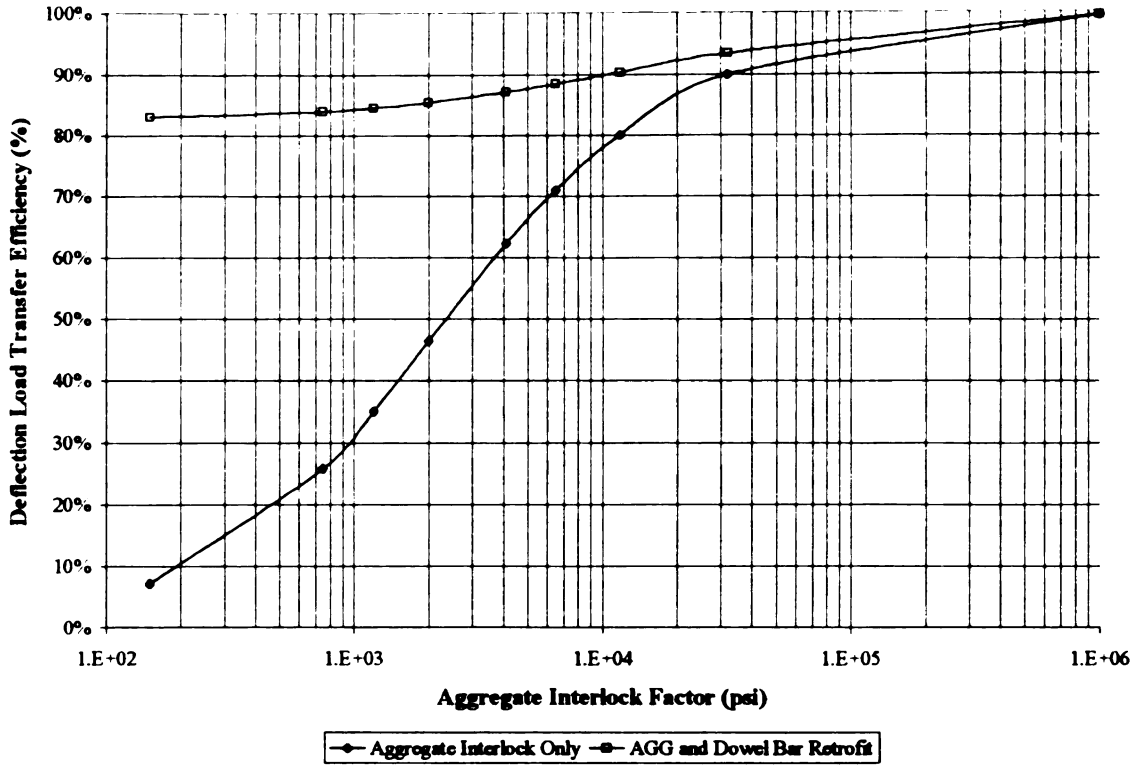

Figure B-3. LTE_δ with Respect to AGG Before and After Dowel Bar Retrofit for h=6" (152 mm), k=100 psi/in (27.1 kPa/mm), and ΔT=-15°F (-8.3°C).

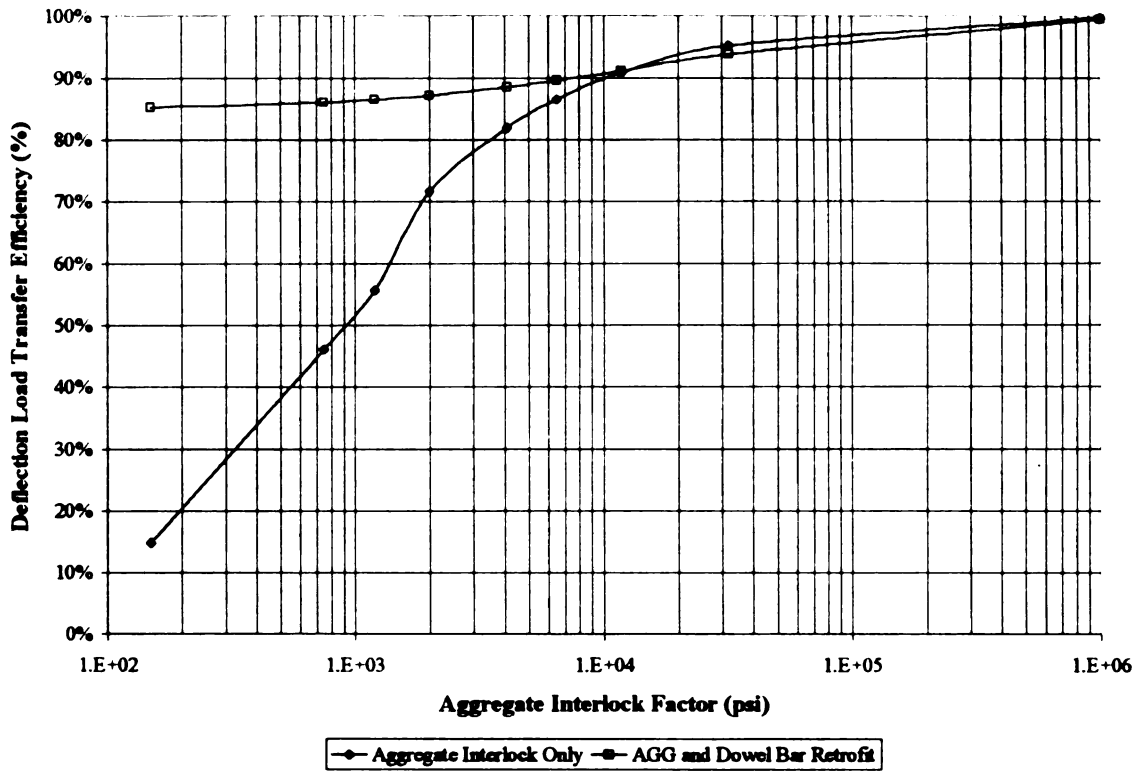

Figure B-4. LTE_δ with Respect to AGG Before and After Dowel Bar Retrofit for h=6" (152 mm), k=250 psi/in (67.9 kPa/mm), and ΔT=0°F (0°C).

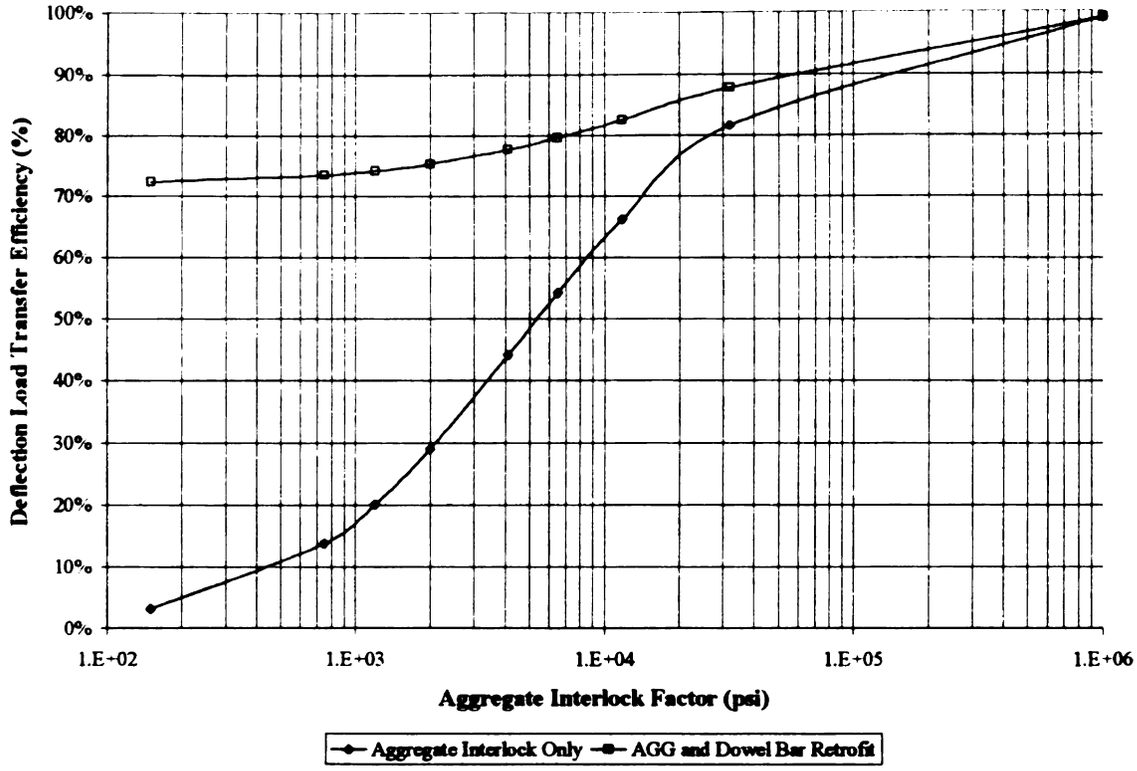

Figure B-5. LTE_δ with Respect to AGG Before and After Dowel Bar Retrofit for h=6" (152 mm), k=250 psi/in (67.9 kPa/mm), and ΔT=+15°F (+8.3°C).

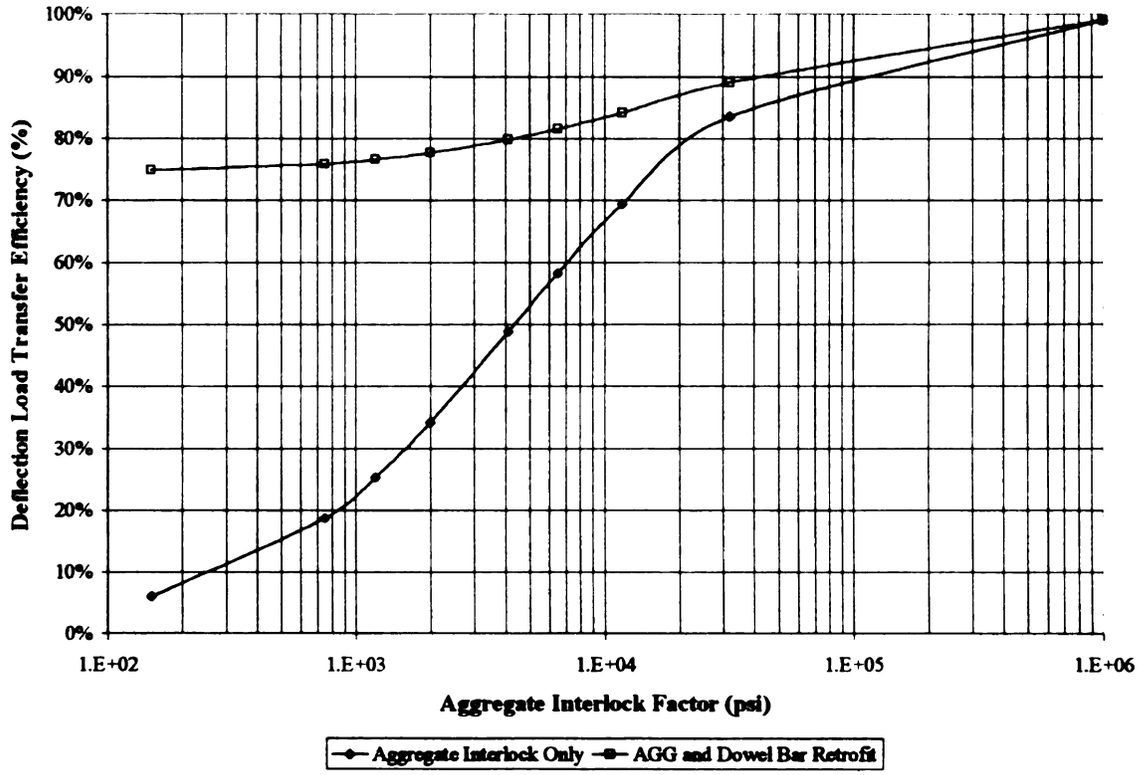

Figure B-6. LTE_δ with Respect to AGG Before and After Dowel Bar Retrofit for h=6" (152 mm), k=250 psi/in (67.9 kPa/mm), and ΔT=-15°F (-8.3°C).

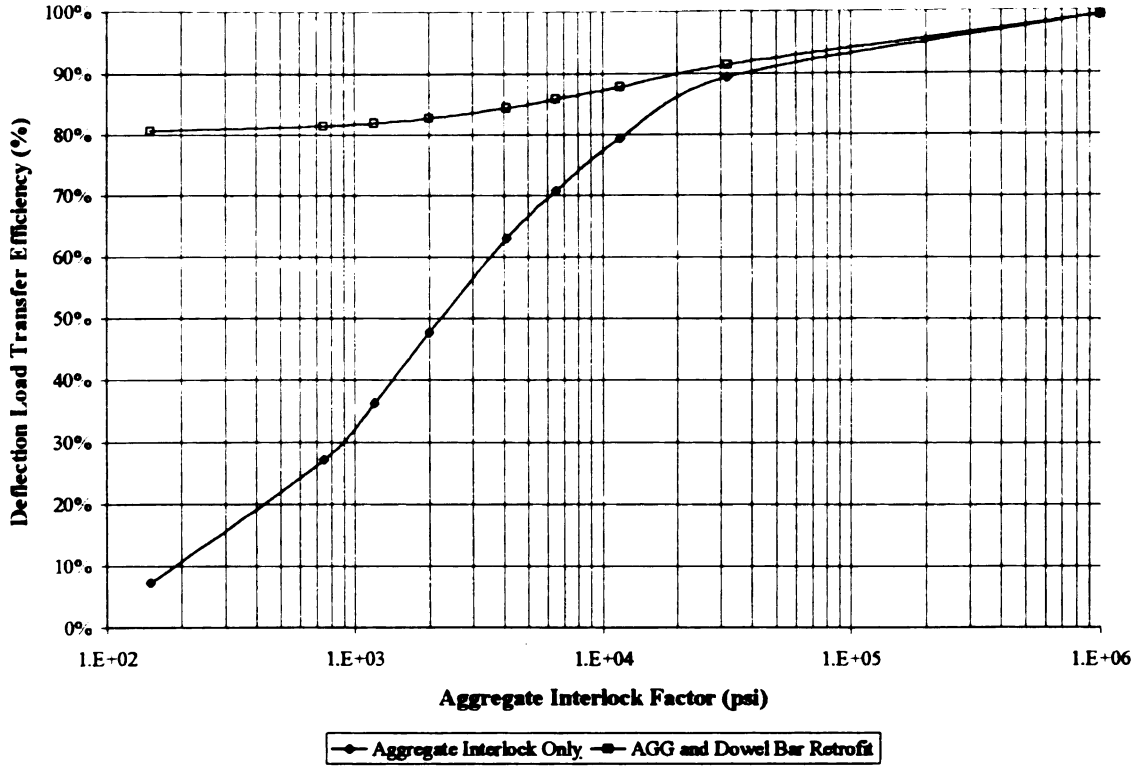

Figure B-7. LTE_δ with Respect to AGG Before and After Dowel Bar Retrofit for h=6" (152 mm), k=400 psi/in (106.8 kPa/mm), and ΔT=0°F (0°C).

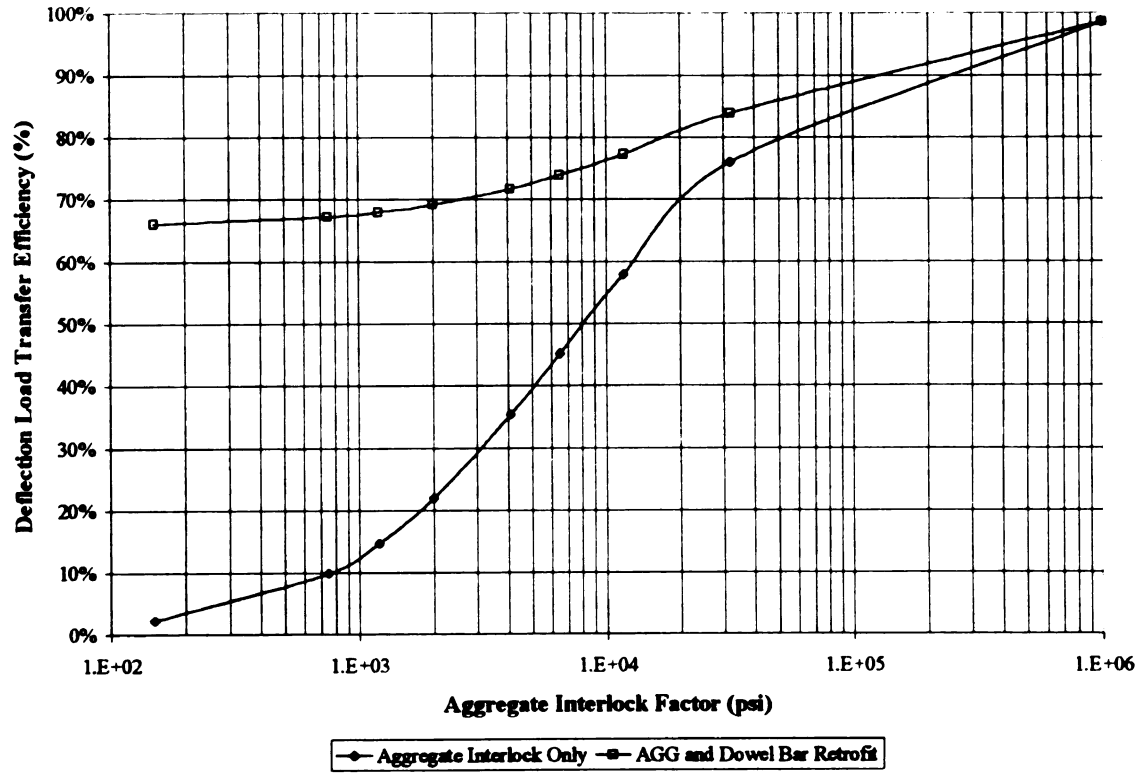

Figure B-8. LTE_δ with Respect to AGG Before and After Dowel Bar Retrofit for h=6" (152 mm), k=400 psi/in (106.8 kPa/mm), and ΔT=+15°F (+8.3°C).

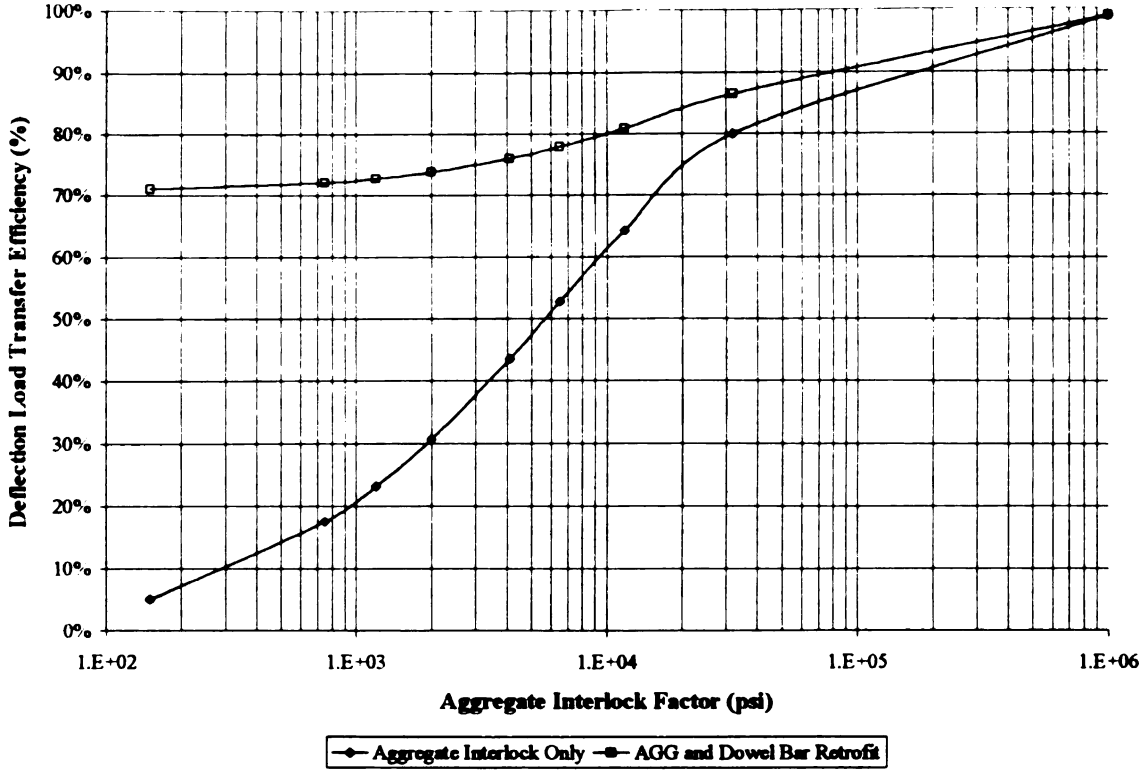

Figure B-9. LTE_δ with Respect to AGG Before and After Dowel Bar Retrofit for h=6" (152 mm), k=400 psi/in (106.8 kPa/mm), and ΔT=-15°F (-8.3°C).

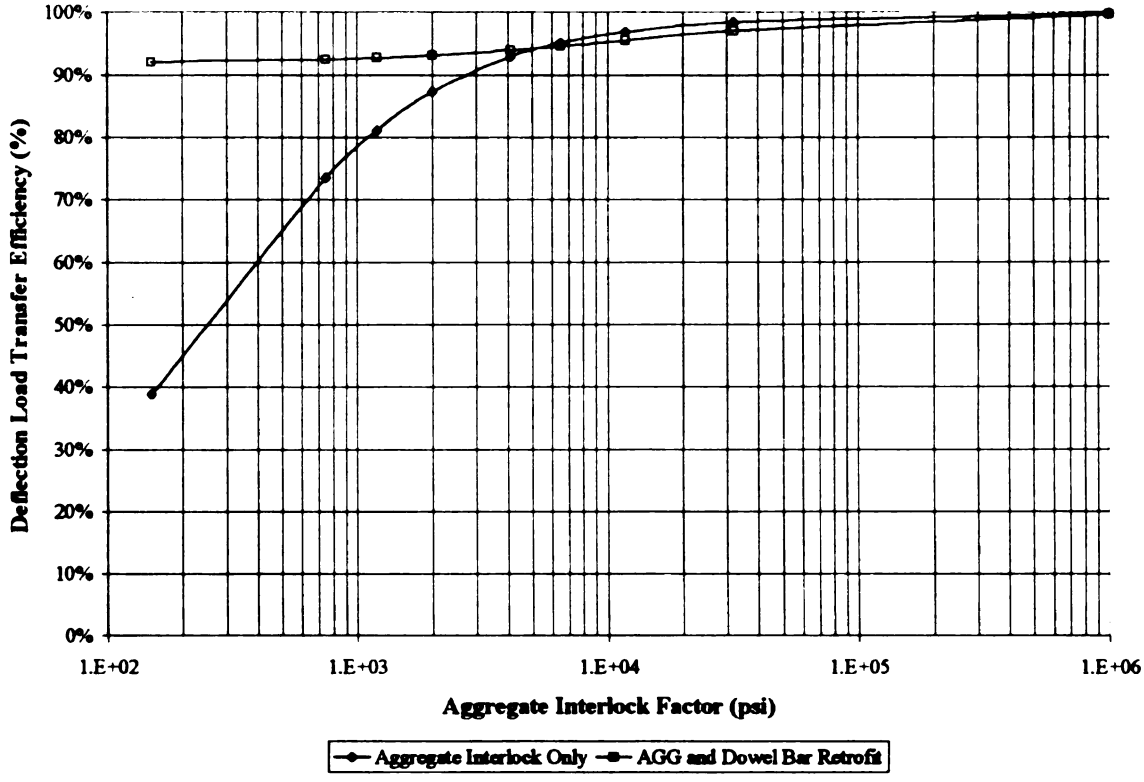

Figure B-10. LTE_δ with Respect to AGG Before and After Dowel Bar Retrofit for h=8" (203 mm), k=100 psi/in (27.1 kPa/mm), and ΔT=0°F (0°C).

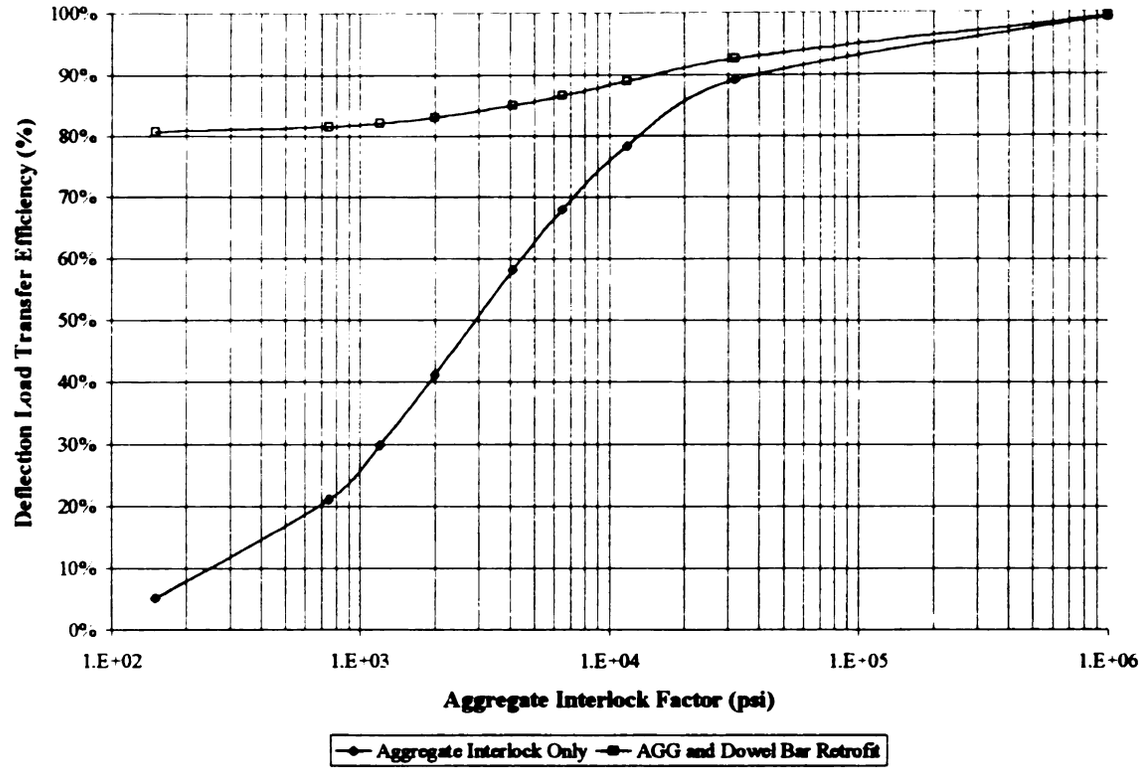

Figure B-11. LTE_δ with Respect to AGG Before and After Dowel Bar Retrofit for h=8" (203 mm), k=100 psi/in (27.1 kPa/mm), and ΔT=+15°F (+8.3°C).

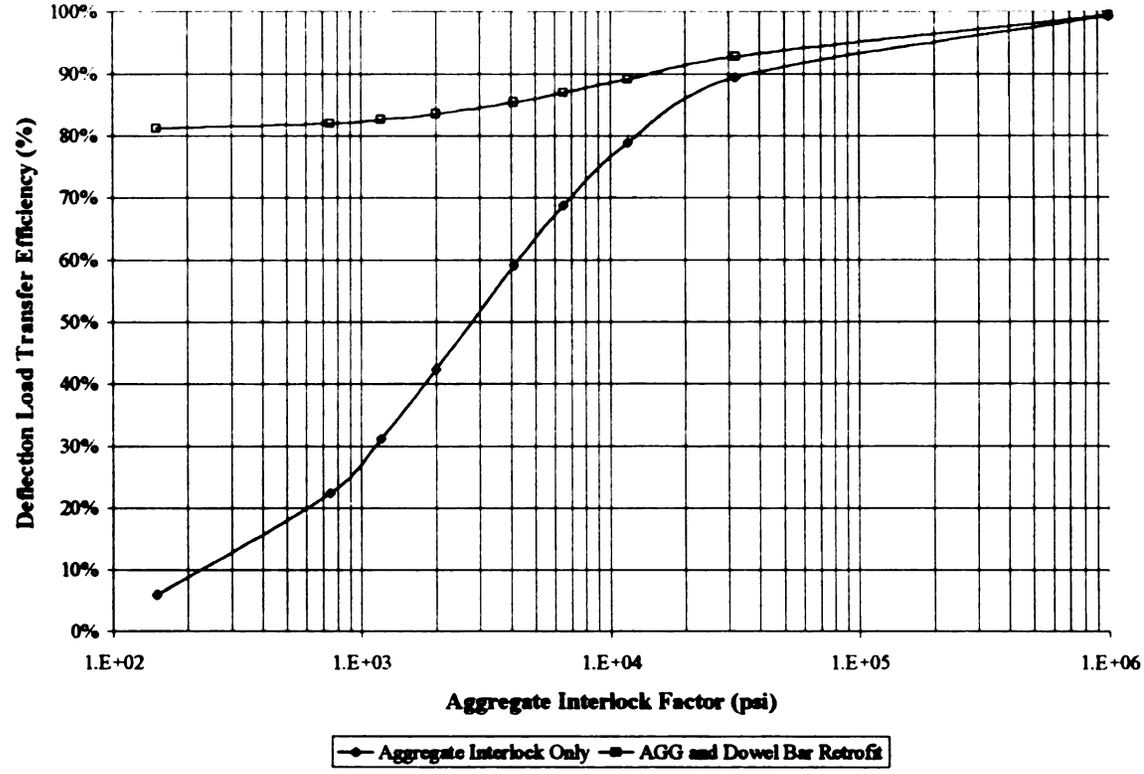

Figure B-12. LTE_δ with Respect to AGG Before and After Dowel Bar Retrofit for h=8" (203 mm), k=100 psi/in (27.1 kPa/mm), and ΔT=-15°F (-8.3°C).

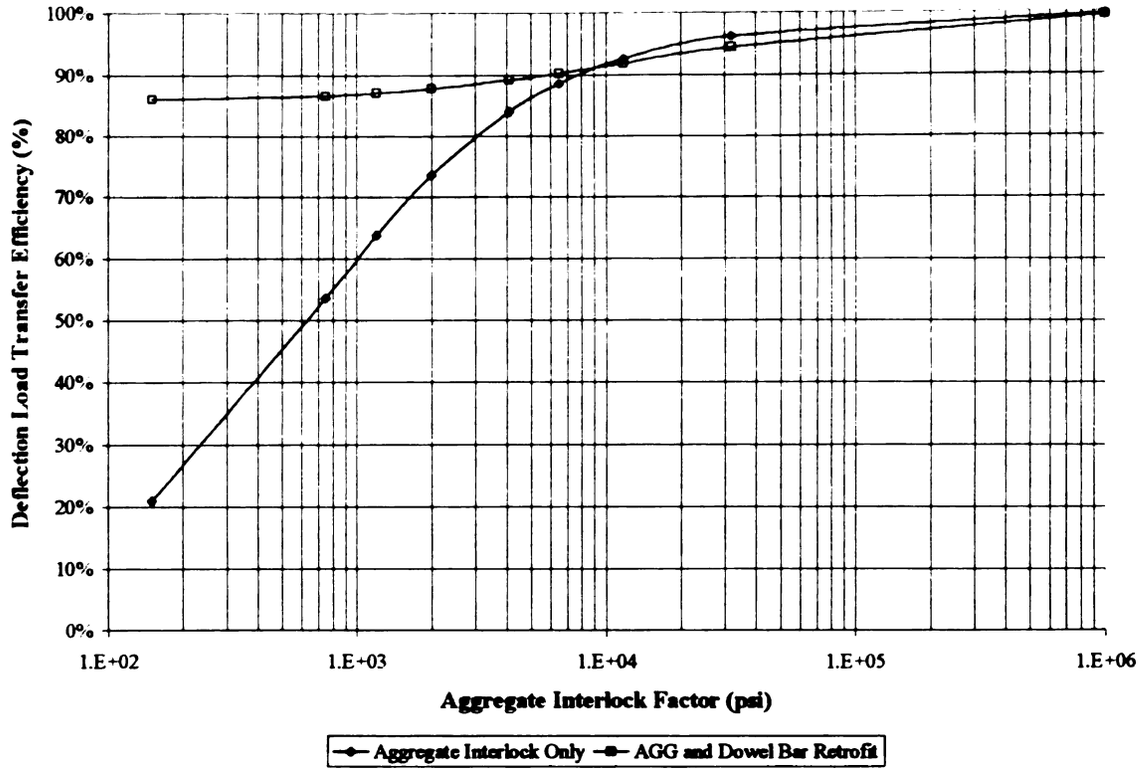

Figure B-13. LTE_δ with Respect to AGG Before and After Dowel Bar Retrofit for h=8" (203 mm), k=250 psi/in (67.9 kPa/mm), and ΔT=0°F (0°C).

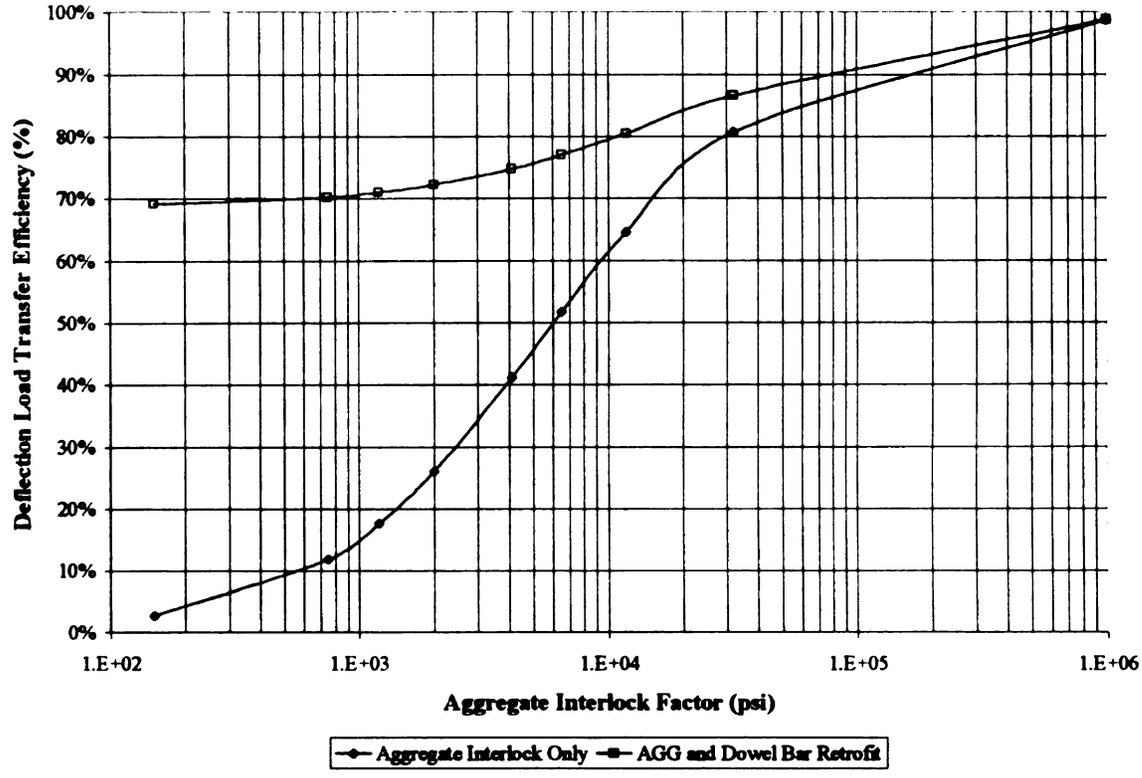

Figure B-14. LTE_δ with Respect to AGG Before and After Dowel Bar Retrofit for h=8" (203 mm), k=250 psi/in (67.9 kPa/mm), and ΔT=+15°F (+8.3°C).

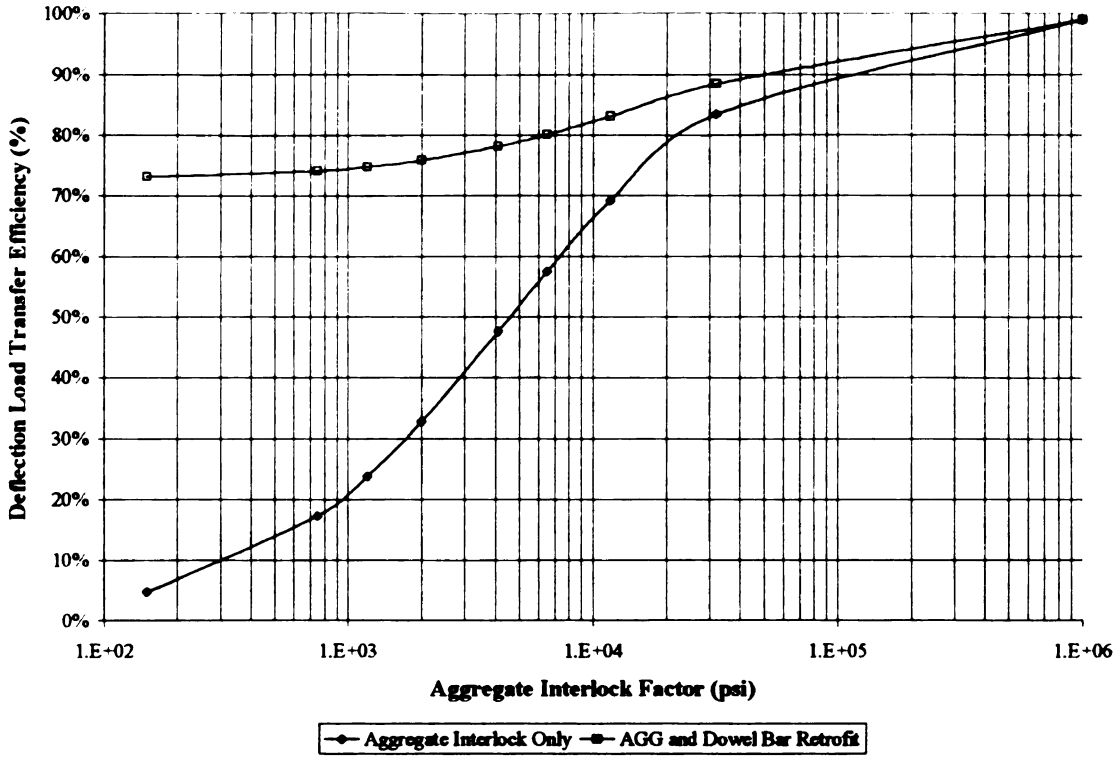

Figure B-15. LTE_δ with Respect to AGG Before and After Dowel Bar Retrofit for h=8" (203 mm), k=250 psi/in (67.9 kPa/mm), and ΔT=-15°F (-8.3°C).

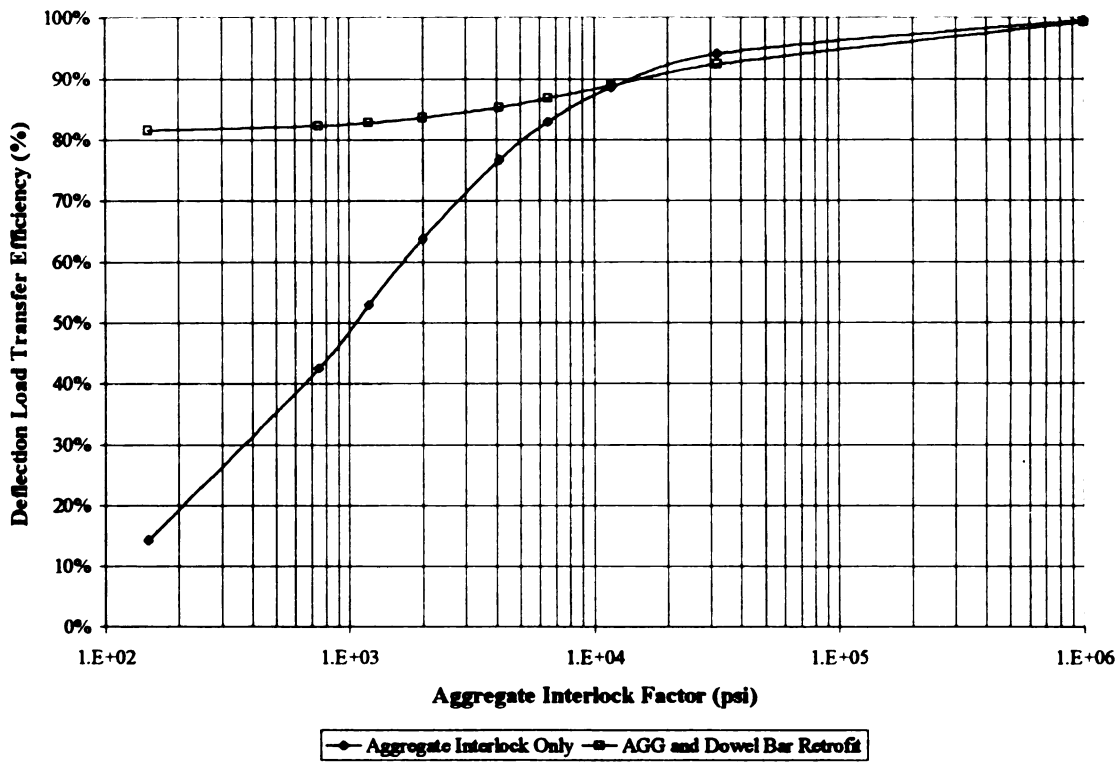

Figure B-16. LTE_δ with Respect to AGG Before and After Dowel Bar Retrofit for h=8" (203 mm), k=400 psi/in (106.8 kPa/mm), and ΔT=0°F (0°C).

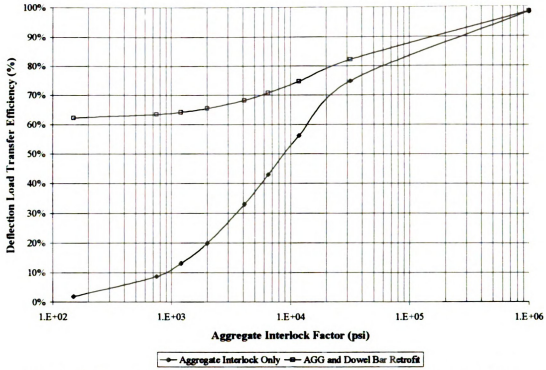

Figure B-17. LTE_δ with Respect to AGG Before and After Dowel Bar Retrofit for h=8" (203 mm), k=400 psi/in (106.8 kPa/mm), and ΔT=+15°F (+8.3°C).

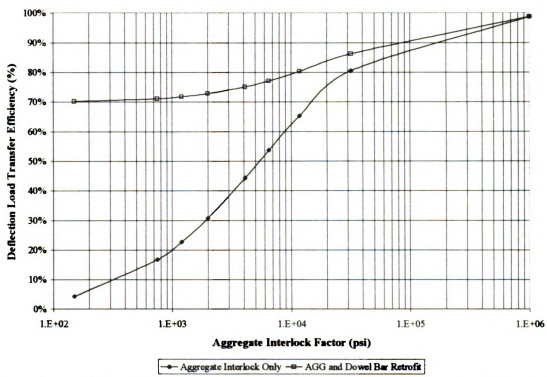

Figure B-18. LTE_δ with Respect to AGG Before and After Dowel Bar Retrofit for h=8" (203 mm), k=400 psi/in (106.8 kPa/mm), and ΔT=-15°F (-8.3°C).

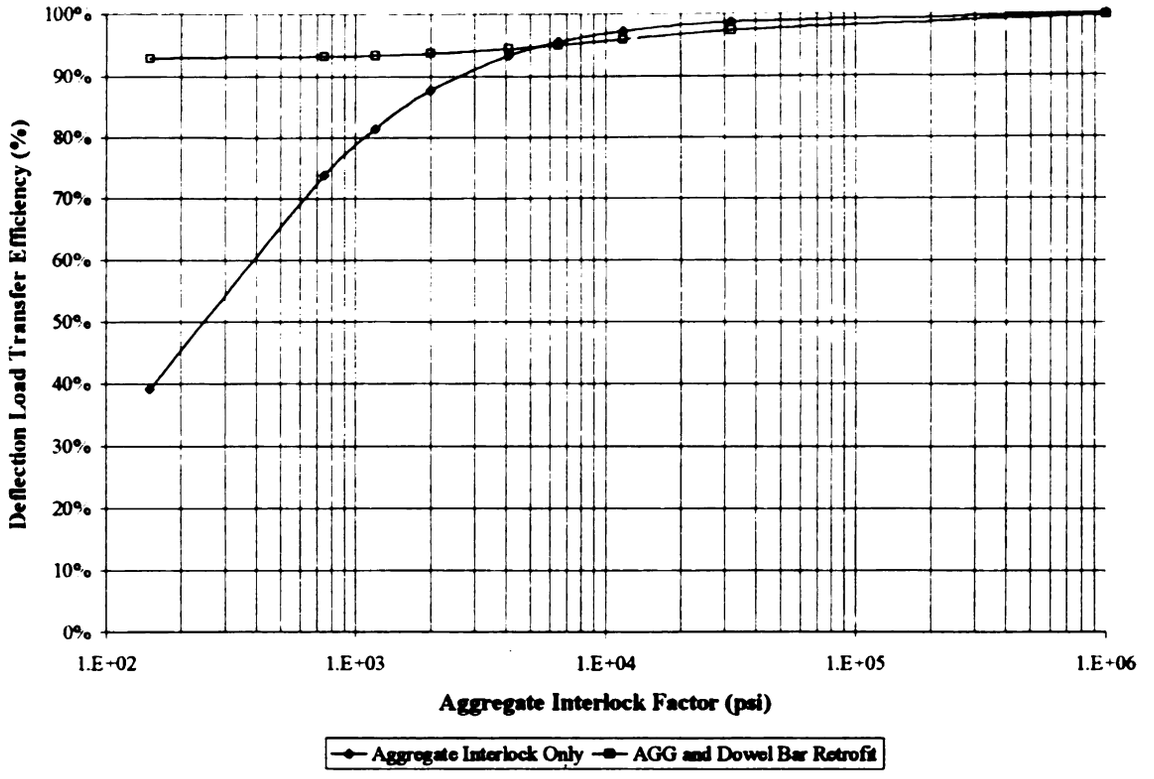

Figure B-19. LTE_δ with Respect to AGG Before and After Dowel Bar Retrofit for h=10" (254 mm), k=100 psi/in (27.1 kPa/mm), and ΔT=0°F (0°C).

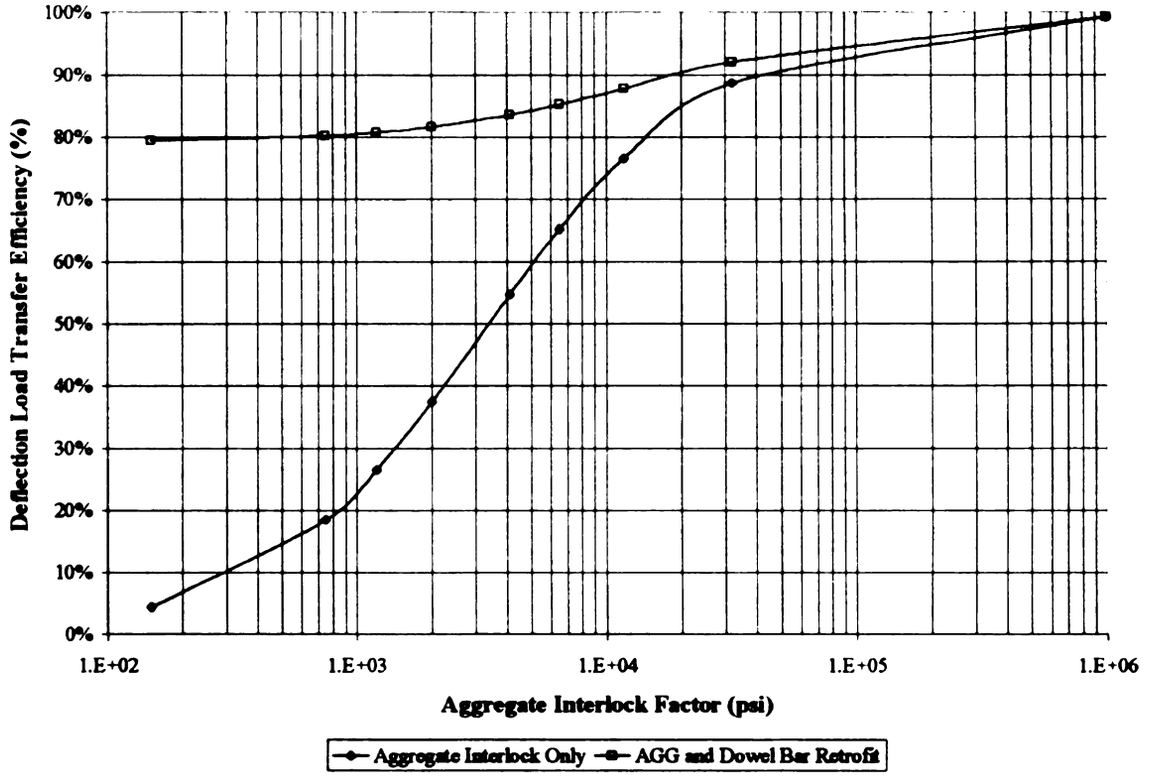

Figure B-20. LTE_δ with Respect to AGG Before and After Dowel Bar Retrofit for h=10" (254 mm), k=100 psi/in (27.1 kPa/mm), and ΔT=+15°F (+8.3°C).

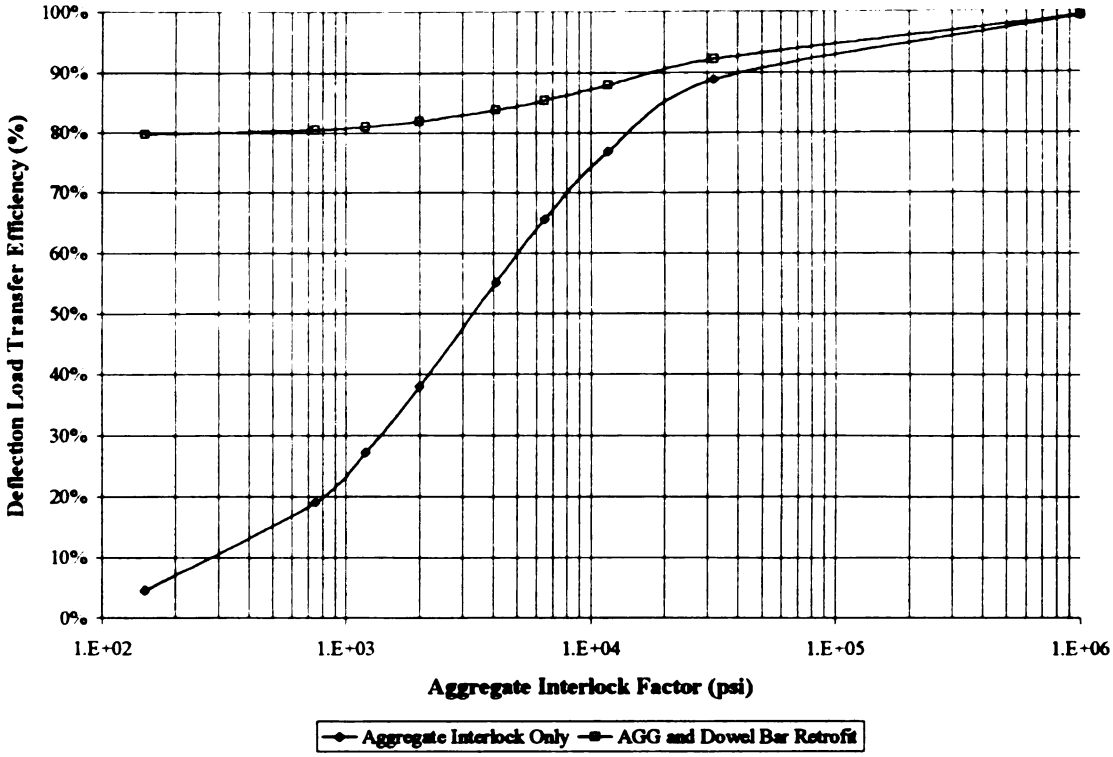

Figure B-21. LTE_δ with Respect to AGG Before and After Dowel Bar Retrofit for h=10" (254 mm), k=100 psi/in (27.1 kPa/mm), and ΔT=-15°F (-8.3°C).

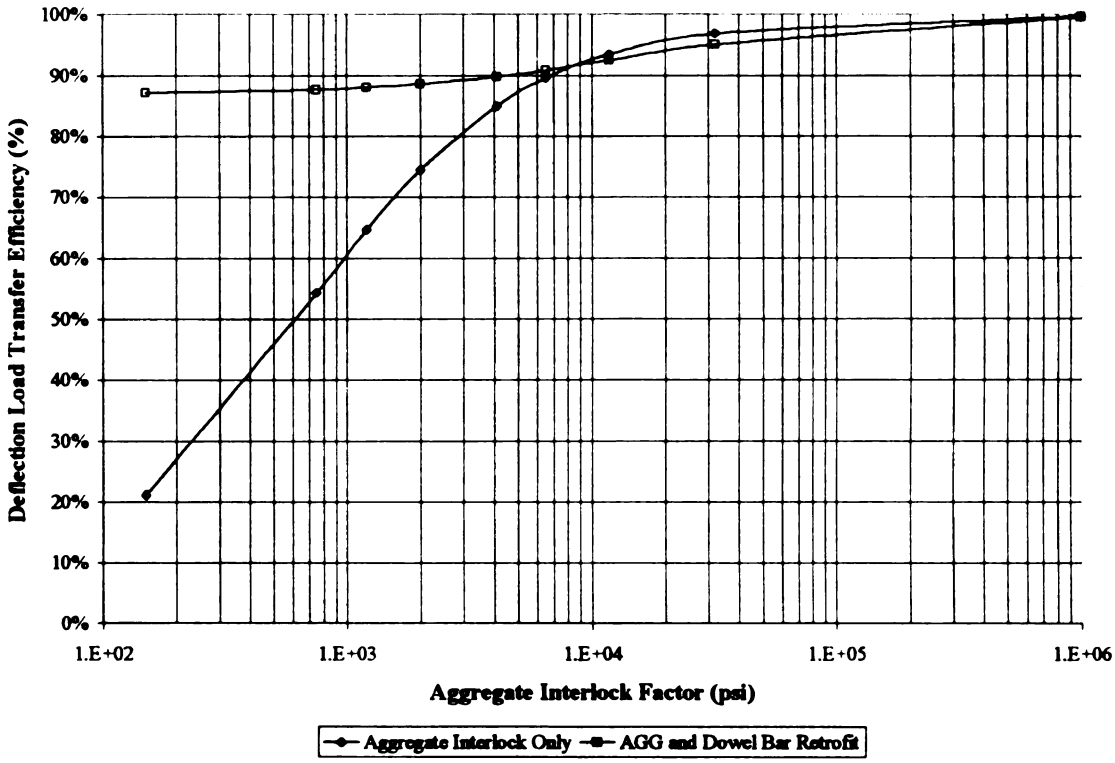

Figure B-22. LTE_δ with Respect to AGG Before and After Dowel Bar Retrofit for h=10" (254 mm), k=250 psi/in (67.9 kPa/mm), and ΔT=0°F (0°C).

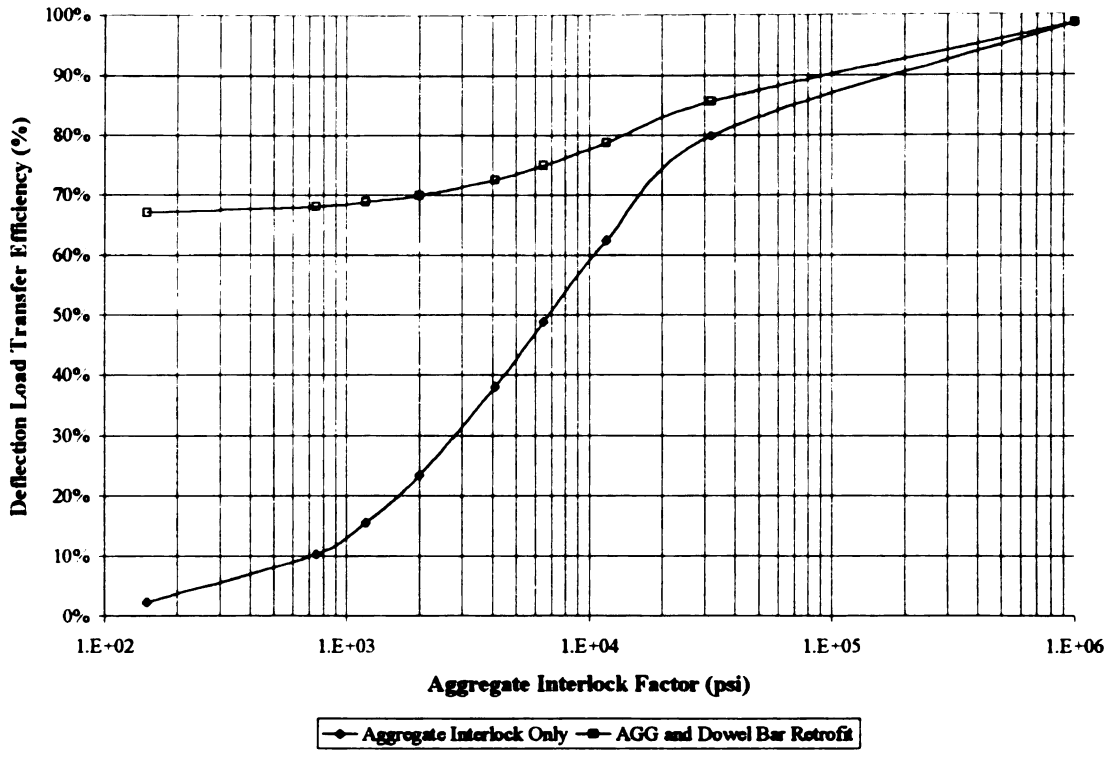

Figure B-23. LTE_δ with Respect to AGG Before and After Dowel Bar Retrofit for h=10" (254 mm), k=250 psi/in (67.9 kPa/mm), and ΔT=+15°F (+8.3°C).

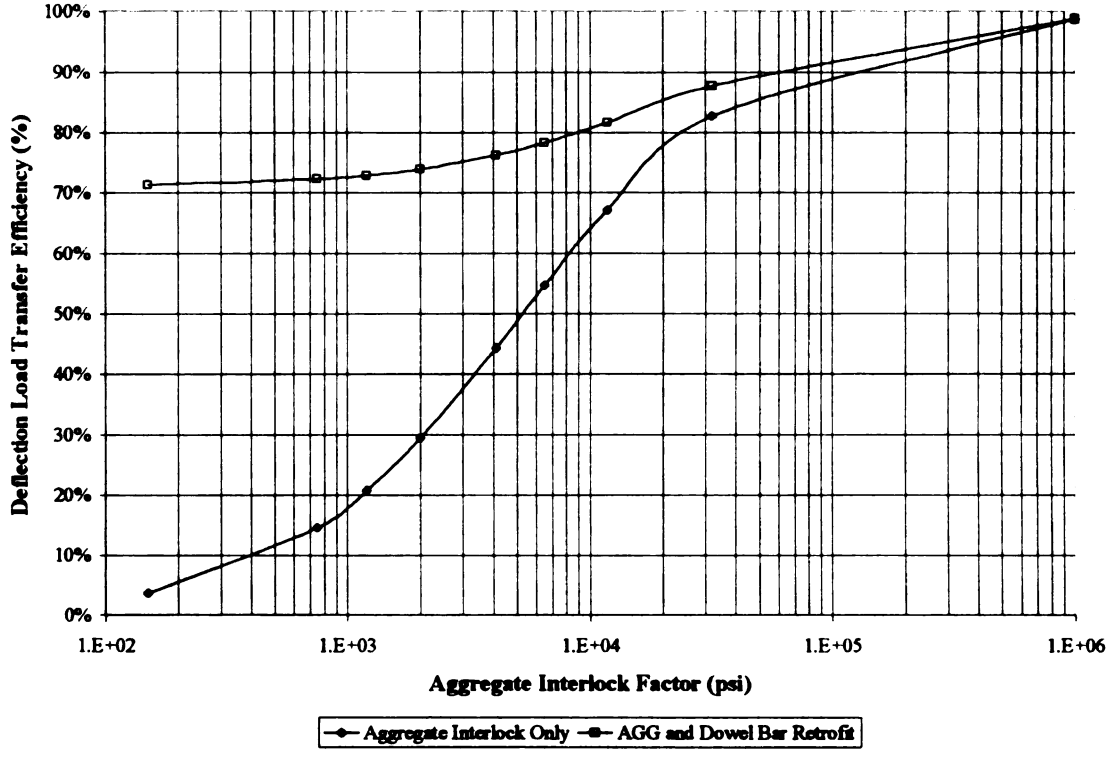

Figure B-24. LTE_δ with Respect to AGG Before and After Dowel Bar Retrofit for h=10" (254 mm), k=250 psi/in (67.9 kPa/mm), and ΔT=-15°F (-8.3°C).

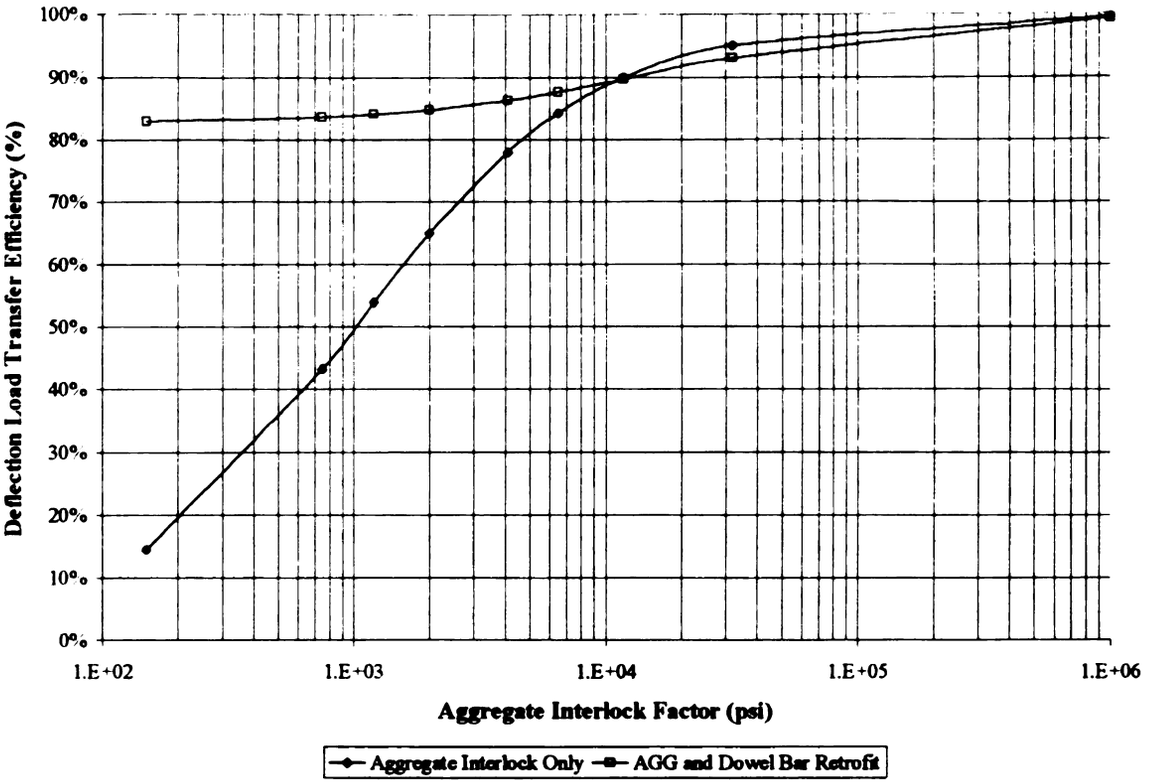

Figure B-25. LTE_δ with Respect to AGG Before and After Dowel Bar Retrofit for h=10" (254 mm), k=400 psi/in (106.8 kPa/mm), and ΔT=0°F (0°C).

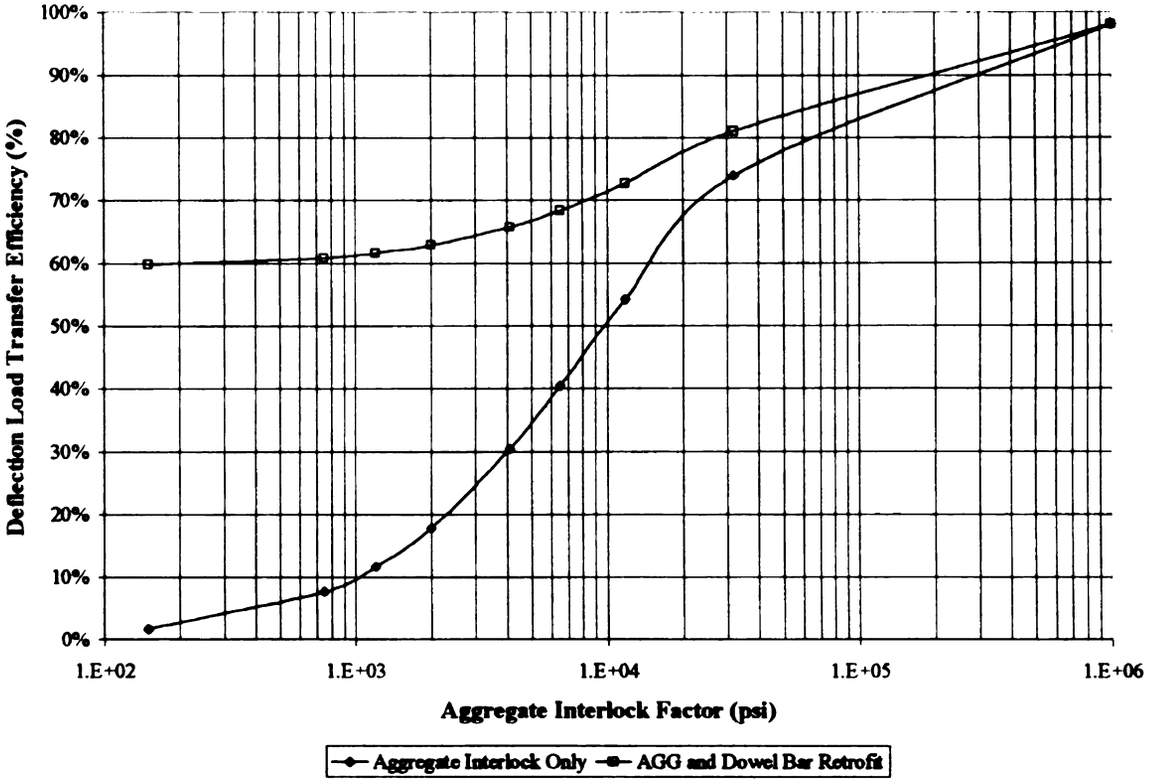

Figure B-26. LTE_δ with Respect to AGG Before and After Dowel Bar Retrofit for h=10" (254 mm), k=400 psi/in (106.8 kPa/mm), and ΔT=+15°F (+8.3°C).

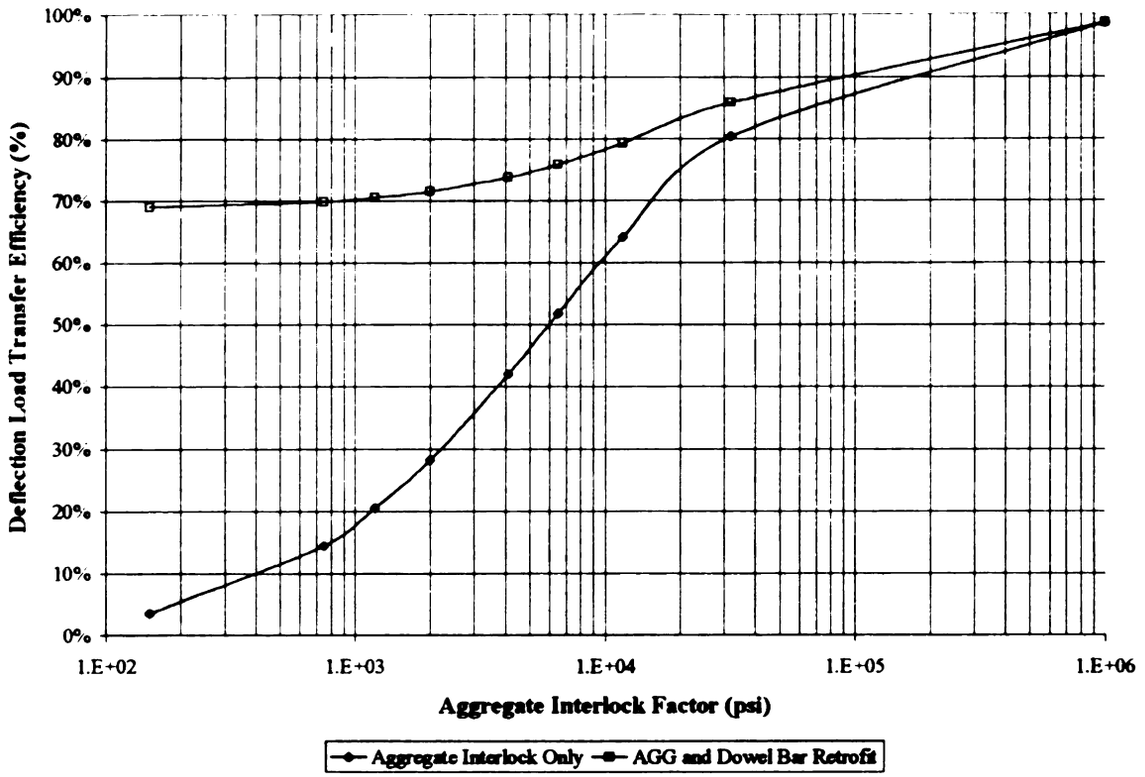

Figure B-27. LTE_δ with Respect to AGG Before and After Dowel Bar Retrofit for h=10" (254 mm), k=400 psi/in (106.8 kPa/mm), and ΔT=-15°F (-8.3°C).

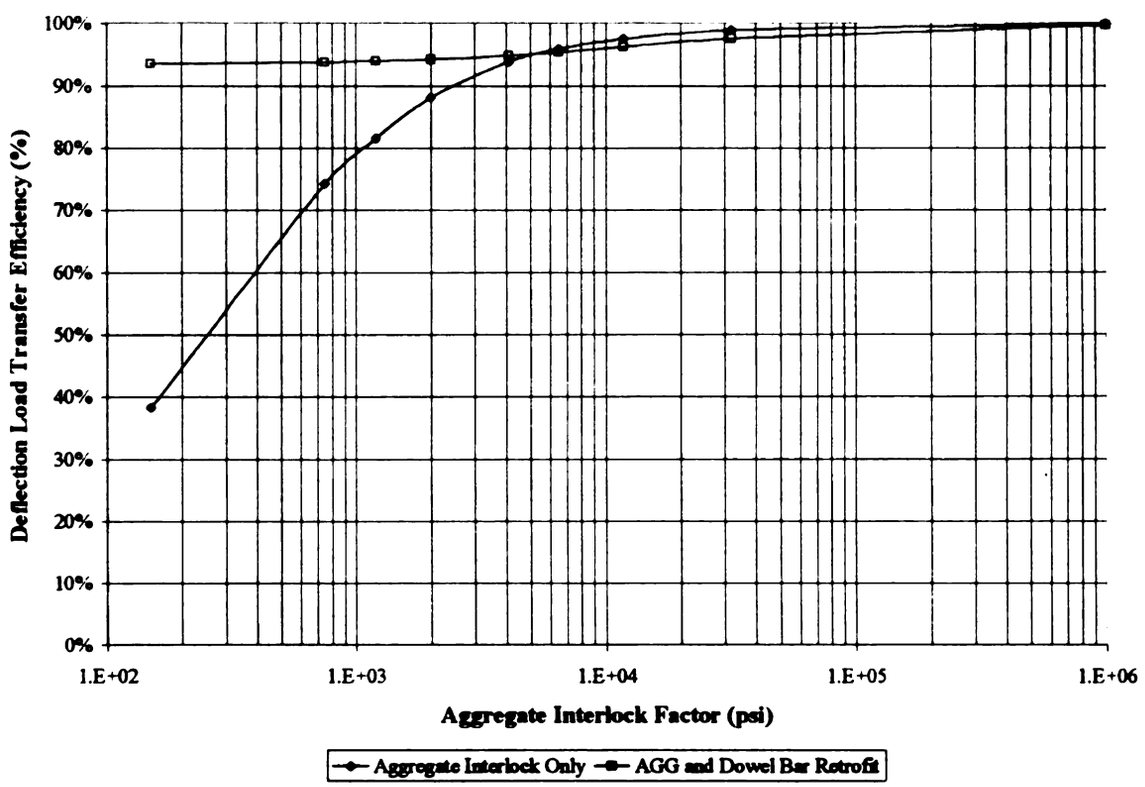

Figure B-28. LTE_δ with Respect to AGG Before and After Dowel Bar Retrofit for h=12" (305 mm), k=100 psi/in (27.1 kPa/mm), and ΔT=0°F (0°C).

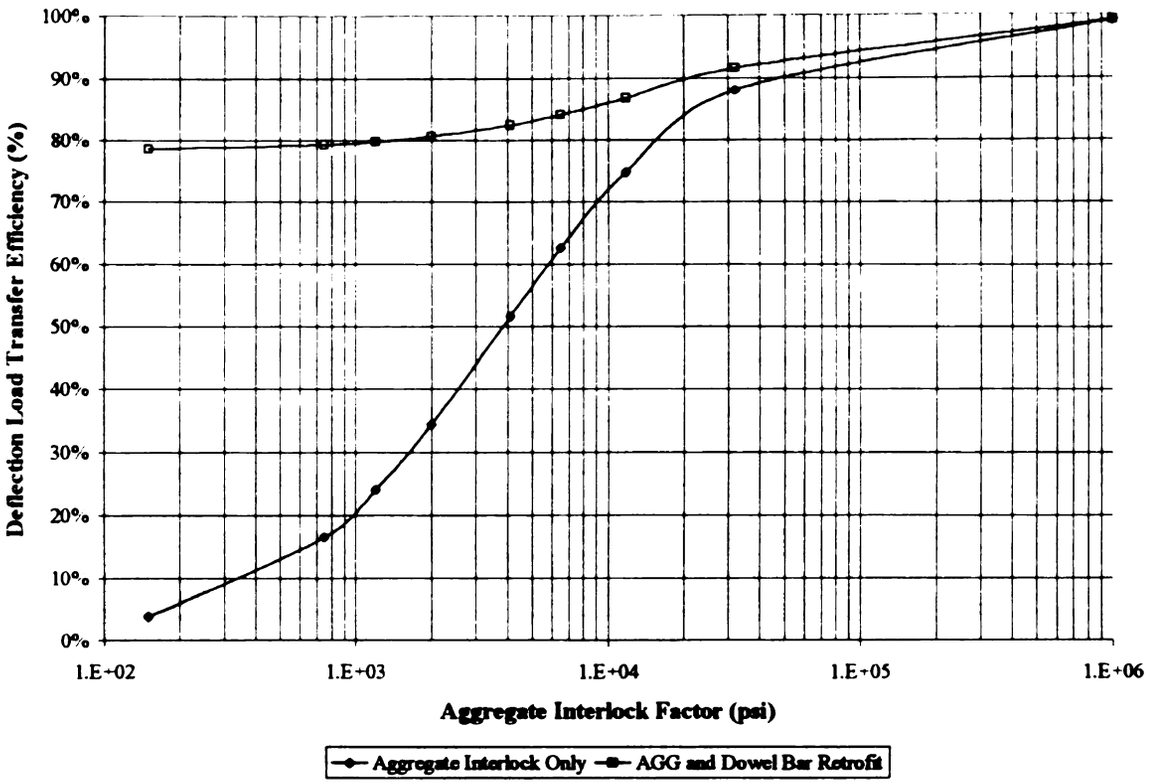

Figure B-29. LTE_δ with Respect to AGG Before and After Dowel Bar Retrofit for h=12" (305 mm), k=100 psi/in (27.1 kPa/mm), and ΔT=+15°F (+8.3°C).

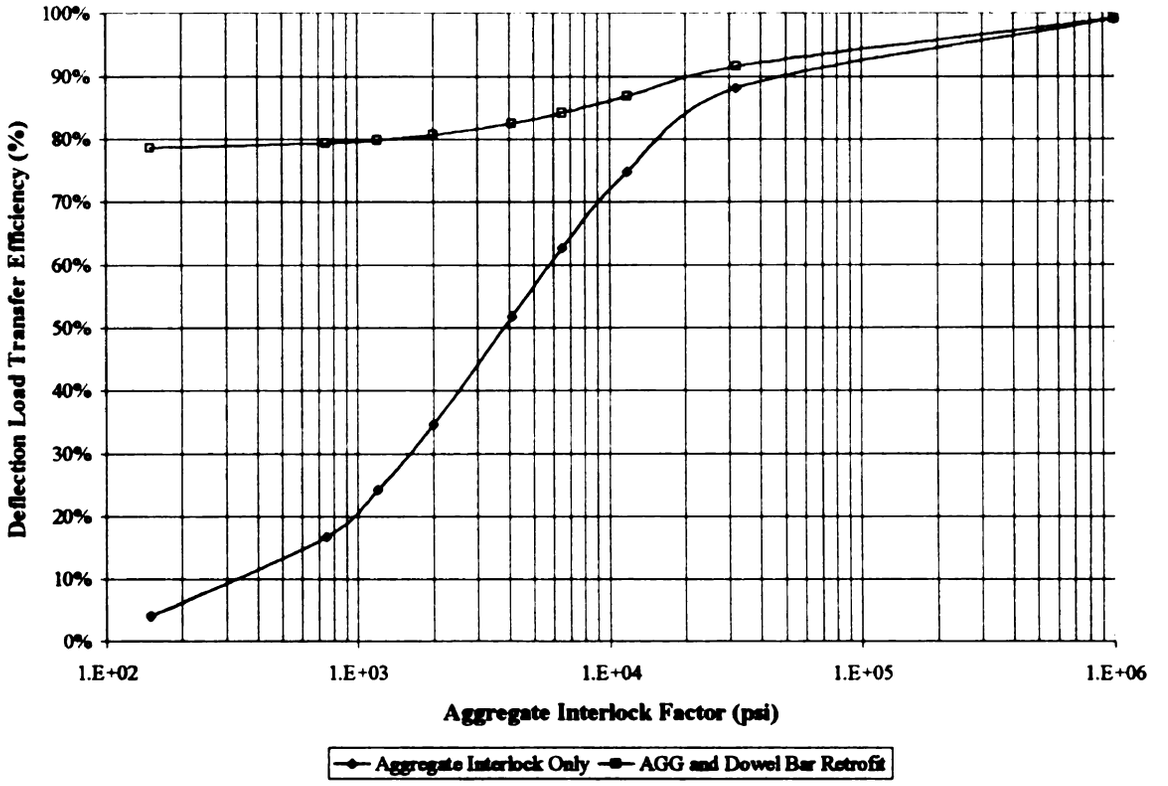

Figure B-30. LTE_δ with Respect to AGG Before and After Dowel Bar Retrofit for h=12" (305 mm), k=100 psi/in (27.1 kPa/mm), and ΔT=-15°F (-8.3°C).

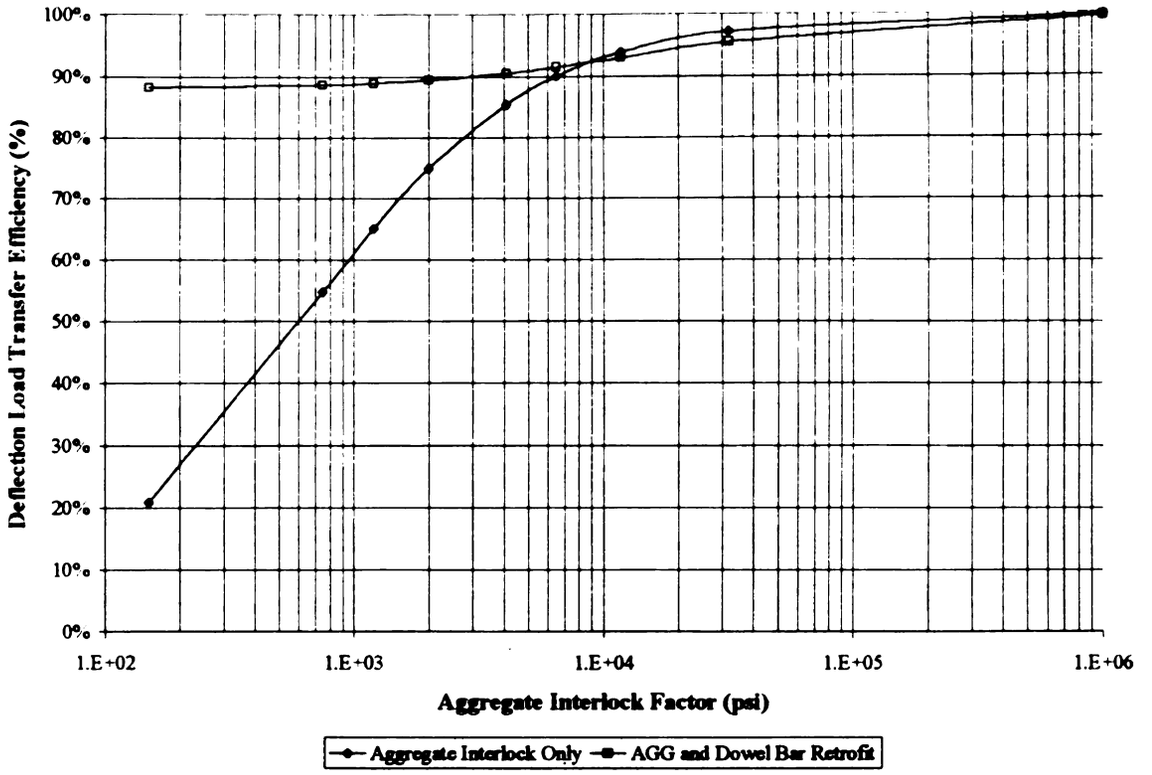

Figure B-31. LTE_δ with Respect to AGG Before and After Dowel Bar Retrofit for h=12" (305 mm), k=250 psi/in (67.9 kPa/mm), and ΔT=0°F (0°C).

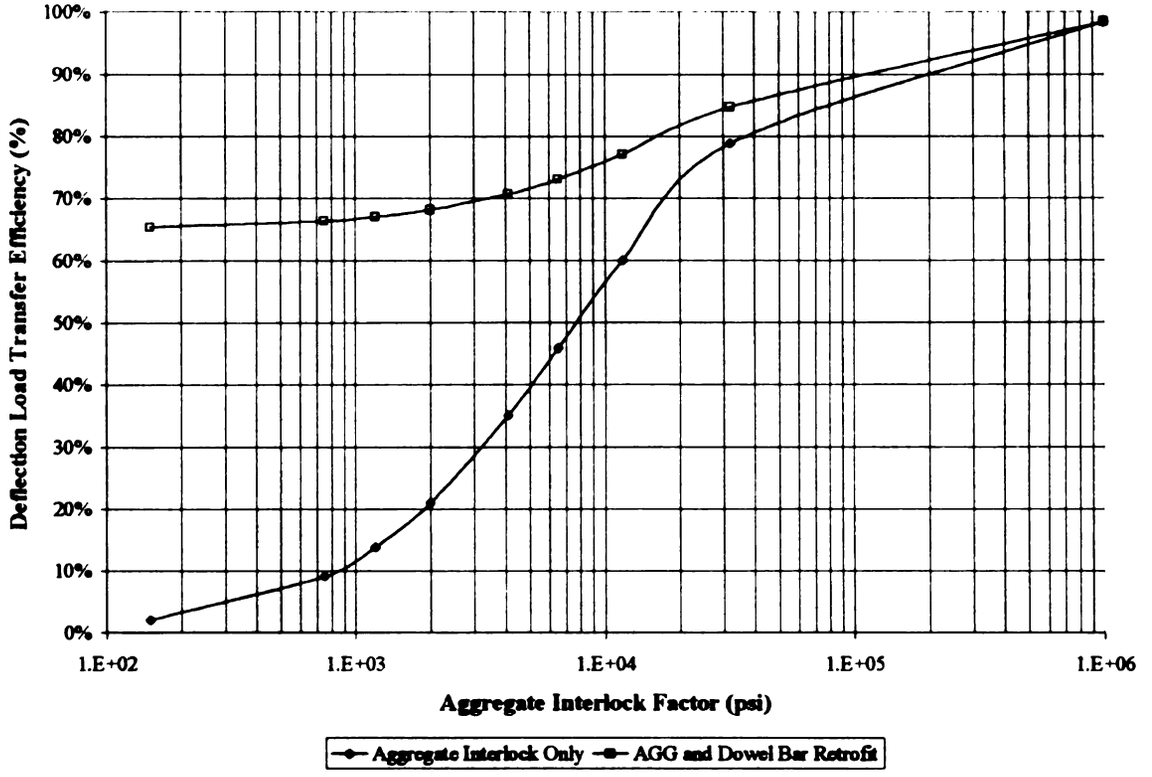

Figure B-32. LTE_δ with Respect to AGG Before and After Dowel Bar Retrofit for h=12" (305 mm), k=250 psi/in (67.9 kPa/mm), and ΔT=+15°F (+8.3°C).

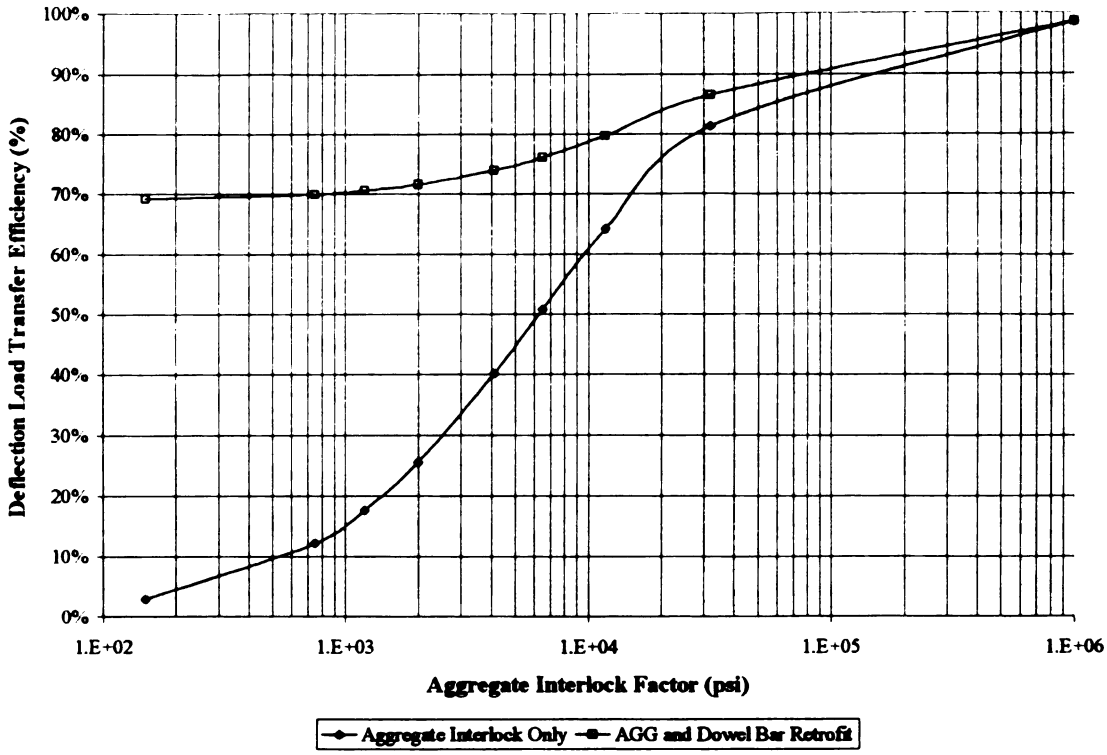

Figure B-33. LTE_δ with Respect to AGG Before and After Dowel Bar Retrofit for h=12" (305 mm), k=250 psi/in (67.9 kPa/mm), and ΔT=-15°F (-8.3°C).

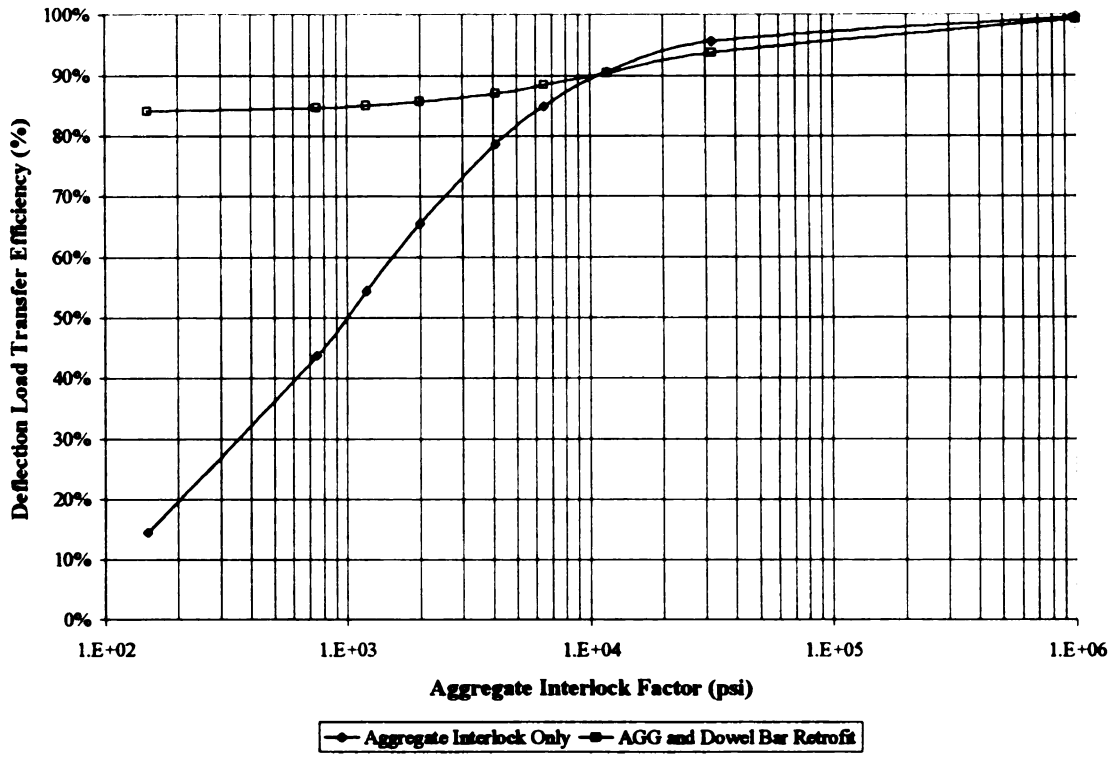

Figure B-34. LTE_δ with Respect to AGG Before and After Dowel Bar Retrofit for h=12" (305 mm), k=400 psi/in (106.8 kPa/mm), and ΔT=0°F (0°C).

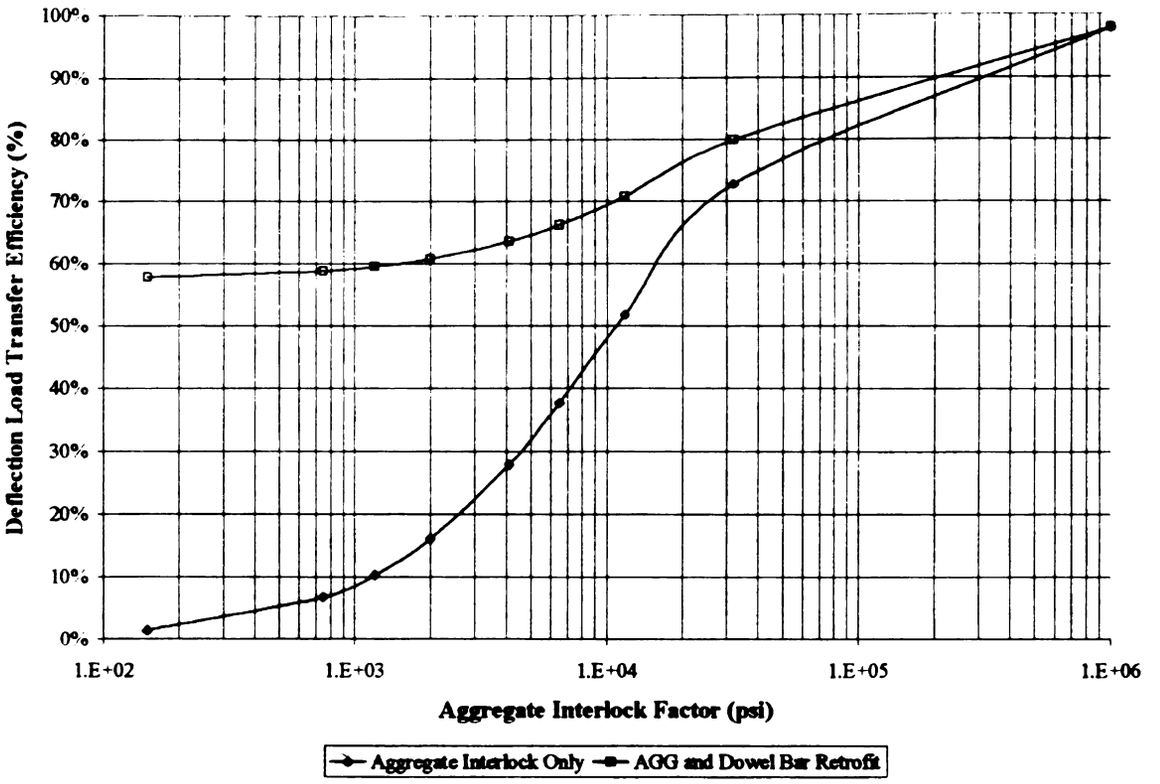

Figure B-35. LTE_δ with Respect to AGG Before and After Dowel Bar Retrofit for h=12" (305 mm), k=400 psi/in (106.8 kPa/mm), and ΔT=+15°F (+8.3°C).

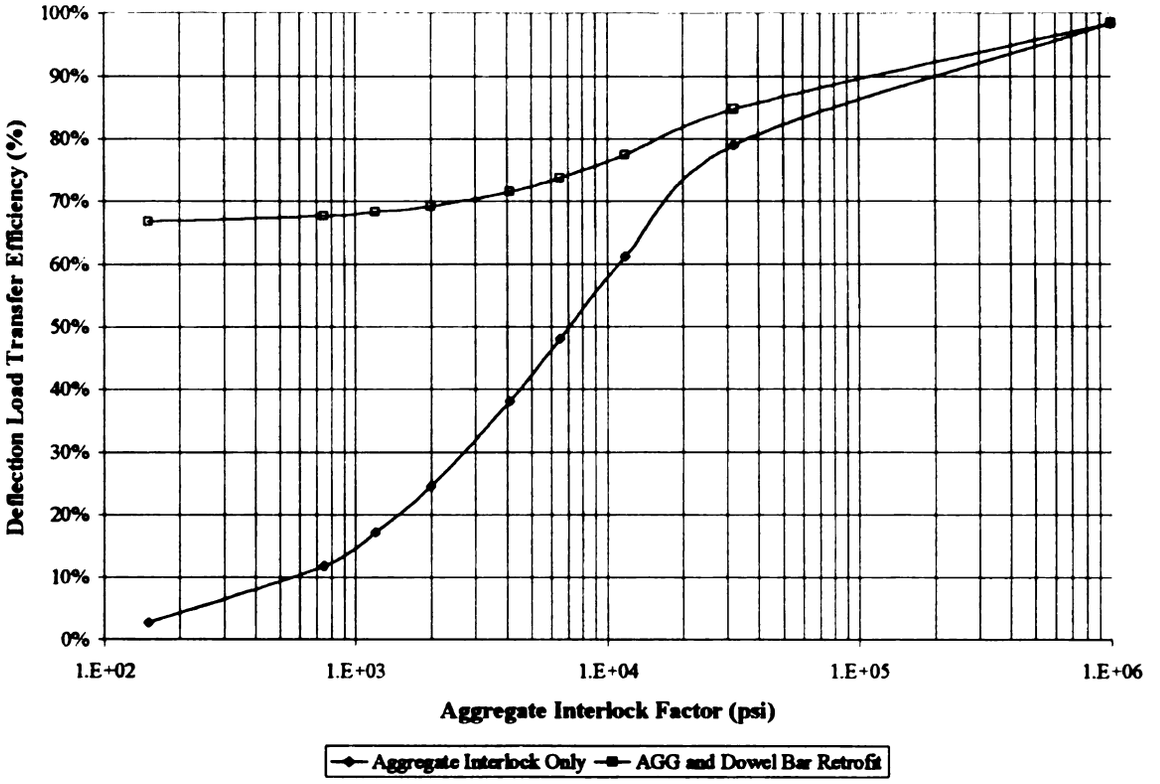

Figure B-36. LTE_δ with Respect to AGG Before and After Dowel Bar Retrofit for h=12" (305 mm), k=400 psi/in (106.8 kPa/mm), and ΔT=-15°F (-8.3°C).

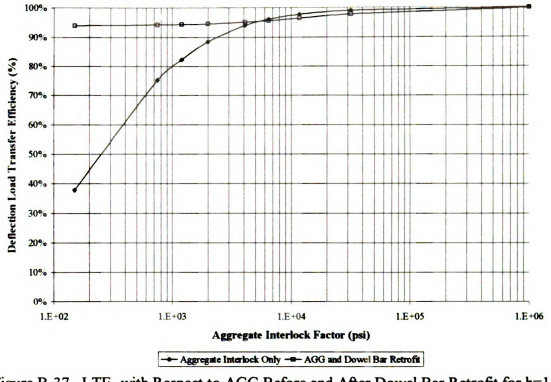

Figure B-37. LTE_δ with Respect to AGG Before and After Dowel Bar Retrofit for h=14" (356 mm), k=100 psi/in (27.1 kPa/mm), and ΔT=0°F (0°C).

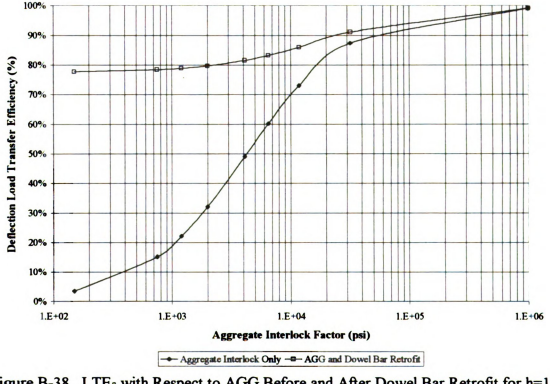

Figure B-38. LTE_δ with Respect to AGG Before and After Dowel Bar Retrofit for h=14" (356 mm), k=100 psi/in (27.1 kPa/mm), and ΔT=+15°F (+8.3°C).

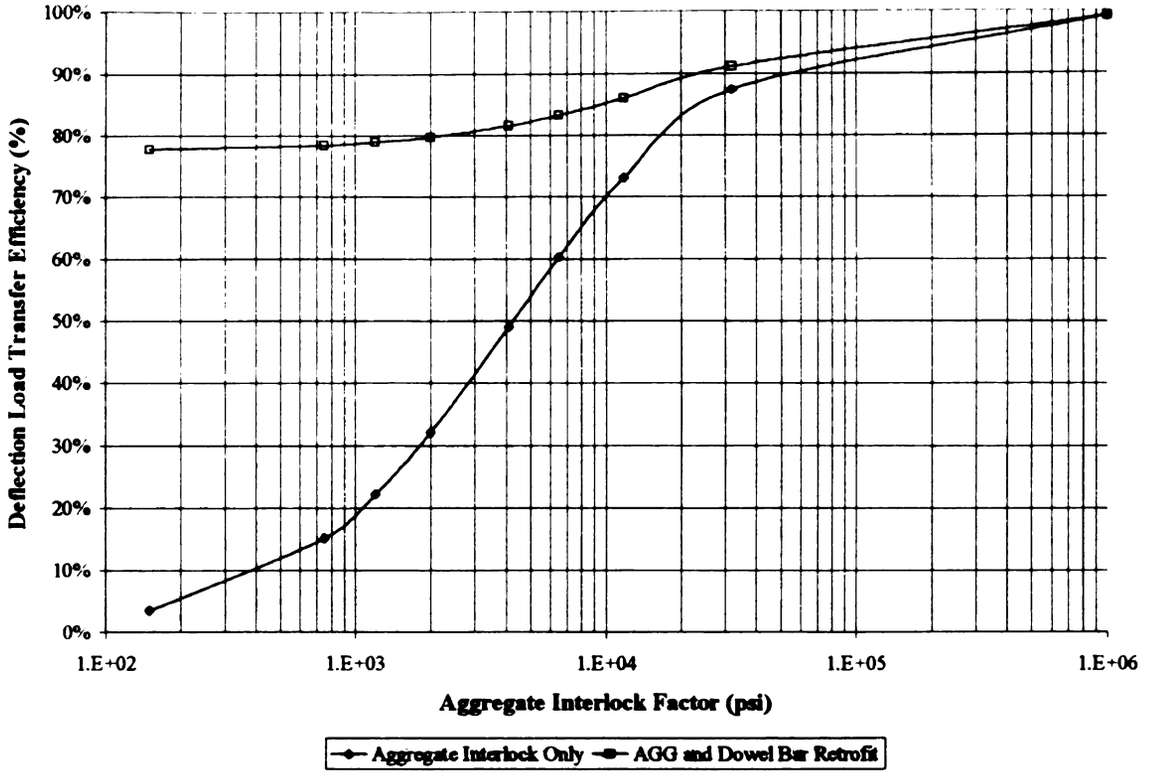

Figure B-39. LTE_δ with Respect to AGG Before and After Dowel Bar Retrofit for h=14" (356 mm), k=100 psi/in (27.1 kPa/mm), and ΔT=-15°F (-8.3°C).

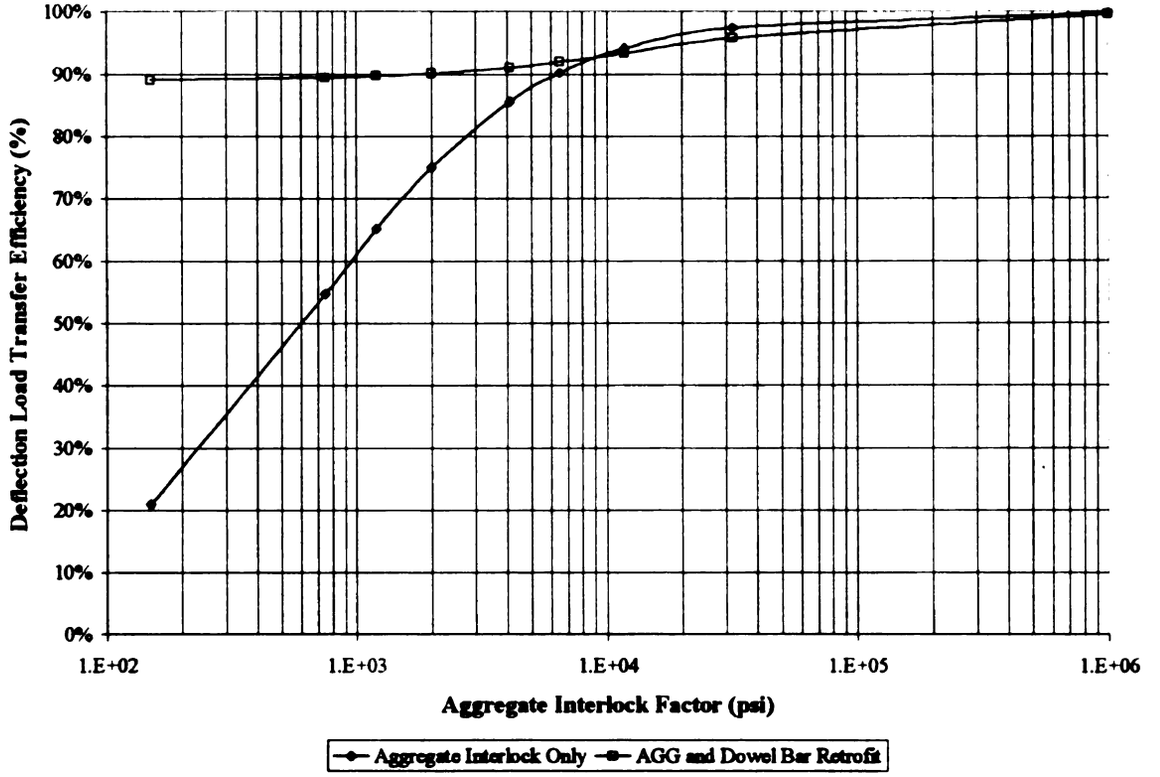

Figure B-40. LTE_δ with Respect to AGG Before and After Dowel Bar Retrofit for h=14" (356 mm), k=250 psi/in (67.9 kPa/mm), and ΔT=0°F (0°C).

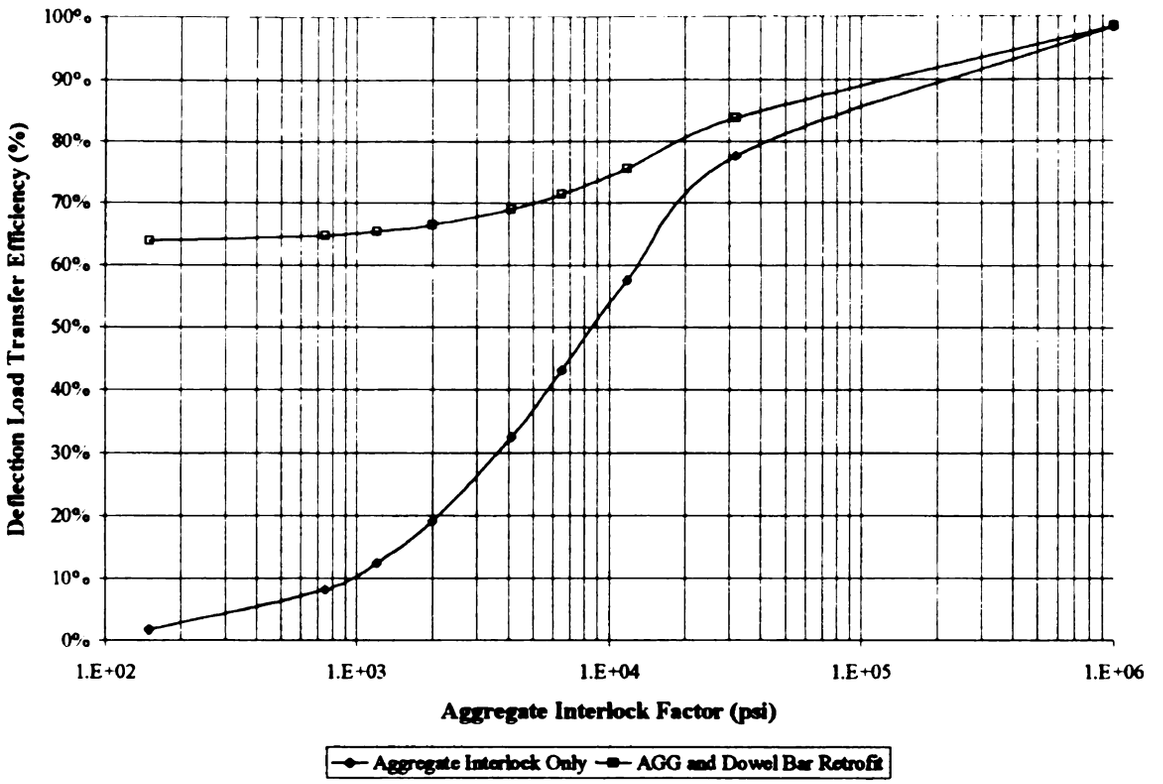

Figure B-41. LTE_δ with Respect to AGG Before and After Dowel Bar Retrofit for h=14" (356 mm), k=250 psi/in (67.9 kPa/mm), and ΔT=+15°F (+8.3°C).

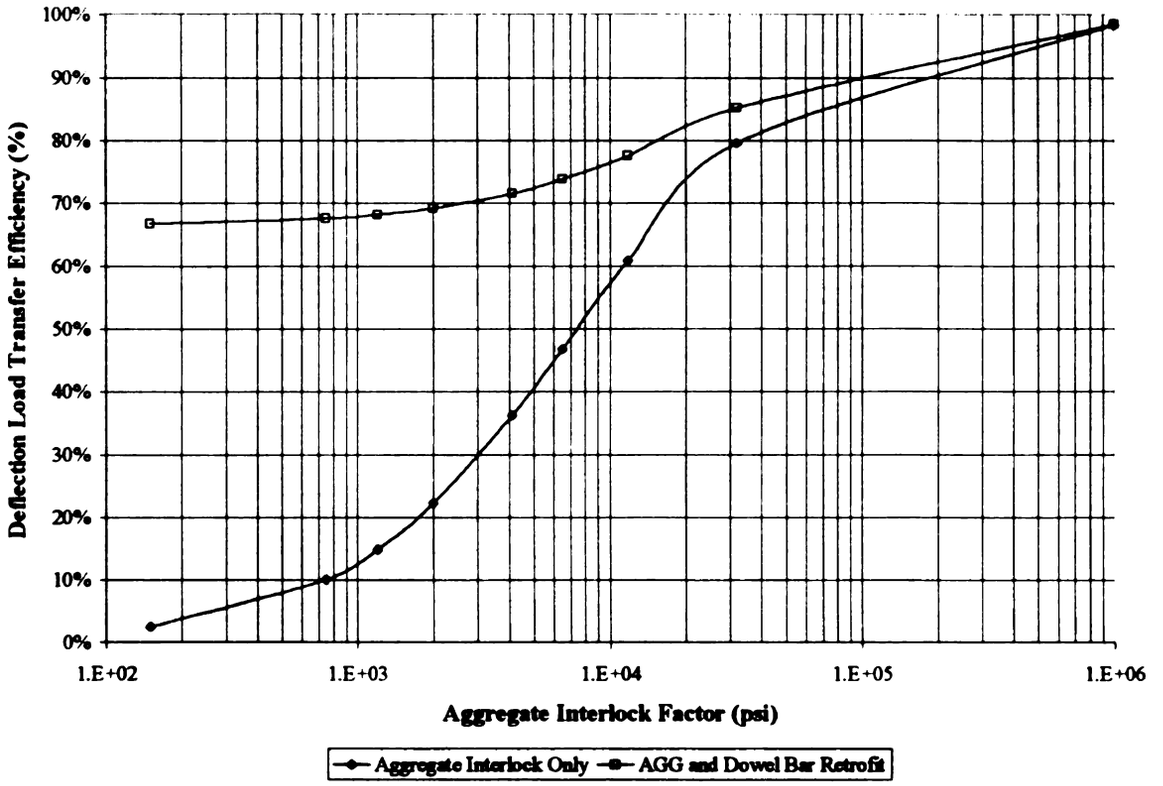

Figure B-42. LTE_δ with Respect to AGG Before and After Dowel Bar Retrofit for h=14" (356 mm), k=250 psi/in (67.9 kPa/mm), and ΔT=-15°F (-8.3°C).

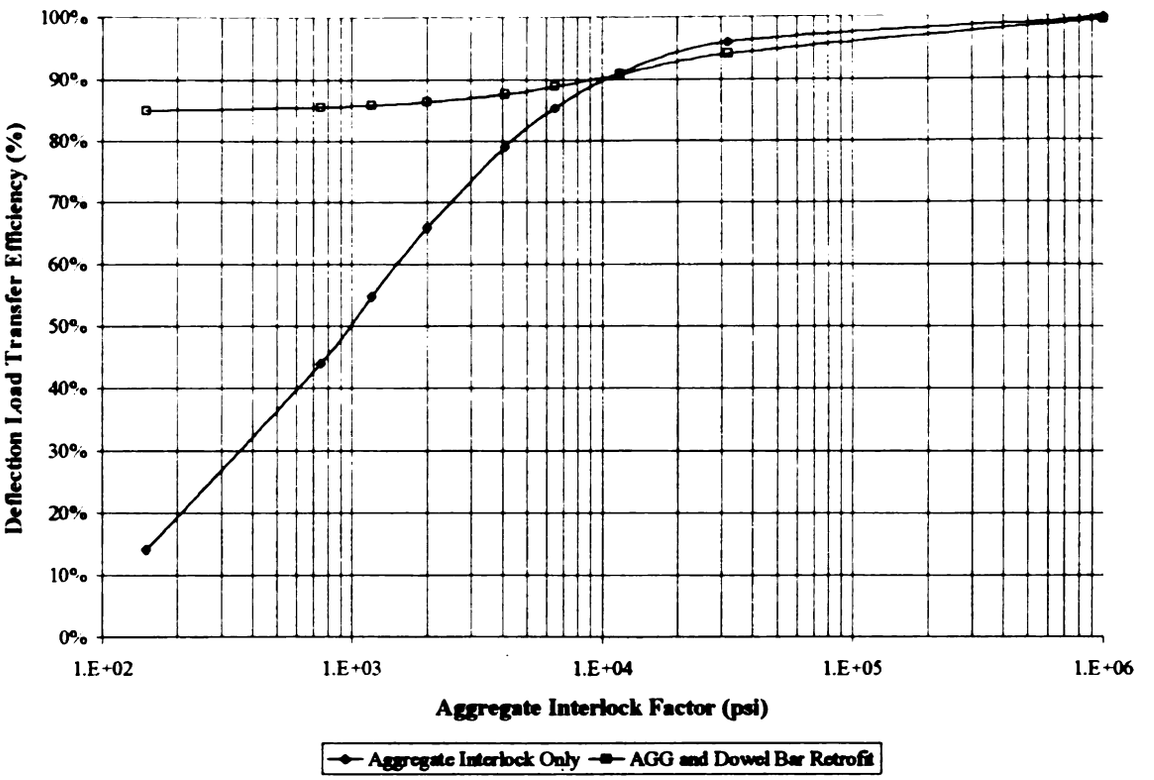

Figure B-43. LTE_δ with Respect to AGG Before and After Dowel Bar Retrofit for h=14" (356 mm), k=400 psi/in (106.8 kPa/mm), and ΔT=0°F (0°C).

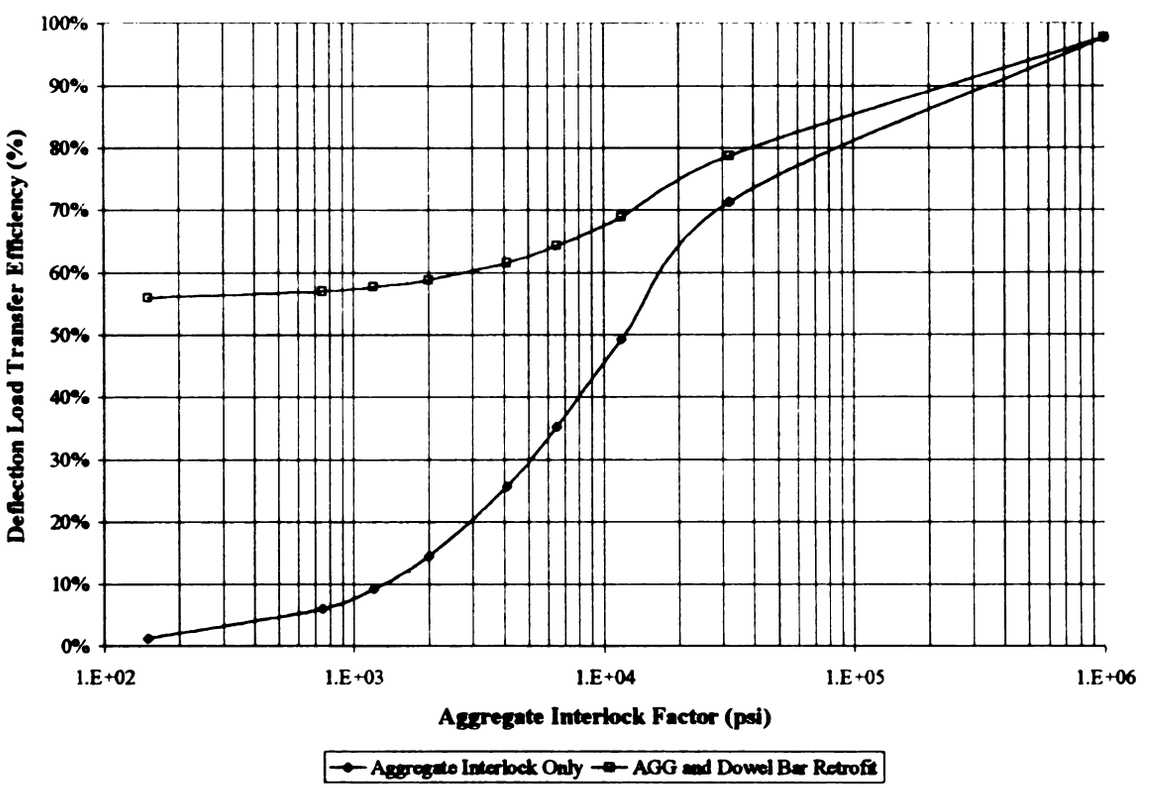

Figure B-44. LTE_δ with Respect to AGG Before and After Dowel Bar Retrofit for h=14" (356 mm), k=400 psi/in (106.8 kPa/mm), and ΔT=+15°F (+8.3°C).

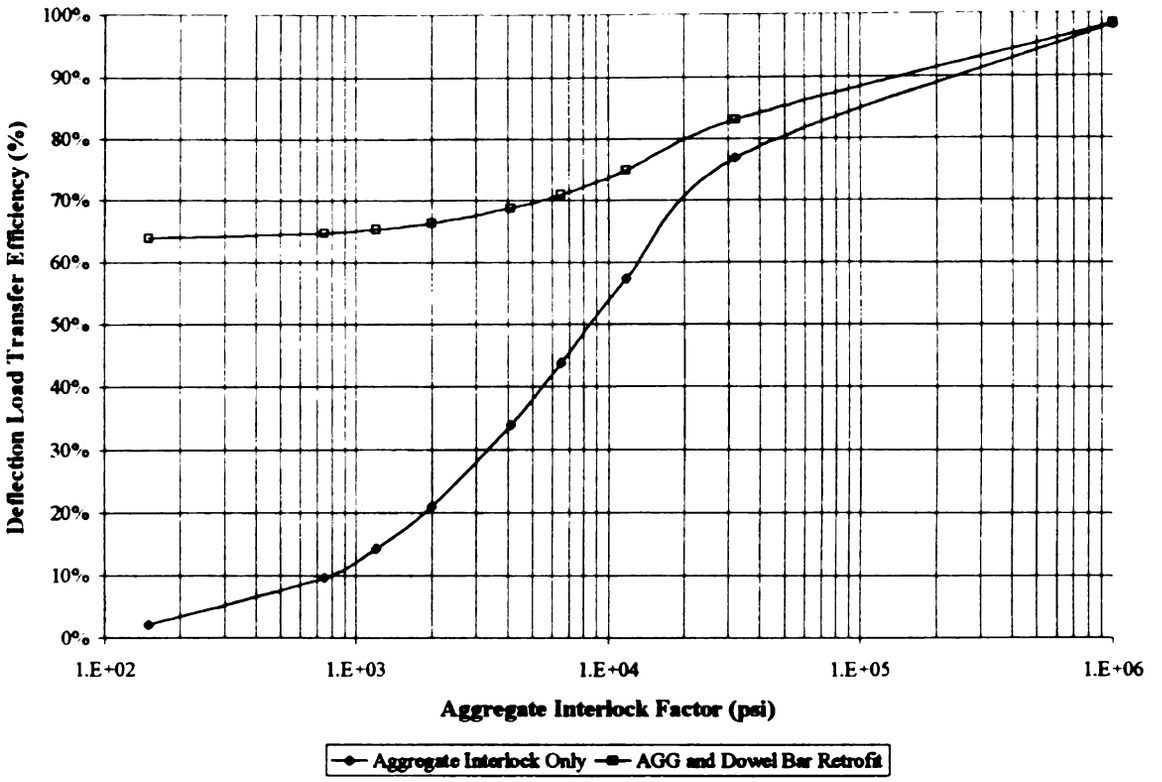

Figure B-45. LTE_δ with Respect to AGG Before and After Dowel Bar Retrofit for h=14" (356 mm), k=400 psi/in (106.8 kPa/mm), and ΔT=-15°F (-8.3°C).

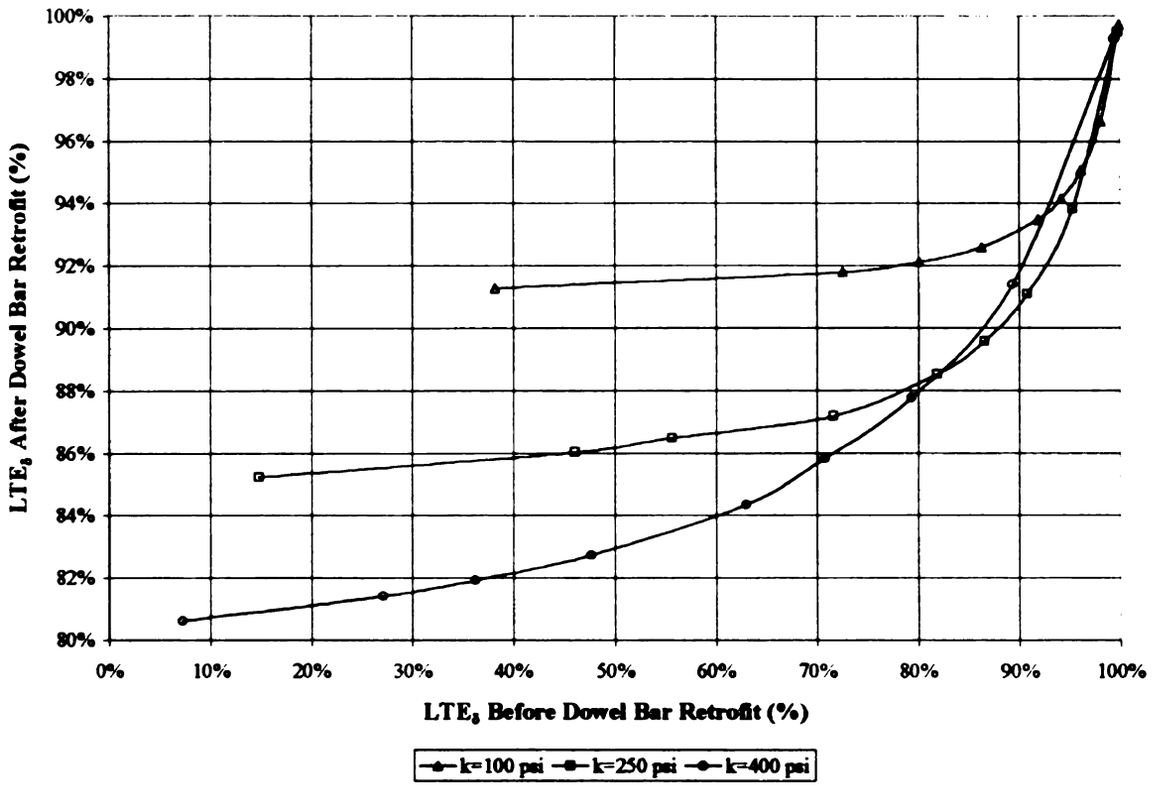

Figure B-46. Analytical Determination of LTE_δ After Dowel Bar Retrofit from Initial LTE_δ for h=6" (152 mm) and ΔT=0°F (0°C).

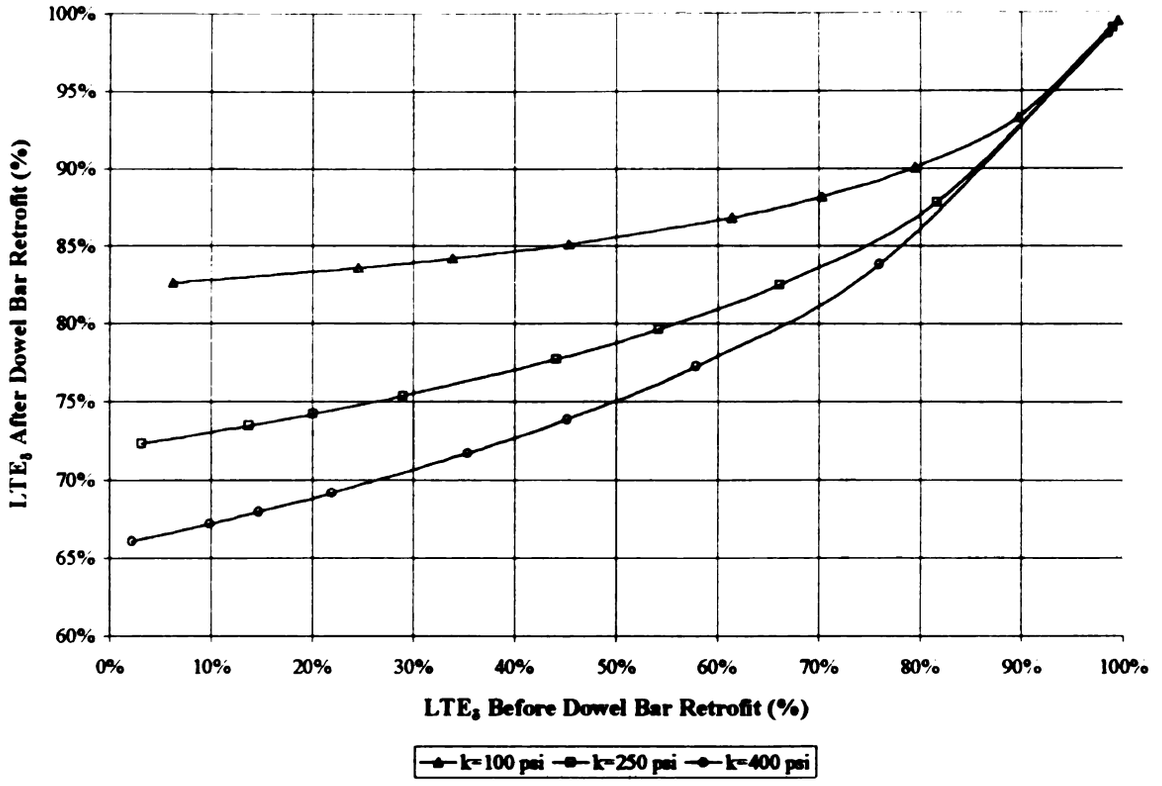

Figure B-47. Analytical Determination of LTE_δ After Dowel Bar Retrofit from Initial LTE_δ for h=6" (152 mm) and ΔT=15°F (8.3°C).

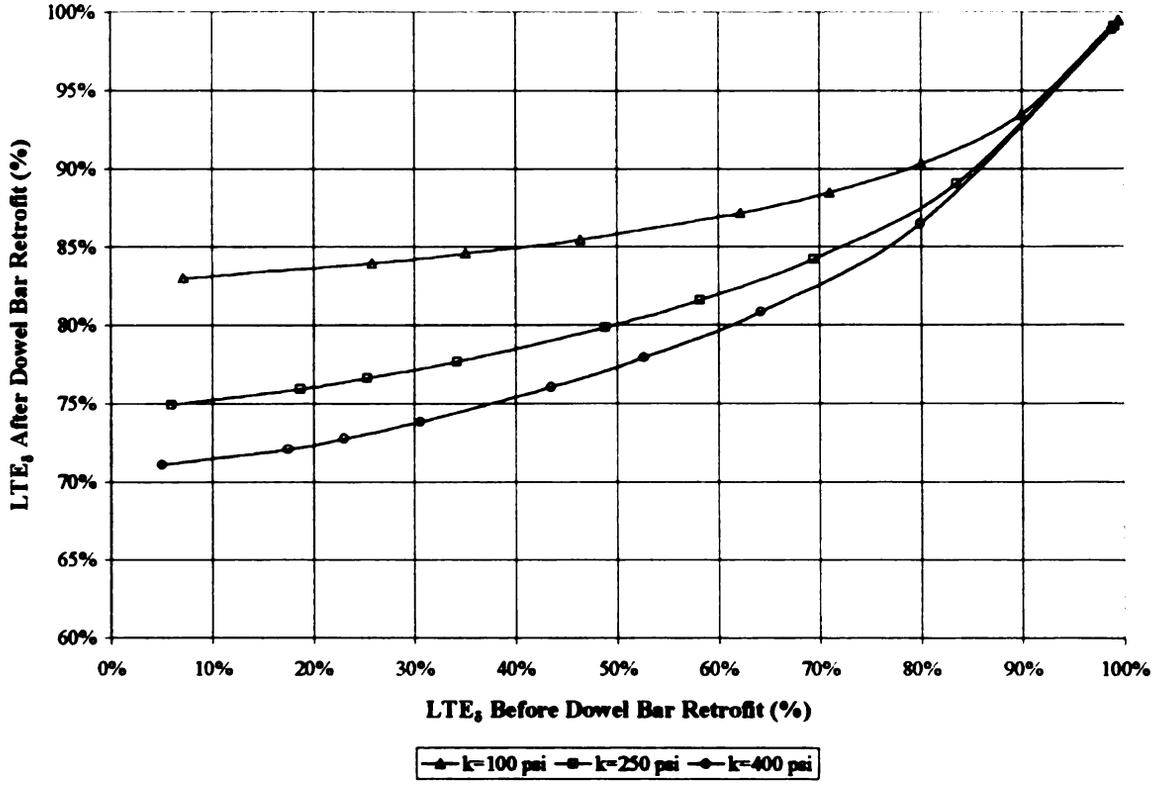

Figure B-48. Analytical Determination of LTE_δ After Dowel Bar Retrofit from Initial LTE_δ for h=6" (152 mm) and ΔT=-15°F (-8.3°C).

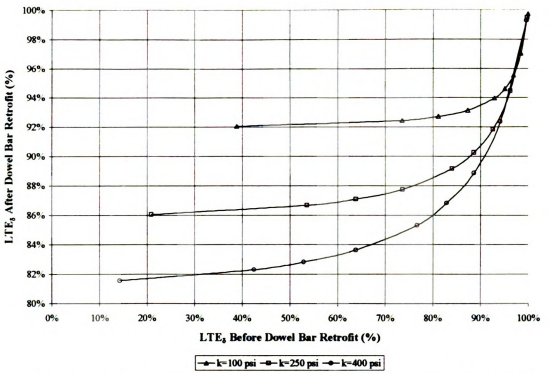

Figure B-49. Analytical Determination of LTE_δ After Dowel Bar Retrofit from Initial LTE_δ for h=8" (203 mm) and ΔT=0°F (0°C).

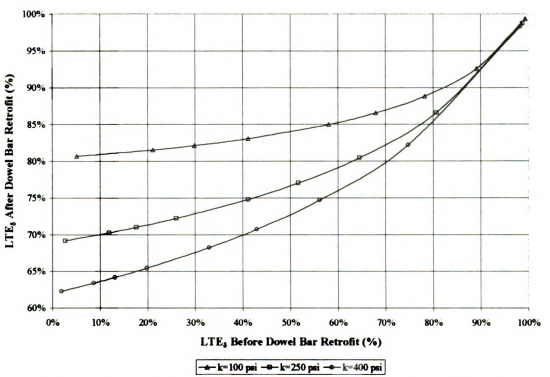

Figure B-50. Analytical Determination of LTE_δ After Dowel Bar Retrofit from Initial LTE_δ for h=8" (203 mm) and ΔT=15°F (8.3°C).

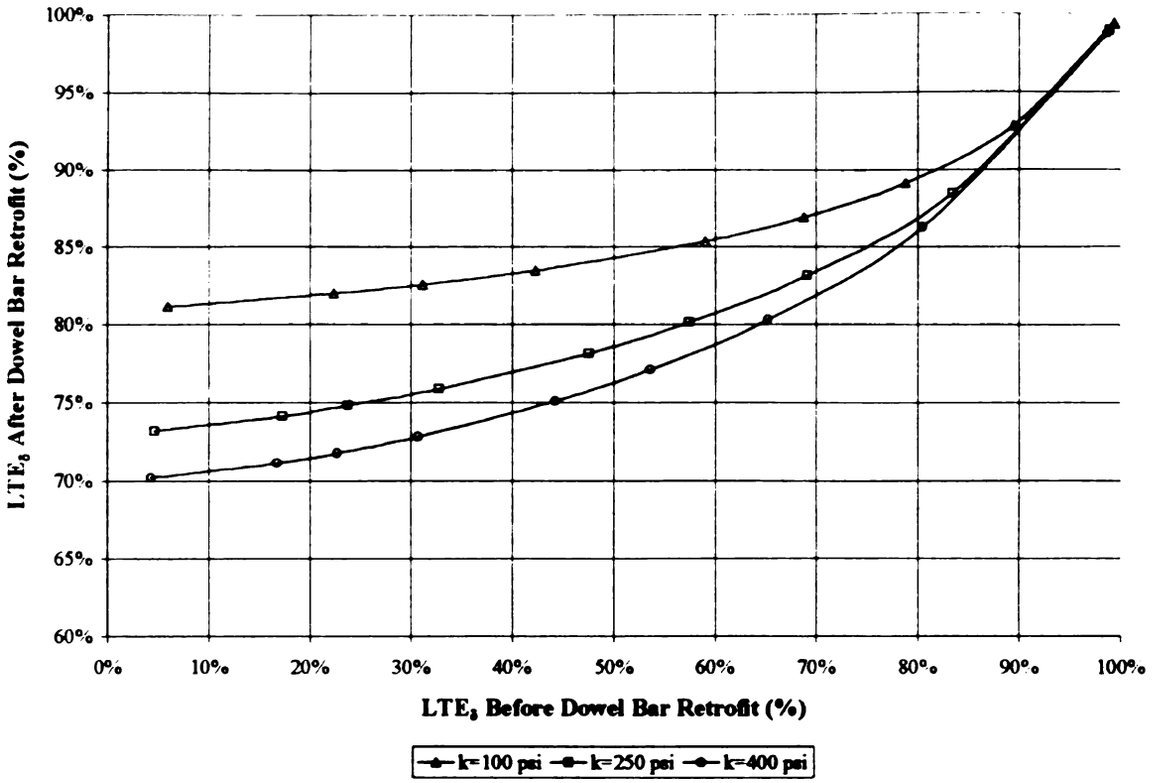

Figure B-51. Analytical Determination of LTE_δ After Dowel Bar Retrofit from Initial LTE_δ for h=8" (203 mm) and ΔT=-15°F (-8.3°C).

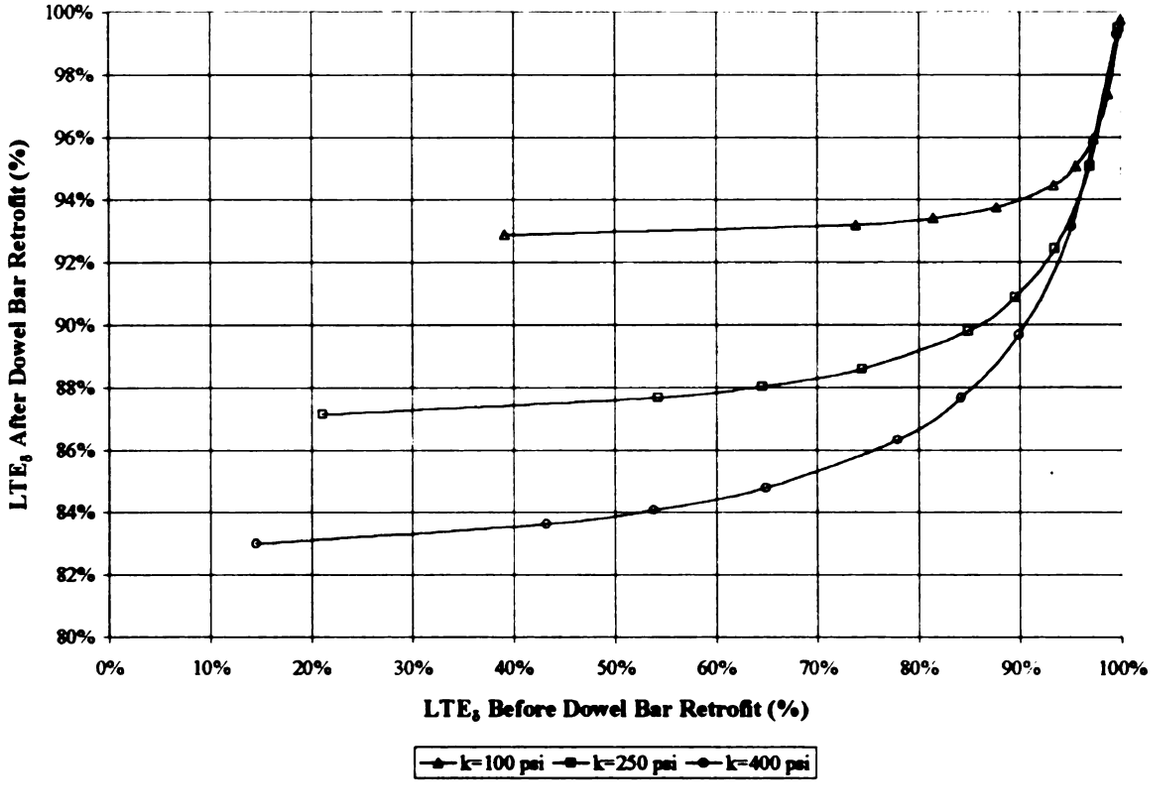

Figure B-52. Analytical Determination of LTE_δ After Dowel Bar Retrofit from Initial LTE_δ for h=10" (254 mm) and ΔT=0°F (0°C).

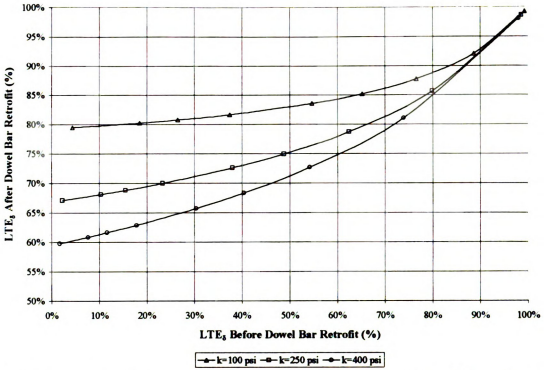

Figure B-53. Analytical Determination of LTE_δ After Dowel Bar Retrofit from Initial LTE_δ for h=10" (254 mm) and ΔT=15°F (8.3°C).

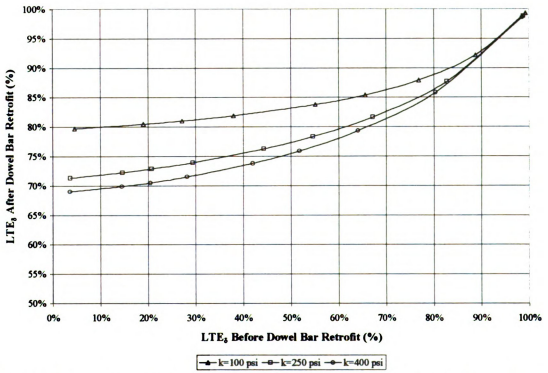

Figure B-54. Analytical Determination of LTE_δ After Dowel Bar Retrofit from Initial LTE_δ for h=10" (254 mm) and ΔT=-15°F (-8.3°C).

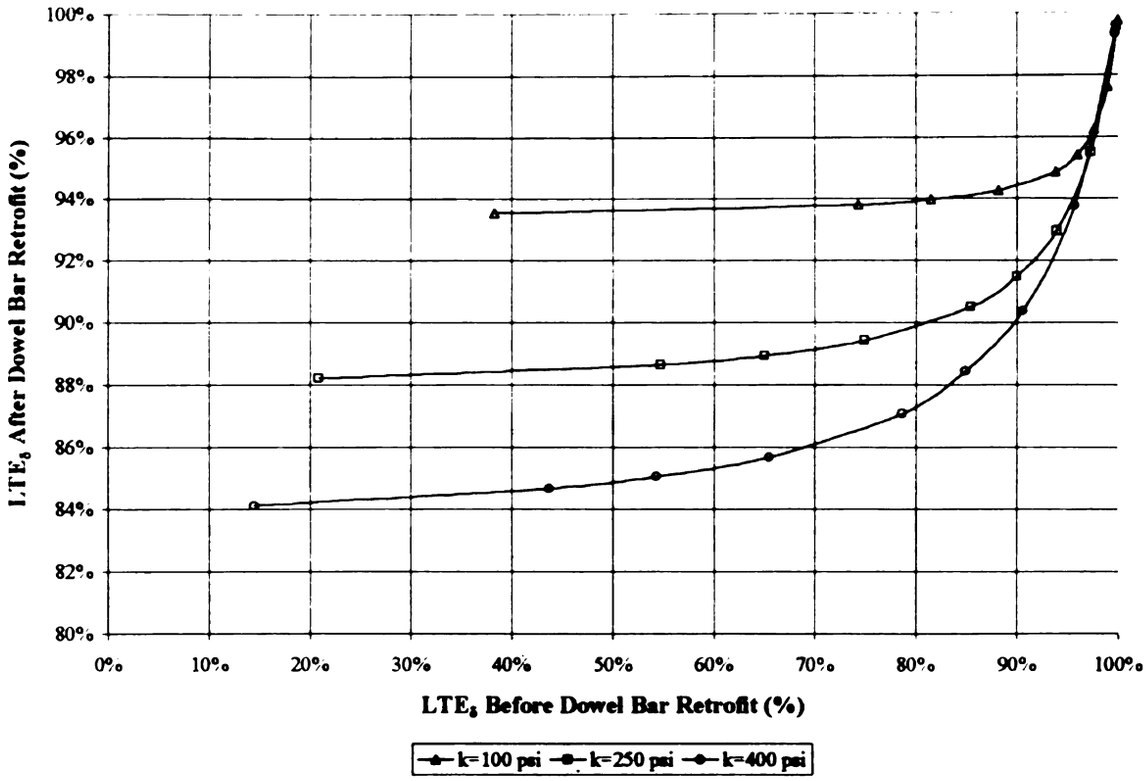

Figure B-55. Analytical Determination of LTE_δ After Dowel Bar Retrofit from Initial LTE_δ for h=12" (305 mm) and ΔT=0°F (0°C).

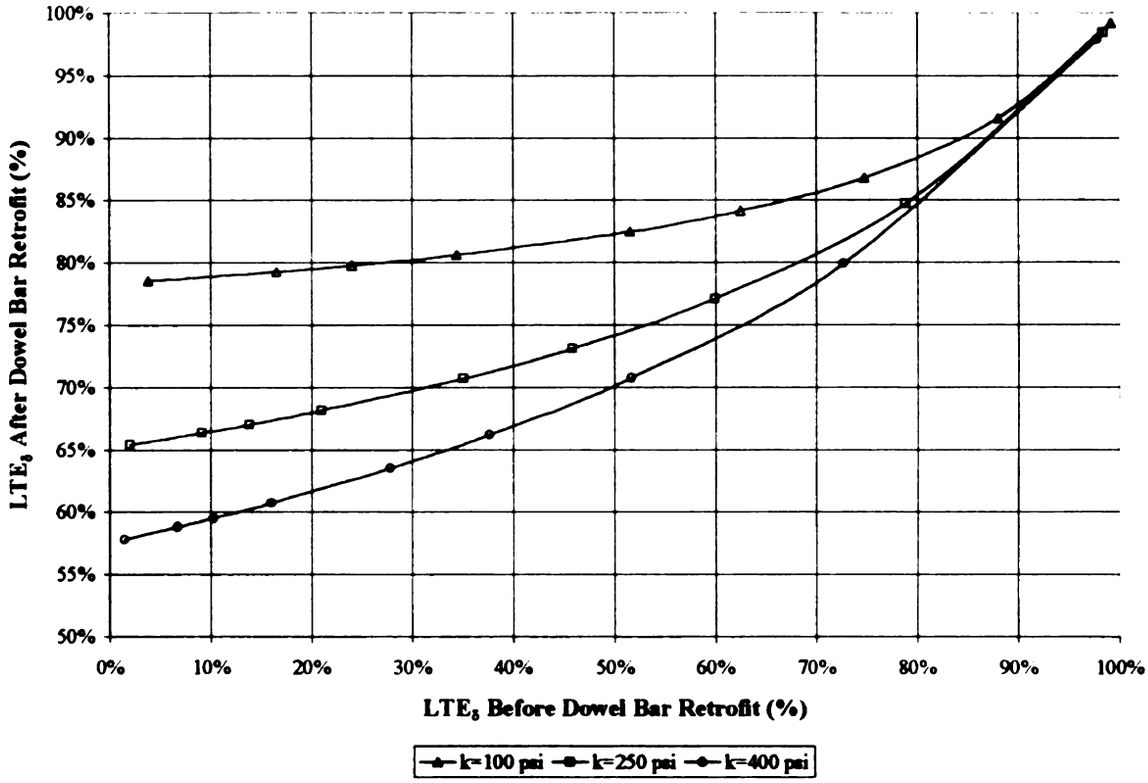

Figure B-56. Analytical Determination of LTE_δ After Dowel Bar Retrofit from Initial LTE_δ for h=12" (305 mm) and ΔT=15°F (8.3°C).

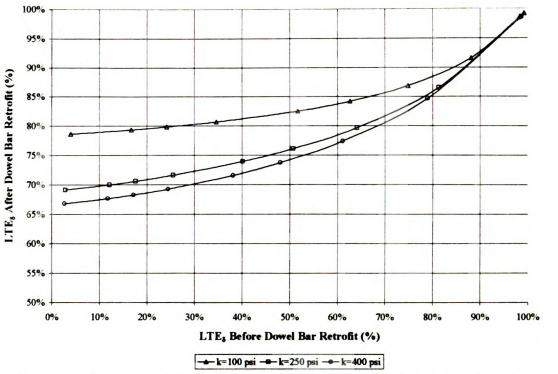

Figure B-57. Analytical Determination of LTE_δ After Dowel Bar Retrofit from Initial LTE_δ for h=12" (305 mm) and ΔT=-15°F (-8.3°C).

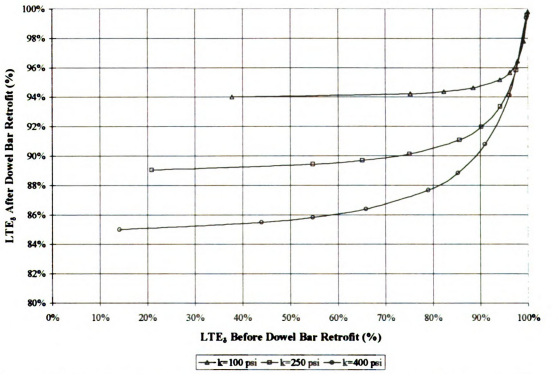

Figure B-58. Analytical Determination of LTE_δ After Dowel Bar Retrofit from Initial LTE_δ for h=14" (356 mm) and ΔT=0°F (0°C).

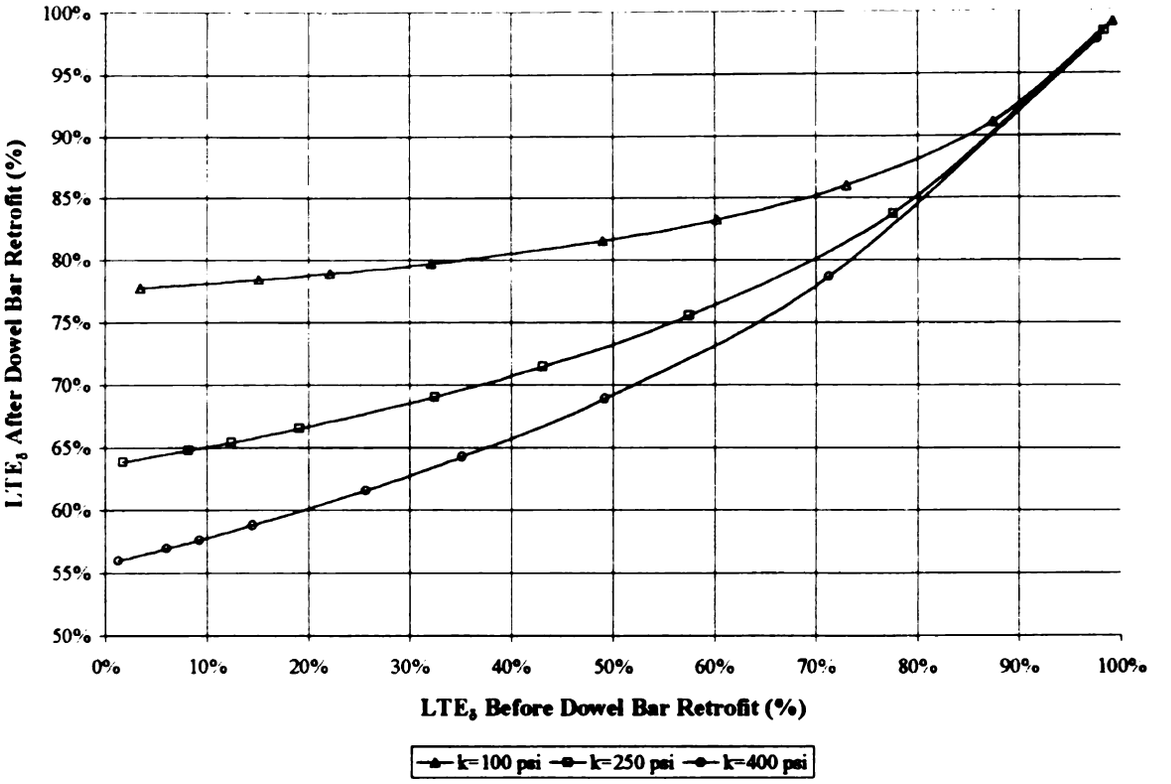

Figure B-59. Analytical Determination of LTE_δ After Dowel Bar Retrofit from Initial LTE_δ for h=14" (356 mm) and ΔT=15°F (8.3°C).

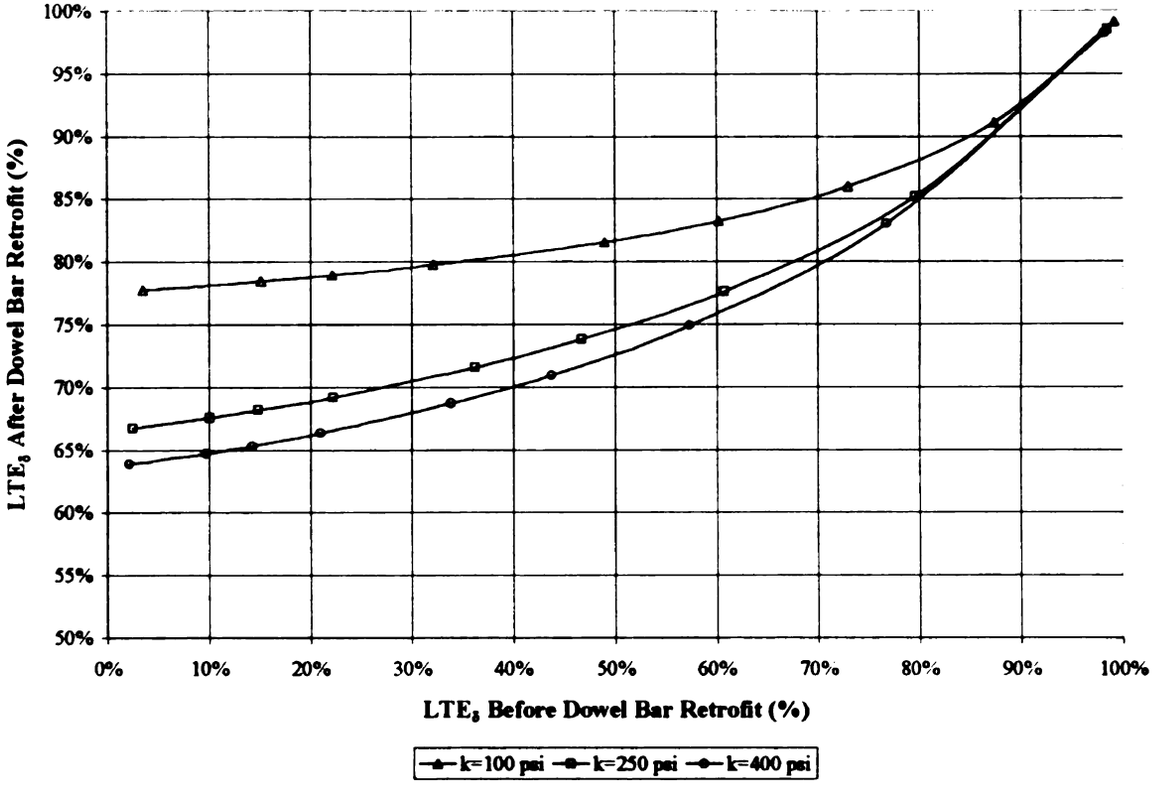

Figure B-60. Analytical Determination of LTE_δ After Dowel Bar Retrofit from Initial LTE_δ for h=14" (356 mm) and ΔT=-15°F (-8.3°C).

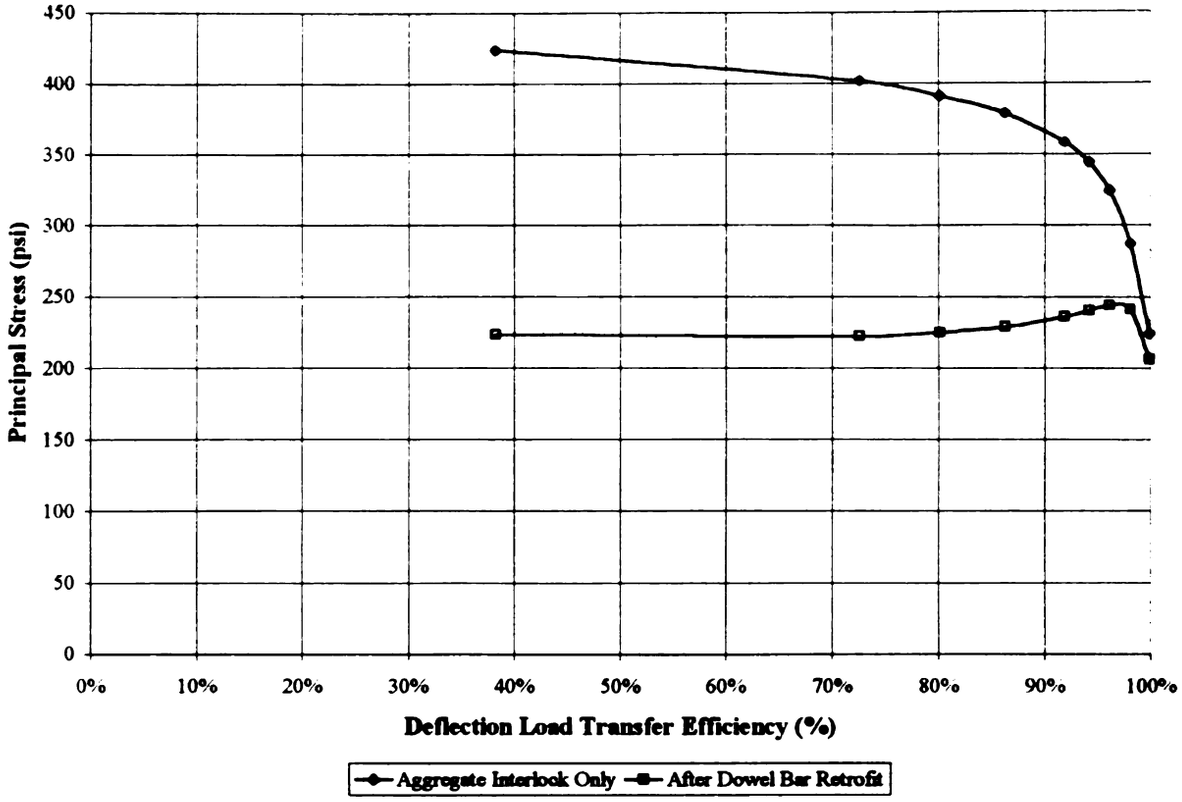

Figure B-61. Principal Tensile Stresses at Crack or Joint Before and After DBR for h=6" (152 mm), k=100 psi/in (27.1 kPa/mm), and ΔT=0°F (0°C).

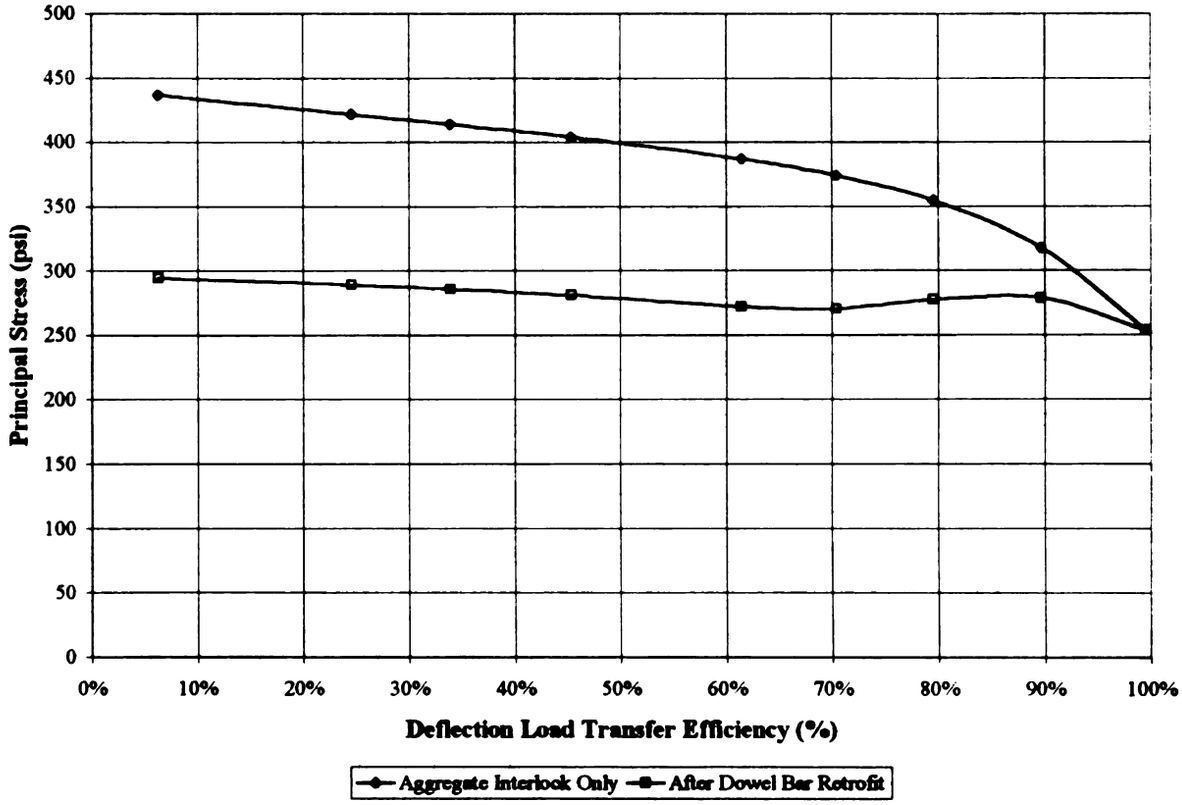

Figure B-62. Principal Tensile Stresses at Crack or Joint Before and After DBR for h=6" (152 mm), k=100 psi/in (27.1 kPa/mm), and ΔT=+15°F (+8.3°C).

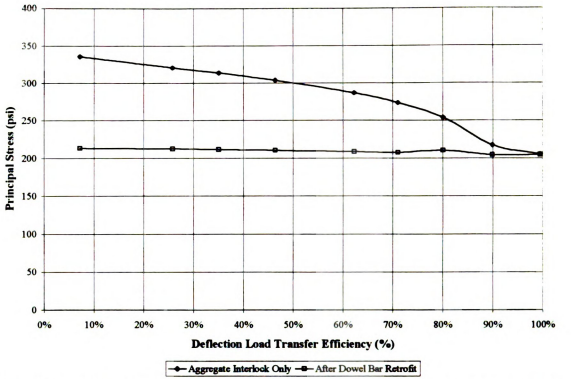

Figure B-63. Principal Tensile Stresses at Crack or Joint Before and After DBR for h=6" (152 mm), k=100 psi/in (27.1 kPa/mm), and ΔT=-15°F (-8.3°C).

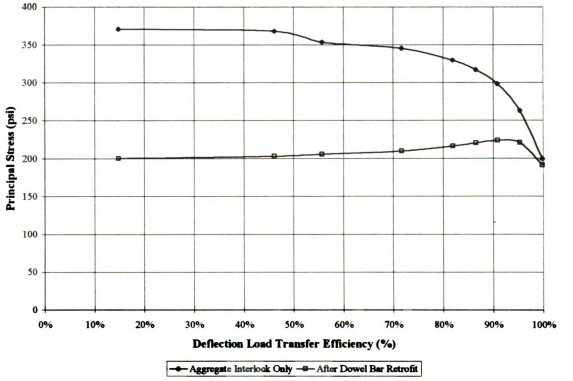

Figure B-64. Principal Tensile Stresses at Crack or Joint Before and After DBR for h=6" (152 mm), k=250 psi/in (67.9 kPa/mm), and ΔT=0°F (0°C).

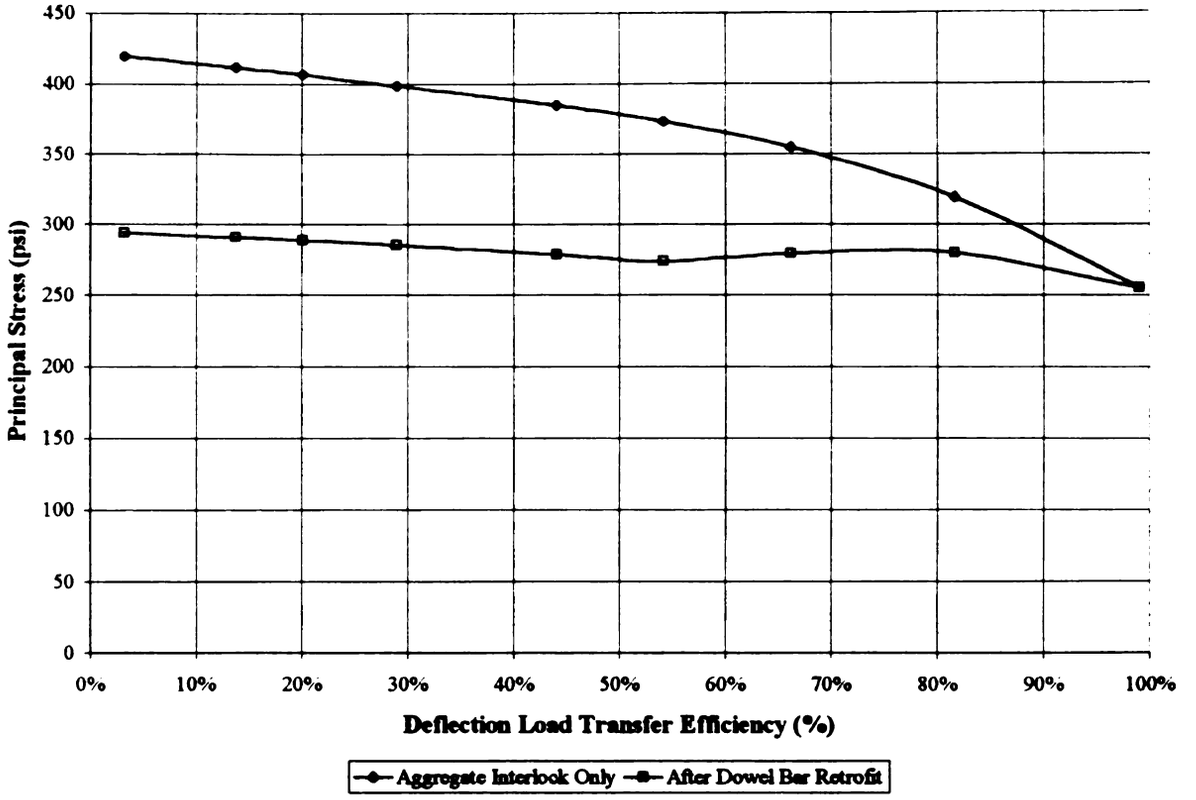

Figure B-65. Principal Tensile Stresses at Crack or Joint Before and After DBR for h=6" (152 mm), k=250 psi/in (67.9 kPa/mm), and ΔT=+15°F (+8.3°C).

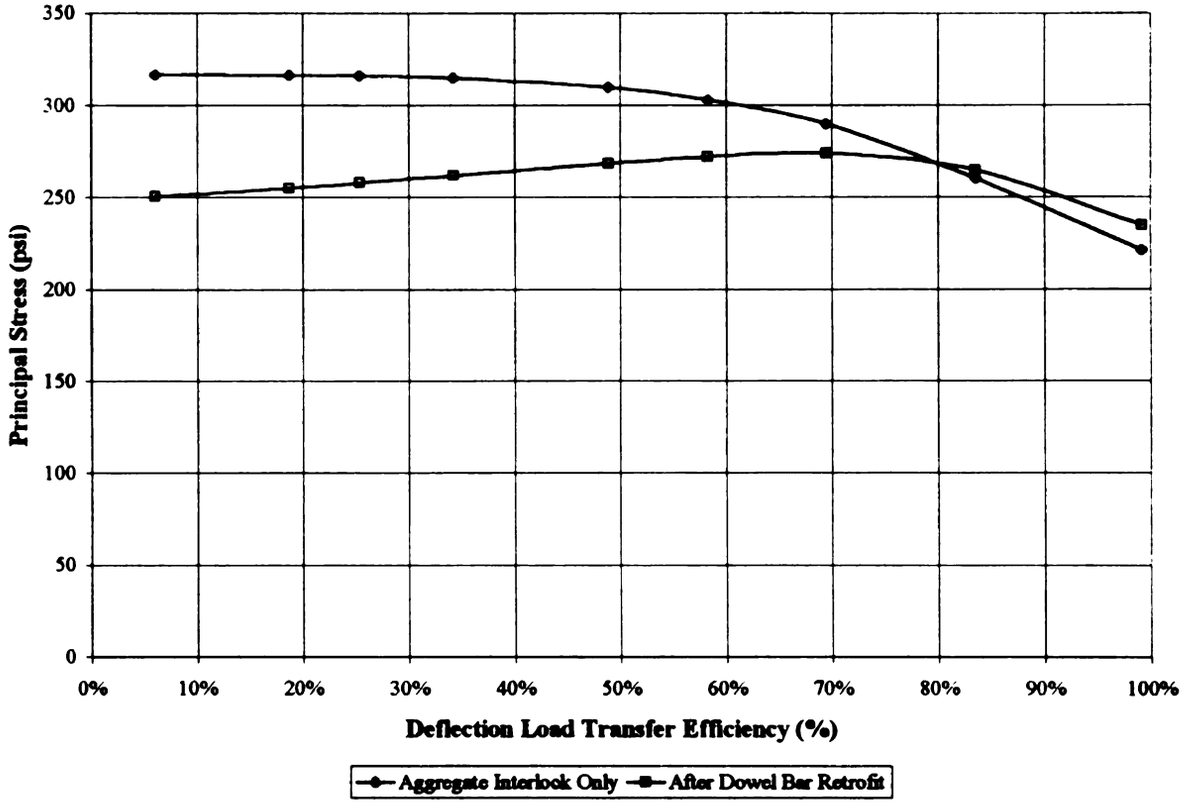

Figure B-66. Principal Tensile Stresses at Crack or Joint Before and After DBR for h=6" (152 mm), k=250 psi/in (67.9 kPa/mm), and ΔT=-15°F (-8.3°C).

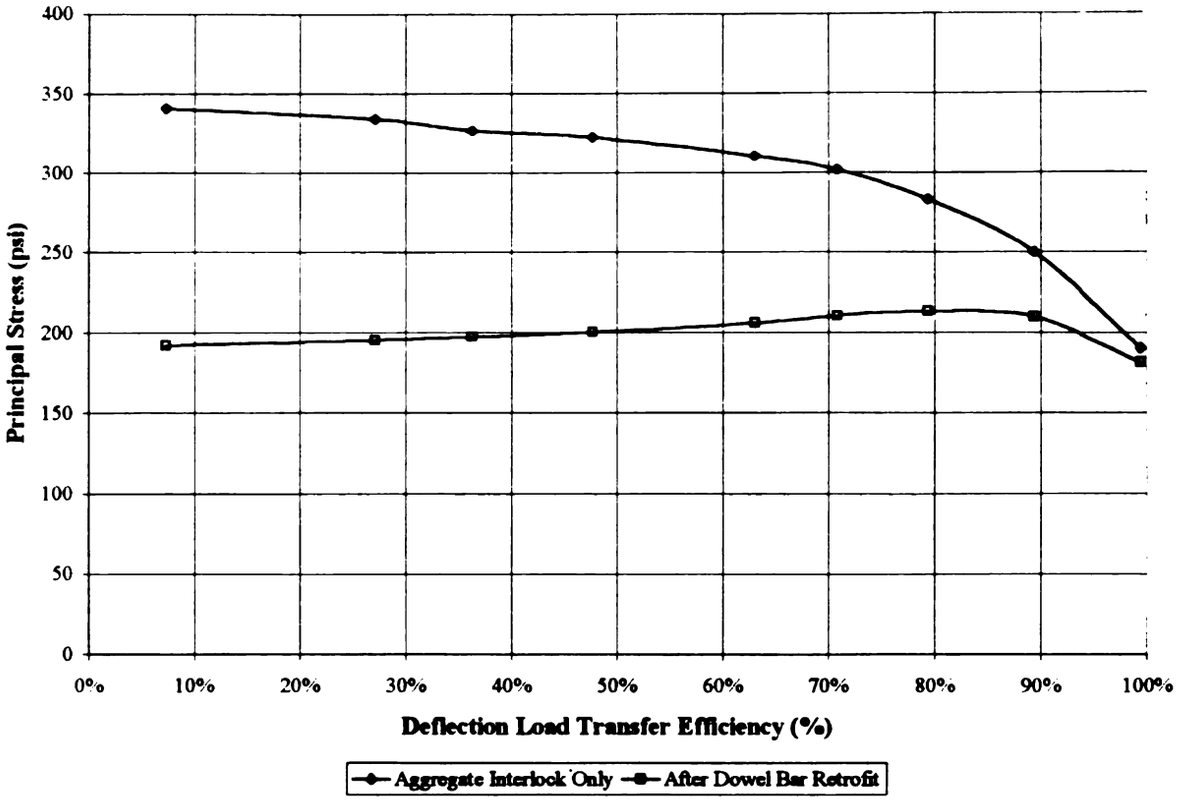

Figure B-67. Principal Tensile Stresses at Crack or Joint Before and After DBR for h=6" (152 mm), k=400 psi/in (106.8 kPa/mm), and ΔT=0°F (0°C).

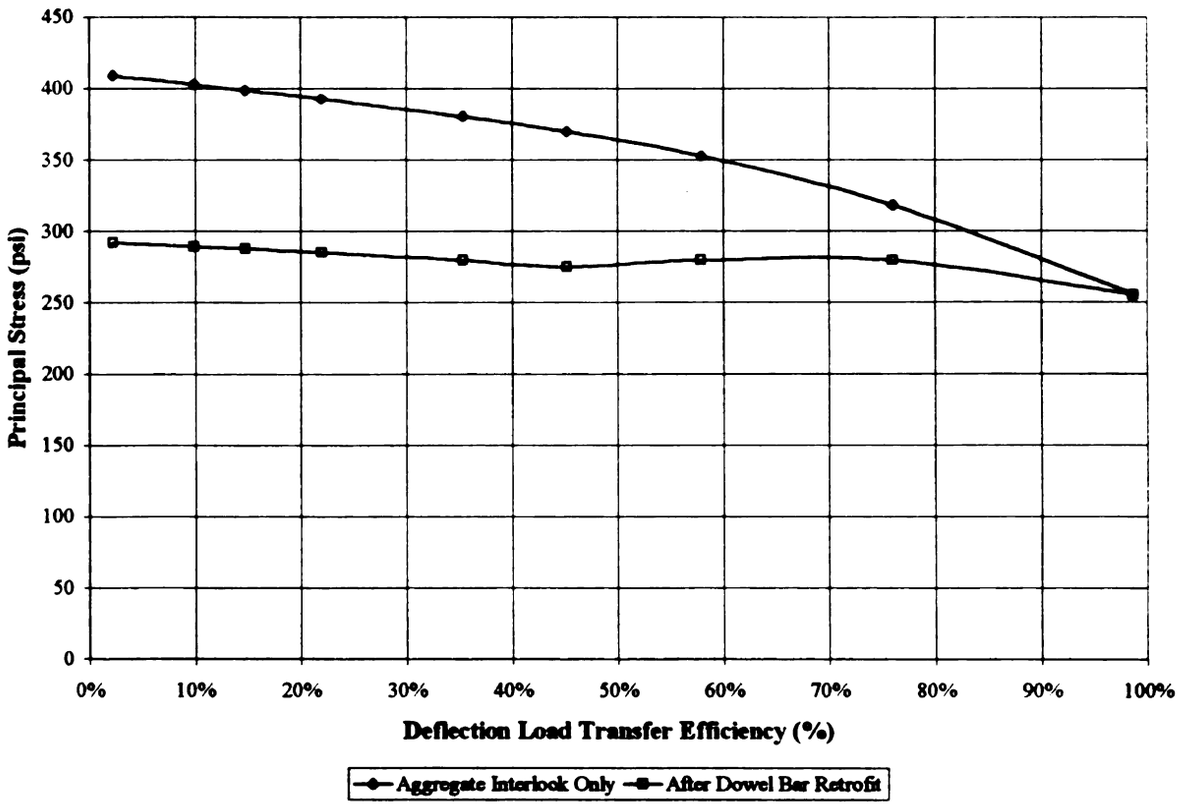

Figure B-68. Principal Tensile Stresses at Crack or Joint Before and After DBR for h=6" (152 mm), k=400 psi/in (106.8 kPa/mm), and ΔT=+15°F (+8.3°C).

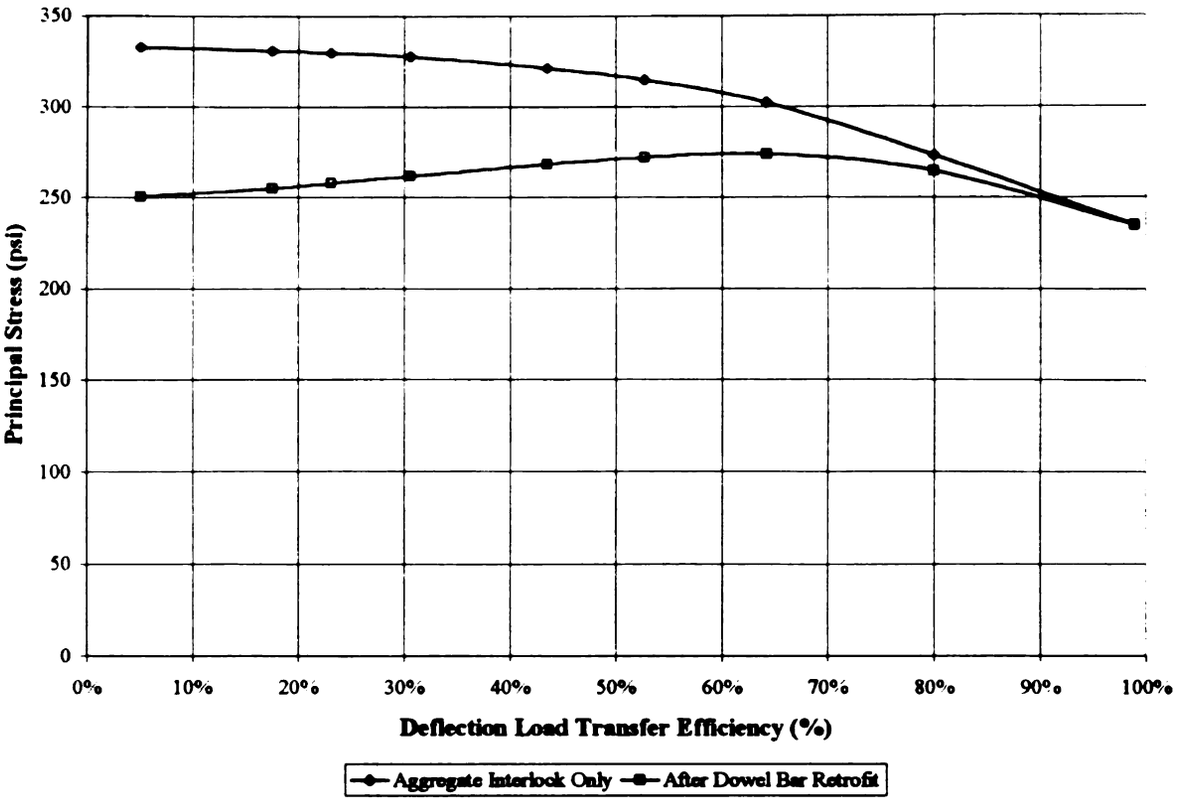

Figure B-69. Principal Tensile Stresses at Crack or Joint Before and After DBR for h=6" (152 mm), k=400 psi/in (106.8 kPa/mm), and ΔT=-15°F (-8.3°C).

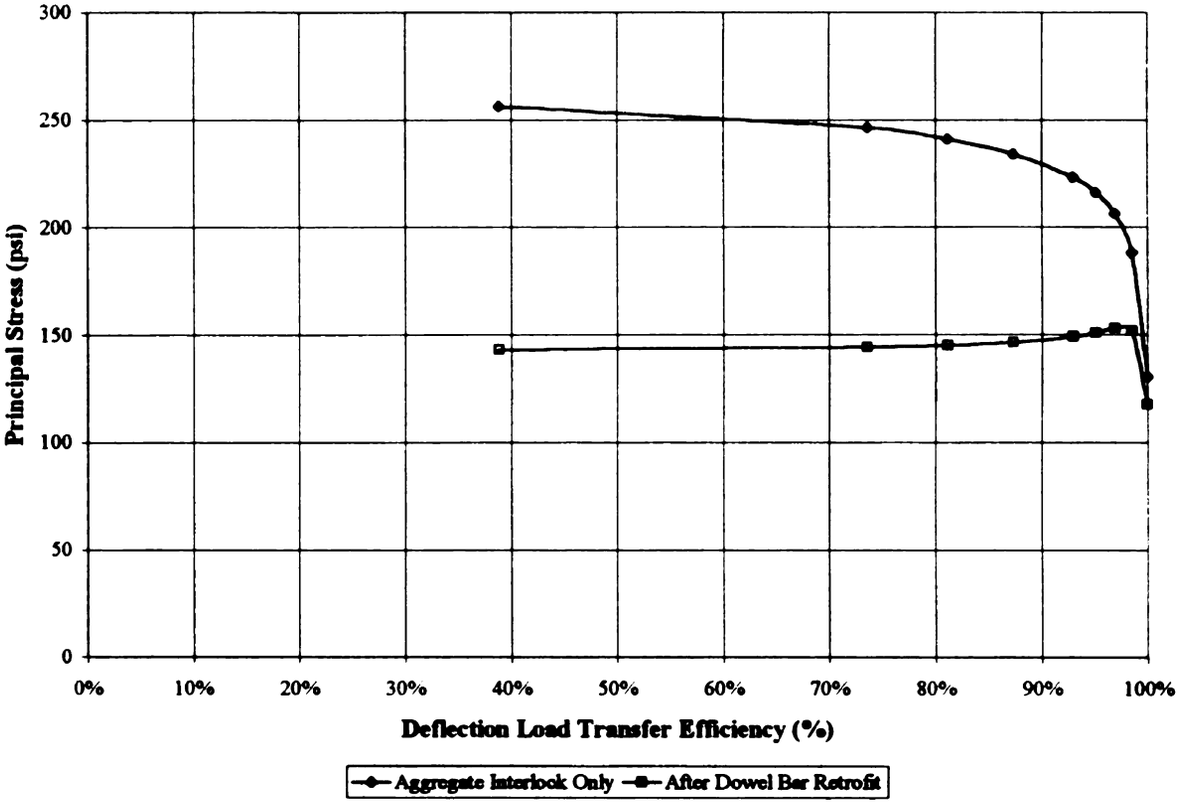

Figure B-70. Principal Tensile Stresses at Crack or Joint Before and After DBR for h=8" (203 mm), k=100 psi/in (27.1 kPa/mm), and ΔT=0°F (0°C).

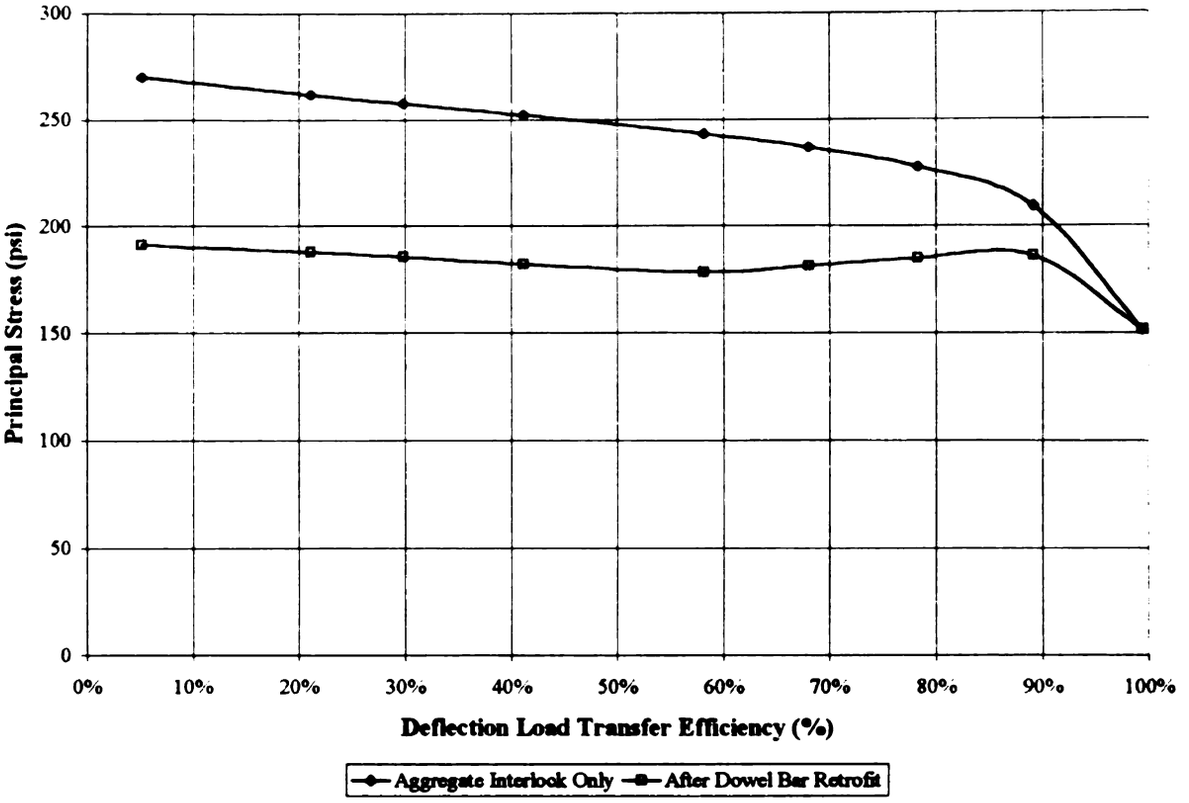

Figure B-71. Principal Tensile Stresses at Crack or Joint Before and After DBR for h=8" (203 mm), k=100 psi/in (27.1 kPa/mm), and ΔT=+15°F (+8.3°C).

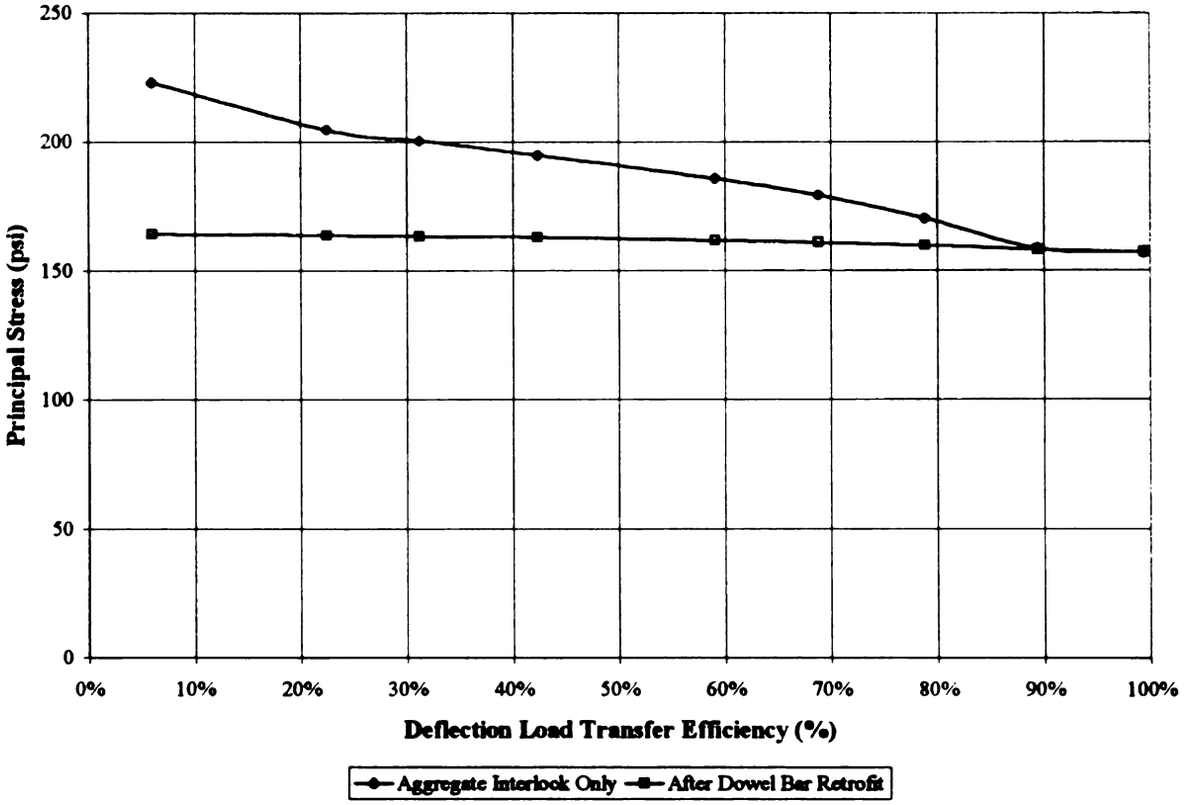

Figure B-72. Principal Tensile Stresses at Crack or Joint Before and After DBR for h=8" (203 mm), k=100 psi/in (27.1 kPa/mm), and ΔT=-15°F (-8.3°C).

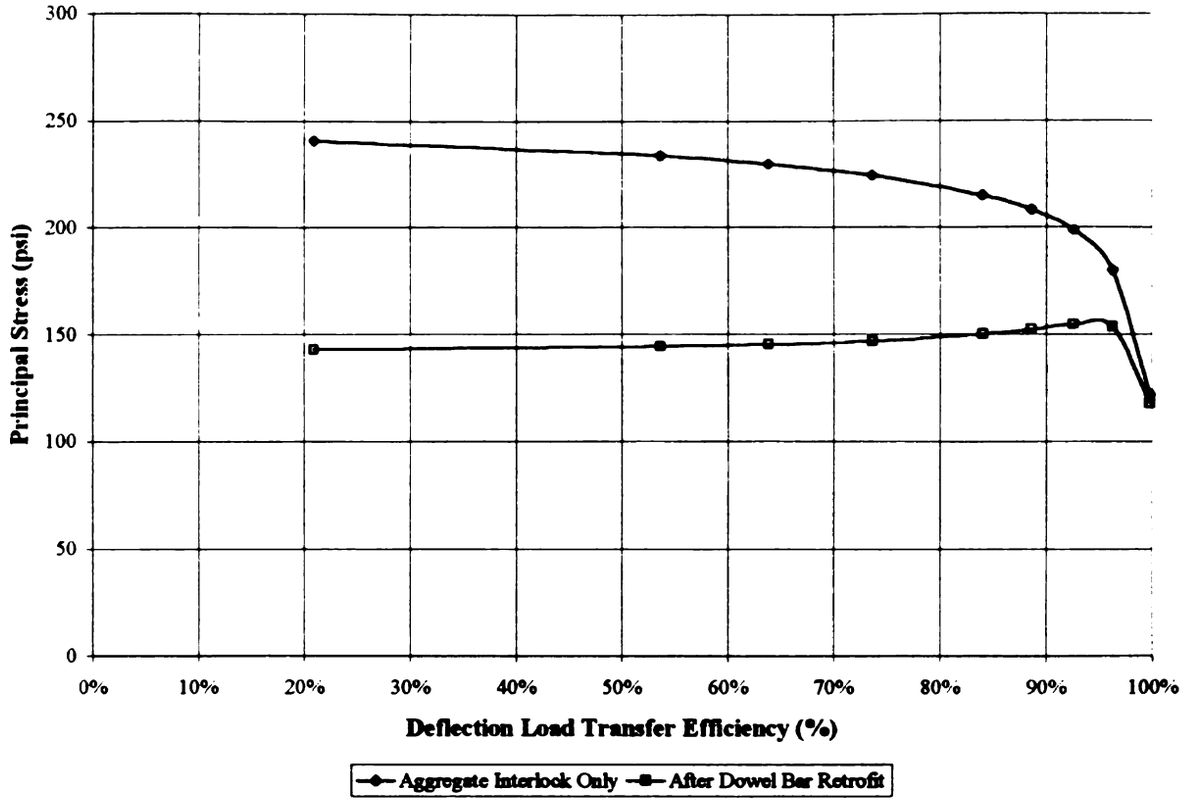

Figure B-73. Principal Tensile Stresses at Crack or Joint Before and After DBR for h=8" (203 mm), k=250 psi/in (67.9 kPa/mm), and ΔT=0°F (0°C).

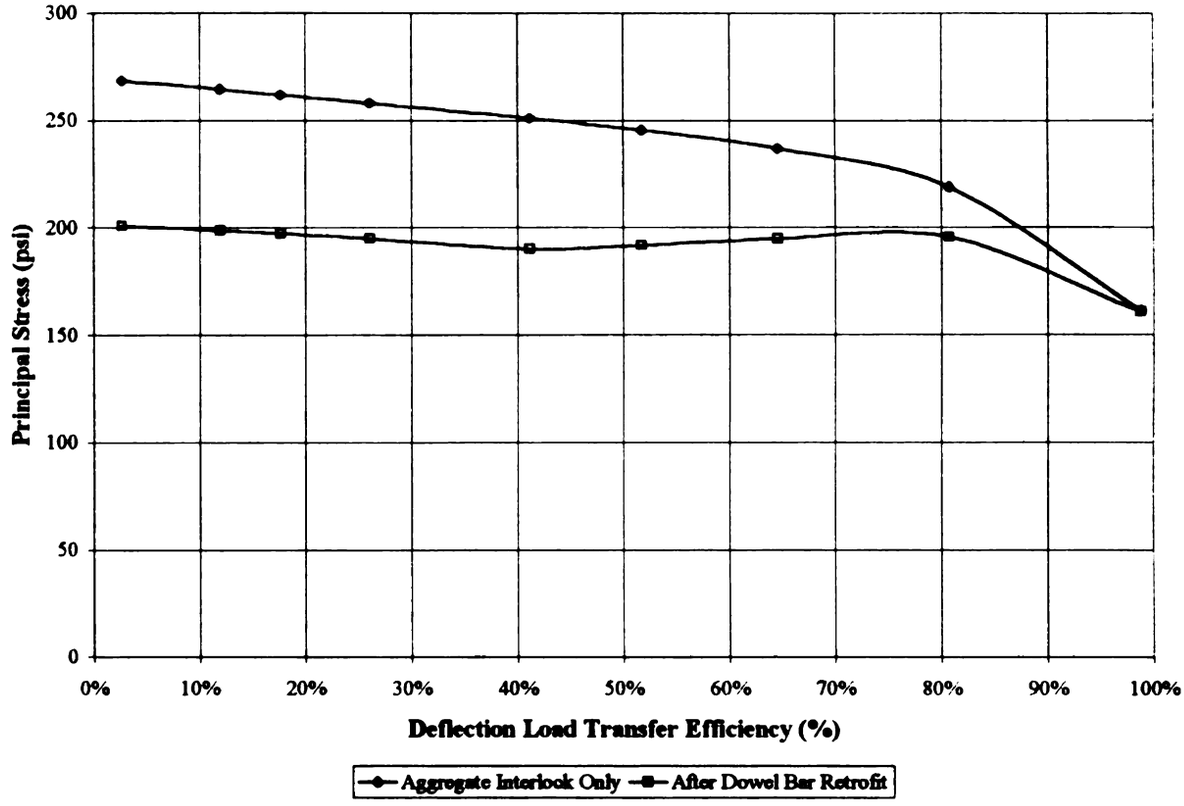

Figure B-74. Principal Tensile Stresses at Crack or Joint Before and After DBR for h=8" (203 mm), k=250 psi/in (67.9 kPa/mm), and ΔT=+15°F (+8.3°C).

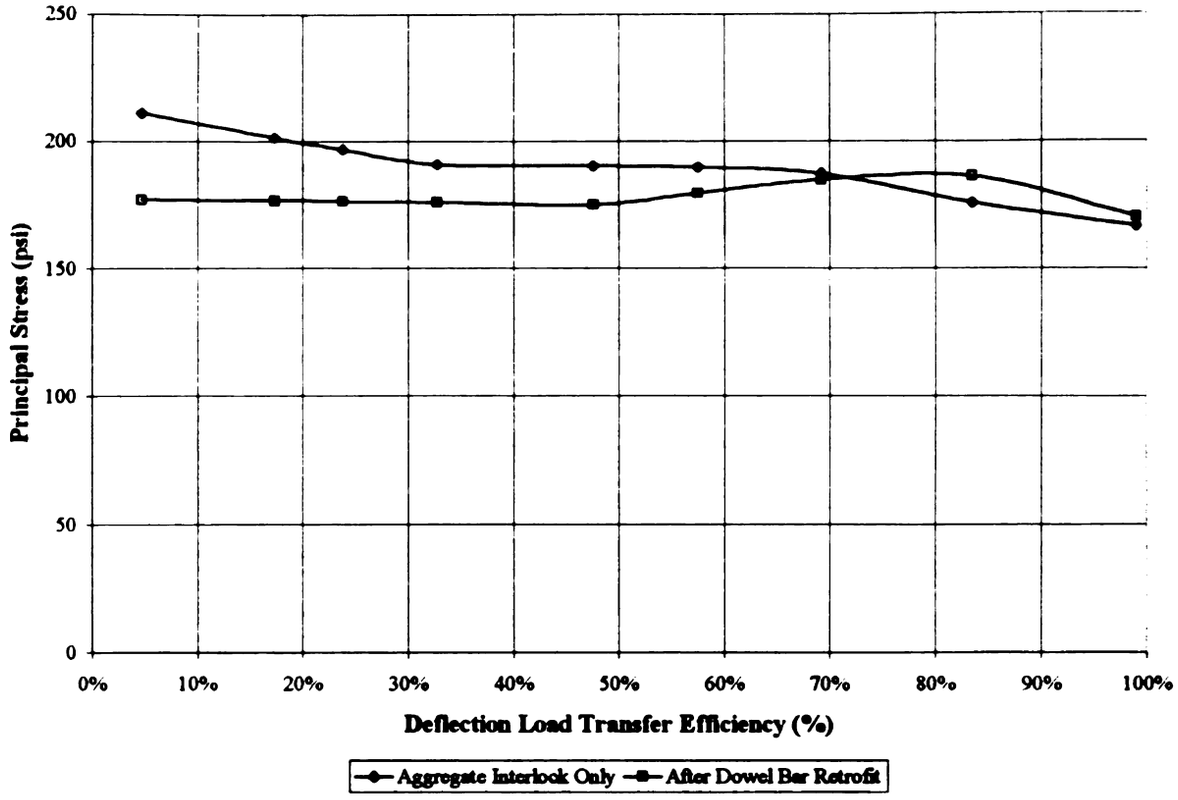

Figure B-75. Principal Tensile Stresses at Crack or Joint Before and After DBR for h=8" (203 mm), k=250 psi/in (67.9 kPa/mm), and ΔT=-15°F (-8.3°C).

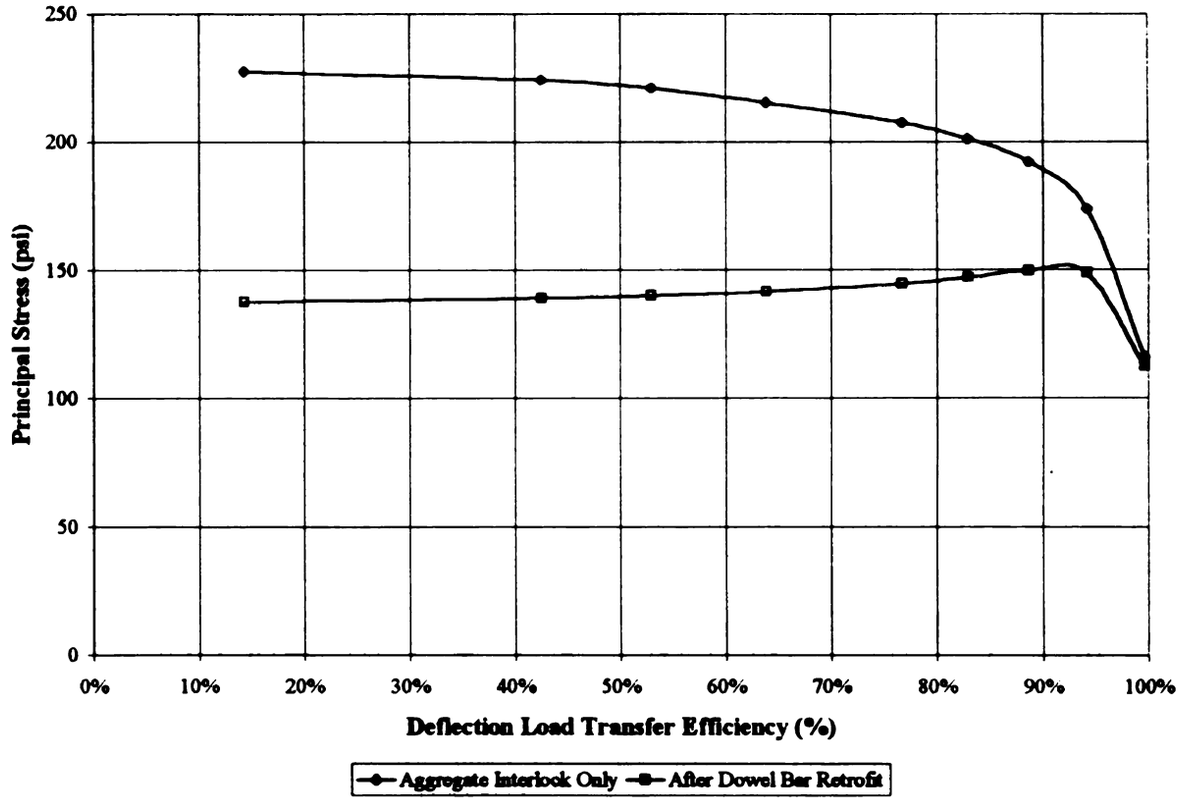

Figure B-76. Principal Tensile Stresses at Crack or Joint Before and After DBR for h=8" (203 mm), k=400 psi/in (106.8 kPa/mm), and ΔT=0°F (0°C).

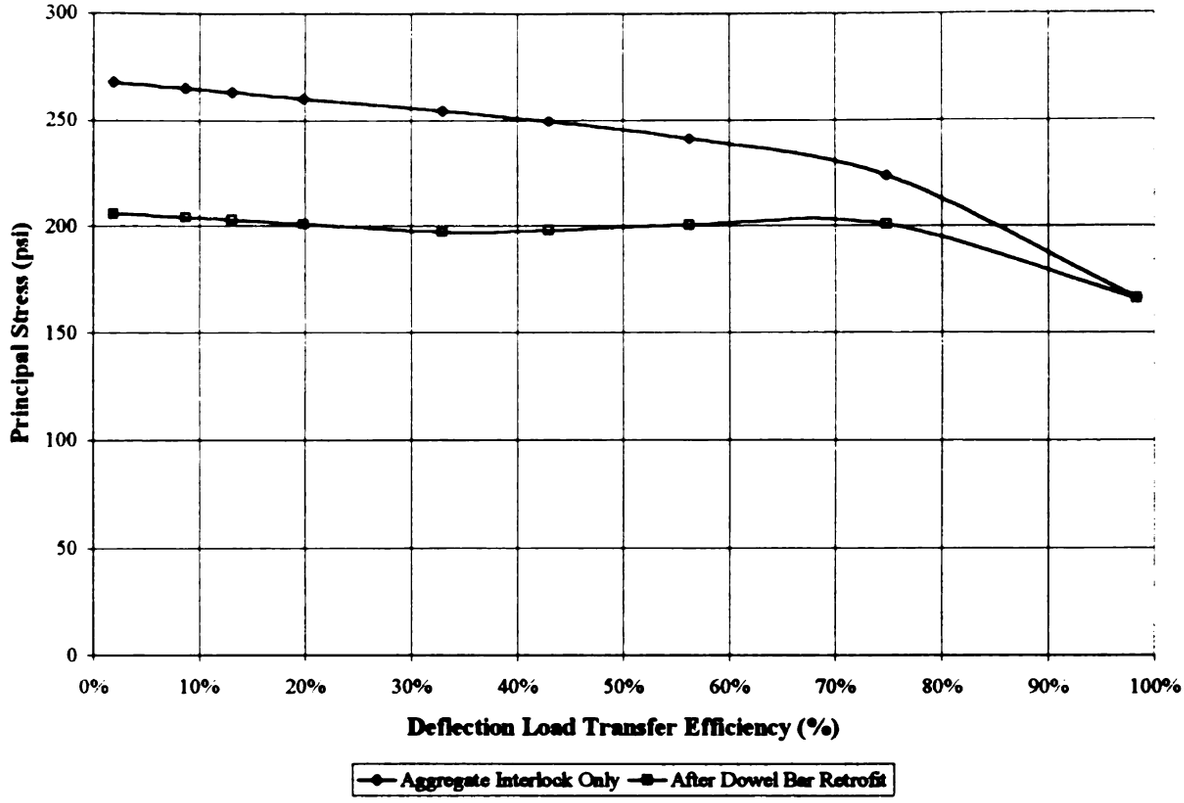

Figure B-77. Principal Tensile Stresses at Crack or Joint Before and After DBR for h=8" (203 mm), k=400 psi/in (106.8 kPa/mm), and ΔT=+15°F (+8.3°C).

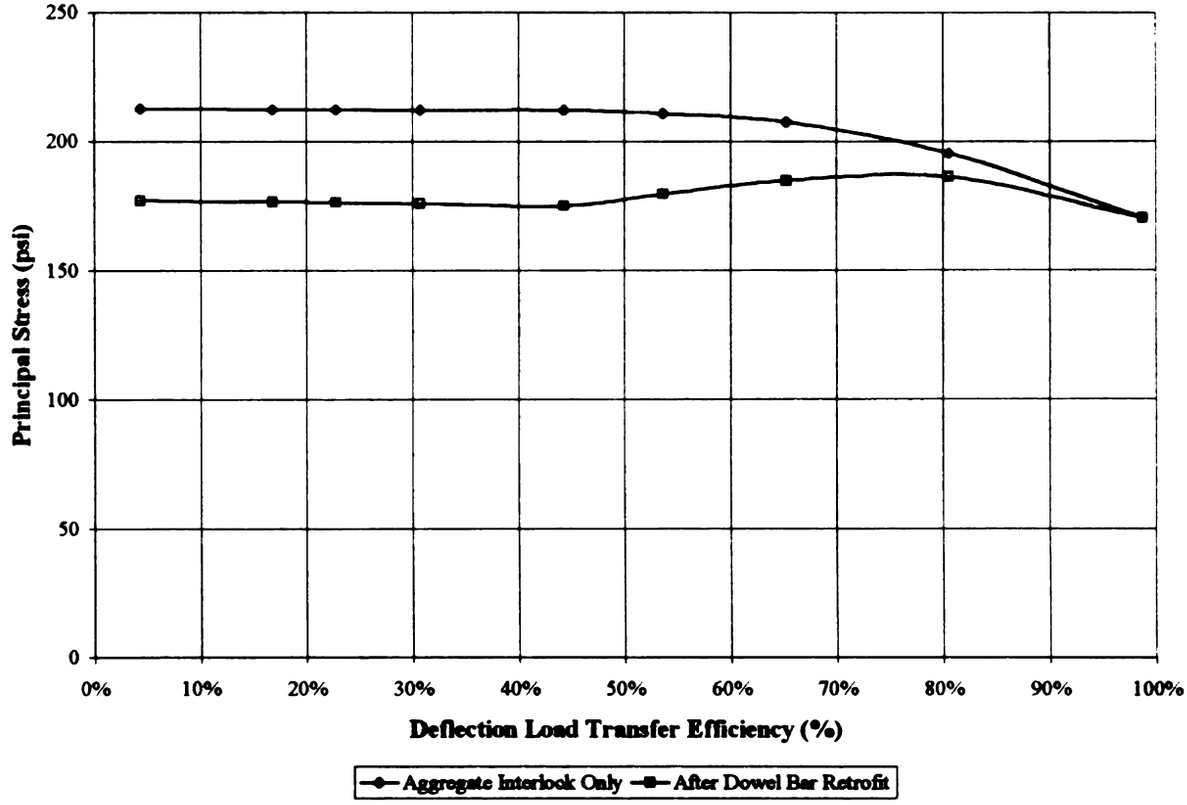

Figure B-78. Principal Tensile Stresses at Crack or Joint Before and After DBR for h=8" (203 mm), k=400 psi/in (106.8 kPa/mm), and ΔT=-15°F (-8.3°C).

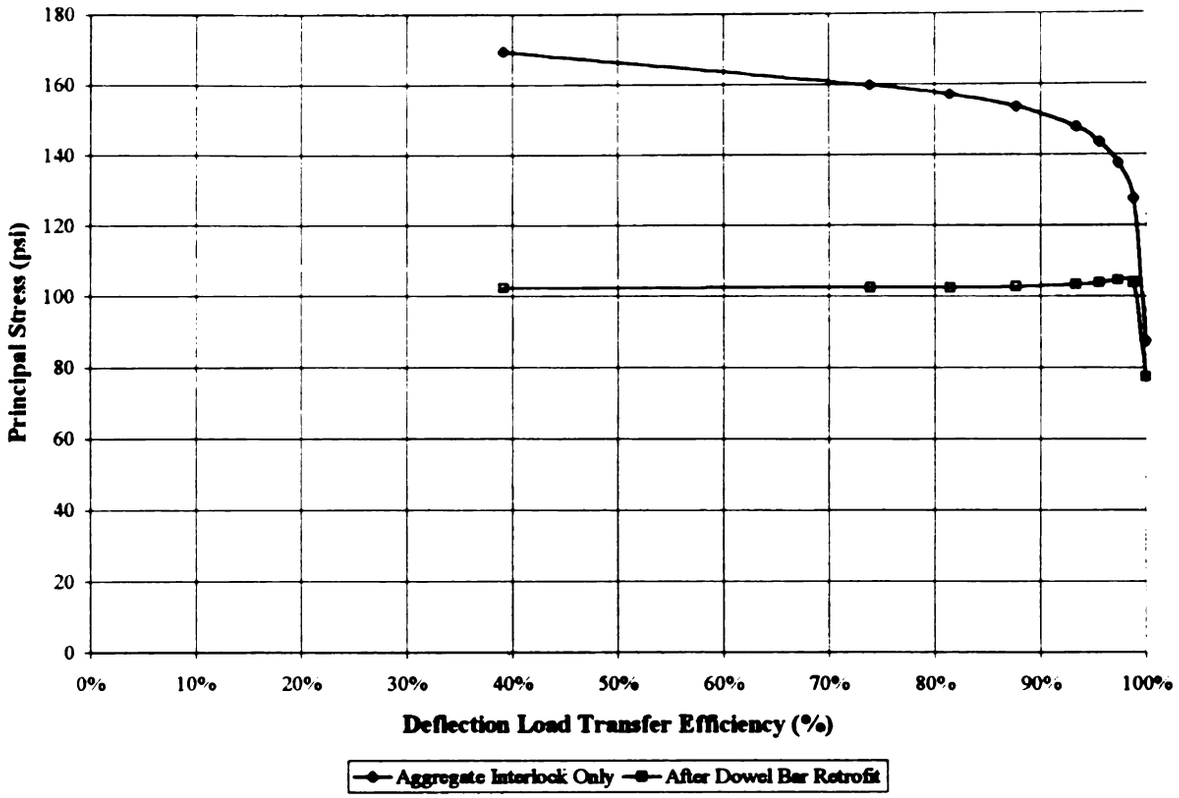

Figure B-79. Principal Tensile Stresses at Crack or Joint Before and After DBR for h=10" (254 mm), k=100 psi/in (27.1 kPa/mm), and ΔT=0°F (0°C).

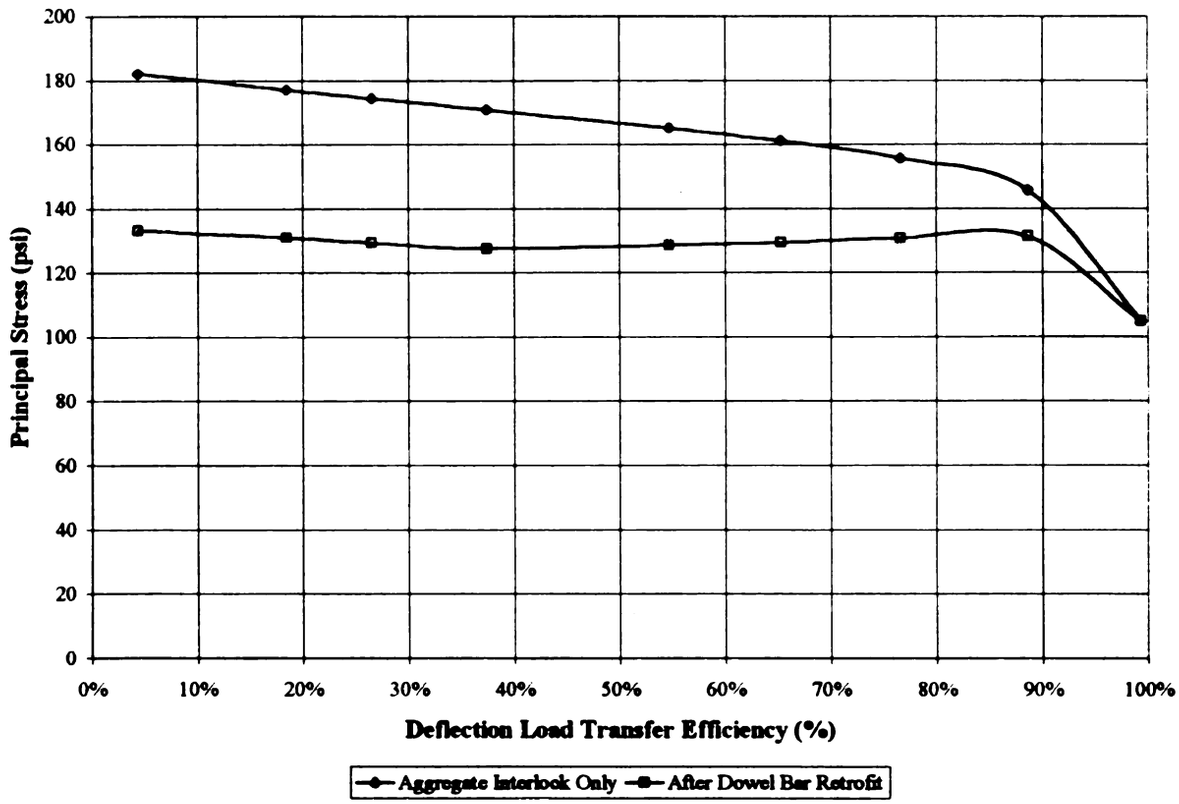

Figure B-80. Principal Tensile Stresses at Crack or Joint Before and After DBR for h=10" (254 mm), k=100 psi/in (27.1 kPa/mm), and ΔT=+15°F (+8.3°C).

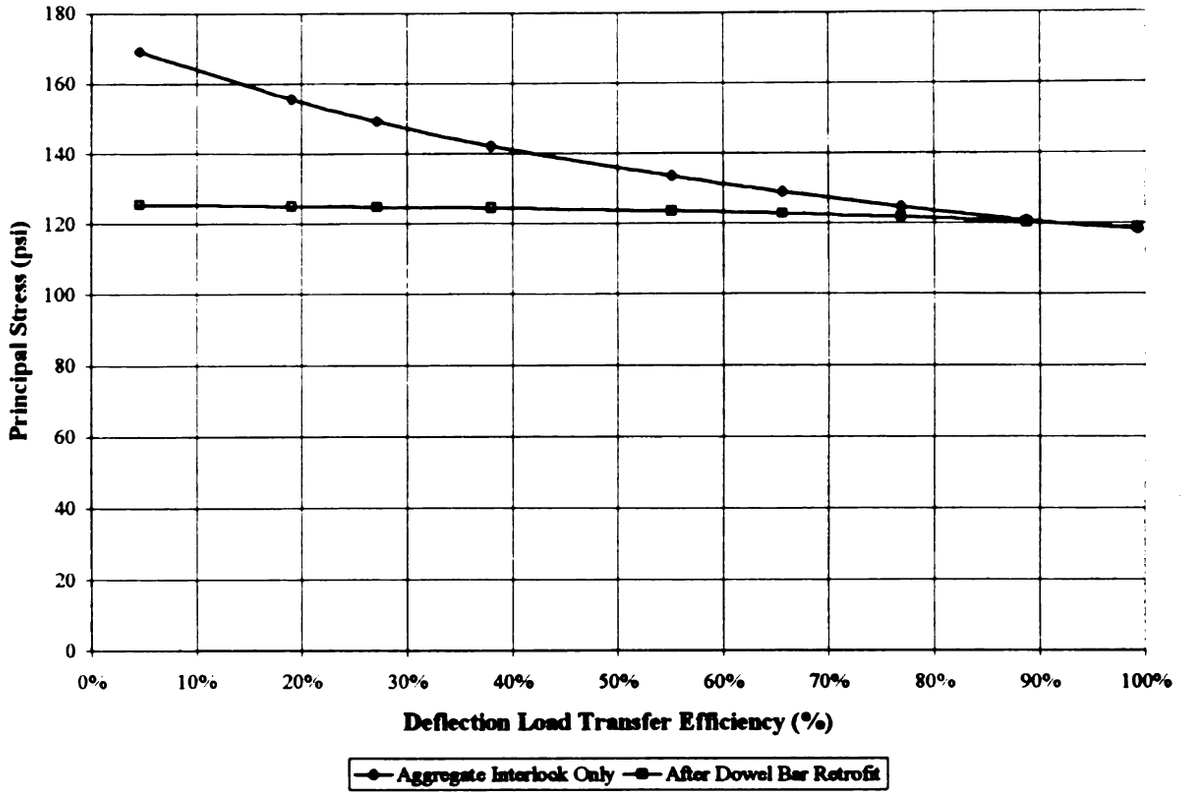

Figure B-81. Principal Tensile Stresses at Crack or Joint Before and After DBR for h=10" (254 mm), k=100 psi/in (27.1 kPa/mm), and ΔT=-15°F (-8.3°C).

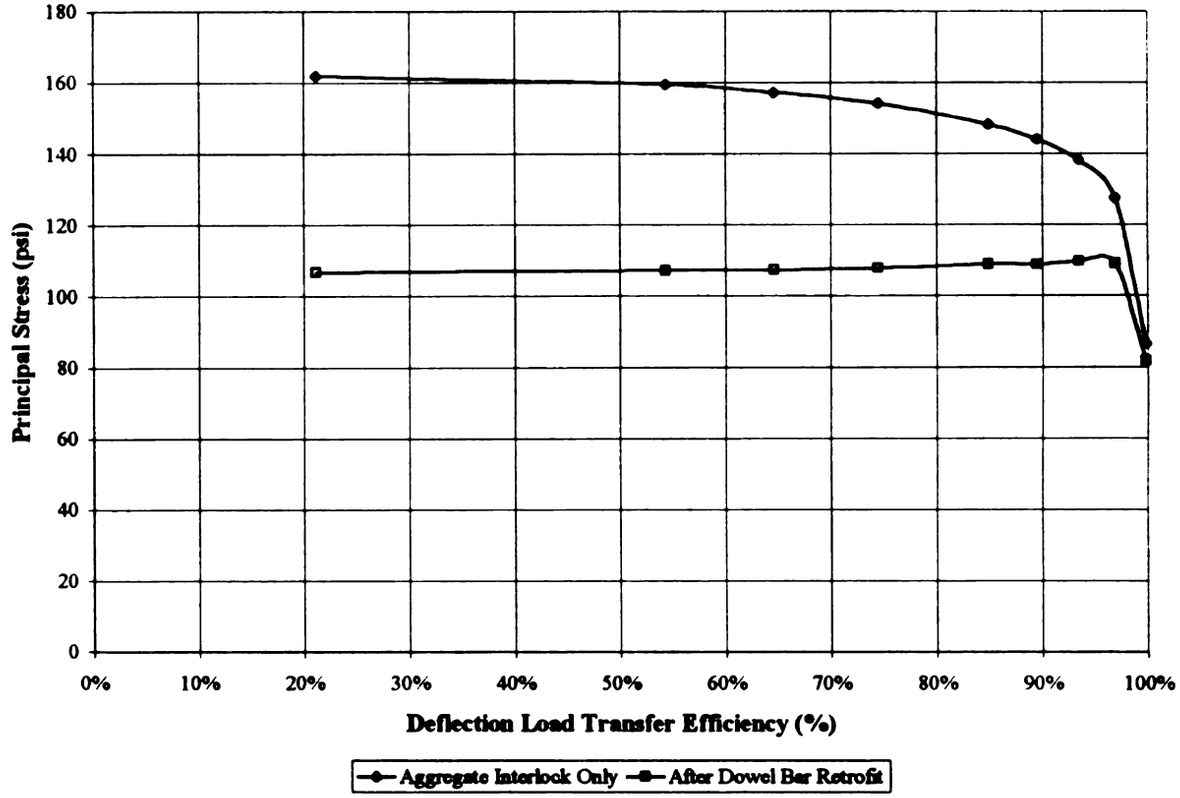

Figure B-82. Principal Tensile Stresses at Crack or Joint Before and After DBR for h=10" (254 mm), k=250 psi/in (67.9 kPa/mm), and ΔT=0°F (0°C).

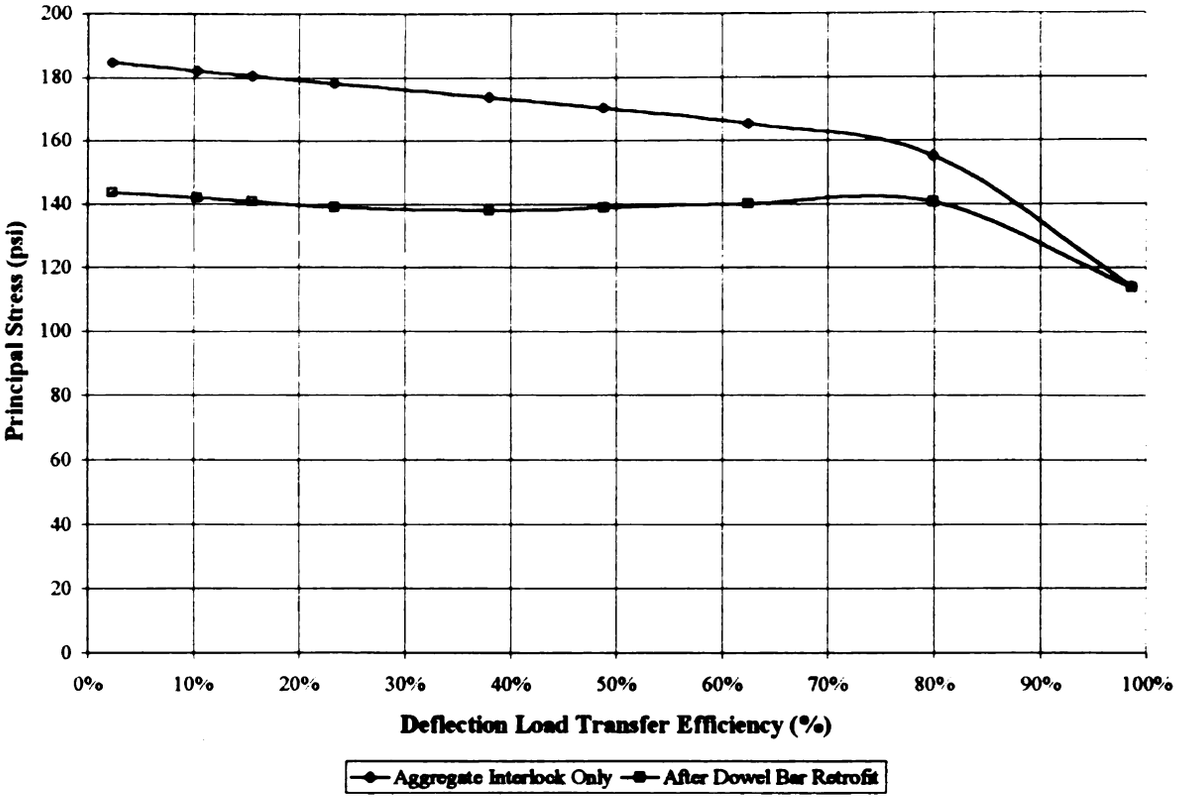

Figure B-83. Principal Tensile Stresses at Crack or Joint Before and After DBR for h=10" (254 mm), k=250 psi/in (67.9 kPa/mm), and ΔT=+15°F (+8.3°C).

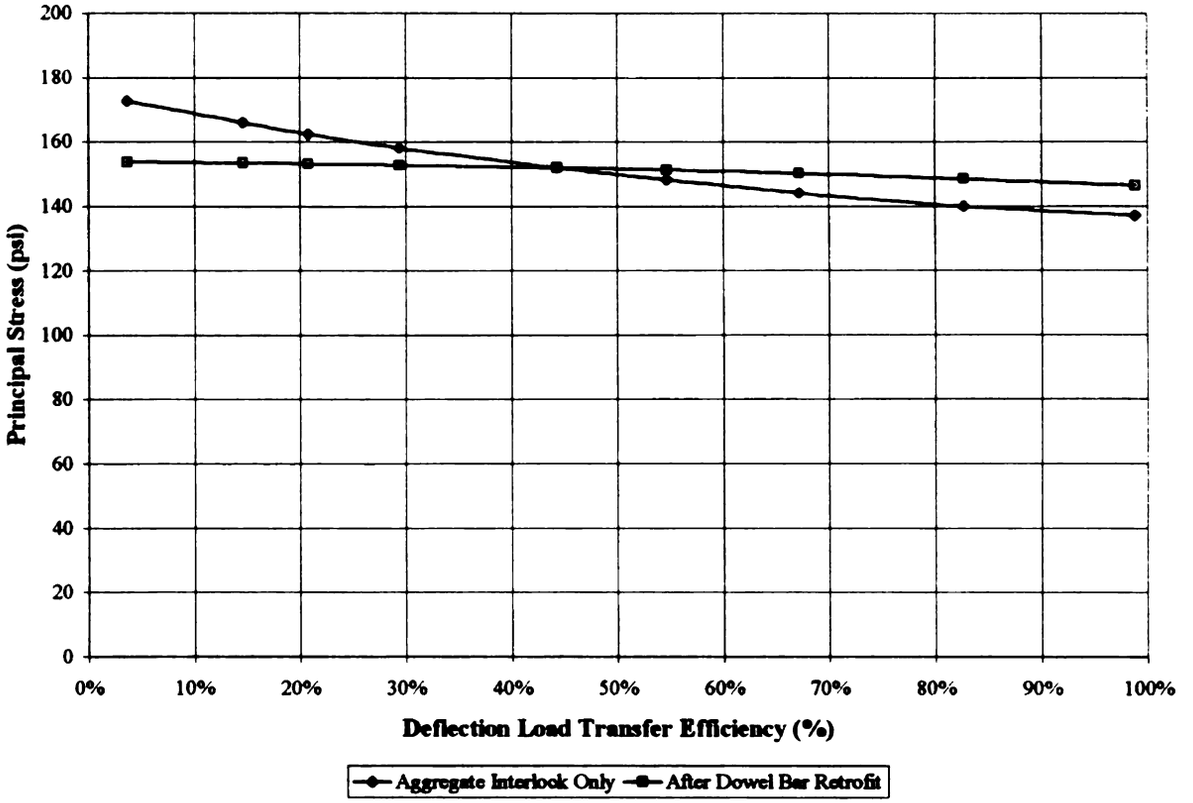

Figure B-84. Principal Tensile Stresses at Crack or Joint Before and After DBR for h=10" (254 mm), k=250 psi/in (67.9 kPa/mm), and ΔT=-15°F (-8.3°C).

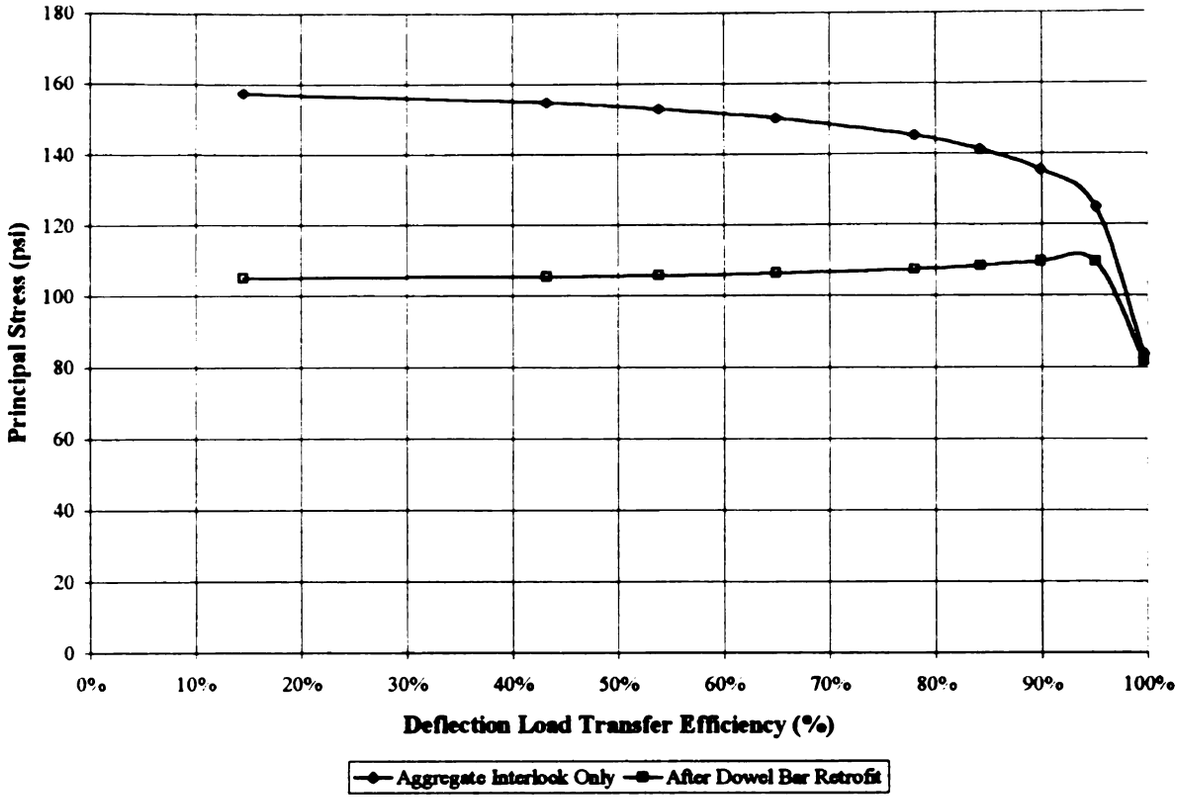

Figure B-85. Principal Tensile Stresses at Crack or Joint Before and After DBR for h=10" (254 mm), k=400 psi/in (106.8 kPa/mm), and ΔT=0°F (0°C).

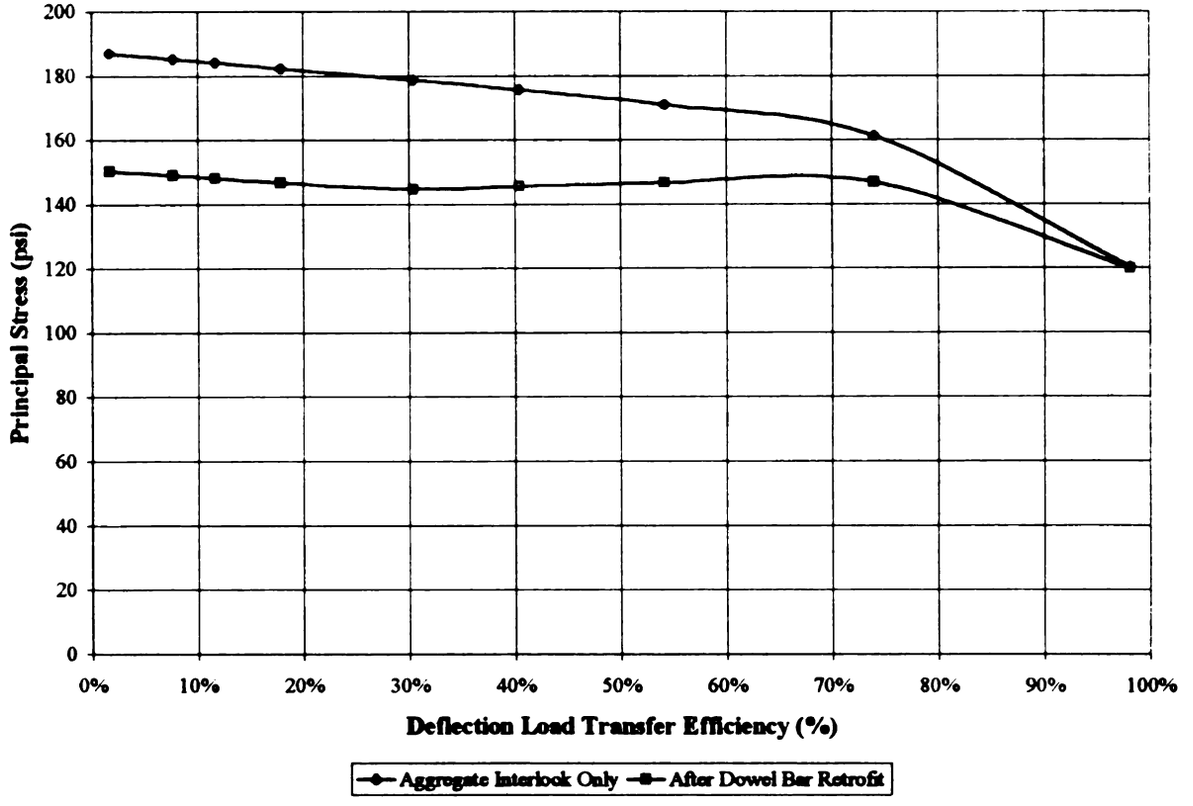

Figure B-86. Principal Tensile Stresses at Crack or Joint Before and After DBR for h=10" (254 mm), k=400 psi/in (106.8 kPa/mm), and ΔT=+15°F (+8.3°C).

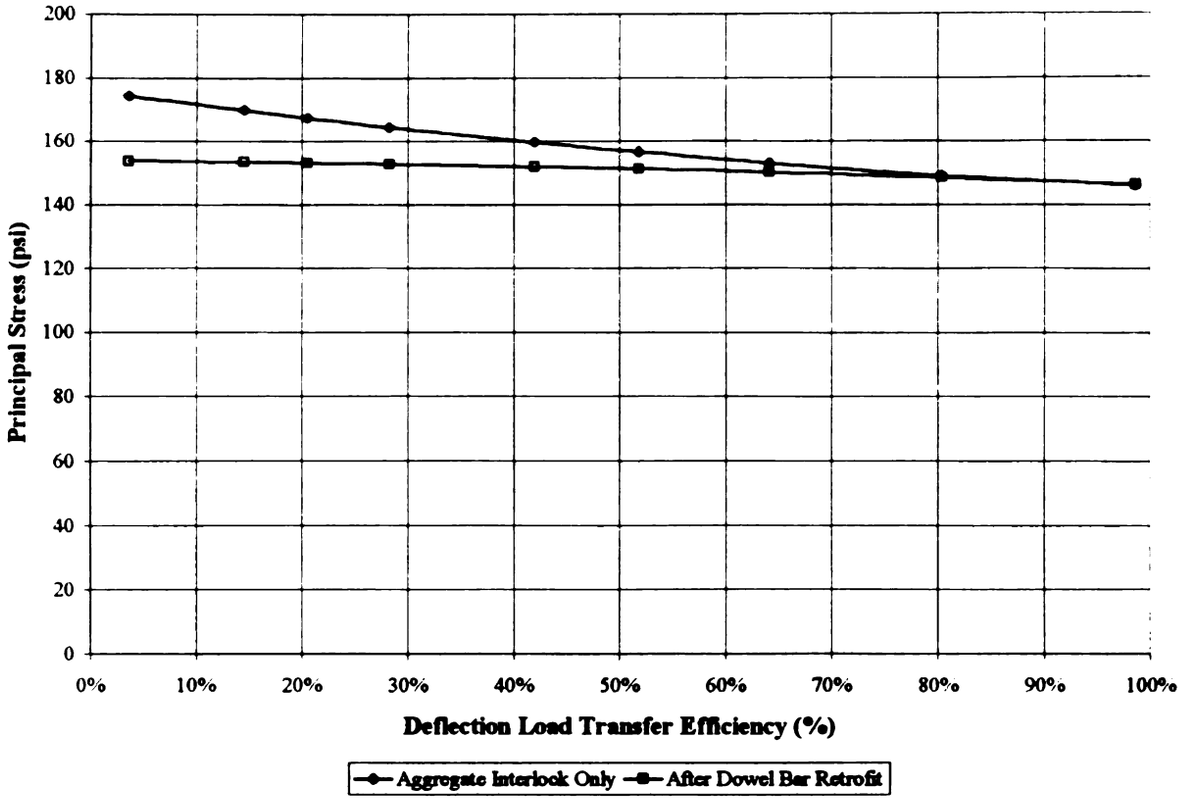

Figure B-87. Principal Tensile Stresses at Crack or Joint Before and After DBR for h=10" (254 mm), k=400 psi/in (106.8 kPa/mm), and ΔT=-15°F (-8.3°C).

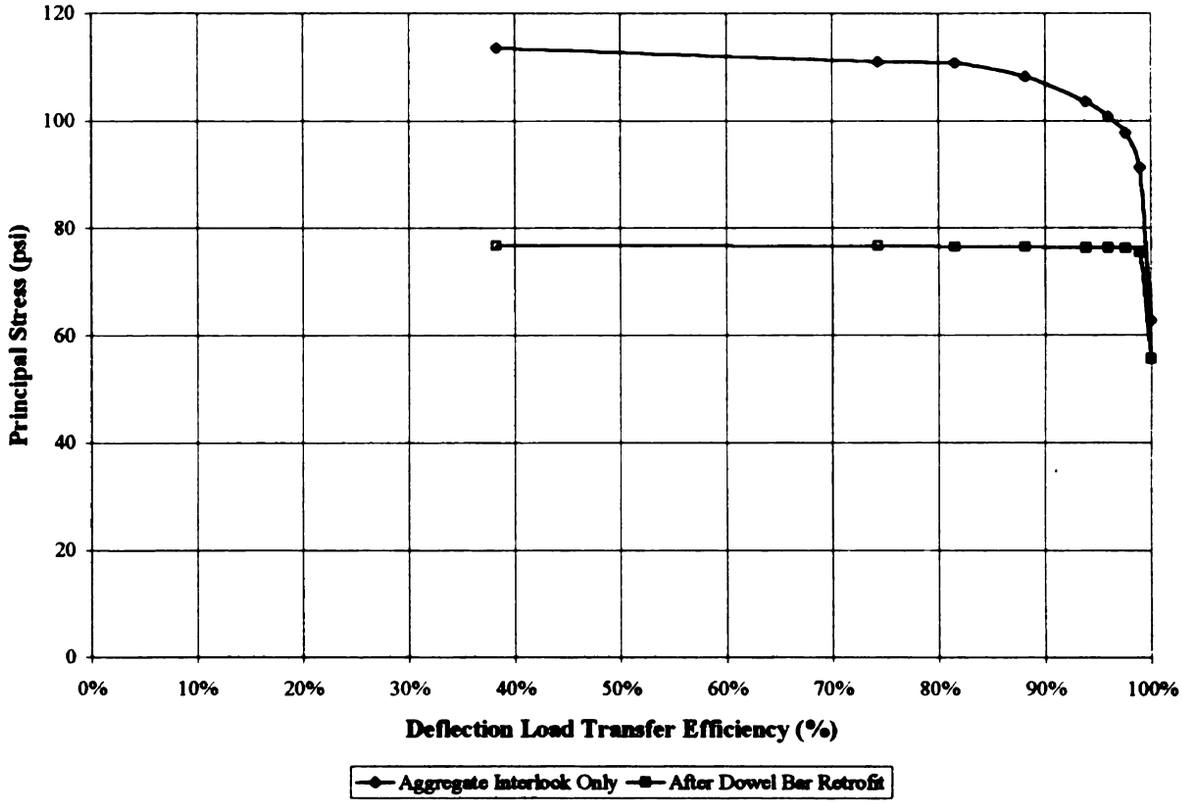

Figure B-88. Principal Tensile Stresses at Crack or Joint Before and After DBR for h=12" (305 mm), k=100 psi/in (27.1 kPa/mm), and ΔT=0°F (0°C).

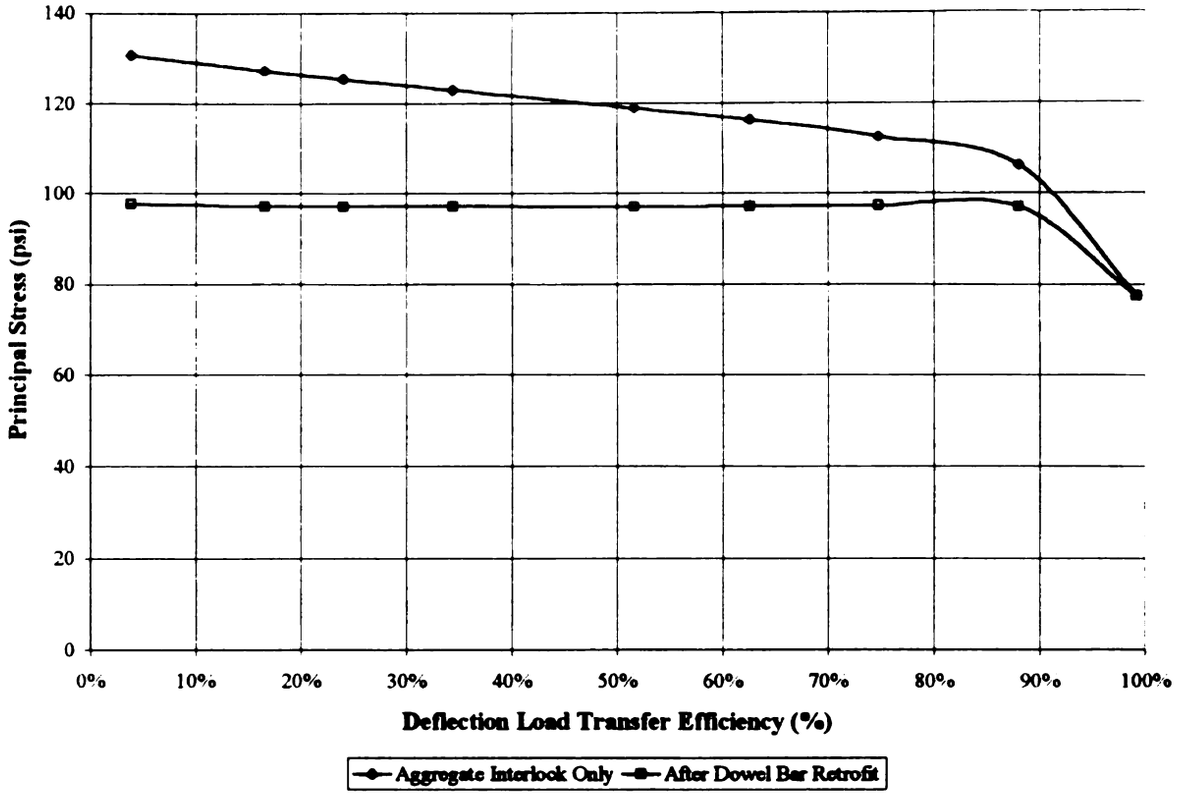

Figure B-89. Principal Tensile Stresses at Crack or Joint Before and After DBR for h=12" (305 mm), k=100 psi/in (27.1 kPa/mm), and ΔT=+15°F (+8.3°C).

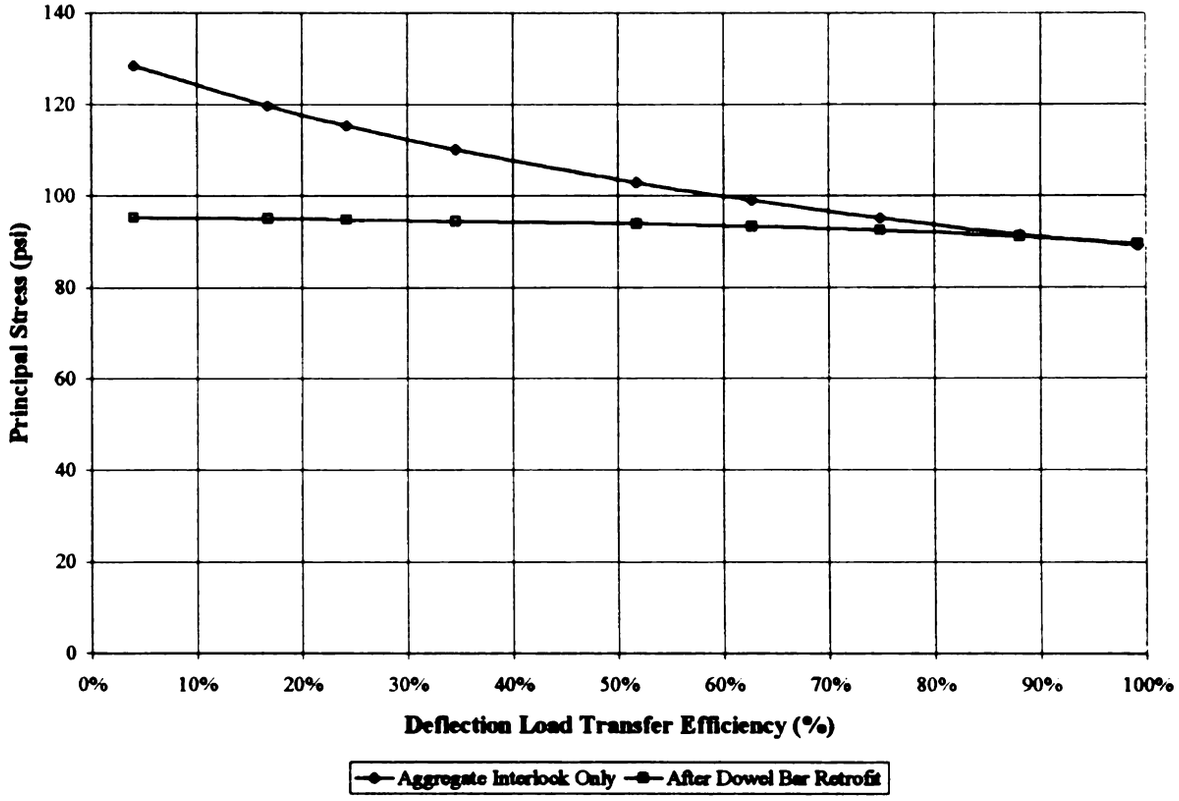

Figure B-90. Principal Tensile Stresses at Crack or Joint Before and After DBR for h=12" (305 mm), k=100 psi/in (27.1 kPa/mm), and ΔT=-15°F (-8.3°C).

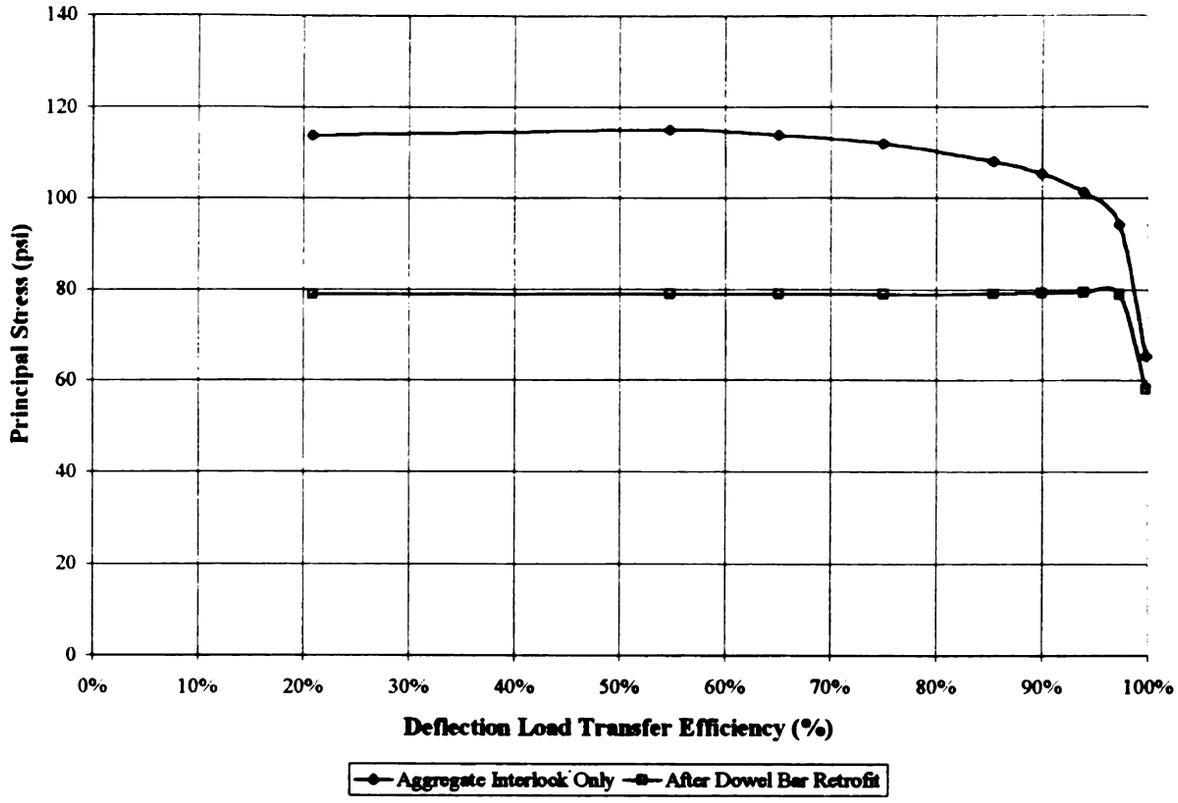

Figure B-91. Principal Tensile Stresses at Crack or Joint Before and After DBR for h=12" (305 mm), k=250 psi/in (67.9 kPa/mm), and ΔT=0°F (0°C).

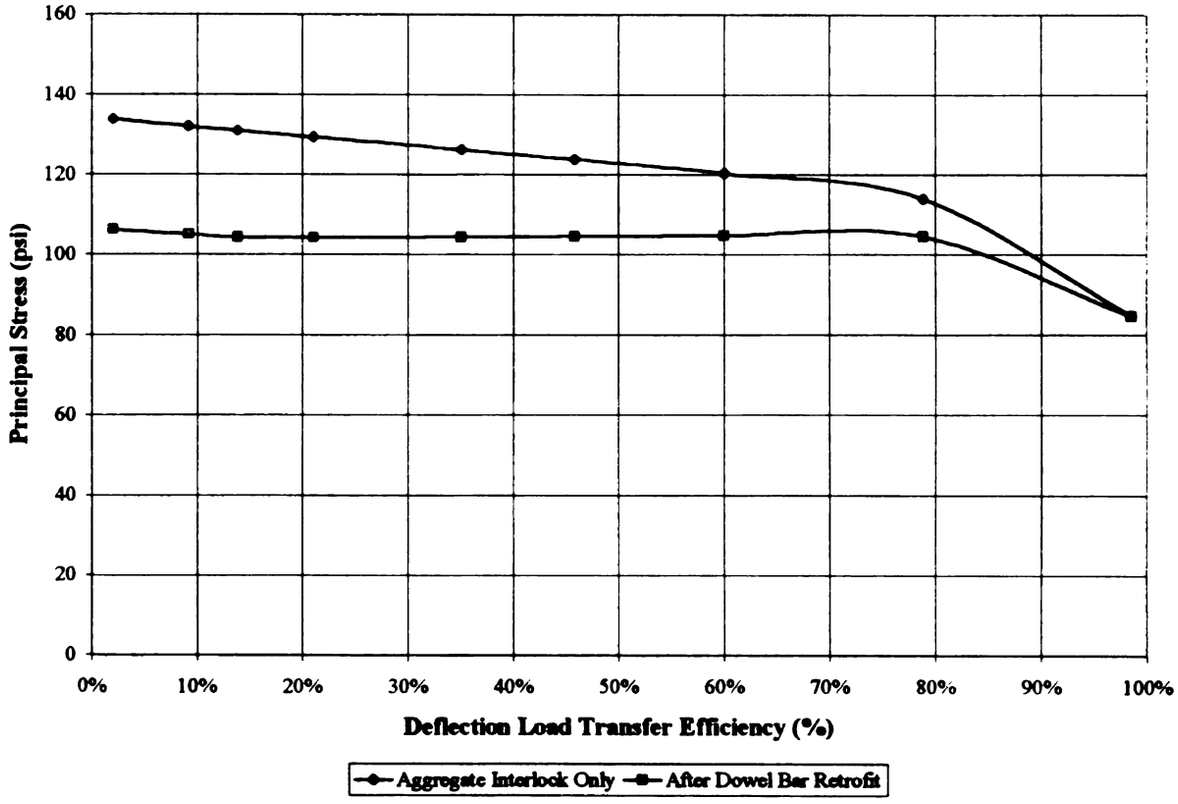

Figure B-92. Principal Tensile Stresses at Crack or Joint Before and After DBR for h=12" (305 mm), k=250 psi/in (67.9 kPa/mm), and ΔT=+15°F (+8.3°C).

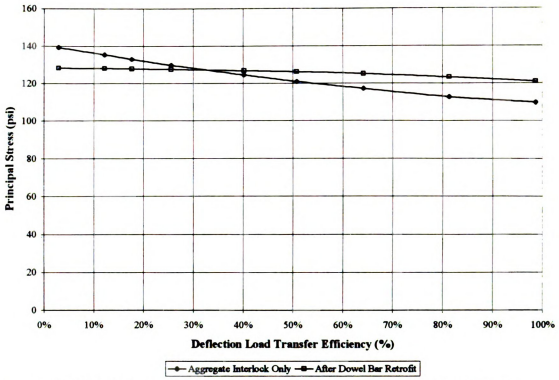

Figure B-93. Principal Tensile Stresses at Crack or Joint Before and After DBR for h=12" (305 mm), k=250 psi/in (67.9 kPa/mm), and ΔT=-15°F (-8.3°C).

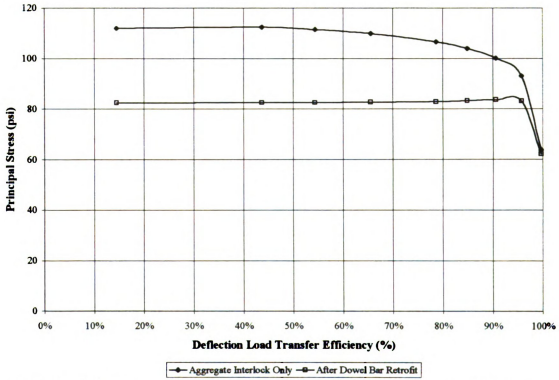

Figure B-94. Principal Tensile Stresses at Crack or Joint Before and After DBR for h=12" (305 mm), k=400 psi/in (106.8 kPa/mm), and ΔT=0°F (0°C).

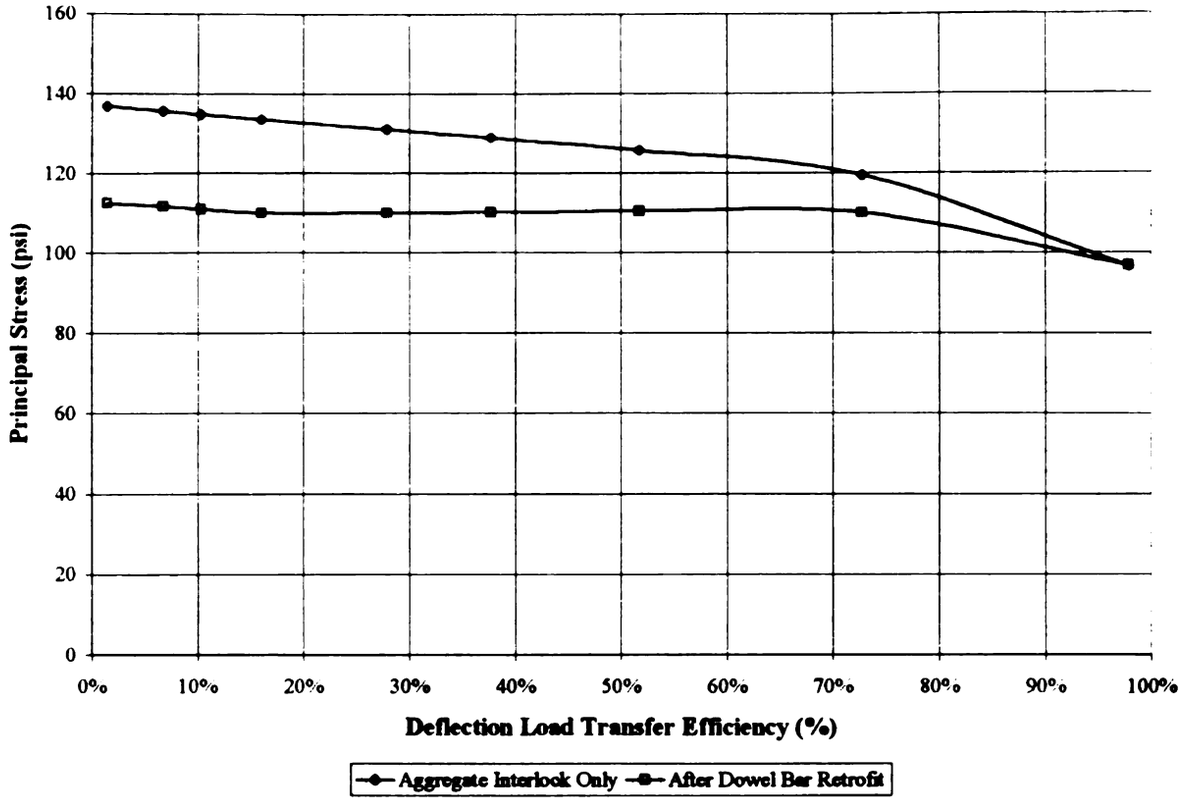

Figure B-95. Principal Tensile Stresses at Crack or Joint Before and After DBR for h=12" (305 mm), k=400 psi/in (106.8 kPa/mm), and ΔT=+15°F (+8.3°C).

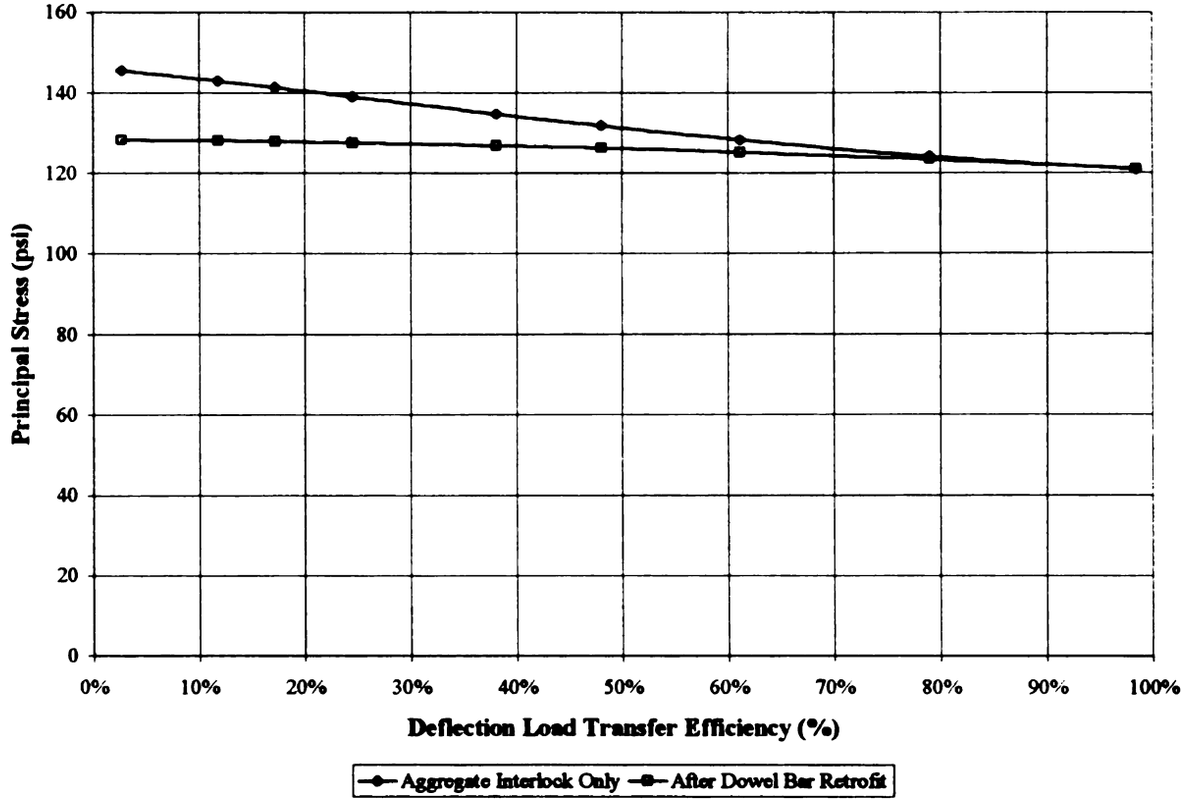

Figure B-96. Principal Tensile Stresses at Crack or Joint Before and After DBR for h=12" (305 mm), k=400 psi/in (106.8 kPa/mm), and ΔT=-15°F (-8.3°C).

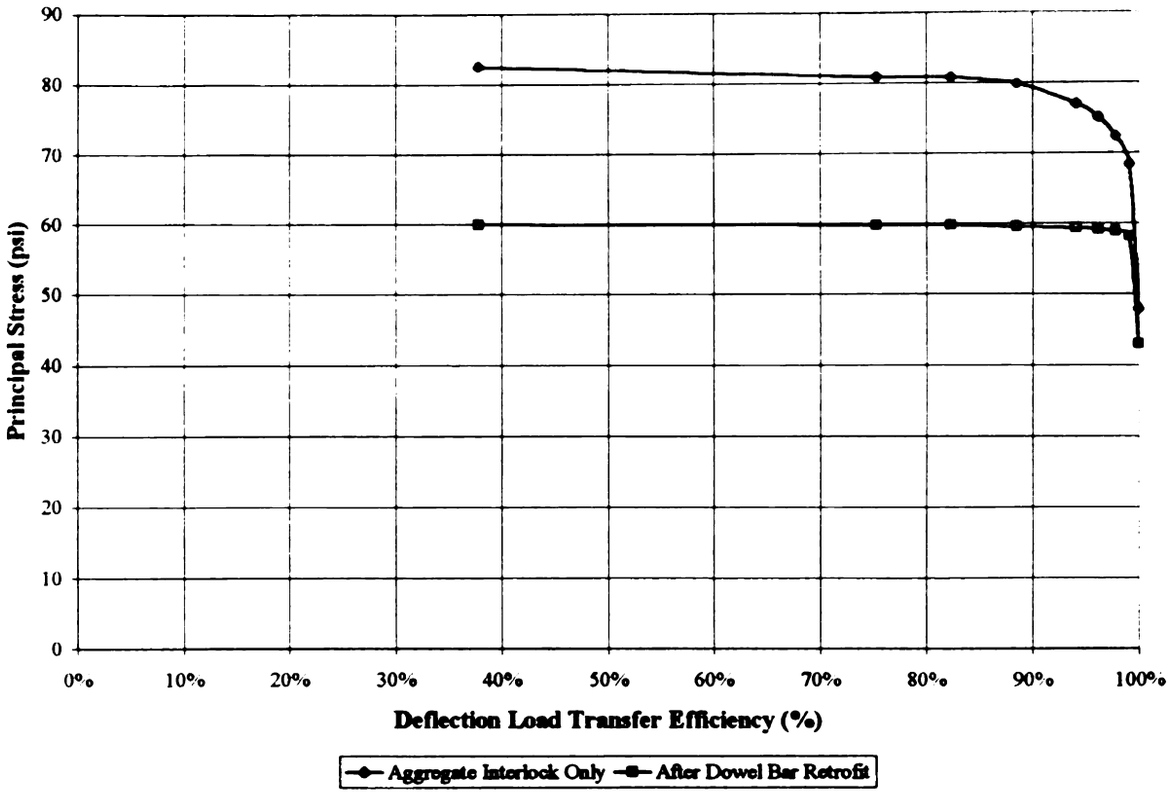

Figure B-97. Principal Tensile Stresses at Crack or Joint Before and After DBR for h=14" (356 mm), k=100 psi/in (27.1 kPa/mm), and ΔT=0°F (0°C).

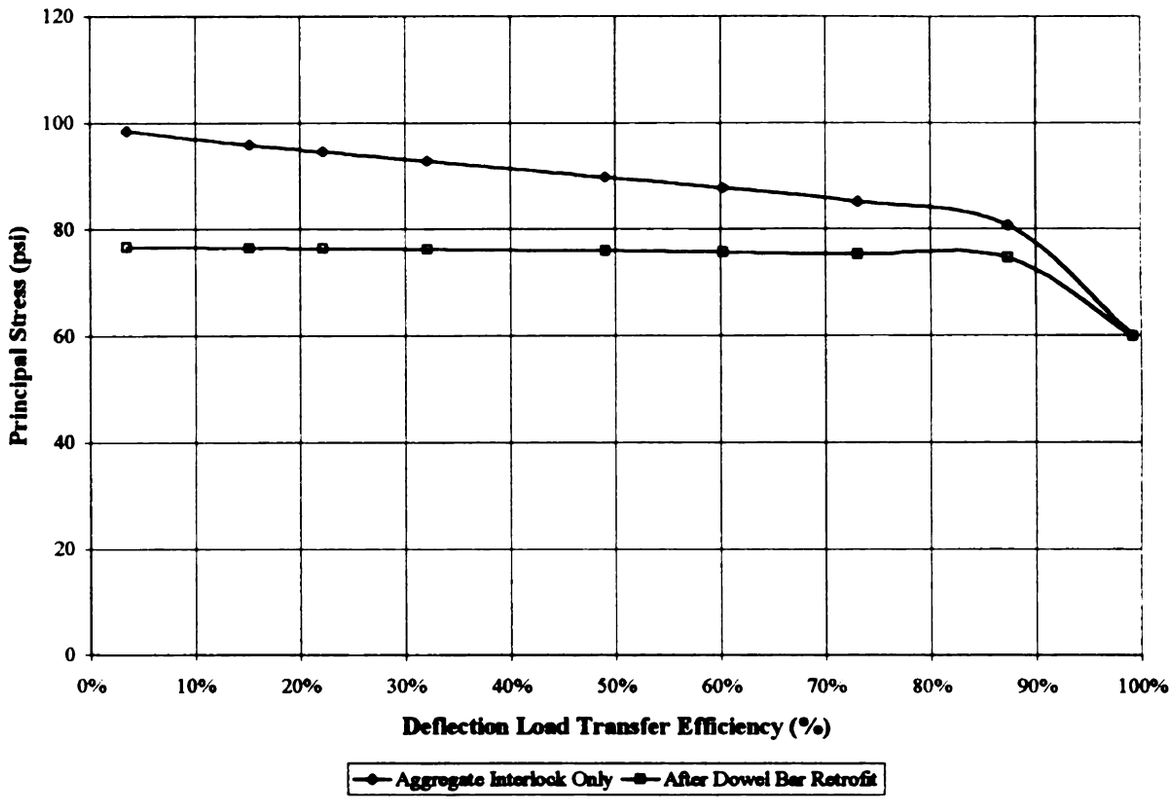

Figure B-98. Principal Tensile Stresses at Crack or Joint Before and After DBR for h=14" (356 mm), k=100 psi/in (27.1 kPa/mm), and ΔT=+15°F (+8.3°C).

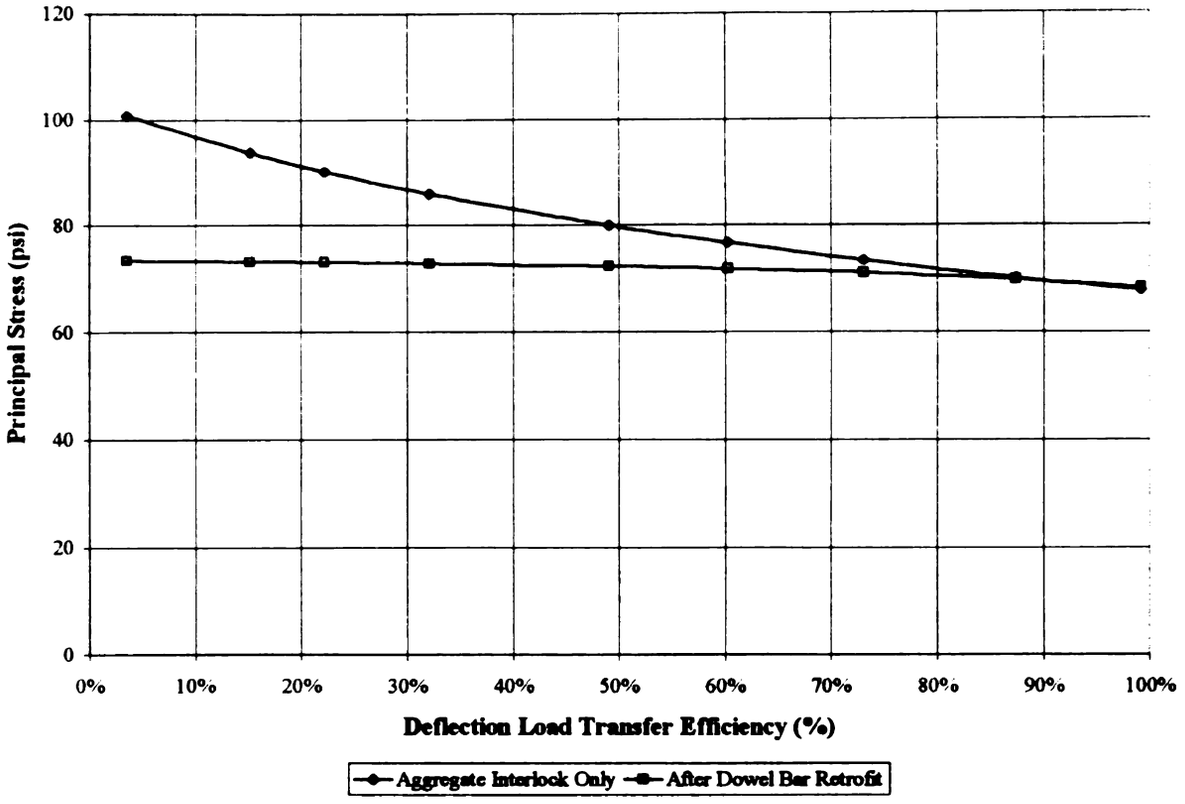

Figure B-99. Principal Tensile Stresses at Crack or Joint Before and After DBR for h=14" (356 mm), k=100 psi/in (27.1 kPa/mm), and ΔT=-15°F (-8.3°C).

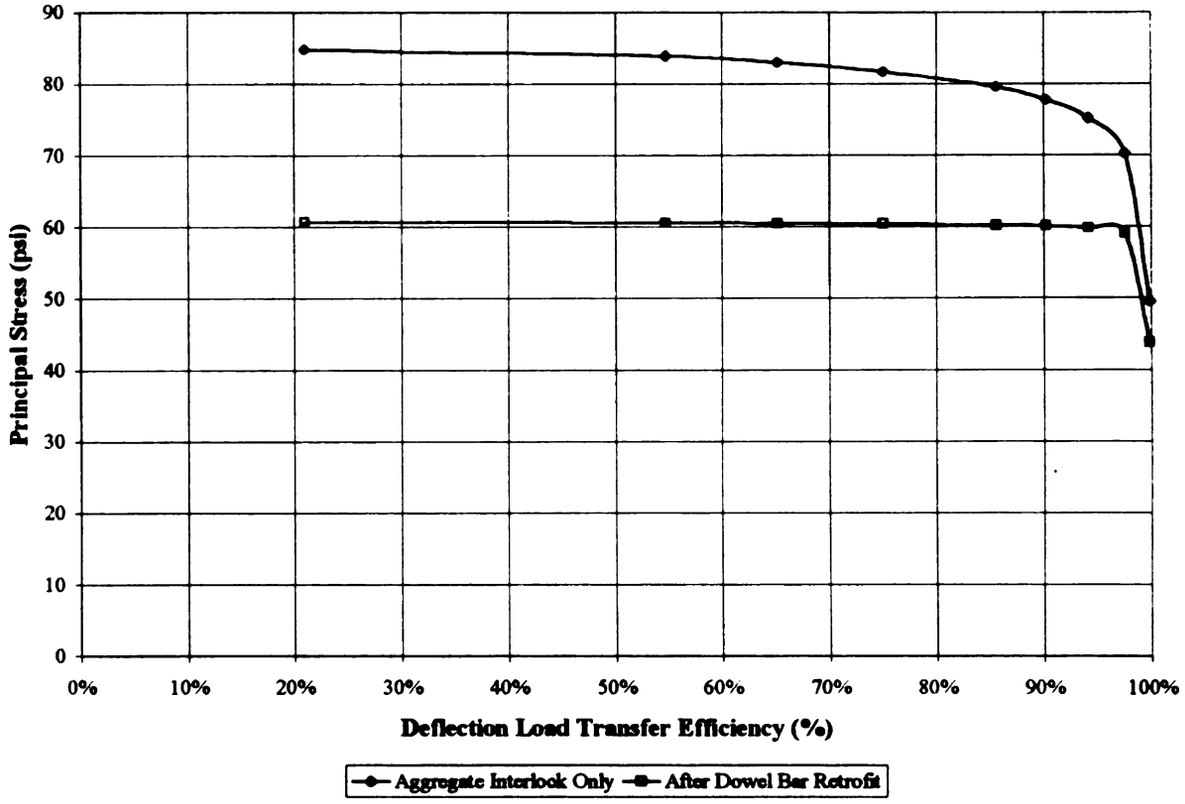

Figure B-100. Principal Tensile Stresses at Crack or Joint Before and After DBR for h=14" (356 mm), k=250 psi/in (67.9 kPa/mm), and ΔT=0°F (0°C).

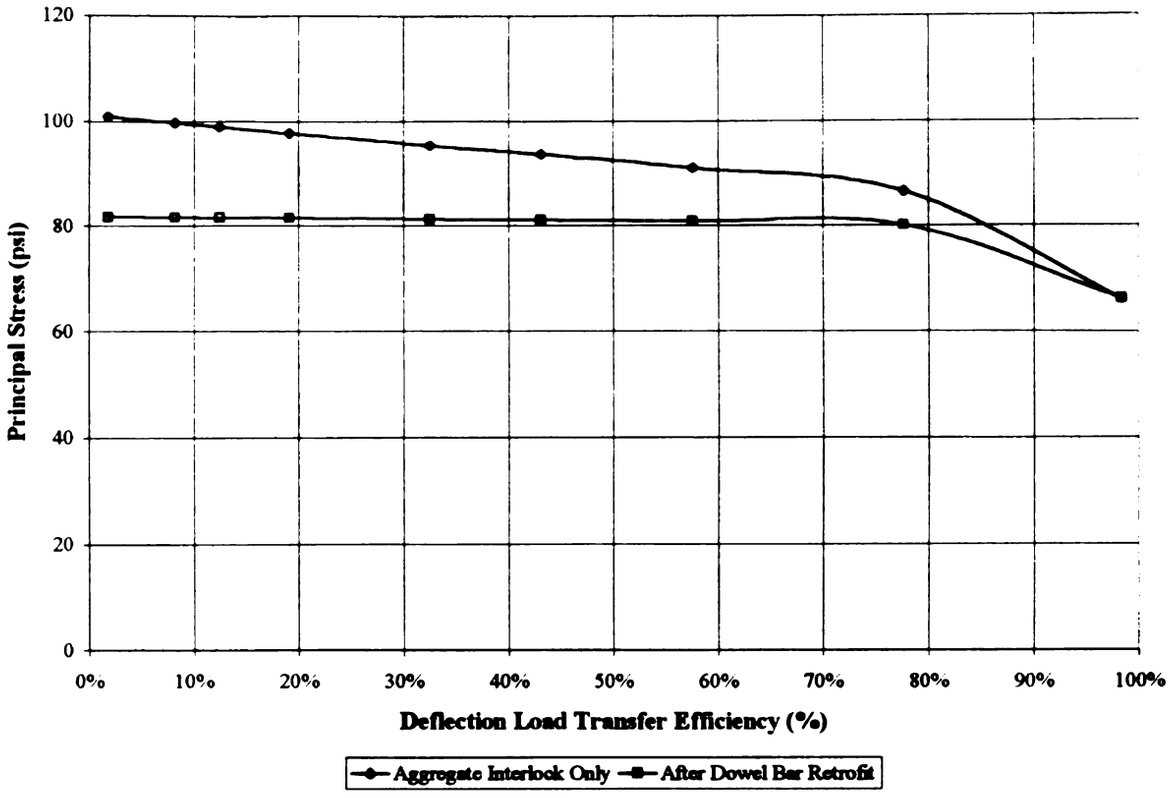

Figure B-101. Principal Tensile Stresses at Crack or Joint Before and After DBR for h=14" (356 mm), k=250 psi/in (67.9 kPa/mm), and ΔT=+15°F (+8.3°C).

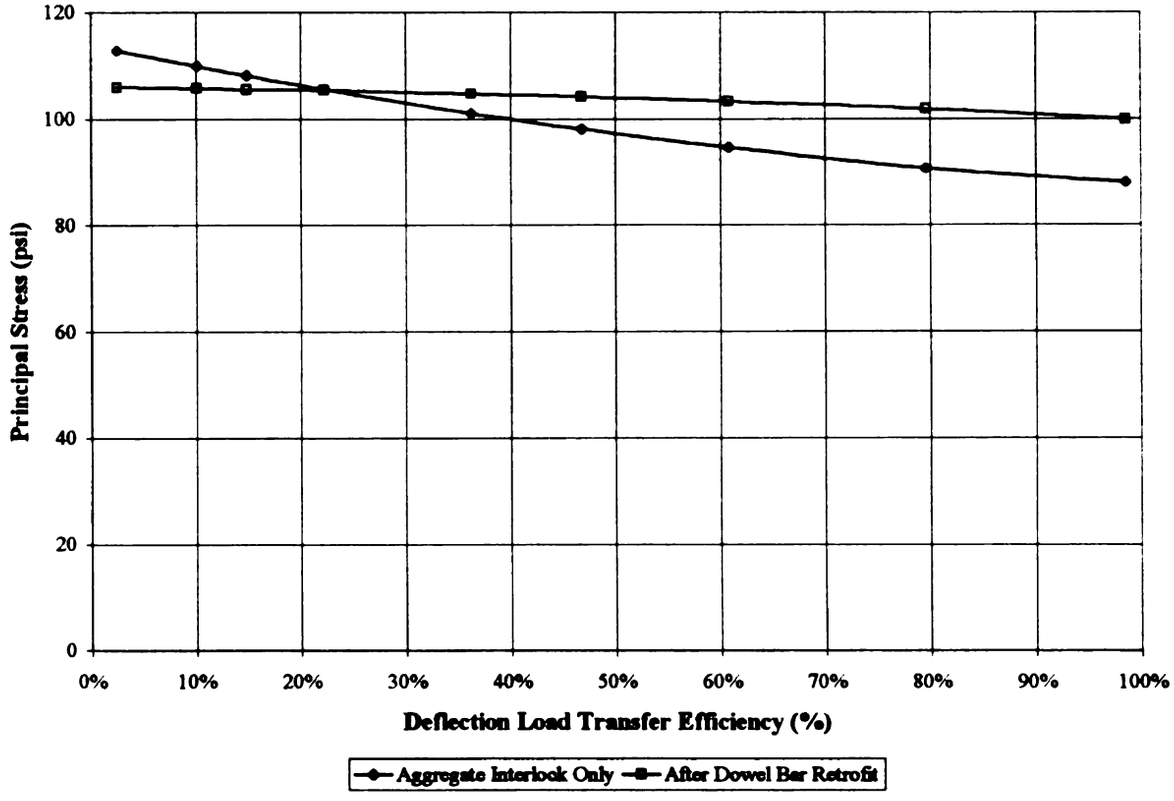

Figure B-102. Principal Tensile Stresses at Crack or Joint Before and After DBR for h=14" (356 mm), k=250 psi/in (67.9 kPa/mm), and ΔT=-15°F (-8.3°C).

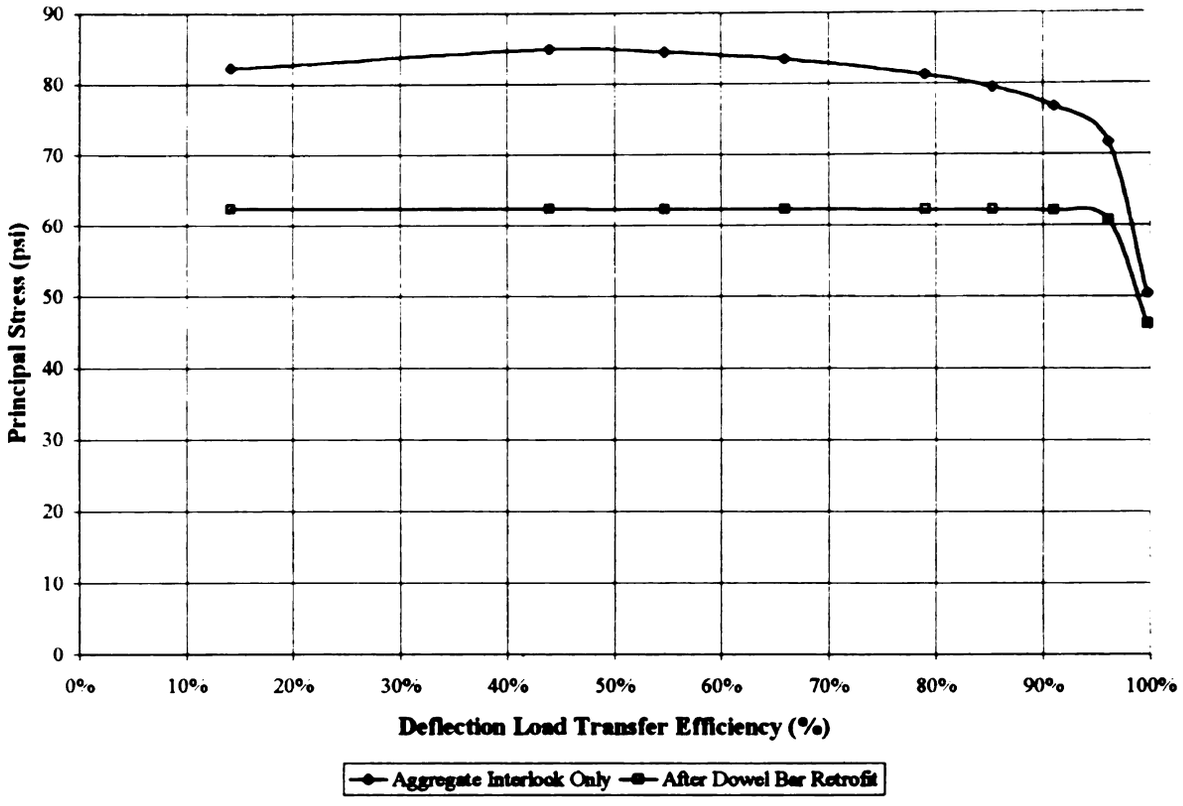

Figure B-103. Principal Tensile Stresses at Crack or Joint Before and After DBR for h=14" (356 mm), k=400 psi/in (106.8 kPa/mm), and ΔT=0°F (0°C).

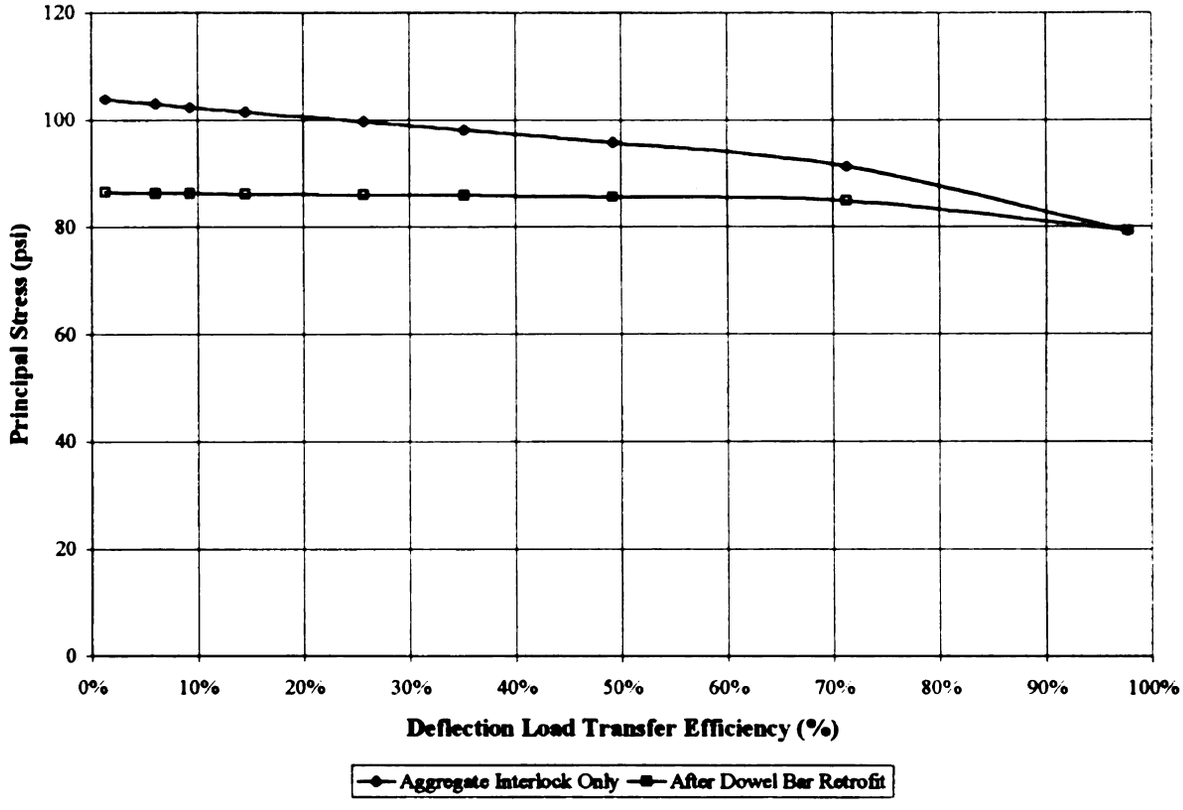

Figure B-104. Principal Tensile Stresses at Crack or Joint Before and After DBR for h=14" (356 mm), k=400 psi/in (106.8 kPa/mm), and ΔT=+15°F (+8.3°C).

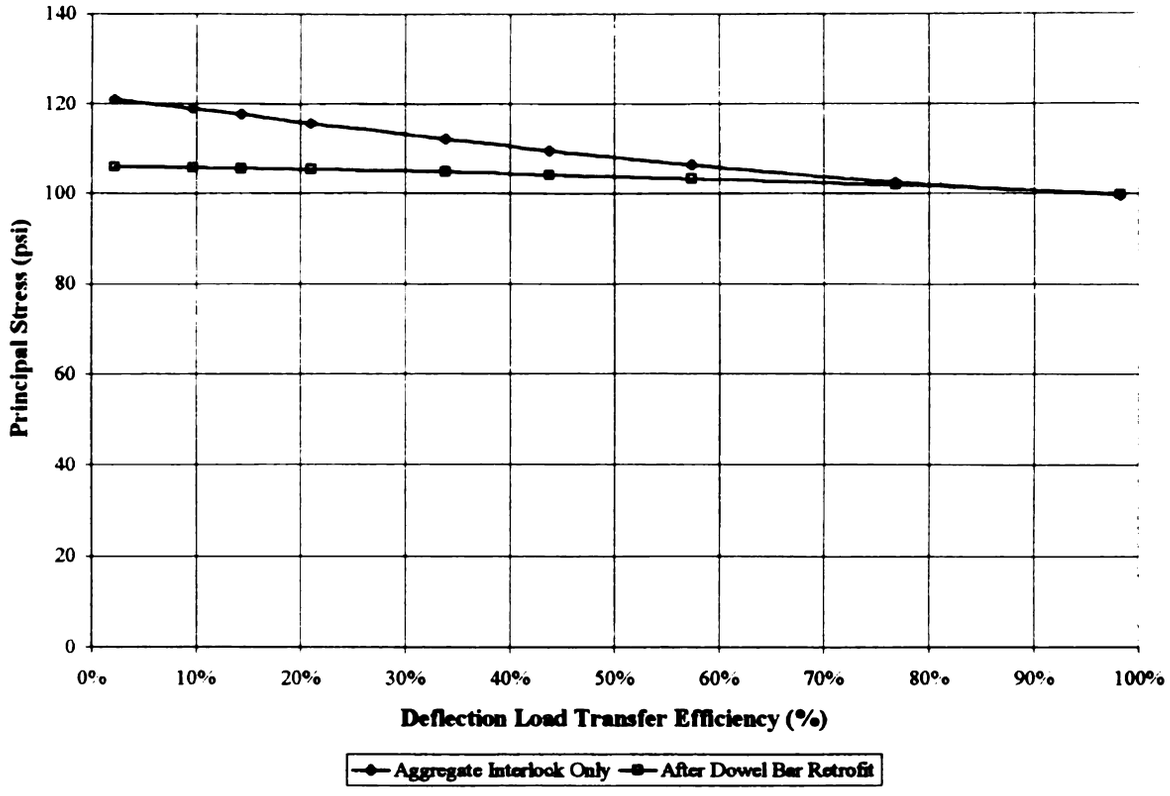

Figure B-105. Principal Tensile Stresses at Crack or Joint Before and After DBR for h=14" (356 mm), k=400 psi/in (106.8 kPa/mm), and ΔT=-15°F (-8.3°C).

APPENDIX C: CATALOG OF RCC DESIGN THICKNESSES

Table C-1. RCC Design Thicknesses for a 12 Kip Single Axle Load and k=100 psi/in.

	$\sigma_{allowable}$ (psi)	Positive Gradient 0%			Positive Gradient 25%			Positive Gradient 50%		
		Neg. Grad 0%	Neg. Grad 25%	Neg. Grad 50%	Neg. Grad 0%	Neg. Grad 25%	Neg. Grad 50%	Neg. Grad 0%	Neg. Grad 25%	Neg. Grad 50%
Lateral Load Reliability 75%	150	9.0	9.5	10.0	11.0	12.0	14.0	15.0	15.0+	15.0+
	200	7.5	7.5	7.0	8.5	9.0	9.0	11.0	11.0	13.0
	250	6.5	6.5	6.0	7.5	7.0	6.5	8.0	8.0	8.0
	300	6.0	5.5	5.5	6.5	6.0	6.0	7.0	7.0	6.5
	350	5.0	5.0	5.0	5.5	5.5	5.0	6.0	6.0	5.5
	400	5.0	5.0	5.0	5.0	5.0	5.0	5.5	5.0	5.0
Lateral Load Reliability 95%	150	10.0	10.5	11.0	12.0	13.0	15.0	15.0+	15.0+	15.0+
	200	8.5	8.0	8.0	10.0	10.0	10.0	11.5	12.0	13.0
	250	7.0	7.0	6.5	8.0	7.5	7.5	9.0	9.0	9.0
	300	6.5	6.0	6.0	7.0	6.5	6.5	7.5	7.5	7.5
	350	5.5	5.5	5.0	6.0	6.0	5.5	6.5	6.5	6.0
	400	5.0	5.0	5.0	5.5	5.5	5.0	6.0	5.5	5.5
Lateral Load Reliability 99%	200	10.0	10.0	9.0	11.0	11.0	11.0	13.5	14.0	15.0
	250	8.5	8.0	7.5	9.5	9.0	8.5	11.0	11.0	10.0
	300	7.5	7.0	6.5	8.0	7.5	7.0	9.0	8.5	8.0
	350	7.0	6.5	6.0	7.0	7.0	6.5	8.0	7.5	7.0
	400	6.0	6.0	5.5	6.5	6.0	6.0	7.0	6.5	6.0
	450	6.0	5.5	5.0	6.0	5.5	5.5	6.5	6.0	6.0

Table C-2. RCC Design Thicknesses for a 12 Kip Single Axle Load and k=250 psi/in.

	$\sigma_{allowable}$ (psi)	Positive Gradient 0%			Positive Gradient 25%			Positive Gradient 50%		
		Neg. Grad 0%	Neg. Grad 25%	Neg. Grad 50%	Neg. Grad 0%	Neg. Grad 25%	Neg. Grad 50%	Neg. Grad 0%	Neg. Grad 25%	Neg. Grad 50%
Lateral Load Reliability 75%	100	9.5	11.0	15.0	13.0	15.0+	15.0+	15.0+	15.0+	15.0+
	150	7.0	7.5	8.0	8.5	9.5	11.5	11.5	14.5	15.0+
	200	6.0	6.0	6.0	7.0	7.0	7.0	8.0	8.5	10.0
	250	5.0	5.0	5.0	6.0	5.5	5.5	6.5	6.5	6.5
	300	5.0	5.0	5.0	5.0	5.0	5.0	5.5	5.5	5.5
	350	5.0	5.0	5.0	5.0	5.0	5.0	5.0	5.0	5.0
Lateral Load Reliability 95%	100	10.5	13.0	15.0	14.0	15.0+	15.0+	15.0+	15.0+	15.0+
	150	8.0	8.0	8.5	9.5	10.5	13.0	12.5	15.0	15.0+
	200	6.5	6.5	6.0	7.5	7.5	7.5	9.0	9.5	10.5
	250	5.5	5.5	5.5	6.0	6.0	6.0	7.0	7.0	7.0
	300	5.0	5.0	5.0	5.5	5.5	5.0	6.0	6.0	5.5
	350	5.0	5.0	5.0	5.0	5.0	5.0	5.0	5.0	5.0
Lateral Load Reliability 99%	150	9.5	9.5	10.0	11.0	12.0	14.0	15.0	15.0+	15.0+
	200	8.5	7.5	7.0	9.0	9.0	9.0	11.0	11.0	12.0
	250	6.5	6.5	6.0	7.5	7.0	6.5	8.0	8.0	8.0
	300	6.0	5.5	5.0	6.5	6.0	5.5	7.0	6.5	6.0
	350	5.5	5.0	5.0	5.5	5.5	5.0	6.0	6.0	5.5
	400	5.0	5.0	5.0	5.0	5.0	5.0	5.5	5.0	5.0

Table C-3. RCC Design Thicknesses for a 12 Kip Single Axle Load and k=400 psi/in.

	$\sigma_{allowable}$ (psi)	Positive Gradient 0%			Positive Gradient 25%			Positive Gradient 50%		
		Neg. Grad 0%	Neg. Grad 25%	Neg. Grad 50%	Neg. Grad 0%	Neg. Grad 25%	Neg. Grad 50%	Neg. Grad 0%	Neg. Grad 25%	Neg. Grad 50%
Lateral Load Reliability 75%	100	9.0	10.5	15.0	12.0	15.0+	15.0+	15.0+	15.0+	15.0+
	150	7.0	7.0	7.5	8.0	9.0	11.0	11.0	14.0	15.0+
	200	6.0	6.0	6.0	6.5	6.5	7.0	7.5	8.0	9.5
	250	5.0	5.0	5.0	5.5	5.5	5.5	6.0	6.5	6.5
	300	5.0	5.0	5.0	5.0	5.0	5.0	5.5	5.5	5.5
	350	5.0	5.0	5.0	5.0	5.0	5.0	5.0	5.0	5.0
Lateral Load Reliability 95%	100	10.0	11.0	15.0	13.0	15.0+	15.0+	15.0+	15.0+	15.0+
	150	7.5	8.0	8.0	9.0	10.0	12.0	11.5	15.0	15.0+
	200	6.0	6.0	6.0	7.0	7.0	7.5	8.0	9.0	10.0
	250	5.5	5.0	5.0	6.0	6.0	6.0	6.5	6.5	7.0
	300	5.0	5.0	5.0	5.0	5.0	5.0	5.5	5.5	5.5
	350	5.0	5.0	5.0	5.0	5.0	5.0	5.0	5.0	5.0
Lateral Load Reliability 99%	150	9.0	13.0	9.5	10.5	11.5	14.0	13.5	15.0+	15.0+
	200	7.5	9.0	7.0	8.0	8.5	8.5	10.0	10.5	11.5
	250	6.5	7.0	5.5	7.0	6.5	6.5	8.0	7.5	7.5
	300	5.5	5.5	5.0	6.0	6.0	5.5	6.5	6.5	6.0
	350	5.0	5.0	5.0	5.5	5.0	5.0	6.0	5.5	5.0
	400	5.0	5.0	5.0	5.0	5.0	5.0	5.0	5.0	5.0

Table C-4. RCC Design Thicknesses for an 18 Kip Single Axle Load and k=100 psi/in.

	$\sigma_{allowable}$ (psi)	Positive Gradient 0%			Positive Gradient 25%			Positive Gradient 50%		
		Neg. Grad 0%	Neg. Grad 25%	Neg. Grad 50%	Neg. Grad 0%	Neg. Grad 25%	Neg. Grad 50%	Neg. Grad 0%	Neg. Grad 25%	Neg. Grad 50%
Lateral Load Reliability 75%	150	10.5	10.5	10.5	12.5	12.5	14.0	15.0+	15.0+	15.0+
	200	8.5	8.0	8.0	11.0	9.5	9.5	11.5	11.5	12.0
	250	7.5	7.0	7.0	8.0	8.0	7.5	9.0	9.0	9.0
	300	6.5	6.0	5.5	7.0	6.5	6.0	8.0	7.5	7.0
	350	6.0	5.5	5.0	6.5	6.0	5.5	7.0	6.5	6.0
	400	5.5	5.0	5.0	5.5	5.0	5.0	6.0	6.0	5.5
Lateral Load Reliability 95%	200	9.0	9.0	8.5	11.0	10.5	10.0	12.5	12.5	13.0
	250	8.0	7.5	7.0	9.0	8.5	8.0	10.0	10.0	9.5
	300	7.0	6.5	6.0	7.5	7.5	7.0	8.5	8.0	7.5
	350	6.0	6.0	5.5	7.0	6.5	6.0	7.5	7.0	6.5
	400	6.5	5.5	5.0	6.0	6.0	5.5	6.5	6.5	6.0
	450	5.5	5.0	5.0	5.5	5.5	5.0	6.0	6.0	5.0
Lateral Load Reliability 99%	200	11.0	10.5	10.0	12.5	12.0	11.5	14.5	14.5	14.0
	250	9.5	9.0	8.0	10.5	10.0	9.0	13.0	11.5	11.0
	300	8.5	8.0	7.5	9.0	8.5	8.0	10.0	9.5	9.0
	350	7.5	7	7.0	8.0	7.5	7.0	8.0	8.0	7.5
	400	7.0	6.5	6.0	7.5	7.0	6.5	7.0	7.5	7.0
	450	6.5	6.0	6.0	7.0	6.5	6.0	6.5	7.0	6.5

Table C-5. RCC Design Thicknesses for an 18 Kip Single Axle Load and k=250 psi/in.

	$\sigma_{allowable}$ (psi)	Positive Gradient 0%			Positive Gradient 25%			Positive Gradient 50%		
		Neg. Grad 0%	Neg. Grad 25%	Neg. Grad 50%	Neg. Grad 0%	Neg. Grad 25%	Neg. Grad 50%	Neg. Grad 0%	Neg. Grad 25%	Neg. Grad 50%
Lateral Load Reliability 75%	150	9.0	9.5	10.0	11.0	12.0	14.0	15.0	15.0+	15.0+
	200	7.5	7.5	7.0	8.5	9.0	9.0	10.5	11.0	12.0
	250	6.5	6.5	6.0	7.0	7.0	7.0	8.0	8.0	8.0
	300	6.0	5.5	5.5	6.5	6.0	6.5	7.0	7.0	6.5
	350	5.0	5.0	5.0	5.5	5.5	5.0	6.0	6.0	5.5
	400	5.0	5.0	5.0	5.0	5.0	5.0	5.5	5.0	5.0
Lateral Load Reliability 95%	150	10.0	10.5	10.5	12.0	13.0	15.0	15.0+	15.0+	15.0+
	200	8.5	8.0	8.0	9.5	9.5	9.5	11.0	12.0	13.0
	250	7.0	7.0	7.0	8.0	7.5	7.5	9.0	9.0	9.0
	300	6.5	6.0	6.0	7.0	6.5	6.5	7.5	7.5	7.0
	350	6.0	5.5	5.5	6.0	6.0	5.5	6.5	6.5	6.0
	400	5.0	5.0	5.0	5.5	5.5	5.0	6.0	5.5	5.5
Lateral Load Reliability 99%	200	10.0	9.5	9.5	11.0	11.0	11.0	13.5	14.0	14.5
	250	8.5	8.0	8.0	9.5	9.0	8.5	11.0	10.5	10.0
	300	7.5	7.0	7.0	8.0	7.5	7.0	9.0	8.5	8.0
	350	7.0	6.5	6.5	7.0	7.0	6.5	8.0	7.5	7.0
	400	6.0	6.0	6.0	6.5	6.0	6.0	7.0	6.5	6.0
	450	6.0	5.5	5.5	6.0	6.0	5.5	6.5	6.0	6.0

Table C-6. RCC Design Thicknesses for an 18 Kip Single Axle Load and k=400 psi/in.

	$\sigma_{allowable}$ (psi)	Positive Gradient 0%			Positive Gradient 25%			Positive Gradient 50%		
		Neg. Grad 0%	Neg. Grad 25%	Neg. Grad 50%	Neg. Grad 0%	Neg. Grad 25%	Neg. Grad 50%	Neg. Grad 0%	Neg. Grad 25%	Neg. Grad 50%
Lateral Load Reliability 75%	150	8.5	9.0	9.5	10.5	11.5	14.0	14.0	15.0+	15.0+
	200	7.0	7.0	7.0	8.0	8.5	8.5	10.0	10.5	12.0
	250	6.0	6.0	6.0	7.0	7.0	6.5	8.0	8.0	8.0
	300	5.5	5.5	5.0	6.0	6.0	5.5	6.5	6.5	6.5
	350	5.0	5.0	5.0	5.5	5.0	5.0	6.0	5.5	5.5
	400	5.0	5.0	5.0	5.0	5.0	5.0	5.0	5.0	5.0
Lateral Load Reliability 95%	150	9.5	10.0	10.5	11.5	12.5	15.0	15.0	15.0+	15.0+
	200	8.0	7.5	7.5	9.0	9.0	9.0	11.0	11.0	13.0
	250	7.0	6.5	6.5	7.5	7.5	7.0	8.5	8.5	8.5
	300	6.0	6.0	6.0	6.5	6.5	6.0	7.0	7.0	7.0
	350	5.5	5.0	5.0	6.0	5.5	5.5	6.5	6.0	6.0
	400	5.0	5.0	5.0	5.0	5.0	5.0	5.5	5.5	5.0
Lateral Load Reliability 99%	200	9.5	9.0	9.0	10.5	10.5	10.5	12.5	11.0	14.5
	250	8.0	7.5	7.5	9.0	8.5	8.0	10.0	10.0	9.5
	300	7.0	6.5	6.5	7.5	7.0	7.0	8.5	8.0	7.5
	350	6.5	6.0	6.0	7.0	6.5	6.5	7.5	7.0	6.5
	400	6.0	5.5	5.5	6.0	6.0	6.0	6.5	6.0	6.0
	450	5.5	5.0	5.0	5.5	5.5	5.5	6.0	5.5	5.5

Table C-7. RCC Design Thicknesses for a 24 Kip Tandem Axle Load and k=100 psi/in.

	$\sigma_{allowable}$ (psi)	Positive Gradient 0%			Positive Gradient 25%			Positive Gradient 50%		
		Neg. Grad 0%	Neg. Grad 25%	Neg. Grad 50%	Neg. Grad 0%	Neg. Grad 25%	Neg. Grad 50%	Neg. Grad 0%	Neg. Grad 25%	Neg. Grad 50%
Lateral Load Reliability 75%	100	10.5	11.5	14.0	14.5	15.0+	15.0+	15.0+	15.0+	15.0+
	150	7.5	7.5	8.0	9.0	10.0	11.5	12.0	14.5	15.0+
	200	6.0	6.0	6.0	7.0	7.0	7.5	8.5	9.0	10.0
	250	5.0	5.0	5.0	6.0	5.5	5.5	6.5	6.5	7.0
	300	5.0	5.0	5.0	5.0	5.0	5.0	5.5	5.5	5.0
	350	5.0	5.0	5.0	5.0	5.0	5.0	5.0	5.0	5.0
Lateral Load Reliability 95%	100	11.0	13.0	15.0	15.0+	15.0+	15.0+	15.0+	15.0+	15.0+
	150	8.0	8.5	8.5	10.0	11.0	12.5	13.0	15.0	15.0+
	200	6.5	6.5	6.5	7.5	8.0	8.0	9.0	10.0	10.5
	250	5.5	5.5	5.0	6.5	6.0	6.0	7.0	7.0	7.5
	300	5.0	5.0	5.0	5.5	5.0	5.0	6.0	6.0	6.0
	350	5.0	5.0	5.0	5.0	5.0	5.0	5.0	5.0	5.0
Lateral Load Reliability 99%	100	14.0	15.0	15.0+	15.0+	15.0+	15.0+	15.0+	15.0+	15.0+
	150	10.0	10.0	10.5	12.0	13.0	13.5	15.0	15.0+	15.0+
	200	8.0	8.0	7.5	9.0	9.0	9.0	11.0	11.5	12.0
	250	7.0	6.5	6.0	7.5	7.5	7.0	8.5	8.5	8.5
	300	6.0	5.5	5.5	6.5	6.0	6.0	7.0	7.0	6.5
	350	5.5	5.0	5.0	5.5	5.5	5.0	6.0	6.0	5.5

Table C-8. RCC Design Thicknesses for a 24 Kip Tandem Axle Load and k=250 psi/in.

	$\sigma_{allowable}$ (psi)	Positive Gradient 0%			Positive Gradient 25%			Positive Gradient 50%		
		Neg. Grad 0%	Neg. Grad 25%	Neg. Grad 50%	Neg. Grad 0%	Neg. Grad 25%	Neg. Grad 50%	Neg. Grad 0%	Neg. Grad 25%	Neg. Grad 50%
Lateral Load Reliability 75%	100	8.5	10.0	14.0	12.0	15.0+	15.0+	15.0+	15.0+	15.0+
	150	6.5	7.0	7.5	8.0	9.0	11.0	10.5	13.5	15.0+
	200	5.5	5.5	5.5	6.0	6.5	7.0	7.5	8.0	9.0
	250	5.0	5.0	5.0	5.5	5.5	5.5	6.0	6.0	6.0
	300	5.0	5.0	5.0	5.0	5.0	5.0	5.0	5.0	5.0
	350	5.0	5.0	5.0	5.0	5.0	5.0	5.0	5.0	5.0
Lateral Load Reliability 95%	100	9.5	11.0	15.0	13.5	15.0+	15.0+	15.0+	15.0+	15.0+
	150	7.0	7.5	8.0	8.5	9.5	12.0	11.5	14.5	15.0+
	200	6.0	6.0	6.0	6.5	7.0	7.5	8.0	8.5	10.0
	250	5.0	5.0	5.0	5.5	5.5	5.5	6.5	6.5	6.5
	300	5.0	5.0	5.0	5.0	5.0	5.0	5.5	5.5	5.5
	350	5.0	5.0	5.0	5.0	5.0	5.0	5.0	5.0	5.0
Lateral Load Reliability 99%	150	8.5	9.0	9.5	10.5	11.0	13.5	13.5	15.0+	15.0+
	200	7.0	7.0	7.0	8.0	8.0	8.5	9.5	10.0	11.0
	250	6.0	6.0	5.5	6.5	6.5	6.5	7.5	7.5	7.5
	300	5.5	5.0	5.0	5.5	5.5	5.5	6.0	6.0	6.0
	350	5.0	5.0	5.0	5.0	5.0	5.0	5.5	5.5	5.0
	400	5.0	5.0	5.0	5.0	5.0	5.0	5.0	5.0	5.0

Table C-9. RCC Design Thicknesses for a 24 Kip Tandem Axle Load and k=400 psi/in.

	$\sigma_{allowable}$ (psi)	Positive Gradient 0%			Positive Gradient 25%			Positive Gradient 50%		
		Neg. Grad 0%	Neg. Grad 25%	Neg. Grad 50%	Neg. Grad 0%	Neg. Grad 25%	Neg. Grad 50%	Neg. Grad 0%	Neg. Grad 25%	Neg. Grad 50%
Lateral Load Reliability 75%	100	8.0	9.5	13.5	11.0	15.0+	15.0+	15.0+	15.0+	15.0+
	150	6.5	6.5	7.0	7.5	8.5	10.5	10.0	13.0	15.0+
	200	5.5	5.5	5.5	6.0	6.5	7.0	7.0	7.5	9.0
	250	5.0	5.0	5.0	5.0	5.0	5.5	5.5	6.0	6.5
	300	5.0	5.0	5.0	5.0	5.0	5.0	5.0	5.0	5.0
	350	5.0	5.0	5.0	5.0	5.0	5.0	5.0	5.0	5.0
Lateral Load Reliability 95%	100	9.0	10.5	14.5	12.5	15.0+	15.0+	15.0+	15.0+	15.0+
	150	7.0	7.0	7.5	8.0	9.0	11.0	10.5	14.0	15.0+
	200	5.5	6.0	6.0	6.5	6.5	7.0	7.5	8.0	9.5
	250	5.0	5.0	5.0	5.5	5.5	5.5	6.5	6.0	6.5
	300	5.0	5.0	5.0	5.0	5.0	5.0	5.0	5.5	5.5
	350	5.0	5.0	5.0	5.0	5.0	5.0	5.0	5.0	5.0
Lateral Load Reliability 99%	100	10.5	12.0	15.0+	15.0+	15.0+	15.0+	15.0+	15.0+	15.0+
	150	8.0	8.0	9.0	9.5	10.5	13.0	12.5	15.0+	15.0+
	200	6.5	6.5	6.5	7.5	7.5	8.0	8.5	9.0	10.5
	250	5.5	5.5	5.5	6.0	6.0	6.0	7.0	7.0	7.0
	300	5.0	5.0	5.0	5.5	5.5	5.0	6.0	6.0	6.0
	350	5.0	5.0	5.0	5.0	5.0	5.0	5.0	5.0	5.0

Table C-10. RCC Design Thicknesses for a 30 Kip Tandem Axle Load and k=100 psi/in.

	$\sigma_{allowable}$ (psi)	Positive Gradient 0%			Positive Gradient 25%			Positive Gradient 50%		
		Neg. Grad 0%	Neg. Grad 25%	Neg. Grad 50%	Neg. Grad 0%	Neg. Grad 25%	Neg. Grad 50%	Neg. Grad 0%	Neg. Grad 25%	Neg. Grad 50%
Lateral Load Reliability 75%	150	9.0	9.0	9.0	11.0	12.0	13.0	14.5	15.0+	15.0+
	200	7.0	7.0	7.0	8.5	8.5	8.5	10.5	10.5	11.5
	250	5.5	6.0	5.5	7.0	7.0	6.5	8.0	8.0	8.0
	300	5.0	5.0	5.0	6.0	6.0	5.5	6.5	6.5	6.0
	350	5.0	5.0	5.0	5.5	5.0	5.0	6.0	5.5	5.0
	400	5.0	5.0	5.0	5.0	5.0	5.0	5.0	5.0	5.0
Lateral Load Reliability 95%	150	10.0	10.0	10.0	12.5	13.0	14.0	15.0+	15.0+	15.0+
	200	8.0	8.0	7.5	9.0	9.0	9.0	11.0	11.5	12.0
	250	7.0	6.5	6.0	7.5	7.5	7.0	8.5	8.5	8.5
	300	6.0	5.5	5.5	6.5	6.0	6.0	7.0	7.0	7.0
	350	5.5	5.0	5.0	6.0	5.5	5.0	6.0	6.0	5.5
	400	5.0	5.0	5.0	5.0	5.0	5.0	5.5	5.5	5.0
Lateral Load Reliability 99%	200	9.5	9.5	9.0	11.0	11.0	10.5	13.0	13.0	13.5
	250	8.0	7.5	7.5	9.0	9.0	8.5	105.0	10.0	10.0
	300	7.0	6.5	6.0	7.5	7.5	7.0	8.5	8.5	8.0
	350	6.5	6.0	5.5	7.0	6.5	6.0	7.5	7.0	6.5
	400	6.0	5.5	5.0	6.0	6.0	5.5	6.5	6.0	6.0
	450	5.5	5.0	5.0	5.5	5.5	5.0	5.0	5.5	5.5

Table C-11. RCC Design Thicknesses for a 30 Kip Tandem Axle Load and k=250 psi/in.

	$\sigma_{allowable}$ (psi)	Positive Gradient 0%			Positive Gradient 25%			Positive Gradient 50%		
		Neg. Grad 0%	Neg. Grad 25%	Neg. Grad 50%	Neg. Grad 0%	Neg. Grad 25%	Neg. Grad 50%	Neg. Grad 0%	Neg. Grad 25%	Neg. Grad 50%
Lateral Load Reliability 75%	100	10.5	12.0	15.0+	15.0	15.0+	15.0+	15.0+	15.0+	15.0+
	150	8.0	8.0	8.5	9.5	10.5	13.0	12.5	15.0+	15.0+
	200	6.5	6.5	6.5	7.5	7.5	8.0	8.5	9.5	10.5
	250	5.5	5.5	5.5	6.0	6.0	6.0	7.0	7.0	7.0
	300	5.0	5.0	5.0	5.5	5.5	5.0	6.0	6.0	6.0
	350	5.0	5.0	5.0	5.0	5.0	5.0	5.0	5.0	5.0
Lateral Load Reliability 95%	150	8.5	9.0	9.0	10.5	11.5	13.5	14.0	15.0+	15.0+
	200	7.0	7.0	7.0	8.0	8.0	8.5	9.5	10.5	11.5
	250	6.0	6.0	6.0	6.5	6.5	6.5	7.5	7.5	8.0
	300	5.5	5.0	5.0	6.0	5.5	5.5	6.5	6.0	6.0
	350	5.0	5.0	5.0	5.0	5.0	5.0	5.5	5.5	5.5
	400	5.0	5.0	5.0	5.0	5.0	5.0	5.0	5.0	5.0
Lateral Load Reliability 99%	150	10.0	10.5	10.5	12.5	13.5	15.0+	15.0+	15.0+	15.0+
	200	8.0	8.0	8.0	9.5	9.5	10.0	11.5	12.0	13.0
	250	7.0	7.0	7.0	7.5	7.5	7.5	9.0	9.0	9.0
	300	6.0	6.0	6.0	6.5	6.5	6.0	7.5	7.0	7.0
	350	5.5	5.5	5.5	6.0	5.5	5.5	6.5	6.0	6.0
	400	5.0	5.0	5.0	5.5	5.0	5.0	6.0	5.5	5.0

Table C-12. RCC Design Thicknesses for a 30 Kip Tandem Axle Load and k=400 psi/in.

	$\sigma_{allowable}$ (psi)	Positive Gradient 0%			Positive Gradient 25%			Positive Gradient 50%		
		Neg. Grad 0%	Neg. Grad 25%	Neg. Grad 50%	Neg. Grad 0%	Neg. Grad 25%	Neg. Grad 50%	Neg. Grad 0%	Neg. Grad 25%	Neg. Grad 50%
Lateral Load Reliability 75%	100	9.5	11.0	15.0+	13.5	15.0+	15.0+	15.0+	15.0+	15.0+
	150	7.5	7.5	8.5	9.0	10.0	12.0	11.5	15.0+	15.0+
	200	6.0	6.5	6.5	7.0	7.0	7.5	8.0	9.0	10.5
	250	5.5	5.5	5.5	6.0	6.0	6.0	6.5	7.0	7.0
	300	5.0	5.0	5.0	5.0	5.0	5.0	6.0	6.0	6.0
	350	5.0	5.0	5.0	5.0	5.0	5.0	5.0	5.0	5.0
Lateral Load Reliability 95%	100	10.5	13.0	15.0+	15.0+	15.0+	15.0+	15.0+	15.0+	15.0+
	150	8.0	8.5	9.0	9.5	10.5	13.0	12.5	15.0+	15.0+
	200	6.5	6.5	7.0	7.5	7.5	8.0	9.0	9.5	11.0
	250	6.0	5.5	5.5	6.5	6.5	6.5	7.0	7.0	7.5
	300	5.0	5.0	5.0	5.5	5.5	5.5	6.0	6.0	6.0
	350	5.0	5.0	5.0	5.0	5.0	5.0	5.5	5.5	5.0
Lateral Load Reliability 99%	150	9.5	9.5	10.5	11.5	12.5	15.0+	15.0+	15.0+	15.0+
	200	7.5	7.5	7.5	8.5	9.0	9.0	10.5	11.0	12.5
	250	6.5	6.5	6.5	7.0	7.0	7.0	8.0	8.0	8.0
	300	6.0	5.5	5.5	6.5	6.5	6.0	7.0	7.0	6.5
	350	5.5	5.0	5.0	5.5	5.5	5.0	6.0	6.0	5.5
	400	5.0	5.0	5.0	5.0	5.0	5.0	5.5	5.5	5.0

Table C-13. RCC Design Thicknesses for a 36 Kip Tandem Axle Load and k=100 psi/in.

	$\sigma_{allowable}$ (psi)	Positive Gradient 0%			Positive Gradient 25%			Positive Gradient 50%		
		Neg. Grad 0%	Neg. Grad 25%	Neg. Grad 50%	Neg. Grad 0%	Neg. Grad 25%	Neg. Grad 50%	Neg. Grad 0%	Neg. Grad 25%	Neg. Grad 50%
Lateral Load Reliability 75%	150	10.0	10.0	10.0	12,5	13.0	14.0	15.0+	15.0+	15.0+
	200	8.0	7.5	7.5	9.0	9.0	9.0	11.0	11.5	12.0
	250	6.5	6.5	6.0	7.5	7.5	7.0	8.5	8.5	8.5
	300	6.0	5.5	5.0	6.5	6.0	6.0	7.0	7.0	6.5
	350	5.0	5.0	5.0	5.5	5.5	5.0	6.0	6.0	5.5
	400	5.0	5.0	5.0	5.0	5.0	5.0	5.5	5.0	5.0
Lateral Load Reliability 95%	200	8.5	8.5	8.0	10.0	10.0	10.0	12.5	12.5	13.0
	250	7.5	7.0	7.5	8.0	8.0	8.0	9.5	9.5	9.0
	300	6.5	6.0	6.5	7.0	7.0	6.5	8.0	7.5	7.5
	350	6.0	5.5	5.0	6.0	6.0	5.5	7.0	6.5	5.5
	400	5.0	5.0	5.0	5.5	5.5	5.0	6.0	5.5	5.0
	450	5.0	5.0	5.0	5.0	5.0	5.0	5.5	5.0	5.0
Lateral Load Reliability 99%	250	9.0	8.5	8.0	10.0	9.5	9.0	11.5	11.0	10.5
	300	7.5	7.5	7.0	8.5	8.0	7.5	9.5	9.0	8.5
	350	7.0	6.5	6.0	7.5	7.0	6.5	8.0	8.0	7.5
	400	6.0	6.0	5.5	6.5	6.0	6.0	7.0	7.0	6.5
	450	6.0	5.5	5.0	6.0	6.0	5.5	6.5	6.0	5.0
	500	5.5	5.0	5.0	5.5	5.5	5.0	5.0	5.5	5.5

Table C-14. RCC Design Thicknesses for a 36 Kip Tandem Axle Load and k=250 psi/in.

	$\sigma_{allowable}$ (psi)	Positive Gradient 0%			Positive Gradient 25%			Positive Gradient 50%		
		Neg. Grad 0%	Neg. Grad 25%	Neg. Grad 50%	Neg. Grad 0%	Neg. Grad 25%	Neg. Grad 50%	Neg. Grad 0%	Neg. Grad 25%	Neg. Grad 50%
Lateral Load Reliability 75%	150	8.5	8.5	9.5	10.5	11.0	13.5	14.0	15.0+	15.0+
	200	7.0	7.0	7.5	8.0	8.0	8.5	9.5	10.0	11.0
	250	6.0	6.0	6.0	6.5	6.5	6.5	7.5	7.5	8.0
	300	5.5	5.0	5.0	6.0	5.5	5.5	6.5	6.0	6.0
	350	5.0	5.0	5.0	5.0	5.0	5.0	5.5	5.5	5.5
	400	5.0	5.0	5.0	5.0	5.0	5.0	5.0	5.0	5.0
Lateral Load Reliability 95%	150	9.0	9.5	10.0	11.0	12.5	14.5	15.0	15.0+	15.0+
	200	7.5	7.5	7.5	8.5	9.0	9.0	10.5	11.0	12.5
	250	6.5	6.0	6.0	7.0	7.0	7.0	8.0	8.0	8.5
	300	5.5	5.5	5.5	6.0	6.0	6.0	7.0	6.5	6.5
	350	5.0	5.0	5.0	5.5	5.5	5.0	6.0	6.0	5.5
	400	5.0	5.0	5.0	5.0	5.0	5.0	5.5	5.5	5.0
Lateral Load Reliability 99%	200	9.0	9.0	9.0	10.5	10.5	10.5	12.5	13.0	14.0
	250	7.5	7.5	7.0	8.5	8.5	8.0	9.5	9.5	10.0
	300	6.5	6.5	6.0	7.0	7.0	6.5	8.0	8.0	7.6
	350	6.0	6.0	5.5	6.5	6.0	6.0	7.0	6.5	6.5
	400	5.5	5.5	5.0	6.0	5.5	5.5	6.0	6.0	5.5
	450	5.0	5.0	5.0	5.5	5.0	5.0	5.5	5.5	5.0

Table C-15. RCC Design Thicknesses for a 36 Kip Tandem Axle Load and k=400 psi/in.

	$\sigma_{allowable}$ (psi)	Positive Gradient 0%			Positive Gradient 25%			Positive Gradient 50%		
		Neg. Grad 0%	Neg. Grad 25%	Neg. Grad 50%	Neg. Grad 0%	Neg. Grad 25%	Neg. Grad 50%	Neg. Grad 0%	Neg. Grad 25%	Neg. Grad 50%
Lateral Load Reliability 75%	150	8.0	8.0	9.0	9.5	10.5	11.0	12.5	15.0+	15.0+
	200	6.5	7.0	7.0	7.5	7.5	8.0	9.0	9.5	11.0
	250	5.5	5.5	6.0	6.0	6.5	6.5	7.0	7.0	7.5
	300	5.0	5.0	5.0	5.5	5.5	5.5	6.0	6.0	6.0
	350	5.0	5.0	5.0	5.0	5.0	5.0	5.5	5.5	5.5
	400	5.0	5.0	5.0	5.0	5.0	5.0	5.0	5.0	5.0
Lateral Load Reliability 95%	150	8.5	9.0	9.5	10.5	11.5	14.0	14.0	15.0+	15.0+
	200	7.0	7.0	7.0	8.0	8.0	8.5	9.5	10.5	12.0
	250	6.0	6.0	6.0	7.0	7.0	7.0	7.5	7.5	8.0
	300	5.5	5.5	5.0	6.0	6.0	6.0	6.5	6.5	6.5
	350	5.0	5.0	5.0	5.5	5.0	5.0	6.0	5.5	5.5
	400	5.0	5.0	5.0	5.0	5.0	5.0	5.0	5.0	5.0
Lateral Load Reliability 99%	200	8.5	8.5	8.0	9.5	9.5	10.0	11.5	13.0	13.0
	250	7.0	7.0	7.0	8.0	8.0	7.5	9.0	9.0	9.0
	300	6.5	6.0	6.0	7.0	6.5	6.5	7.5	7.5	7.0
	350	6.0	5.5	5.0	6.0	6.0	5.5	6.5	6.5	6.0
	400	5.0	5.0	5.0	5.5	5.5	5.0	6.5	5.5	5.5
	450	5.0	5.0	5.0	5.0	5.0	5.0	5.0	5.0	5.0

APPENDIX D: RAW LOAD TRANSFER DATA

Table D-1. LTE Tests on Transverse Cracks (After Pittman [6]).

Location	Area	Date(s) Tested	Statistic	Temp. (°F)	LTE_δ (%)	Crack Spacing (ft.)	Crack Width (in.)
Austin, TX	Central Freight	Sep-91	Mean	111.7	85	31.9	0.021
			Std Dev	8.48	9	16.3	0.026
			COV	8%	11%	51%	126%
			# of Tests	75	76	76	5
			Maximum	126	93	84	0.068
			Minimum	101	35	7.3	0.003
			Range	25	58	76.7	0.065
	Tuscany Way	Sep-91	Mean	71	62	30.5	0.051
			Std Dev	0.31	15	11.1	0.064
			COV	0%	24%	36%	125%
			# of Tests	25	25	25	18
			Maximum	71	85	53	0.300
			Minimum	70	33	13.6	0.013
			Range	1	52	39.4	0.287
		Jan-92	Mean	60	55	30.5	0.059
			Std Dev	0	13	11.1	0.069
			COV	0%	24%	36%	117%
			# of Tests	24	24	25	18
			Maximum	60	83	53	0.320
			Minimum	60	32	13.6	0.013
			Range	0	51	39.4	0.307
Ft. Campbell, KY	63rd Chemical Company	Jan-91	Mean	43.5	24.3	79.6	0.244
			Std Dev	1.97	12.1	28.2	0.132
			COV	5%	50%	35%	54%
			# of Tests	78	78	78	78
			Maximum	46	83.5	155.6	0.550
			Minimum	40	13.1	24.7	0.010
			Range	6	70.4	110.9	0.540
		Aug-91	Mean	112	77	81.0	0.134
			Std Dev	--	9	28.3	0.096
			COV	--	11%	35%	72%
			# of Tests	86	86	86	86
			Maximum	127	89	135.6	0.425
			Minimum	96	22	24.7	0.008
			Range	31	67	110.9	0.418

Table D-1. LTE Tests on Transverse Cracks (After Pittman [6]) (cont'd).

Location	Area	Date(s) Tested	Statistic	Temp. (°F)	LTE_δ (%)	Crack Spacing (ft.)	Crack Width (in.)
Ft. Drum, NY	PN69A Site 1	Aug-91	Mean	104	78	44.1	0.051
			Std Dev	--	17	26.0	0.035
			COV	--	22%	59%	69%
			# of Tests	40	42	41	24
			Maximum	116	93	106.3	0.175
			Minimum	98	11	8.4	0.001
			Range	18	82	97.9	0.174
	PN69A Site 2	Aug-91	Mean	71	40.4	29.6	0.067
			Std Dev	--	19.8	21.7	0.028
			COV	--	49%	73%	41%
			# of Tests	24	25	25	18
			Maximum	74	88.1	86.55	0.110
			Minimum	65	9.3	8.4	0.018
			Range	9	78.8	78.15	0.093
	PN69B	Aug-91	Mean	93	78	31.8	0.043
			Std Dev	--	14	12.9	0.036
			COV	--	18%	41%	82%
			# of Tests	95	95	95	52
			Maximum	112	91	76.3	0.150
			Minimum	79	25	13.2	0.008
			Range	33	66	63.1	0.1425
	PN187	Apr-90	Mean	65.6	88	--	--
			Std Dev	4.13	6	--	--
			COV	6%	7%	--	--
			# of Tests	16	16	--	--
			Maximum	72	96.2	--	--
			Minimum	61	70.2	--	--
			Range	11	26	--	--
		Aug-91	Mean	87	83	34.34	0.024
			Std Dev	--	9	14.58	0.017
			COV	--	11%	42%	68%
			# of Tests	15	15	15	12
			Maximum	91	90	58.85	0.055
			Minimum	81	62	16.00	0.008
			Range	10	28	42.85	0.0475

Table D-1. LTE Tests on Transverse Cracks (After Pittman [6]) (cont'd).

Location	Area	Date(s) Tested	Statistic	Temp. (°F)	LTE_δ (%)	Crack Spacing (ft.)	Crack Width (in.)
Ft. Drum, NY cont'd	PN203	Aug-91	Mean	91	80	29.8	0.010
			Std Dev	0	0	0.0	0.000
			COV	0%	0%	0%	0%
			# of Tests	1	1	1	1
			Maximum	91	80	29.8	0.010
			Minimum	91	80	29.8	0.010
			Range	0	0	0	0
Ft. Hood, TX	Bldg. 26027	Mar-85	Mean	60	64	51.5	--
			Std Dev	0	14	17.8	--
			COV	0%	22%	35%	--
			# of Tests	129	129	129	--
			Maximum	60	88	89.6	--
			Minimum	60	18	10.5	--
			Range	0	70	79.1	--
		Feb-90	Mean	61.8	30		--
			Std Dev	2.02	18		--
			COV	3%	60%	#DIV/0!	--
			# of Tests	27	27	129	--
			Maximum	64	73	67	--
			Minimum	60	1	13.2	--
			Range	4	72	53.8	--
		Aug-91	Mean	95.21	86	28.20	0.107
			Std Dev	0.78	7	12.90	0.105
			COV	--	8%	46%	99%
			# of Tests	42	45	45	45
			Maximum	98	97	57.45	0.375
			Minimum	95	53	5.25	0.005
			Range	3	44	52.20	0.37
	Bldg. 38033	Feb-90	Mean	75	88	27.60	--
			Std Dev	0	9	9.70	--
			COV	0%	10%	35%	--
			# of Tests	30	30	30	--
			Maximum	75	99	51.00	--
			Minimum	75	48	14.80	--
			Range	0	51	36.20	--

Table D-1. LTE Tests on Transverse Cracks (After Pittman [6]) (cont'd).

Location	Area	Date(s) Tested	Statistic	Temp. (°F)	LTE_δ (%)	Crack Spacing (ft.)	Crack Width (in.)
Ft. Hood, TX cont'd	Bldg. 38033 cont'd	Sep-91	Mean	113.12	86	26.50	0.055
			Std Dev	3.028	4	9.10	0.028
			COV	3%	5%	34%	51%
			# of Tests	50	51	51	51
			Maximum	116	93	54.50	0.125
			Minimum	110	75	14.80	0.005
			Range	6	18	39.70	0.12
	Bldg. 3850	Feb-90	Mean	63	32	25.30	--
			Std Dev	0	18	6.90	--
			COV	0%	56%	27%	--
			# of Tests	42	42	42	--
			Maximum	63	84	41.30	--
			Minimum	63	14	15.40	--
			Range	0	70	25.90	--
		Sep-91	Mean	85.95	54	23.90	0.064
			Std Dev	5.7	21	15.10	0.042
			COV	7%	39%	63%	66%
			# of Tests	64	66	66	66
			Maximum	96	92	103.40	0.175
			Minimum	84	12.8	7.45	0.003
			Range	12	79.2	95.95	0.1725
	Wash Rack	Feb-90	Mean	67	63	--	--
			Std Dev	0	21	--	--
			COV	0%	33%	--	--
			# of Tests	11	11	--	--
			Maximum	67	92	--	--
			Minimum	67	36	--	--
			Range	0	56	--	--
		Sep-91	Mean	88.5	40	40.50	0.094
			Std Dev	1.12	9	20.20	0.080
			COV	1%	23%	50%	84%
			# of Tests	13	13	13	13
			Maximum	89	65	79.05	0.275
			Minimum	86	28	15.40	0.020
			Range	3	37	63.65	0.255

Table D-1. LTE Tests on Transverse Cracks (After Pittman [6]) (cont'd).

Location	Area	Date(s) Tested	Statistic	Temp. (°F)	LTE_δ (%)	Crack Spacing (ft.)	Crack Width (in.)
Ft. Hood, TX cont'd	Tank Trail	Feb-90	Mean	67	95	--	--
			Std Dev	0	4	--	--
			COV	0%	4%	--	--
			# of Tests	11	11	--	--
			Maximum	67	100	--	--
			Minimum	67	85	--	--
			Range	0	15	--	--
		Sep-91	Mean	101	93	32.20	0.073
			Std Dev	0	4	11.60	0.053
			COV	0%	4%	36%	73%
			# of Tests	20	20	20	19
			Maximum	101	99	63.50	0.175
			Minimum	101	85	9.70	0.018
			Range	0	14	53.80	0.1575
Spring Hill, TN (Saturn Plant)	Zenith Road	Jan-91	Mean	55	88	15.2	0.005
			Std Dev	0	0	0.0	0.000
			COV	0%	0%	0%	0%
			# of Tests	1	1	1	1
			Maximum	55	88	15.15	0.005
			Minimum	55	88	15.15	0.005
			Range	0	0	0	0.000

Table D-2. LTE Tests on Transverse Joints (after Wu and Todres [39]).

Slab No.	Joint Spacing (ft.)	Average RCC Thickness (in.)	1992			1993		
			Load (lb)	LTE_δ (%)	Average LTE_δ (%)	Load (lb)	LTE_δ (%)	Average LTE_δ (%)
1	14.8	6.5	6328	80	82	6598	82	83
			9405	82		9556	83	
			12760	82		12673	84	
	14.8	6.5	6225	78	79	6305	77	78
			9215	79		9199	78	
			12292	80		12300	79	
	14.8	6.5	6098	77	78	6384	80	80
			9271	78		9405	80	
			12284	79		12490	80	
2	14.8	6.5	7066	61	60	6550	54	57
			9770	60		9493	58	
			12554	60		12490	60	
	14.8	6.5	6891	70	68	6320	67	65
			9461	66		9247	65	
			12014	67		12379	64	
	14.8	6.5	6035	51	55	6431	73	72
			9175	55		9461	72	
			12054	59		12570	71	
3	14.8	6.5	6217	77	77	6614	88	87
			9358	77		9540	87	
			12379	77		12609	87	
	14.8	6.5	6788	81	79	6416	76	76
			9223	79		9382	76	
			12102	79		12546	77	
	14.8	6.5	6495	79	80	6416	79	79
			9413	80		9382	80	
			12411	80		12546	80	
4	14.8	6.5	6273	79	79	6558	79	80
			9326	79		9540	80	
			12371	80		12665	80	
	14.8	6.5	6201	82	81	6313	72	73
			9167	80		9286	73	
			12213	82		12387	74	
	14.8	6.5	6424	83	83	6313	79	79
			9382	84		9318	79	
			12347	83		12482	79	

Table D-2. LTE Tests on Transverse Joints (after Wu and Todres [39]) (cont'd).

Slab No.	Joint Spacing (ft.)	Average RCC Thickness (in.)	1992			1993		
			Load (lb)	LTE_δ (%)	Average LTE_δ (%)	Load (lb)	LTE_δ (%)	Average LTE_δ (%)
5	21.3	6.7	6320	73	75	6297	74	75
			9255	76		9215	75	
			12276	76		12157	76	
	21.3	6.7	6201	73	73	6257	69	70
			9167	73		9318	70	
			12229	73		12411	71	
	21.3	6.7	6384	75	75	6352	77	76
			9342	74		9382	76	
			12355	75		12514	76	
6	21.3	8.5	6368	61	65	6297	41	46
			9223	65		9358	46	
			12173	67		12316	50	
	21.3	8.5	6114	50	52	6217	41	46
			9025	52		9207	47	
			12086	54		12419	51	
	21.3	8.5	6305	42	45	6471	78	78
			9302	45		9445	78	
			12268	48		12657	79	
7	21.3	8.5	7082	42	48	6313	66	67
			9873	49		9389	67	
			12149	53		12213	68	
	21.3	8.5	6241	70	69	6424	64	66
			9136	68		9405	67	
			12189	69		12538	68	
	21.3	8.5	6416	54	56	6225	63	62
			9397	56		9239	62	
			12308	58		12363	61	
8	32.8	8.3	6360	55	56	6297	72	71
			9239	56		9294	70	
			12181	56		12244	69	
	32.8	8.3	6209	65	63	6273	64	63
			9120	62		9255	64	
			12141	61		12292	63	
	32.8	8.3	6907	68	66	5932	38	42
			9516	66		9001	42	
			12268	65		12205	45	

Table D-2. LTE Tests on Transverse Joints (after Wu and Todres [39]) (cont'd).

Slab No.	Joint Spacing (ft.)	Average RCC Thickness (in.)	1992			1993		
			Load (lb)	LTE_δ (%)	Average LTE_δ (%)	Load (lb)	LTE_δ (%)	Average LTE_δ (%)
9	32.8	8.3	6701	60	65	6233	74	74
			9635	66		9302	74	
			12078	68		12316	74	
	32.8	8.3	6257	74	74	6233	71	72
			9239	75		9120	72	
			12260	74		12197	73	
	32.8	8.3	6495	74	74	6249	39	42
			9429	75		9199	42	
			12387	73		12292	45	
10	32.8	8.1	6487	54	56	6225	75	75
			9175	57		9318	76	
			11967	59		12141	75	
	32.8	8.1	6209	67	67	6217	60	60
			9072	68		9271	60	
			12062	67		12332	61	
	32.8	8.1	6463	72	72	6344	67	68
			9421	73		9358	68	
			12340	73		12482	68	
11	49.2	8.0	6558	68	70	6162	56	59
			9080	70		9199	59	
			11800	71		12070	61	
	49.2	8.0	6067	59	60	6114	23	28
			9001	60		8977	28	
			11935	60		12062	32	
	49.2	8.0	6463	62	62	6336	61	63
			9421	62		9255	64	
			12347	62		12419	65	
12	49.2	7.5	6186	60	64	6368	62	63
			9207	65		9374	63	
			12022	67		12316	64	
	49.2	7.5	6257	66	67	6114	51	52
			9080	67		9152	52	
			12070	68		12276	53	
	49.2	7.5	6408	68	70	6328	64	66
			9326	71		9239	67	
			12292	71		12379	67	

Table D-2. LTE Tests on Transverse Joints (after Wu and Todres [39]) (cont'd).

Slab No.	Joint Spacing (ft.)	Average RCC Thickness (in.)	1992			1993		
			Load (lb)	LTE_δ (%)	Average LTE_δ (%)	Load (lb)	LTE_δ (%)	Average LTE_δ (%)
13	49.2	7.5	6075	84	85	6408	77	79
			9183	84		9397	80	
			12260	85		12435	81	
	49.2	7.5	6090	82	83	6328	79	81
			9056	83		9231	81	
			12086	84		12363	82	
	49.2	7.5	6376	81	82	6336	66	67
			9302	84		9302	67	
			12260	82		12490	68	
				AVERAGE	69.1		AVERAGE	67.2
				COV	15.2%		COV	19.4%

APPENDIX E: GUIDE FOR LIMITING SUBGRADE STRESS

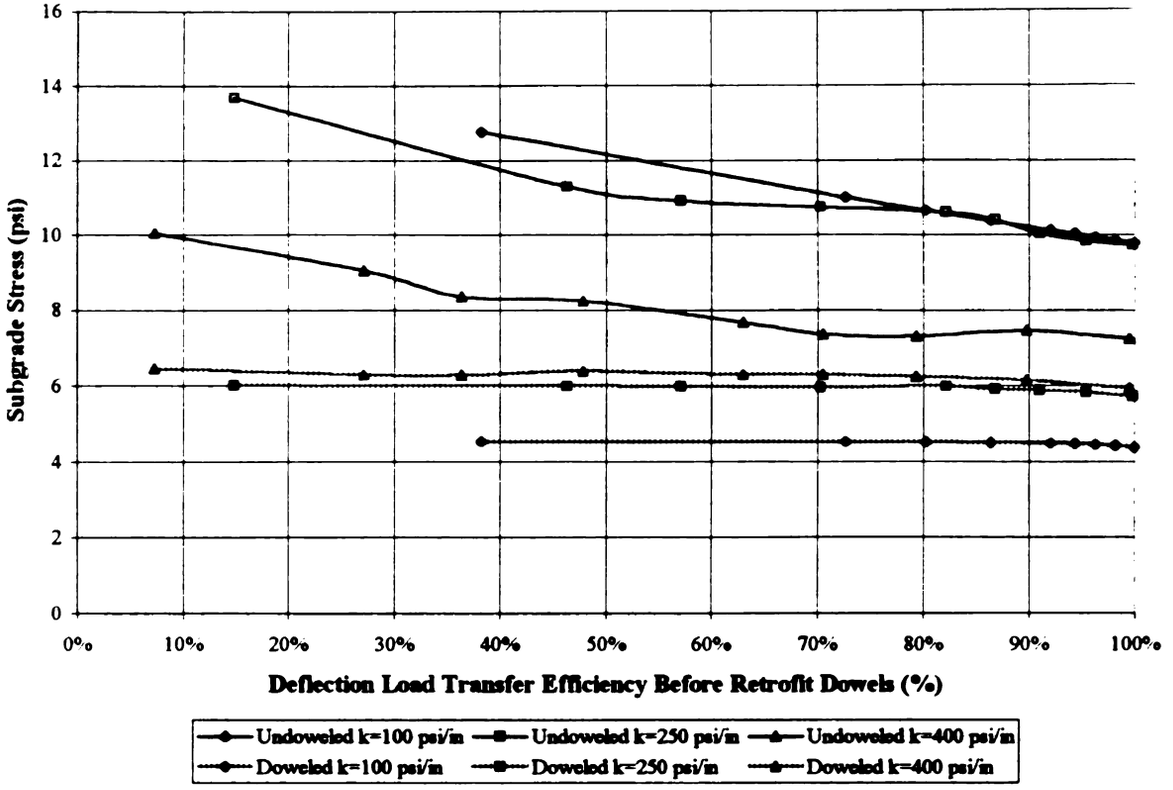

Figure E-1. Subgrade Stresses for a 12 kip (53.4 kN) Dual-Tired Single Axle on a 6" (152 mm) RCC Pavement Before and After Retrofit Dowels.

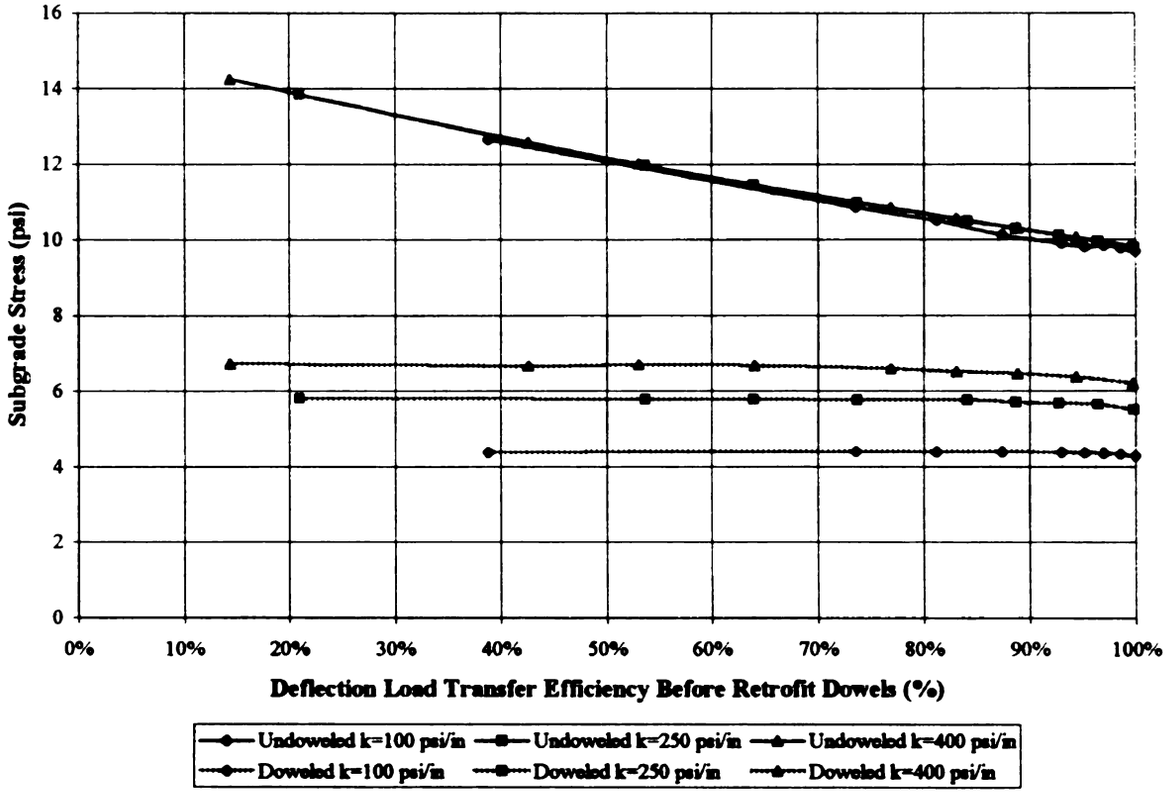

Figure E-2. Subgrade Stresses for a 12 kip (53.4 kN) Dual-Tired Single Axle on an 8" (203 mm) RCC Pavement Before and After Retrofit Dowels.

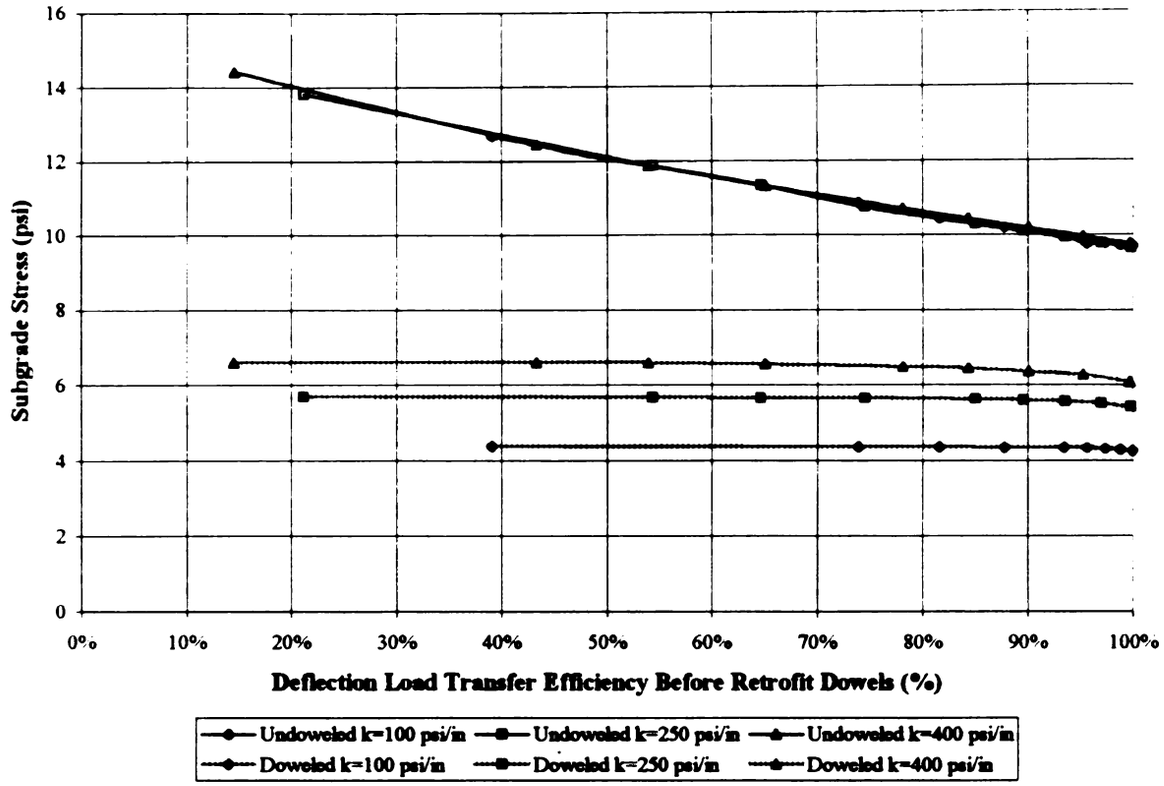

Figure E-3. Subgrade Stresses for a 12 kip (53.4 kN) Dual-Tired Single Axle on a 10" (254 mm) RCC Pavement Before and After Retrofit Dowels.

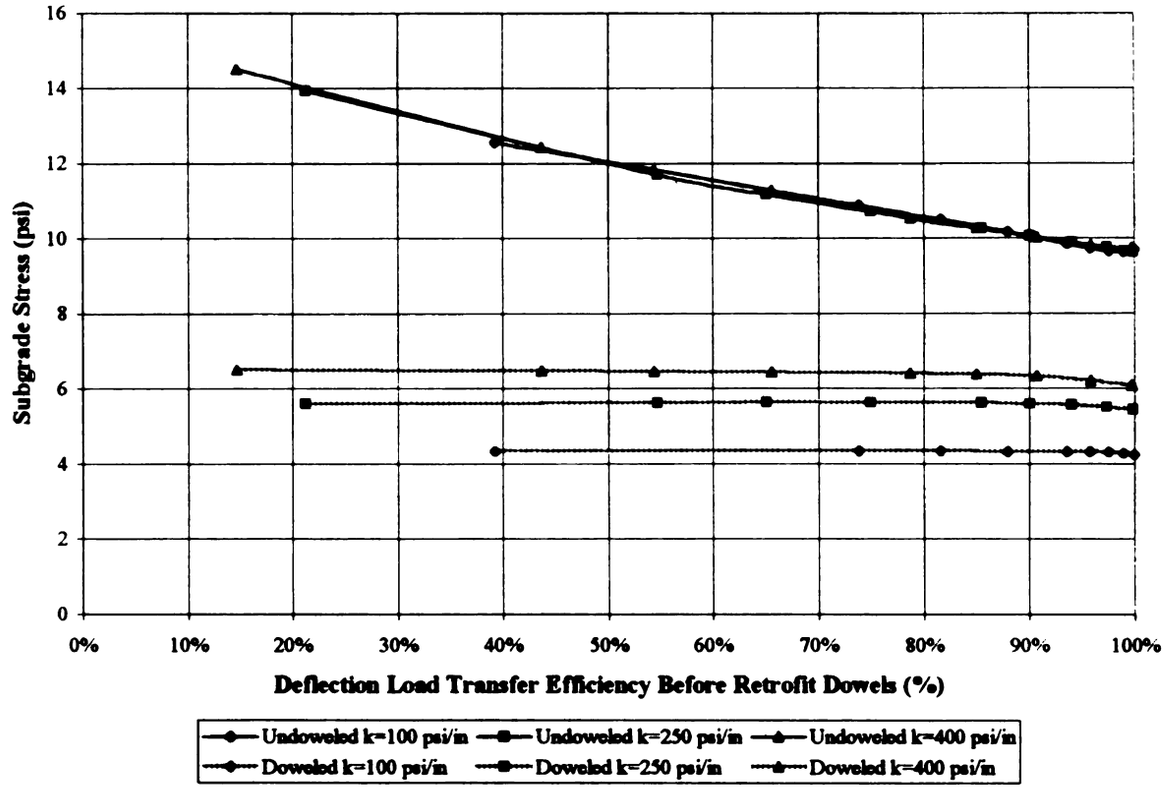

Figure E-4. Subgrade Stresses for a 12 kip (53.4 kN) Dual-Tired Single Axle on a 12" (305 mm) RCC Pavement Before and After Retrofit Dowels.

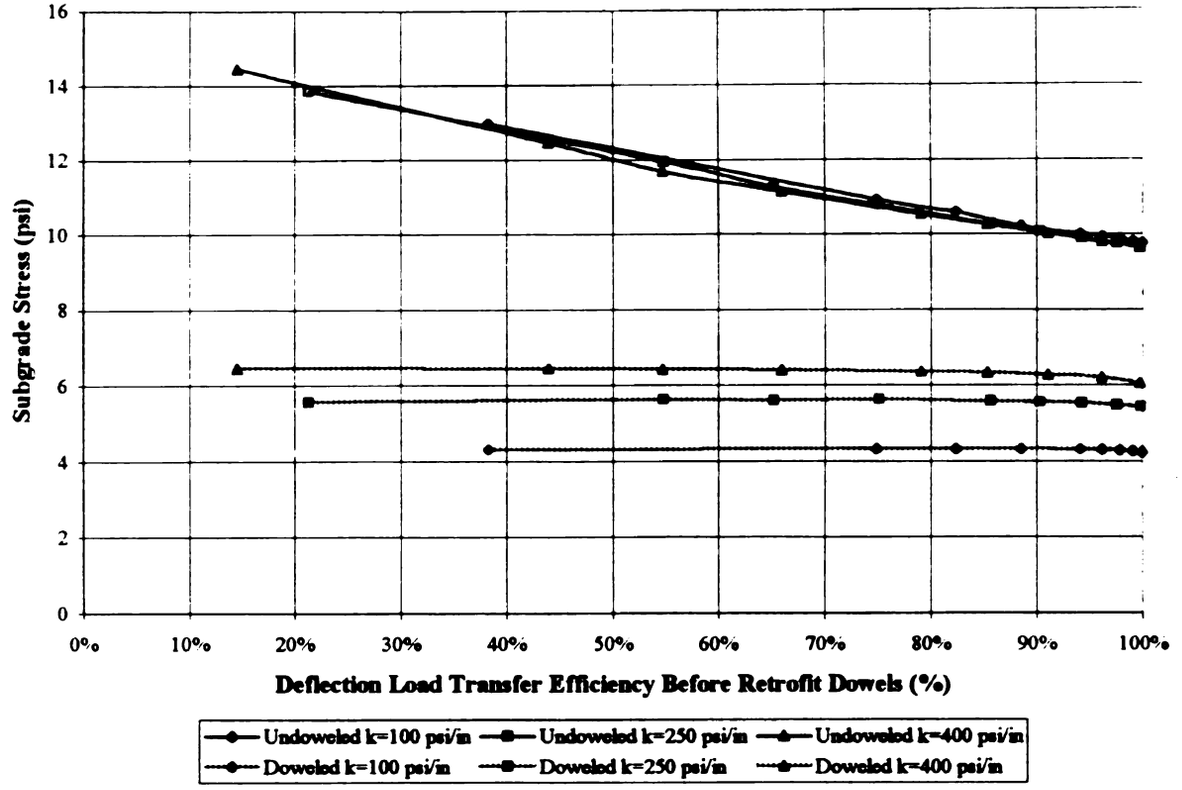

Figure E-5. Subgrade Stresses for a 12 kip (53.4 kN) Dual-Tired Single Axle on a 14" (356 mm) RCC Pavement Before and After Retrofit Dowels.

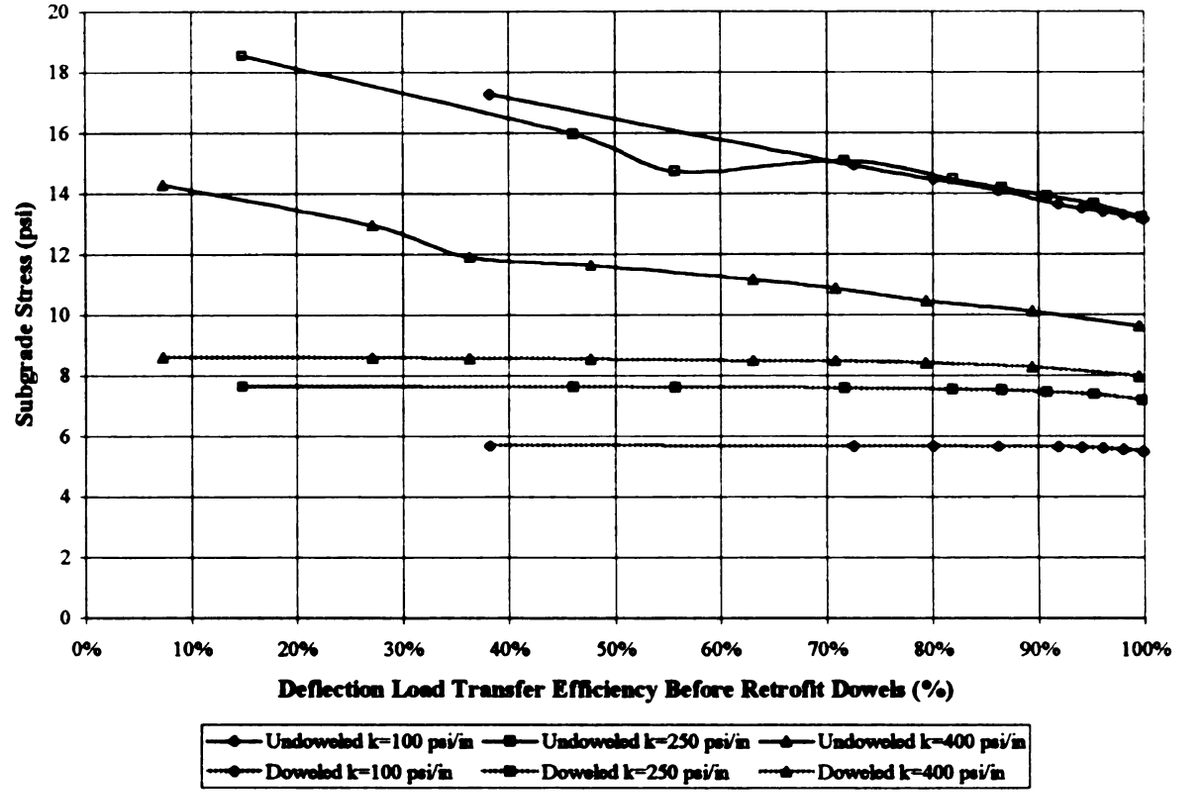

Figure E-6. Subgrade Stresses for a 18 kip (80.1 kN) Dual-Tired Single Axle on a 6" (152 mm) RCC Pavement Before and After Retrofit Dowels.

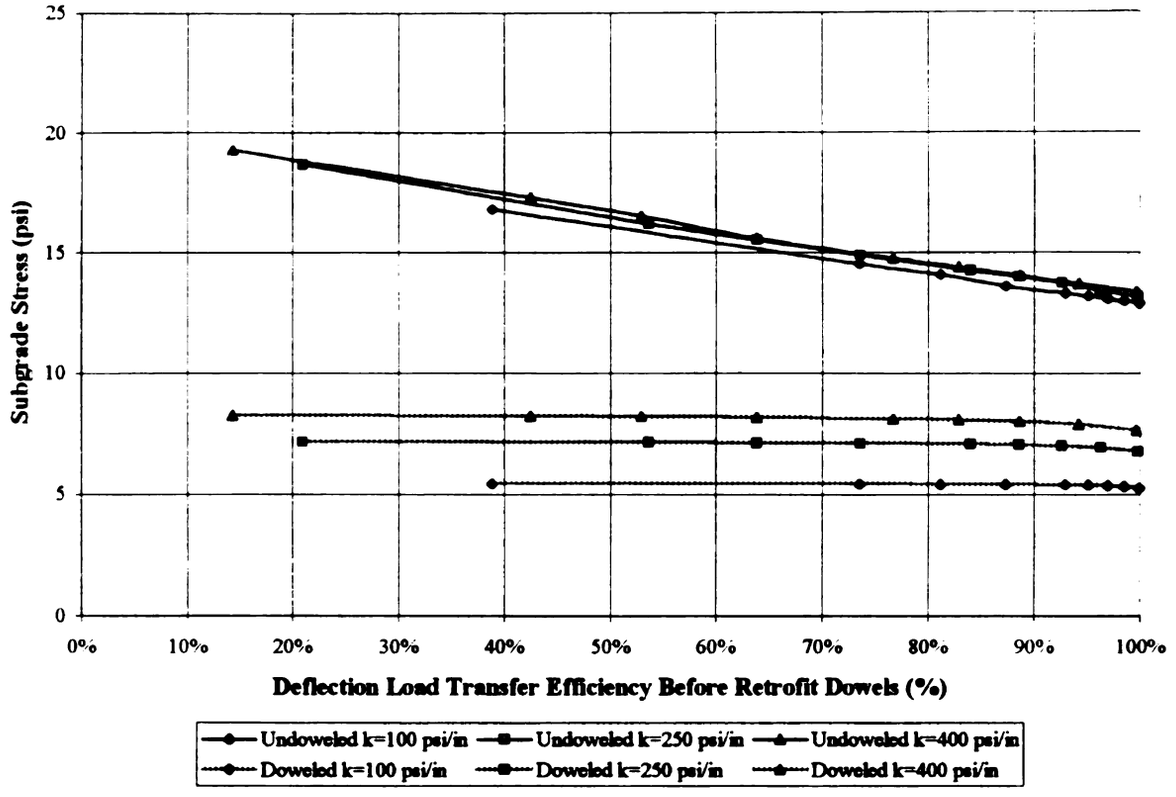

Figure E-7. Subgrade Stresses for a 18 kip (80.1 kN) Dual-Tired Single Axle on an 8" (203 mm) RCC Pavement Before and After Retrofit Dowels.

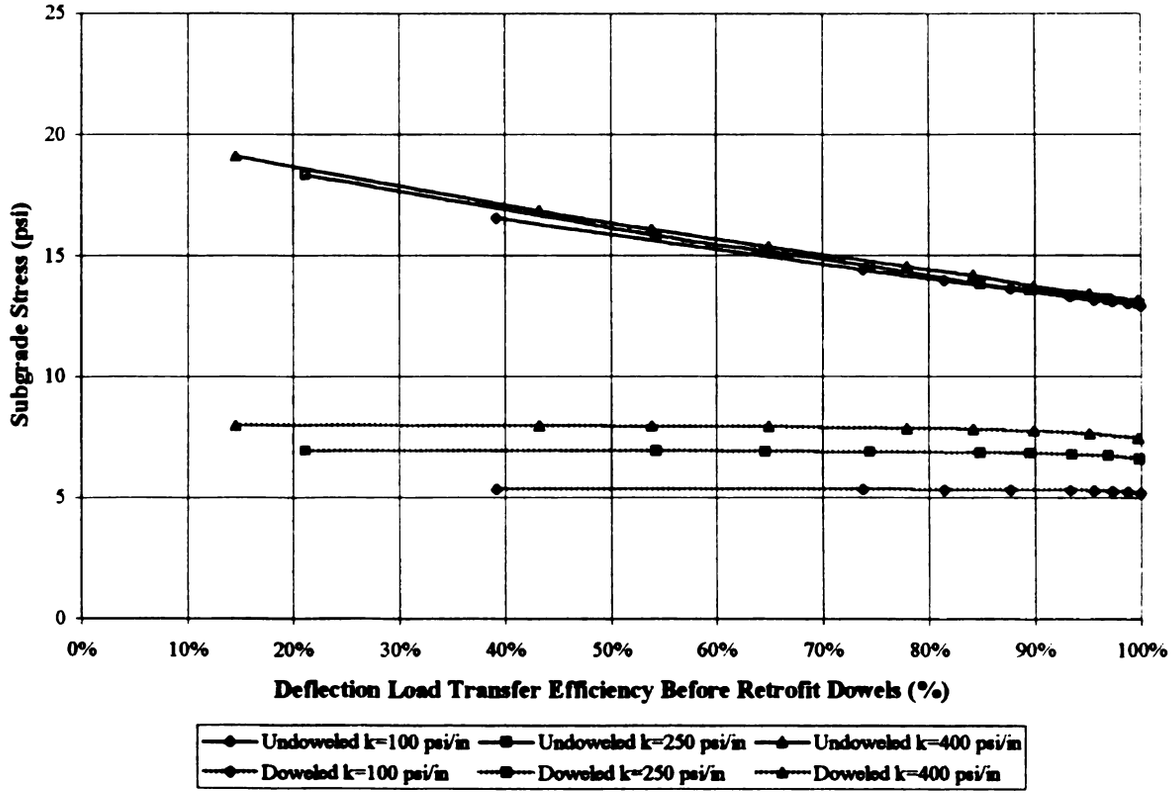

Figure E-8. Subgrade Stresses for a 18 kip (80.1 kN) Dual-Tired Single Axle on a 10" (254 mm) RCC Pavement Before and After Retrofit Dowels.

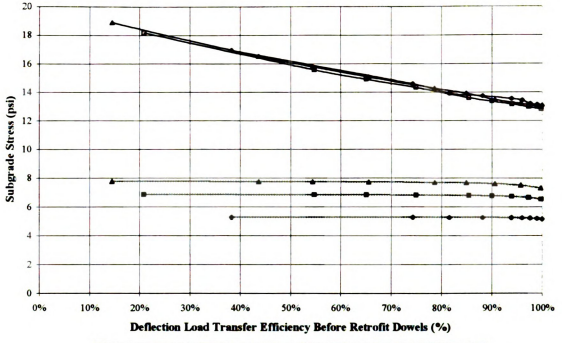

Figure E-9. Subgrade Stresses for a 18 kip (80.1 kN) Dual-Tired Single Axle on a 12" (305 mm) RCC Pavement Before and After Retrofit Dowels.

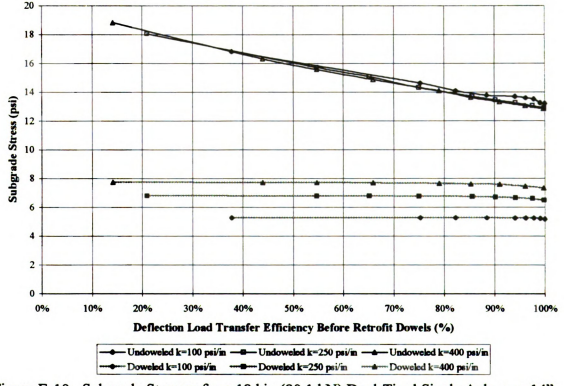

Figure E-10. Subgrade Stresses for a 18 kip (80.1 kN) Dual-Tired Single Axle on a 14" (356 mm) RCC Pavement Before and After Retrofit Dowels.

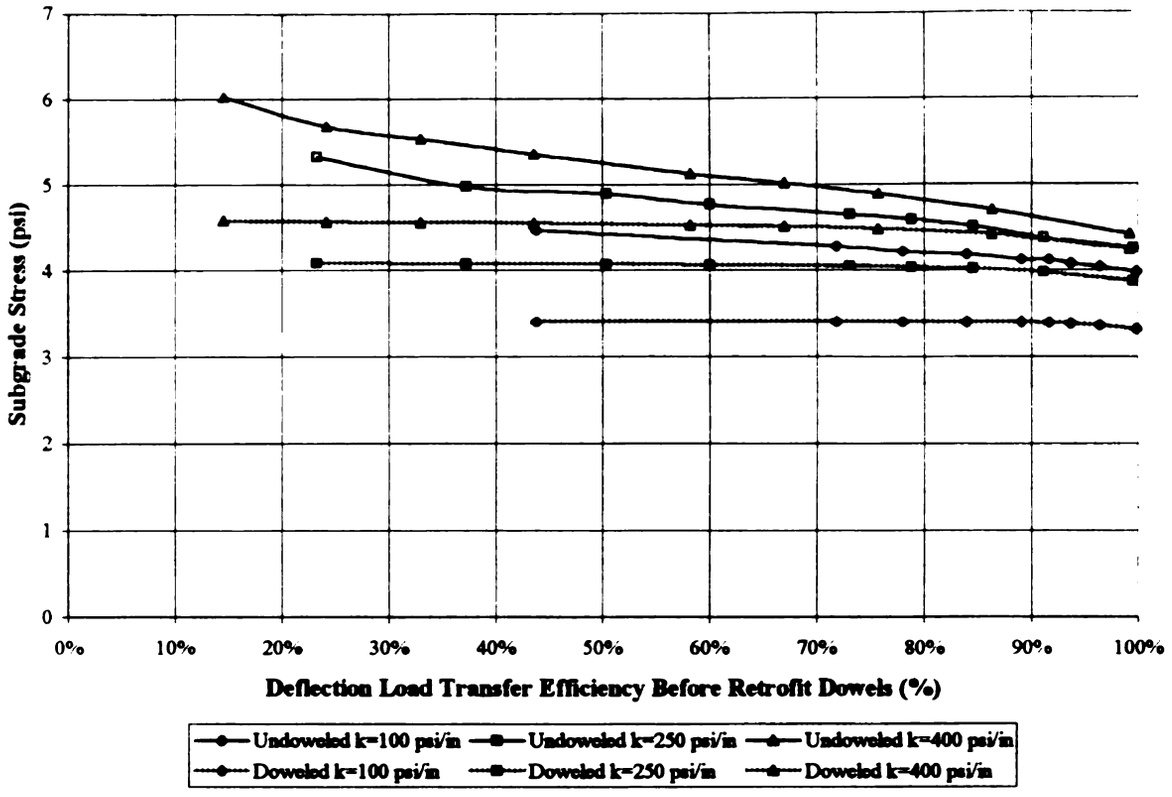

Figure E-11. Subgrade Stresses for a 24 kip (106.8 kN) Dual-Tired Tandem Axle on a 6" (152 mm) RCC Pavement Before and After Retrofit Dowels.

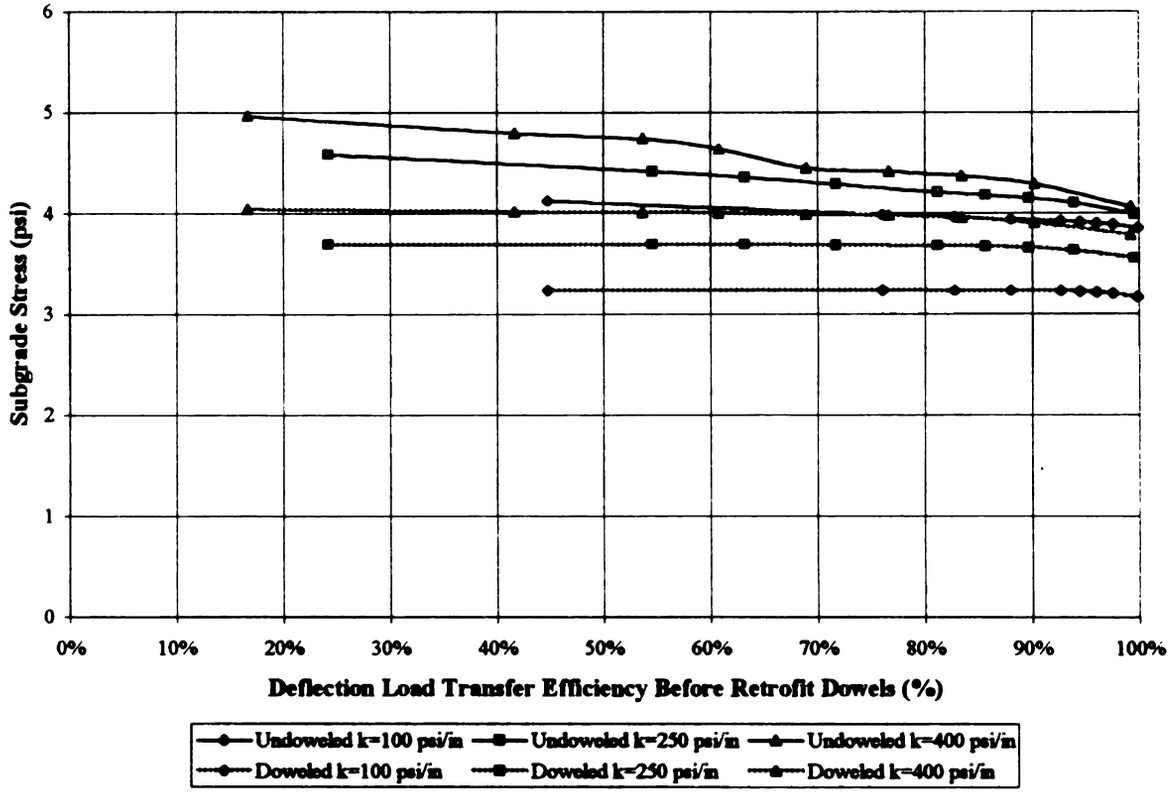

Figure E-12. Subgrade Stresses for a 24 kip (106.8 kN) Dual-Tired Tandem Axle on an 8" (203 mm) RCC Pavement Before and After Retrofit Dowels.

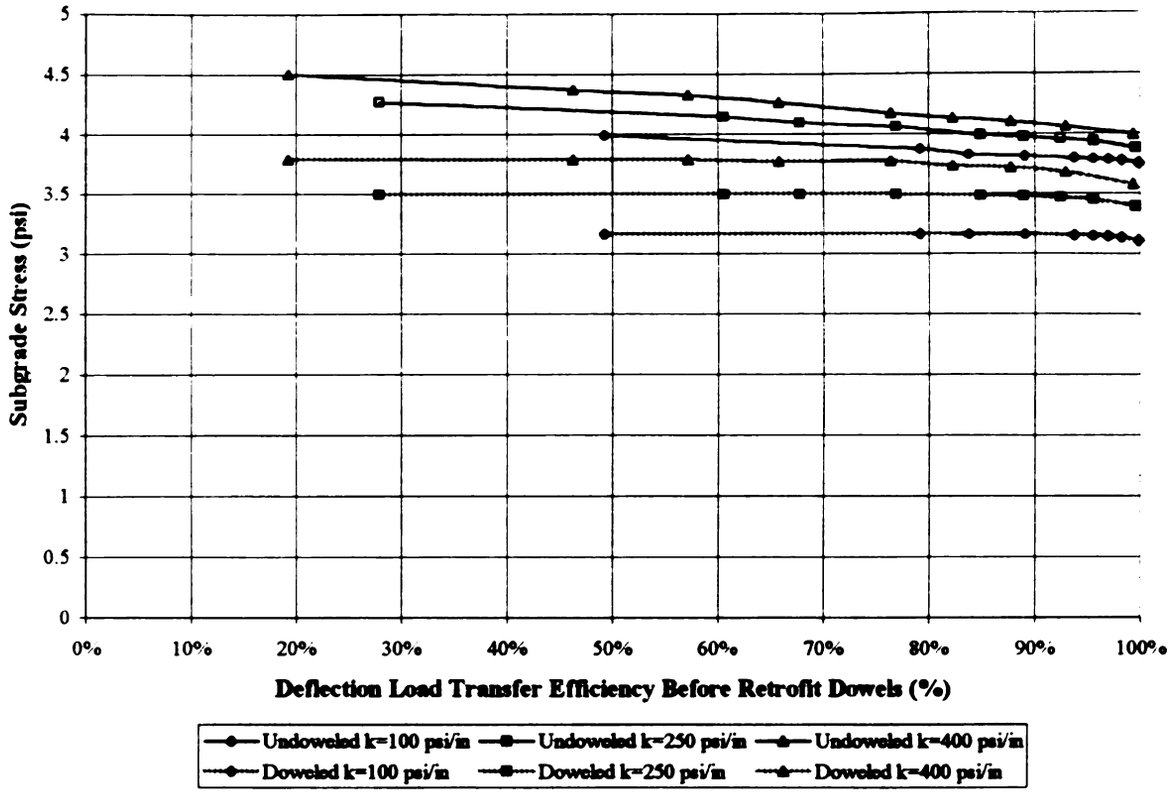

Figure E-13. Subgrade Stresses for a 24 kip (106.8 kN) Dual-Tired Tandem Axle on a 10" (254 mm) RCC Pavement Before and After Retrofit Dowels.

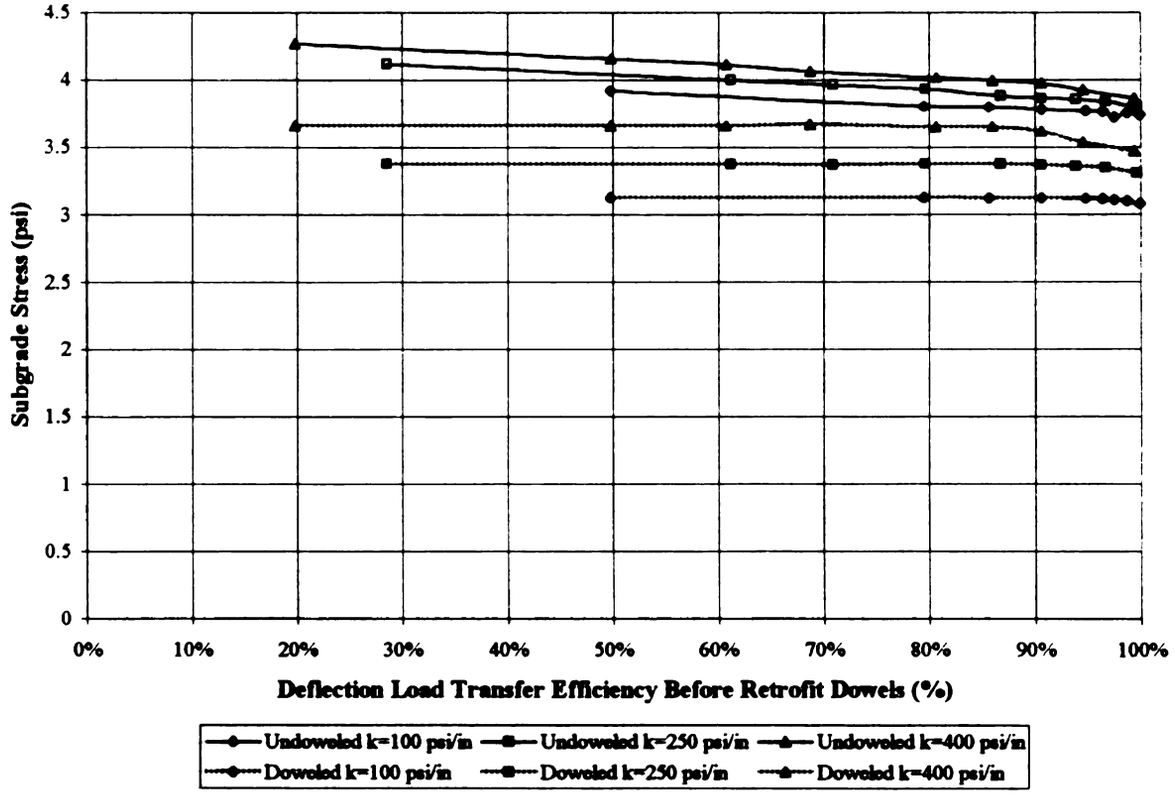

Figure E-14. Subgrade Stresses for a 24 kip (106.8 kN) Dual-Tired Tandem Axle on a 12" (305 mm) RCC Pavement Before and After Retrofit Dowels.

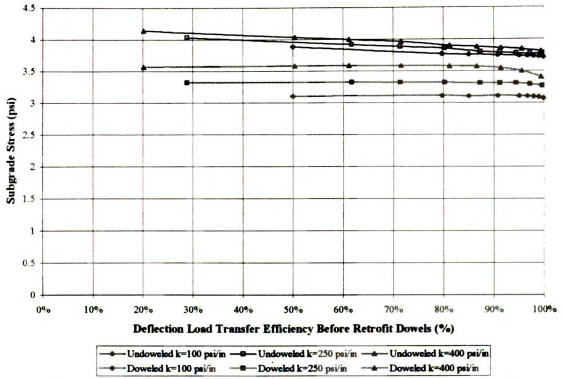

Figure E-15. Subgrade Stresses for a 24 kip (106.8 kN) Dual-Tired Tandem Axle on a 14" (356 mm) RCC Pavement Before and After Retrofit Dowels.

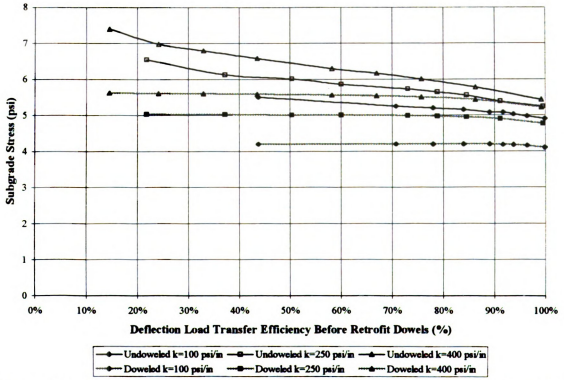

Figure E-16. Subgrade Stresses for a 30 kip (133.4 kN) Dual-Tired Tandem Axle on a 6" (152 mm) RCC Pavement Before and After Retrofit Dowels.

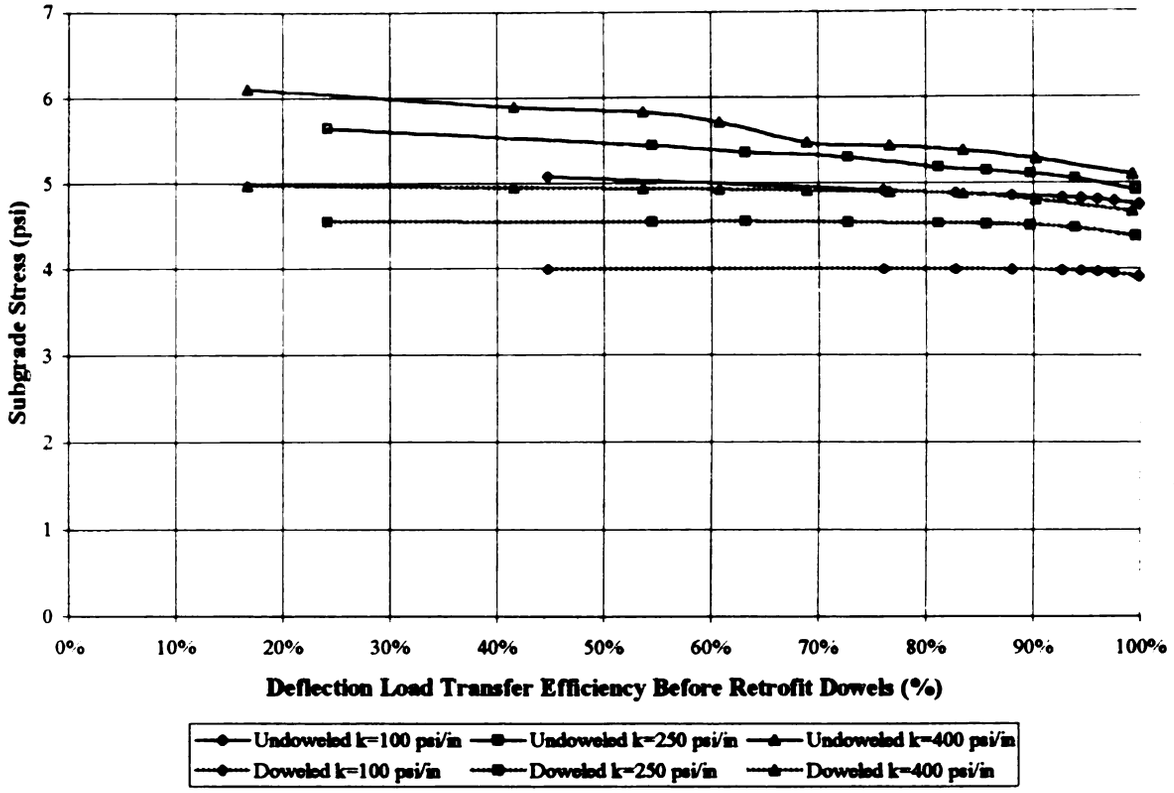

Figure E-17. Subgrade Stresses for a 30 kip (133.4 kN) Dual-Tired Tandem Axle on an 8" (203 mm) RCC Pavement Before and After Retrofit Dowels.

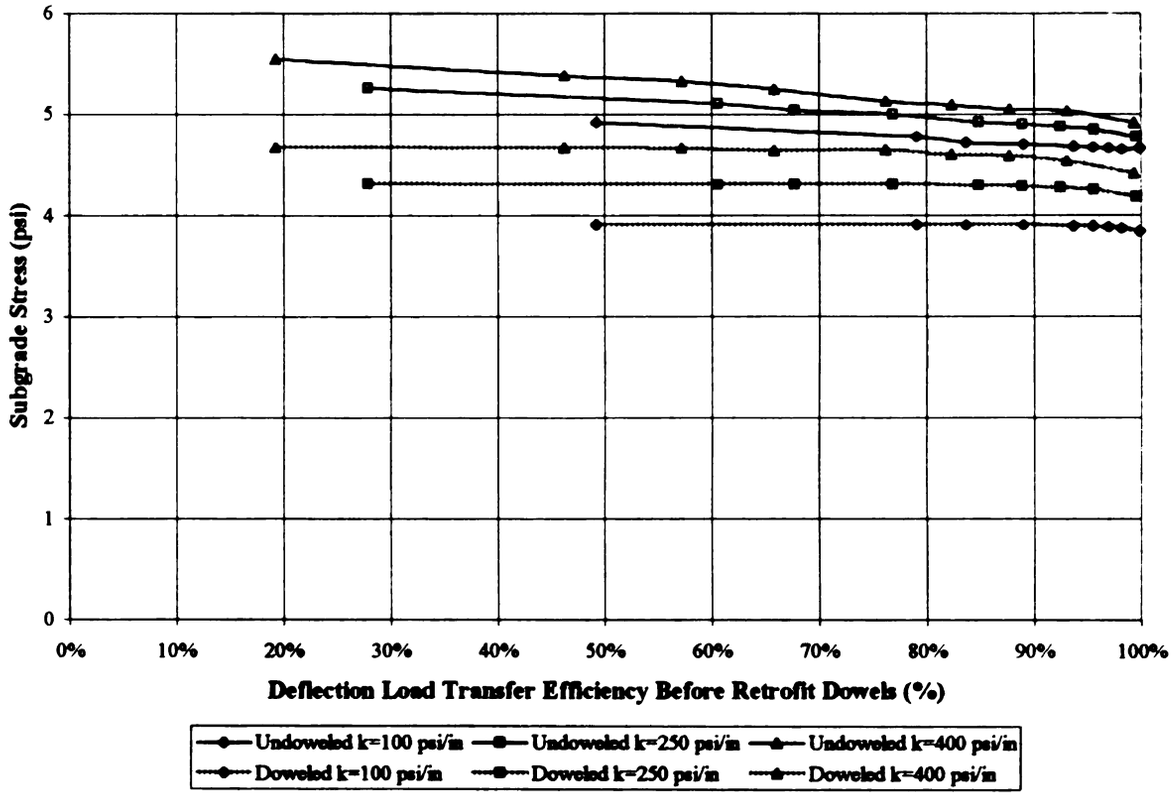

Figure E-18. Subgrade Stresses for a 30 kip (133.4 kN) Dual-Tired Tandem Axle on a 10" (254 mm) RCC Pavement Before and After Retrofit Dowels.

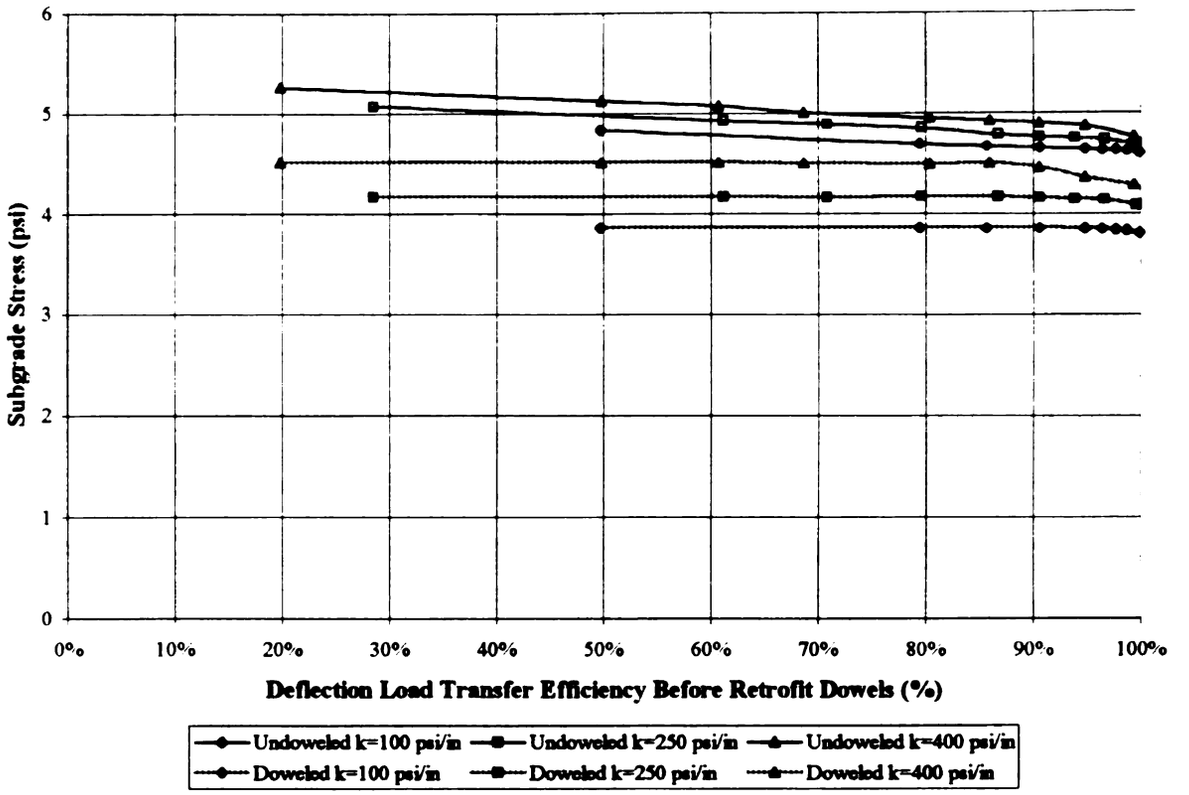

Figure E-19. Subgrade Stresses for a 30 kip (133.4 kN) Dual-Tired Tandem Axle on a 12" (305 mm) RCC Pavement Before and After Retrofit Dowels.

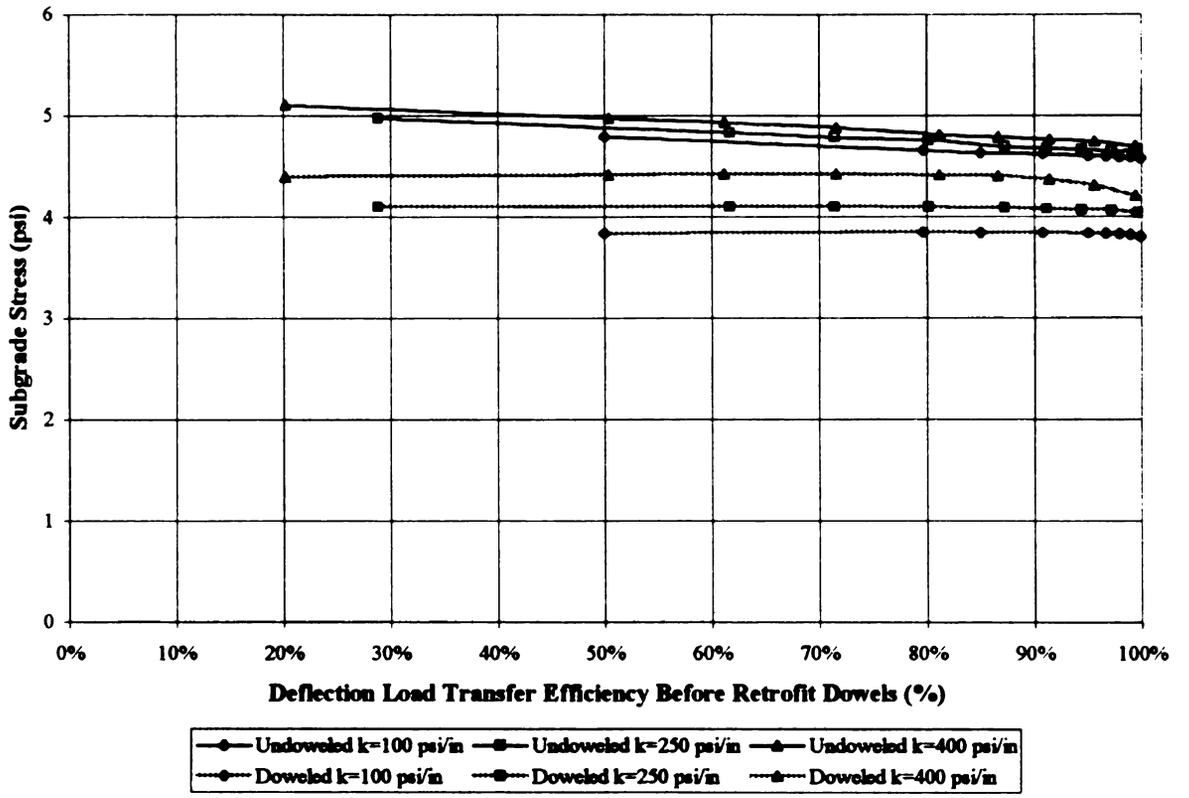

Figure E-20. Subgrade Stresses for a 30 kip (133.4 kN) Dual-Tired Tandem Axle on a 14" (356 mm) RCC Pavement Before and After Retrofit Dowels.

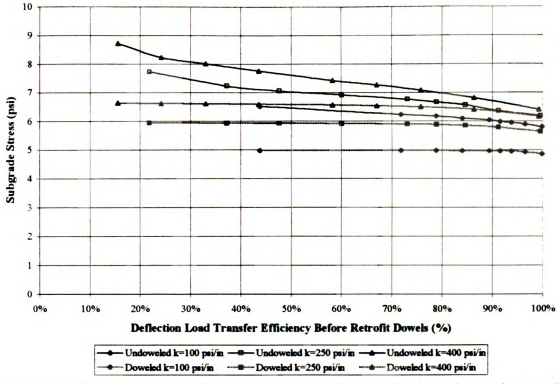

Figure E-21. Subgrade Stresses for a 36 kip (160.1 kN) Dual-Tired Tandem Axle on a 6" (152 mm) RCC Pavement Before and After Retrofit Dowels.

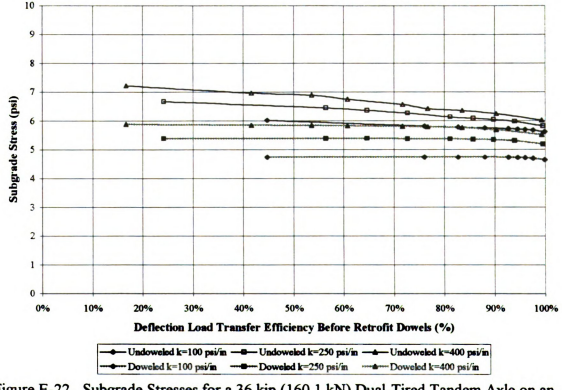

Figure E-22. Subgrade Stresses for a 36 kip (160.1 kN) Dual-Tired Tandem Axle on an 8" (203 mm) RCC Pavement Before and After Retrofit Dowels.

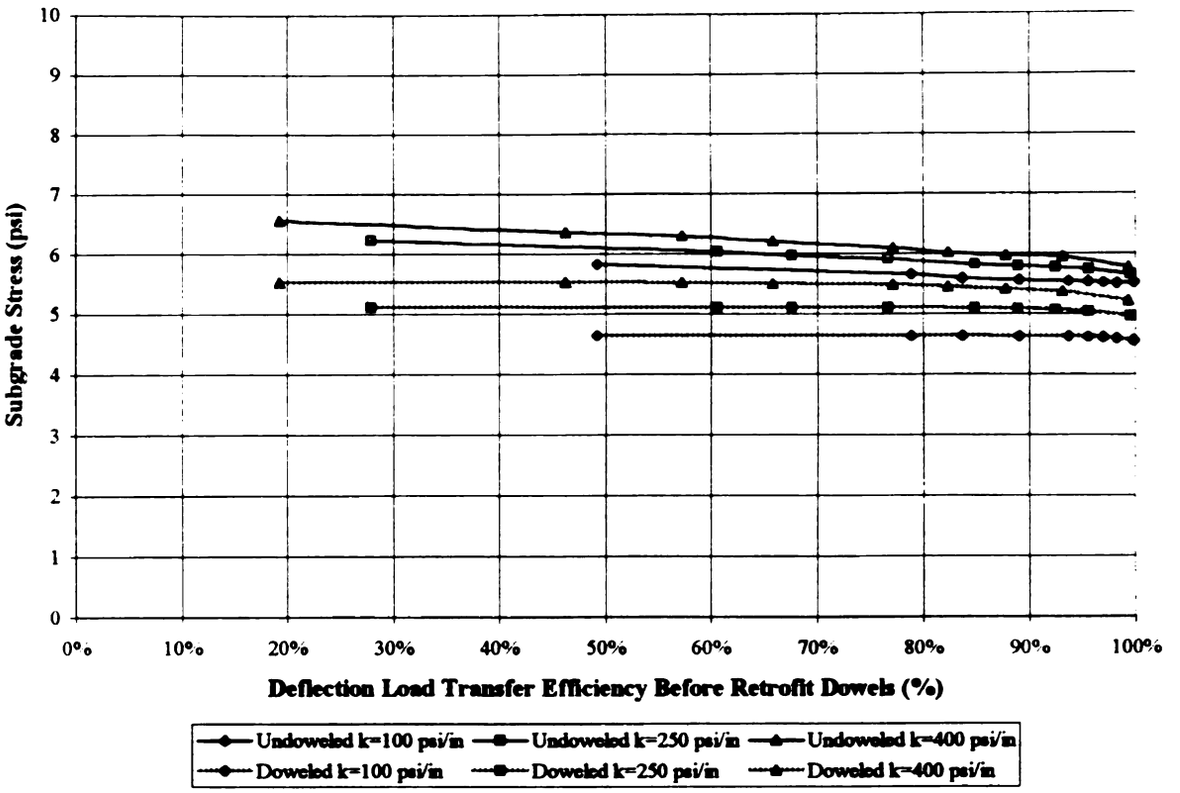

Figure E-23. Subgrade Stresses for a 36 kip (160.1 kN) Dual-Tired Tandem Axle on a 10" (254 mm) RCC Pavement Before and After Retrofit Dowels.

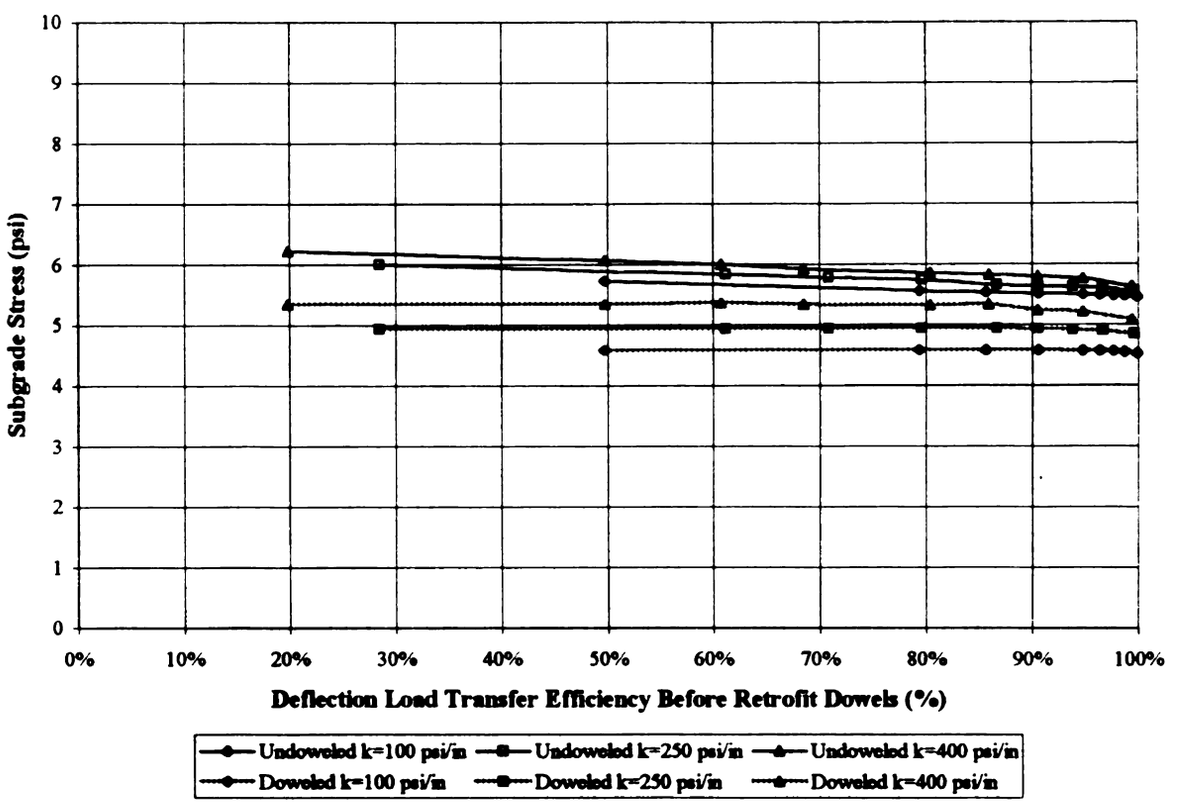

Figure E-24. Subgrade Stresses for a 36 kip (160.1 kN) Dual-Tired Tandem Axle on a 12" (305 mm) RCC Pavement Before and After Retrofit Dowels.

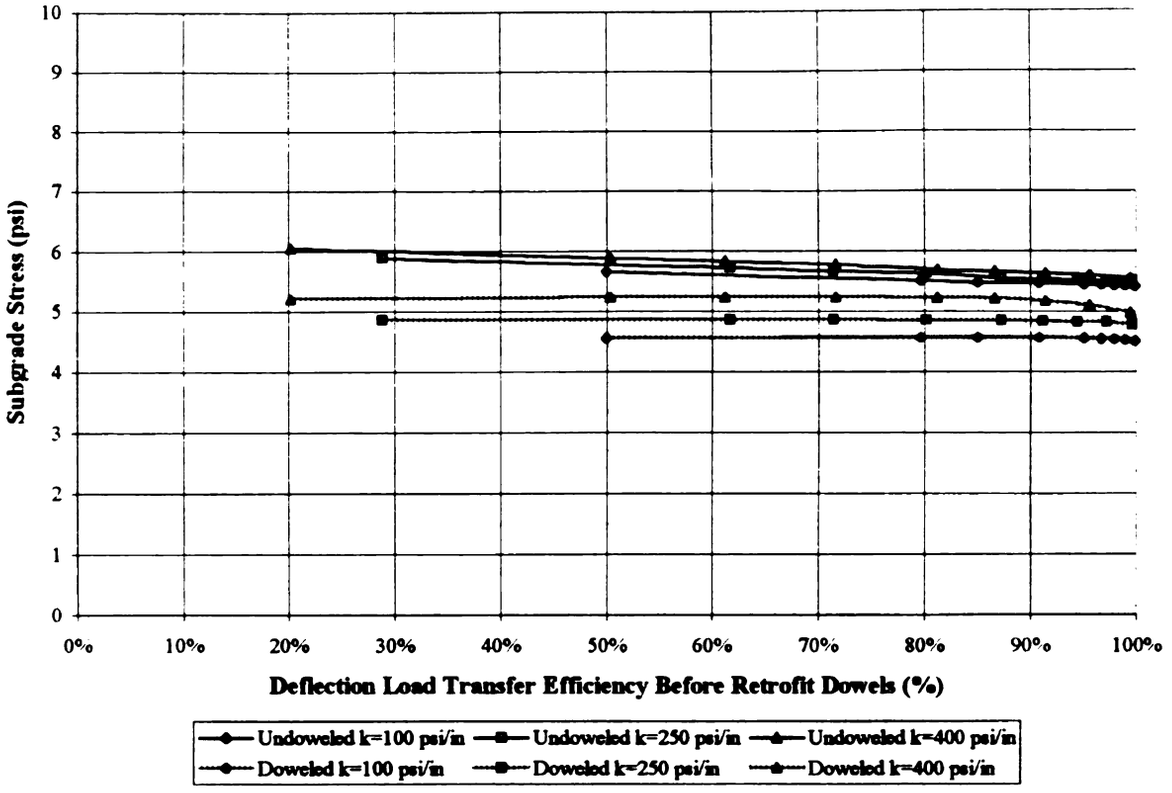

Figure E-25. Subgrade Stresses for a 36 kip (160.1 kN) Dual-Tired Tandem Axle on a 14" (356 mm) RCC Pavement Before and After Retrofit Dowels.

REFERENCES

- REFERENCES -

1. Pittman, D.W. *Development of a Design Procedure for Roller-Compacted Concrete (RCC) Pavements*. Ph.D. dissertation. University of Texas, Austin, TX. 1993.

2. Pittman, D.W. Construction of Roller-Compacted Concrete Pavements. *Transportation Research Record 1062*, TRB, National Research Council, Washington, D.C., 1986, pp. 13-19.

3. Roller-Compacted Concrete Pavements; Design and Construction, TM 5-822-7. *Standard Practice Manual for Concrete Pavement – Appendix D*. U.S. Army Corps of Engineers, Department of the Army, Washington, D.C.

4. *Suggested Specifications for Roller Compacted Concrete Paving for Municipal and Industrial Applications*, CP014.01P. Canadian Portland Cement Association (CPCA), Ottawa, ON, CA, 1995.

5. Stewart, R.F., and C.J. Schexnayder. Construction Techniques for Roller-Compacted Concrete. *Transportation Research Record 1062*, TRB, National Research Council, Washington, D.C., 1986, pp. 32-37.

6. White, T.D. Mix Design, Thickness Design, and Construction of Roller-Compacted Concrete Pavement. *Transportation Research Record 1062*, TRB, National Research Council, Washington, D.C., 1986, pp. 1-6.

7. Munn, W.D. Roller Compacted Concrete Paves Factory Roads. *Highway & Heavy Construction*, Sept. 1989.

8. Piggott, R.W. Roller-Compacted Concrete for Heavy-Duty Pavements: Past Performance, Recent Projects, and Recommended Construction Methods. *Transportation Research Record 1062*, TRB, National Research Council, Washington, D.C., 1986, pp. 7-12.

9. Cortez, E.R., and J.A. Gerlach. Roller-Compacted Concrete Pavement Construction at Fort Drum, New York. *Transportation Research Record 1282*, TRB, National Research Council, Washington, D.C., 1990, pp. 8-17.

10. Al-Abdul Wahhab, H.I., and I.M. Asi. Optimization of Roller-Compacted Concrete for Local Application. *Transportation Research Record 1458*, TRB, National Research Council, Washington, D.C., 1994, pp. 1-7.

11. State-of-the-Art Report on Roller-Compacted Concrete Pavements, ACI 325.10R-95. *ACI Manual of Concrete Practice*, American Concrete Institute, Detroit, MI, 1995.

12. Tayabji, S.D., and P.A. Okamoto. Engineering Properties of Roller-Compacted Concrete. *Transportation Research Record 1136*, TRB, National Research Council, Washington, D.C., 1987, pp. 33-45.

13. Nanni, A. Properties and Design of Fiber Reinforced Roller Compacted Concrete. *Transportation Research Record 1226*, TRB, National Research Council, Washington, D.C., 1989, pp. 61-68.

14. *Structural Design of Roller-Compacted Concrete for Industrial Pavements.* IS233.01. Portland Cement Association (PCA), Skokie, IL, 1987.

15. Piggott, R.W. *Roller Compacted Concrete Pavements – A Study of Long Term Performance.* PCA R&D Serial No. 2261. Portland Cement Association (PCA), Skokie, IL, 1999.

16. Ragan, S.A. Evaluation of the Frost Resistance of Roller-Compacted Concrete Pavements. *Transportation Research Record 1062*, TRB, National Research Council, Washington, D.C., 1986, pp. 25-32.

17. Pigeon, M., and V.M. Malhotra. Frost Resistance of Roller-Compacted High-Volume Fly Ash Concrete. *Journal of Materials in Civil Engineering*, Nov. 1995, pp. 208-211.

18. Dolen, T.P. Freeze-Thaw Durability of Roller-Compacted Concrete (Part II). *A Paper Prepared for the 1996 Spring Convention of the American Concrete Institute*, Denver, CO, Mar. 1996.

19. Petrie, R.E., and S.C. Matthews. Roller Compacted Concrete Pavements: Recent Australian Developments and Prospects for the 90s. *Proceedings of the 15th Australian Road Research Board Conference*, Melbourne, Australia, 1990, pp. 65-87.

20. Jameson, G.W., Sharp, K.G., Bailey, D.P., and R.A. Warwick. A Field Trial of the Use of Roller Compacted Concrete in High-Speed Traffic Applications. *Proceedings of the 15th Australian Road Research Board Conference*, Melbourne, Australia, 1990, pp. 143-168.

21. Todres, H.A., Jacobs, A.P., Haug, P., and T.J. McLaughlin. *An Experimental Section of Roller Compacted Concrete Arterial Road in Edmonton, Alberta.* PCA R&D Serial No. 1980. Portland Cement Association, 1992.

22. Wu, C.L., and H.A. Todres. *Improving Roller Compacted Concrete Pavement Technology: Pavement Evaluation and Thickness Design.* PCA R&D Serial No. 2016. Portland Cement Association, 1995.

23. Smith, K.D., H.T. Yu, M.J. Wade, D.G. Peshkin, and M.I. Darter. *Performance of Concrete Pavements, Volume I - Field Investigation.* Report FHWA-RD-94-177. FHWA, U.S. Department of Transportation, 1997.

24. Hall, K.T. Backcalculation Solutions for Concrete Pavements. *A Paper Prepared for Long-Term Pavement Performance Data Analysis*. Report SHRP-P-20. SHRP, National Research Council, 1992.

25. Darter, M.I., K.T. Hall, and C. Kuo. *Support under Portland Cement Concrete Pavements*. NCHRP Report 372. TRB, National Research Council, 1995.

26. Wu, C.L., and H.A. Todres. *Non-Destructive Evaluation of Roller Compacted Concrete Pavements at Fort Drum, New York*. PCA R&D Serial No. 2012. Portland Cement Association, 1994.

27. Ioannides, A.M., and G.T. Korovesis. Aggregate Interlock: A Pure-Shear Load Transfer Mechanism. *Transportation Research Record 1286*, TRB, National Research Council, Washington, D.C., 1990, pp. 14-24.

28. Benkelman, A.C. Tests of Aggregate Interlock at Joints and Cracks. *Engineering News-Record*, Vol. 111, No. 8, Aug. 24, 1933, pp. 227-232.

29. Buch, N.J. *Development of Empirical-Mechanistic Based Faulting Models in the Design of Plain Jointed Concrete Pavements*. Ph.D. Dissertation. Texas A&M University, College Station, TX, 1995.

30. Nanni, A., Ludwig, D.A., and J.E. Shoenberger. Physico-Mechanical Properties and Load Transfer Efficiency of RCC Pavement. *American Concrete Institute (ACI) Materials Journal*, Vol. 93, No. 4, pp. 356-361.

31. Teller, L.W., and H.D. Cashell. Performance of Dowels Under Repetitive Loading. *Public Roads*, Vol. 30, No. 1, April 1958, pp. 1-24.

32. Kilareski, W.P., M.A. Ozbeki, and D.A. Anderson. *Fourth Cycle of Pavement Research at the Pennsylvania Transportation Research Facility – Vol. 4: Rigid Pavement Joint Evaluation and Full Depth Patch Designs*. Report FHWA/PA-84-026. The Pennsylvania Transportation Institute, The Pennsylvania State University, University Park, PA, December 1984.

33. Ozbeki, M.A., W.P. Kilareski , and D.A. Anderson. Computer Simulation and Field Evaluation of Transverse Joints in Rigid Pavements. *Proceedings of the Third International Conference on Concrete Pavement Design and Rehabilitation*, Purdue University, West Lafayette, IN, Apr. 23-25, 1985, pp. 577-586.

34. Tayabji, S.D., and D.J. Halpenny. Thickness Design of Roller-Compacted Concrete Pavements (Discussion and Closure). *Transportation Research Record 1136*, TRB, National Research Council, Washington, D.C., 1987, pp. 23-32.

35. Huang, Y.H. *Pavement Analysis and Design*. Prentice-Hall, Inc., Englewood Cliffs, NJ, 1993.

36. Shankar, P.R., and C.E. Lee. Lateral Placement of Truck Wheels Within Highway Lanes. *Transportation Research Record 1043*, TRB, National Research Council, Washington, D.C., 1985, pp. 33-39.

37. Benekohal, R.F., K.T. Hall, and H.W. Miller. Effect of Lane Widening on Lateral Distribution of Truck Wheels. *Transportation Research Record 1286*, TRB, National Research Council, Washington, D.C., 1990, pp. 57-66.

38. Taragin, A. Lateral Placements of Trucks on Two-Lane Highways and Four-Lane Divided Highways. *Public Roads*, Vol. 30, No. 3, Aug. 1958, pp. 71-75.

39. Miller, E.J., and G.N. Steuart. Vehicle Lateral Placements on Urban Roads. *Transportation Engineering Journal, ASCE*, Vol. 108, No. TE5, Sept. 1982, pp. 495-508.

40. Taragin, A. Transverse Placement of Vehicles as Related to Cross Section Design. *Proceedings*, HRB, National Research Council, Washington, D.C., Vol. 23, 1943, pp. 342-350.

41. Shankar, P.R. *Lateral Placement of Truck Traffic in Highway Lanes*. Ph.D. Dissertation. University of Texas, Austin, TX, 1984.

42. Poblete, M., R. Valenzuela, and R. Salsilli. Load Transfer in Undoweled Transverse Joints of PCC Pavements. *Transportation Research Record 1207*, TRB, National Research Council, Washington, D.C., 1988, pp. 39-49.

43. Frabizzio, M.A., N. Buch, and J.E. Hiller, Impact of Coarse Aggregates on Transverse Crack Performance in Jointed Concrete Pavements, *ACI Materials Journal*, Vol. 97, No. 3, May-June 2000, pp.325-332.

44. Raja, Z.I., and M.B. Snyder. Factors Affecting Deterioration of Transverse Cracks in Jointed Reinforced Concrete Pavements. *Transportation Research Record 1307*, TRB, National Research Council, Washington, D.C., 1991, pp. 162-168.

45. Snyder M.B., M.J. Reiter, K.T. and M.I. Darter. *Rehabilitation of Concrete Pavements, Volume I – Repair Rehabilitation Techniques*. Report FHWA-RD-88-071. FHWA, U.S. Department of Transportation, 1989.

46. Larson, R.M., D. Peterson, and A. Correa. *Retrofit Load Transfer – Special Demonstration Project SP-204*. Report FHWA-SA-98-047. FHWA, U.S. Department of Transportation, 1998.

47. Mamlouk, M.S., M. Eacker, and E. Owusu-Antwi. *Dowel Retrofitting – A Viable Method for Preventative Maintenance*. Presented at the 79th Annual Meeting of the Transportation Research Board, TRB, National Research Council, Washington, D.C., 2000.

48. Pierce, L.M. Portland Cement Concrete Pavement Rehabilitation in Washington State: Case Study. *Transportation Research Record 1449*, TRB, National Research Council, Washington, D.C., 1994, pp. 189-198.

49. Pierce, L.M. Design, Construction, Performance and Future Direction of Dowel Bar Retrofit in Washington State. *Sixth International Purdue Conference on*

Concrete Pavement Design and Materials for High Performance, Vol. 2, Indianapolis, IN, Nov. 18-21, 1997, pp. 87-100.

50. Embacher, R.A. and M.B. Snyder. *Minne-ALF Project Overview and Results of Tests of PCC Slab Specimens Containing Retro-Fit Dowels*. Paper Prepared for the International Conference on Accelerated Pavement Testing, TRB, Reno, NV, 1999.

51. Zaniewski, J.P., and M.S. Mamlouk. *Preventive Maintenance Effectiveness – Preventive Maintenance Treatments*, Report FHWA-SA-96-027, FHWA, U.S. Department of Transportation, 1996.

52. Galehouse, L. Innovative Concepts for Preventative Maintenance. *Transportation Research Record 1627*, TRB, National Research Council, Washington, D.C., 1999, pp. 1-6.